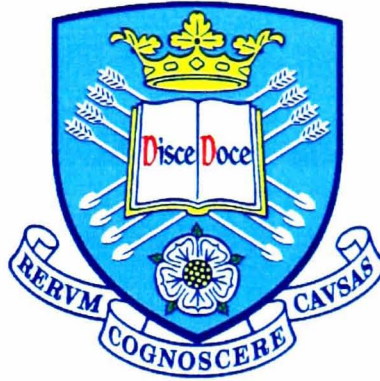


VULNERABILITY OF RC BUILDINGS AND RISK ASSESSMENT FOR CYPRUS



A thesis submitted for the degree of Doctor of Philosophy
in the Faculty of Engineering of the University of Sheffield

By

Nicholas Kyriakides
(B.Eng., Nottingham)

Centre for Cement and Concrete
Department of Civil & Structural Engineering
The University of Sheffield

December 2007

*To Marília for her love and patience and to
my parents for having so much faith in me*

ABSTRACT

Previous studies on Earthquake Risk Assessment (ERA) for Cyprus (Kythreoti, 2001) concluded that a new Peak Ground Acceleration (PGA) attenuation law needs to be derived based on local data and the vulnerability of the building stock needs to be fully re-examined. Field data from recent seismic activity became available and are used to derive a new PGA attenuation law. However, the damage data proved limited and analytical vulnerability curves were found to be necessary. Previous studies on analytical vulnerability underestimate damage from common brittle modes of failures.

A variety of failure modes were simulated by using relatively simple element models, which were calibrated based on experimental data and expert judgment. A modified capacity-spectrum procedure was developed for the estimation of structural response and verified against time-history results. This procedure includes the bilinearisation of softening capacity curves so as to predict the response of structures deteriorating due to a variety of local brittle failure modes.

A new damage index indicator was developed based on fundamental period shift and this was linked to damage limits. Key design parameters from capacity models were treated probabilistically and analytical vulnerability curves were derived for two building types and three design levels. A rapid increase in damage takes place well before the anticipated flexural failure threshold is observed in “Pre” and “Basic” design buildings. This occurs due to the dominance of brittle failure modes. The effect of the hazard spectrum on the vulnerability curves was found to be considerable. In the case of Cyprus, Type 2 spectra (EC-8, 2004) were found to simulate better the earthquake hazard potential.

Annual insurance premium allocated for seismic risk in Cyprus is currently set at 0.06-0.08% of value and this appears to predict the overall risk accurately. However, the use of a single premium for all building types and the entire island leads to underestimation of seismic risk in Pre-seismic buildings. This underestimation is more profound in regions along the southwest coast of the island.

The single most important issue for analytical vulnerability assessment is the definition of an appropriate structural model, which requires sophisticated modelling capabilities to simulate brittle failure modes and further work is recommended.

ACKNOWLEDGMENTS

I would like to express my deepest gratitude and appreciation to my supervisor and friend, Professor Kypros Pilakoutas for his continuous help, support and inspiration during this project. His lateral thinking and guidance helped me overcome successfully any obstacles found in this project. Thank you Kypros.

I also want to thank all my colleagues in room E110, in particular Maurizio and Shaukat, for all their help at the initial and final stages of my work, respectively. Further on, I would like to thank my close friends Panos, Charis, Kyriakos, Sotiris, Yiannis and Sager for all the good times we had in Sheffield, which I will always remember. Special thanks are due to Kyriakos for his valuable help throughout the thesis but most importantly for hosting me in his place for the whole of the writing-up period. Thanks a lot for your generosity.

I would also like to acknowledge the financial assistance offered to me by the University of Sheffield. In addition, my acknowledgements are due to the A.G. Leventis Foundation for providing me with financial support for the period 2002-2005.

The initial part of this work is based on data which were provided from local authorities in Cyprus and for this I am particularly grateful to Mr K. Solomis-Geological Survey Department of Cyprus, and Mr Ch. Kyriakides - Commissioner of the Civil Defence of the Republic of Cyprus.

This work is dedicated to the people I love most in my life and who have “suffered” a lot during the period of my absence from home. Marilia, your love, patience and encouragement kept me going. Thanks for believing in me and although I was miles away from you, I could always sense your presence next to me (binggg!!!!). Mom and Dad, thank you from the bottom of my heart for all the sacrifices you went through for me. Your motivation, encouragement and most importantly confidence in my abilities have been of paramount importance to me. Phanos and Alexis, thanks for the laughs and for your constant support.

TABLE OF CONTENTS

CHAPTER 1

INTRODUCTION

1.1. Introductory Remarks	1
1.2. Research Aims and Objectives.....	4
1.3. Layout of the thesis	5

CHAPTER 2

LITERATURE REVIEW

2.1. Introduction	8
2.2. Background	8
2.3. Methods for vulnerability assessment.....	9
2.3.1 Empirical	9
2.3.2 Expert judgment	12
2.3.3 Analytical	15
2.3.3.1. Simple analytical procedures	15
2.3.3.2. Detailed analytical method procedures	18
2.4. Structural Damage Indicators.....	22
2.4.1 Dynamic parameters assessment.....	23
2.4.2 Displacement parameters	25
2.4.3 Displacement and cumulative damage.....	26
2.5. Conclusions	27

CHAPTER 3

EMPIRICAL RISK ASSESSMENT

3.1.	Introduction-background to empirical risk assessment.....	28
3.2.	Description of Acceleration Data.....	30
3.3.	PGA attenuation relationship by Theodulidis.....	32
3.4.	Derivation of enhanced PGA relationship	33
3.4.1	Comparison of predicted to observed PGA	36
3.5.	Relationship between PGA and MMI.....	38
3.6.	Empirical vulnerability -Introduction	39
3.7.	Data classification	40
3.8.	Identification of damage grade.....	40
3.9.	Empirical Vulnerability curves	41
3.10.	Discussion on the Vulnerability Results	44

CHAPTER 4

STRUCTURAL MODELLING

4.1	Introduction.....	45
4.2	Background on Analysis and Modelling.....	46
4.2.1	Lumped plasticity constitutive models	47
4.2.2	Resistance models	49
4.2.2.1	Flexure	49
4.2.2.2	Shear.....	49
4.2.2.3	Bond.....	51
4.3	Choice of Analytical Tool.....	52
4.3.1.	Drain-3D (Flexure).....	52
4.3.1.1	Material Modelling.....	54
4.3.2.	Drain-3D (Anchorage)	54
4.3.2.1	Pullout Fibres	55

4.3.2.2	Reinforcement local buckling	61
4.3.2.3	Gap Fibre.....	62
4.3.3.	Drain-3D (Shear).....	63
4.3.3.1	Calibration of shear model	64

CHAPTER 5

VERIFICATION OF ANALYTICAL TOOL

5.1.	Data for Verification of Analytical Tool.....	67
5.1.1.	Design Details of the frame.....	68
5.1.2.	Reinforcement detailing	70
5.1.3.	Instrumentation	73
5.2.	Shaking Table Tests	75
5.3.	Observed Damage	75
5.4.	Capacity-Demand.....	77
5.4.1	Post-elastic behaviour	79
5.5.	Strain histories.....	81
5.5.1	First storey response.....	81
5.5.2	Second storey response	83
5.6.	Modelling of the Saclay frame in DRAIN-3D	85
5.6.1	Section modelling.....	85
5.6.2	Material modelling.....	86
5.6.3	Moment-curvature relationships	87
5.6.4	Modelling slip deformations	87
5.6.5	Modelling of joints.....	88
5.6.6	Segment distribution	89
5.6.7	Frame Mass	89
5.6.8	Damping	90
5.7.	Correlation of experimental and analytical dynamic results.....	91
5.8.	General Discussion	96

CHAPTER 6

ANALYTICAL VULNERABILITY ASSESSMENT

6.1	Introduction.....	98
6.2	Prediction of structural response.....	98
6.2.1.	Capacity Envelope	100
6.2.2.	Response Spectrum	104
6.2.3.	Applications of CSM	110
6.3	Quantification of damage potential.....	111
6.4	Probabilistic vulnerability assessment	113
6.4.1	CDP considerations.....	115
6.4.2	Analytical determination of capacity envelope.....	120
6.4.3	Definition of complete damage.....	121
6.4.4	Process for choosing the simulation values	122
6.4.5	Probabilistic vulnerability curves.....	125
6.4.5.1.	LR buildings.....	125
6.4.5.2.	MR buildings.....	127
6.4.5.3.	Comparison with other empirical vulnerability curves.....	129

CHAPTER 7

EARTHQUAKE RISK ASSESSMENT

7.1.	Introduction.....	135
7.2.	Background on EQ-RACY	135
7.3.	Estimation of earthquake risk for the region of Cyprus.....	136

CHAPTER 8

CLOSURE

8.1	Introduction.....	138
8.2	Summary and main conclusions.....	138

8.3 Recommendations for future work 141

REFERENCES

APPENDIX A

DATA FOR EMPIRICAL RISK ASSESSMENT

APPENDIX B

SIMULATION VALUES FOR PROBABILISTIC VUNERABILITY CURVES

APPENDIX C

CROSS-SECTIONAL DETAILS OF SIMULATED FRAMES

LIST OF FIGURES

CHAPTER 1

- Figure 1.1. Examples of common failure modes observed during Kalamata (1986), North Athens (1999)¹ and Limassol (1999) earthquakes. 3

CHAPTER 2

- Figure 2.1. Weighted observational damage statistics (after Rossetto, 2002)..... 11
- Figure 2.2. Qualitative description of RC buildings for damage grade 3..... 14
- Figure 2.3. Vulnerability curves for Cyprus (after Schnabel, 1987). 14
- Figure 2.4. Comparison of displacement demand and capacity for LS2 at PGA=0.5g..... 15
- Figure 2.5. Determination of capacity curves 16
- Figure 2.6. Example of capacity curve and demand spectrum..... 17
- Figure 2.7. Shear failures in joints (Pagni, 2004, Dhakal, 2005 and Pantelides 2000) 20
- Figure 2.8. Normalised natural frequency drop with progressive damage states (after Zembaty et al.,2006) 24

CHAPTER 3

- Figure 3.1 Error in PGA (cm/sec^2) with increased magnitude 33
- Figure 3.2 Error in PGA (cm/sec^2) with increased epicentral distance 33
- Figure 3.3 Summarised schematic of the methodology for PGA attenuation equation. 35
- Figure 3.4 Residual error (cm/sec^2) in the predictions of eq-3-9 for increasing M_s and R. 37
- Figure 3.5 Approximate normal distribution for the residual error in the prediction of eq. 3-9 ($\mu=0$)..... 38
- Figure 3.6 Relationship between PGA (in cm/sec^2) and MMI..... 39
- Figure 3.7 Percentage of buildings for each damage grade (DG) for the range of PGA values. 43
- Figure 3.8 Empirical vulnerability curves for RC and masonry buildings for Cyprus 44

CHAPTER 4

- Figure 4.1. Clough and Johnson lumped plasticity element..... 47
- Figure 4.2. (a) Stiffness degradation with shear deterioration, and (b) Takeda hysteretic model 48
- Figure 4.3. Hysteretic modelling of the moment-curvature relationship (Ghobarah, 1999)48
- Figure 4.4. (a) Shear failure after reinforcement yielding and (b) no shear in joint and poor anchorage of reinforcement (from Biddah, 1997). 50

List of Figures

Figure 4.5.	Hysteretic response of damaged joint (after Walker, 2001)	50
Figure 4.6.	Experimental stress-slip response of anchored reinforcing bar under cyclic push-pull (Viwathanatepa, 1979).....	51
Figure 4.7.	Contribution of flexure, shear and slip deformations to total column displacements (from Sezen, H., 2002).....	52
Figure 4.8.	Section analysis element (Prakash, 1994).....	53
Figure 4.9.	Concrete and steel stress-strain envelopes.....	54
Figure 4.10.	Trilinear backbone curve of pullout fibre	55
Figure 4.11.	Pullout fibre degradation properties (a) Basic trilinear curve decomposed in three parallel components, (b) Stiffness degradation factor (SDF), (c) Strength loss in each component depends on strength degradation factor (STDF or SCDF) and the ratio of accumulated plastic displacement to saturated displacement (ST or SC), and (d) Pinch factor (PF), pinch strength factor (PSF) and plateau factor (PPF).	56
Figure 4.12.	Fibre deformation (reproduced from Prakash, 1994).....	57
Figure 4.13.	Piecewise constant bond distribution for yielded steel.	59
Figure 4.14.	Bond-slip model in CEB (1993)	60
Figure 4.15.	Model for gap fibres	62
Figure 4.16.	Backbone curve of inelastic shear element.....	63
Figure 4.17.	Shear hinge deformation	64

CHAPTER 5

Figure 5.1.	a) Connection detail of steel plate, and b) free rotation of the slab (reproduced from Chaudat, 2005).....	68
Figure 5.2.	Reinforcement details of the elements (Chaudat et al., 2006) and plan view of the frame.	69
Figure 5.3.	Anchorage details of 1st and 2nd storey (a) beams, and (b) columns (Chaudat et al., 2006).	71
Figure 5.4.	Detail of anchorage of column bars at the top of the storey joints (Chaudat, 2005).....	71
Figure 5.5.	(a-d) reproduced from Chaudat, 2005), a) Plan view of the steel box, b) Side view of the steel box, c) Cross-section of a typical steel box, d) Column bar welding detail into the steel base and e) Isometric view of the foundation (obtained from Chaudat, 2005).....	72
Figure 5.6.	Location of Displacement and Acceleration transducers (Chaudat, 2005).....	73
Figure 5.7.	Location of strain gauges on steel bars (reproduced from Chaudat, 2005)	74
Figure 5.8.	Location of strain gauges relative to the column-joint interface.....	74

List of Figures

Figure 5.9.	Spectrum of the acceleration signal (Chaudat, 2005).	75
Figure 5.10.	Damage at the column-joint interface and column length after the 0.2g and 0.4g tests (Chaudat, 2005).	76
Figure 5.11.	Time-history of shear force at 2nd floor after the 0.2g test.	80
Figure 5.12.	Time-histories of base shear force after the 0.2g test.	80
Figure 5.13.	Time-histories of base shear force after the 0.4g test.	81
Figure 5.14.	Strain history of 1 st storey columns (j3pot).....	81
Figure 5.15.	Strain histories of 1 st floor column 3 for 0.3g and 0.4g (j3pot).	82
Figure 5.16.	Strain histories of 1 st floor column 2 for 0.3g and 0.4g (j2pot).	82
Figure 5.17.	1 st storey displacement records.	83
Figure 5.18.	Strain history of 2 nd floor column 3 (j8pot) for 0.3g.....	83
Figure 5.19.	Top storey displacement history at 0.3g.	84
Figure 5.20.	Strain history for j8pot at 0.4g.	84
Figure 5.21.	Top storey displacement history at 0.4g.	85
Figure 5.22.	Layout of the fibre element for the 1st storey columns	86
Figure 5.23.	Stress-strain envelops of concrete and reinforcement steel.	86
Figure 5.24.	Comparison of moment-curvature curves for 1st floor columns.	87
Figure 5.25.	Backbone curve of pullout hinge.	88
Figure 5.26.	Model for elastic shear deformations.....	89
Figure 5.27.	Analytical vs. experimental top storey displacements (0.05g)	91
Figure 5.28.	Analytical vs. experimental top storey displacements (0.10g)	92
Figure 5.29.	Analytical vs. experimental top storey displacement at 0.20g (no bond slip). .	93
Figure 5.30.	Analytical relative displacement history of 2 nd storey at 0.20g (no bond slip).	93
Figure 5.31.	Analytical positive strain results of 2 nd floor (0.2g test).....	93
Figure 5.32.	Analytical vs. experimental top storey displacements at 0.20g with bond slip.	94
Figure 5.33.	Analytical vs. experimental at 0.30g with no bond slip.....	95
Figure 5.34.	Analytical strain results (j8pot) of 2 nd floor (0.3g test) without bond slip.	95
Figure 5.35.	Analytical vs. experimental at 0.30g with bond slip.....	95
Figure 5.36.	Analytical vs. experimental at 0.40g with no bond slip.....	96
Figure 5.37.	Analytical vs. experimental at 0.40g with bond slip.....	96

CHAPTER 6

Figure 6.1	Transformation of push-over curve to capacity diagram	101
Figure 6.2	Idealisation of capacity curve using the ES approximation	102
Figure 6.3	Comparison of the residual error using the two idealization techniques	104
Figure 6.4	Transformation of elastic spectrum based on EC-8 (2004) model for PGA=0.25g and ground type C.....	106
Figure 6.5	Graphical application of N2 method after Fajfar (1999)	108

List of Figures

Figure 6.6	MADRS in FEMA 440 (2005) for use in CSM.....	109
Figure 6.7	Residual error of the simulation study	109
Figure 6.8	Quantities required to define structural behaviour.....	110
Figure 6.9	Schematic of the application to determine PGA using CSM (colouring based on Figure 6.6).....	111
Figure 6.10	Layout of LR and MR simulation frames	119
Figure 6.11	Comparison between time-history and cyclic push-over for different displacement step.....	120
Figure 6.12	Definition of the failure plane.....	122
Figure 6.13	Comparison of analytical curves using 10, 25 and 50 simulations.....	124
Figure 6.14	Analytical vulnerability curves for LR Pre-seismic buildings.....	125
Figure 6.15	Analytical vulnerability curves for LR Basic seismic buildings.....	126
Figure 6.16	Analytical vulnerability curves for LR Modern seismic buildings.....	126
Figure 6.17	Analytical vulnerability curves for MR Pre-seismic buildings.....	128
Figure 6.18	Analytical vulnerability curves for MR Basic seismic buildings.....	128
Figure 6.19	Analytical vulnerability curves for MR Modern seismic buildings.....	128
Figure 6.20	Comparison of vulnerability curves for substandard construction	130
Figure 6.21	Comparison of vulnerability curves for superior construction	130
Figure 6.22	Comparison of vulnerability curves for Substandard construction (Type 2 spectrum)	131
Figure 6.23	Comparison of vulnerability curves for superior construction (Type 2).....	131
Figure 6.24	Analytical vulnerability curves for LR Pre-seismic buildings in Cyprus	132
Figure 6.25	Analytical vulnerability curves for LR Basic designed buildings in Cyprus..	133
Figure 6.26	Analytical vulnerability curves for LR Modern seismic buildings in Cyprus	133
Figure 6.27	Analytical vulnerability curves for MR Pre-seismic buildings in Cyprus	133
Figure 6.28	Analytical vulnerability curves for MR Basic designed buildings in Cyprus.	134
Figure 6.29	Analytical vulnerability curves for MR Modern seismic buildings in Cyprus	134

CHAPTER 7

Figure 7.1	Spreading of risk around the island (Kythreoti, 2001).....	137
------------	--	-----

APPENDIX A

Figure A-1.	Damage Grade classification scheme for RC buildings (EMS-1998).....	A-7
Figure A-2.	Damage Grade classification scheme for Masonry buildings (EMS-1998).....	A-8

APPENDIX C

List of Figures

Figure C-1. Cross-sectional design detail of LR frames for (a) Pre, (b) Basic and (c) Modern seismic design (columns on the left hand side).....C-2

Figure C-2. Cross-sectional detail of MR frames for (a) Pre, (b) Basic and (c) Modern seismic design (columns on the left hand side).....C-3

LIST OF TABLES

CHAPTER 2

Table 2.1.	Format of DPM after Whitman (1974)	10
Table 2.2.	Differentiation of building types into vulnerability classes (EMS, 1998)	13
Table 2.3.	Definition of intensity degrees for MMI=8	14
Table 2.4.	ISD (%) for RC buildings (Rossetto, 2002).....	26

CHAPTER 3

Table 3.1	Repair costs/m ² for each DG for RC buildings in Cyprus (1997 prices)	40
Table 3.2	Repair costs/m ² for each DG for Masonry buildings in Cyprus (1997).....	40
Table 3.3	DR for each damage grade for RC buildings (account for 1997).....	41
Table 3.4	DR for each damage grade for masonry buildings (account for 1997).....	41
Table 3.5	DPM in % values for RC buildings in Cyprus	42
Table 3.6	DPM in % values for Masonry buildings in Cyprus	42

CHAPTER 5

Table 5.1.	Steel Mechanical Properties (Chaudat et al., 2005).....	70
Table 5.2.	Concrete Mechanical Properties (Chaudat et al., 2005).....	70
Table 5.3.	Frequency change after each test (Chaudat, 2006)	76
Table 5.4.	Strength capacities for 1 st and 2 nd floor columns.	78

CHAPTER 6

Table 6.1.	Values used in simulation study	104
Table 6.2.	Values of the parameters used in elastic and design response spectra.....	106
Table 6.3.	Calibration parameters for capacity models.....	114
Table 6.4.	Qualitative description of CDP for the selected periods.....	115
Table 6.5.	Statistical data of PDF for the four key parameters per period.....	116
Table 6.6.	Values for deterministic design parameters for LR (per period)	117
Table 6.7.	Values for deterministic design parameters for MR (per period)	117
Table 6.8.	Loading combinations used in design (per period).....	118
Table 6.9.	Top storey drift at complete damage (as obtained from SD values in HAZUS99 (NIBS, 1999) for an h=6m and h=13m building)	122
Table 6.10.	Latin hypercube sampling procedure using 9 simulation values	124

APPENDIX A

Table A-1. Location and surface geology at the recording stations (Solomis, 2002).....A-2

Table A-2. Main geological formations of Cyprus (after Kythreoti, 2001).....A-3

Table A-3. Magnitude and epicentral location of earthquakes in Cyprus (Solomis, 2002).....A-4

Table A-4. Strong-motion data and surface geology at the recording stations (Solomis, 2002).....A-5

Table A-5. Representative sample of damage data.....A-6

APPENDIX B

Table B-1. Simulation values for key parameters (Pre-seismic buildings).....B-2

Table B-2. Simulation values for key parameters (Basic seismic buildings).....B-3

Table B-3. Simulation values for key parameters (Modern seismic buildings).....B-4

ABBREVIATIONS

ATC	Applied Technology Council
BS	British Standards
CDF	Cumulative distribution function
CDP	Construction and design Practice
CEB	Comite Euro-International du Beton
CSM	Capacity-Spectrum method
CY	Cyprus
DG	Damage Grade
DPM	Damage Probability Matrix
DR	Damage Ratio
EC	Eurocode
EMS	European Macroseismic Scale
EQ-RACY	Earthquake Risk Assessment Cyprus
ERA	Earthquake Risk Assessment
FEMA	Federal Emergency Management Agency
HAZUS	Hazard United States
ISD	Interstorey drift
LR	low-rise buildings
LHS	Latin Hypercube Sampling
MADRS	Modified Acceleration Displacement Response Spectrum
MDR	Mean Damage Ratio
MMI	Modified Mercalli Intensity
MR	mid-rise buildings
NIBS	National Institute of Building Science
PDF	Probability Distribution Function
PGA	Peak Ground Acceleration
POE	Probability of Exceedance
PSF, PPF	pinching strength factor, pinching plateau factor
RC	Reinforced Concrete
SRSS	Square root of sums of squares
STDF, SCDF	tensile and compressive strength degradation factor
ST,SC	saturated displacements in tension and compression
US	United States of America

NOTATION

Latin lower case

a/d	aspect ratio
b	breath of cross-section
d	depth of cross-section
d_{bl}	longitudinal bar diameter
d_{bw}	shear link diameter
f_c	concrete compressive strength
f_s	stress in a reinforcement bar
f_{ys}	steel bar yield strength
f_{yw}	shear link yield strength
h_i	height of floor i
l	anchorage length
m	total mass
m^*	effective modal mass
q	behaviour factor
s	shear link spacing
u_i	uniform random number

Latin upper case

F_d	design shear force capacity
F_y	yield shear force capacity
F_{ult}	ultimate shear force capacity
M_d	design moment capacity
M_L	local magnitude
M_s	surface magnitude
M_y	yield moment capacity
M_{ult}	ultimate moment capacity
N	number of floors
P	error parameter
R	epicentral distance

S	soil parameter
S_{EC}	soil parameter as defined in EC-8 (2004)
SA	spectral acceleration
SD	spectral displacement
$S_d(T_1)$	ordinate of the design spectrum
$T_{initial}$	initial period of vibration
T_{sec}	secant period
V_{rd3}	member ultimate shear capacity
V_{cd}	concrete shear contribution
V_{wd}	shear link contribution
W_i	weight of floor i
A_s	area of steel bar
E_s	steel elastic modulus
E_h	steel hardening modulus

Greek symbols

α_0	mass damping coefficient
α_1	element damping coefficient
α_g	design ground acceleration
β	Park and Ang (1985) experimental constant
δ_m	maximum softening
δ_u	ultimate softening
ε_s	steel strain
ζ	viscous damping ratio
λ	correction factor
μ	mean value
σ	standard deviation
τ_e	bond strength for elastic steel
τ_y	bond strength for yielded strength
Φ_{jl}	j th floor element of the fundamental mode of vibration
ω	angular frequency

Chapter 1

INTRODUCTION

1.1. Introductory Remarks

Recent worldwide experience indicates that even though new design codes have been introduced in most seismic regions, they did not contribute as much to the minimization of earthquake damage to buildings, primarily as a result of the fact that the existing building stock pre-dates modern codes. An unfortunate verification of the above is the recent progressive increase of the amount of sustained economic damage, reaching US \$20 billions per annum for the last decade of the millennium. Mitigation of the unwanted consequences of earthquakes can be planned through Earthquake Risk Assessment (ERA), which is based primarily on the assessment of the earthquake hazard and vulnerability of the building stock. Seismic hazard relates to all physical phenomena which are a consequence of the earthquake (such as strong ground motion, liquefaction, tsunamis, landslides, or even induced fires) and can affect exposed infrastructure and other aspects of human interaction with the environment. The vulnerability of the building stock denotes the amount of damage induced by a given degree of hazard, and is expressed monetarily, as the ratio of the damage to the replacement cost of the item under consideration.

ERA forms the basis for the calculation of premium rates for earthquake insurance purposes and for the determination of the range of the probable maximum loss that would be incurred in the event of a catastrophic earthquake (Kythreoti, 2001). It is also performed as part of earthquake risk mitigation programmes in urban areas, the main aim of which is to reduce fatalities, injuries, construction damage and other economic losses caused by an earthquake.

Work on ERA, conducted by Kythreoti (2001) at the University of Sheffield, provided a framework (EQ-RACY) for earthquake risk assessment, using Cyprus as a case study. The investigation of the vulnerability aspect of ERA was beyond the scope of Kythreoti's work and was dealt with in a rather simplistic manner. A detailed hazard assessment procedure was derived that provided risk estimates at specific locations. Hazard was determined in the form of predicted peak ground acceleration (PGA) for every village and municipality, which enabled a more accurate representation than offered by the use of a single response spectrum in the current hazard map included in the Cypriot seismic code for RC structures (Cyprus Civil Engineers and Architects Association, 1991)

In 1995 accelerometers were installed in various areas around the island by the local Seismological Centre, and those started to provide data after the destructive Paphos 1996 earthquake. Following this earthquake, a governmental authority called "Earthquake Rehabilitation Service" (ERS) was established with responsibility to assess the damage levels and prepare repair strategies. ERS was assigned the role of evaluating the level of damage in each area by site inspections soon after the events. At the onset of this work, the author was granted access to information on both PGA and damage data.

Following this development, it was deemed necessary to analyze the available data in view of the limitations of the existing ERA framework (EQ-RACY). Hence, this study is to some extent a continuation of the previous study by Kythreoti (2001) and will attempt to enhance the PGA attenuation model based on accelerometer recordings and produce empirical vulnerability curves for Cyprus based on damage data. The conclusions of the empirical analysis of the observed data will indicate whether a new framework for vulnerability assessment is required through analytical techniques. These curves should use PGA as the hazard parameter to allow the micro-hazard representation already included in EQ-RACY.

It should be noted that most analytical vulnerability studies concentrate primarily on flexural and to a small extent shear failures in members. In addition, most existing studies fail to address shear and bond deficiencies in joints, which are frequently damaged especially in sub-standard constructions. Field investigations, following earthquakes in Cyprus and Greece, as well as in other Mediterranean countries, show that many different types of failures occur such as the ones shown in Figure 1.1. These

failures include shear failures in joints and columns, short column failures, debonding of column and beam reinforcement and local buckling.



(a) Shear failure in joints



(b) Column bars debonding



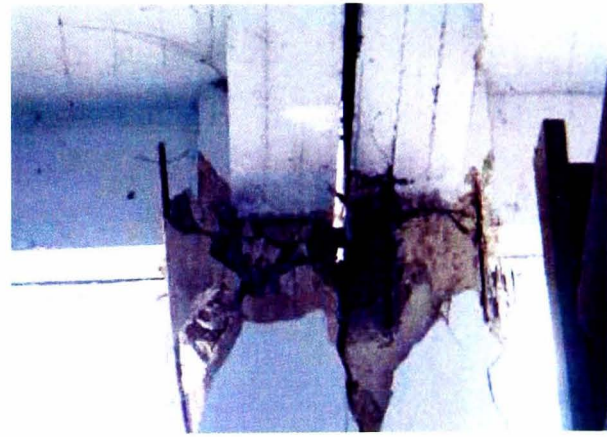
(c) Short column failure



(d) Shear failure in column and local buckling



(e) Short column



(f) Shear failure and column bars debonding

Figure 1.1. Examples of common failure modes observed during Kalamata (1986), North Athens (1999)¹ and Limassol (1999) earthquakes.

¹ From Report No. ESEE 99-4, Elnashai A (1999).

These modes of failure, which in practice for sub-standard construction have a greater impact than flexural failures since they are related to detailing deficiencies, will need to be considered in any future analytical vulnerability study.

1.2. Research Aims and Objectives

This study aims to combine empirical damage data and possibly analytical techniques and develop a framework for improved earthquake vulnerability assessment. The framework will be demonstrated using the island of Cyprus as a case study.

The following objectives are identified as essential for the fulfilment of the main aim:

- Review of the literature on existing methods for vulnerability assessment and select an appropriate hazard attenuation law.
- Establish a reliable local databank for PGA and damage data.
- Evaluate the appropriateness of the existing PGA attenuation models for the area of Cyprus.
- Develop attenuation laws for both PGA and Modified Mercalli Intensity (MMI) based on the local acceleration database.
- Develop empirical vulnerability curves for both reinforced concrete (RC) buildings in Cyprus for the evaluation of the expected damage levels at various hazard levels and assess their ability to represent accurately the vulnerability of the local building stock.
- Identify the most suitable modelling and analytical techniques for the simulation of structural response during earthquakes which capture the typical failure modes expected for the particular class of buildings.
- Verify the analytical tool used for the simulation of structural response.

- Investigate the appropriateness of nonlinear static and dynamic analysis procedures for use in vulnerability assessment.
- Produce a simplified procedure for the estimation of the structural response.
- Choose the most suitable damage indicator for the correlation of structural response and damage potential.
- Produce analytical vulnerability curves and correlate with available data and results from other studies.
- Substitute the enhanced PGA attenuation model and the derived analytical vulnerability curves into the existing ERA framework to estimate the risk for Cyprus.

1.3. Layout of the thesis

In chapter 2, a literature review is presented on vulnerability assessment methods. In the first section, a review of the most comprehensive empirically derived curves takes place which concludes with a discussion on the main drawbacks of such an approach. Following this, a review is conducted on vulnerability curves derived based on expert judgment including an example for the island of Cyprus. In the rest of the review, special emphasis is given on simple and detailed analytical procedures. A discussion follows on the various issues involved in the determination of the structural response and how this can be correlated to structural damage.

Chapter 3 initially includes a brief discussion on PGA attenuation laws for Cyprus and a presentation of the available field data. These are used for the derivation of an improved PGA attenuation law and a comparison with available data is conducted. In the second part, the available damage data are processed and empirical vulnerability curves are derived. It is concluded that very limited information can be derived from the available damage data, and that the problem of vulnerability needs to be addressed analytically, but in a more sophisticated manner than previous studies.

In Chapter 4, the initial sections include a review on modelling issues involved in the derivation of analytical vulnerability curves in light of the anticipated damage potential. Subsequently, an appropriate analytical tool (DRAIN-3D) capable of simulating the previously mentioned damage potential is chosen. The rest of the chapter includes a demonstration of the modelling capabilities of the analytical tool along with details on the calibration process of each model.

The verification of the analytical tool is the objective of Chapter 5. For that purpose, the results from full-scale shaking table tests on an RC frame are compared with simulations results obtained from time-history analysis. The good correlation between actual (from testing) and analytical results leads to the conclusion that the analytical tool can be safely used for the derivation of analytical vulnerability curves.

Chapter 6 examines the various steps towards the derivation of probabilistic analytical vulnerability curves. Initially, the most reliable procedure is chosen to arrive at the estimation of the structural response. The accuracy of this procedure is demonstrated against “exact” values obtained from time-history analysis and results from an alternative capacity-spectrum procedure. Subsequently a damage index, to correlate structural response to damage potential, is selected based on a number of criteria. After establishing the procedure to arrive at the damage potential, the probabilistic nature of vulnerability is addressed and a number of design parameters, to be included in the calibration of capacity models, are selected. The probabilistic distribution function (PDF) of each parameter is established. The Latin Hypercube Sampling method is used to define the simulation values from the corresponding (PDFs). The most representative building types in Cyprus are identified (low and mid rise RC buildings) and separate designs are conducted for each type following “Pre”, “Basic” and “Modern” design guidelines. The last part of the chapter presents the newly derived analytical vulnerability curves and a comparison with the limited empirical data. The curves are modified to account for the characteristics of the local hazard.

Chapter 7 comprises of a small discussion on the existing ERA framework developed by Kythreoti (2001) and a presentation of the enhancements achieved in this study. The calculated risk using the enhanced models is compared with premium values provided by insurance companies in Cyprus.

In the final chapter, the general conclusions, drawn from the work described above, are presented together with recommendations for future research on the topic.

Chapter 2

LITERATURE REVIEW

2.1. Introduction

This chapter provides a review on literature in earthquake vulnerability assessment. Literature on attenuation is given in Chapter 3. After a brief background on the topic, a review of the most widely used methods for vulnerability assessment is given, emphasizing advantages and disadvantages. For each method, the most representative examples found in the literature are given in order to assess their ability to simulate the damage potential observed in recent earthquakes. Special attention is given to the widely used analytical assessment method. The main issues of this method regarding the selection of an appropriate damage indicator and the best representation of seismic hazard parameter are extensively discussed in the last part of the chapter. Finally, a discussion takes place regarding the applicability of these methods for the derivation of vulnerability curves for Cyprus.

2.2. Background

The prediction of damage potential from earthquakes has always been a challenge for the earthquake engineering community. One of the first comprehensive attempts to quantify the expected damage potential for different intensity levels was conducted by Whitman et al. (1974) based on the damage caused by the 1971 San Fernando earthquake. This study introduced for the first time the concept damage ratio (DR). DR is the ratio between repair and replacement value and currently is the most widely used economic damage indicator. Since then, various methods of vulnerability assessment have been developed differing in level of detail and precision. The type of method

chosen depends on the objective of the assessment but also on the availability of data and technology. The objective of such methods is to quantify the level of damage for different levels of seismic exposure. The definition and quantification of damage level and the corresponding representation of earthquake hazard (or seismic exposure) differ for each method. Irrespective of the method used, the distribution of damage for increasing hazard level is referred to as vulnerability curve.

2.3. Methods for vulnerability assessment

The three main approaches used for earthquake vulnerability assessment purposes are:

- Empirical (based on observational data)
- Expert opinion
- Analytical (based on some form of simplified or refined analysis)

2.3.1 Empirical

This method arrives at vulnerability curves by regressing damage data from historical earthquakes against the earthquake hazard. Until recently, the most common representation of hazard was through intensity, which in most cases was defined through the Modified Mercalli Intensity (MMI) scale. A pioneer in compiling statistics on damage to buildings from actual earthquakes was Whitman (1974) using data from approximately 1600 buildings having five or more storeys. MMI scale was used as the earthquake hazard parameter. Damage on the buildings at each MMI level was expressed in the form of a Damage Probability Matrix (DPM). The general form of the DPM as proposed by Whitman (1974) is shown in Table 2.1. Each number in the matrix expresses the probability that a building of a certain building class will experience a particular level of damage as a result of a particular earthquake intensity. The level of damage was expressed quantitatively through DRs (DR=0 for no damage and DR=100 for collapse).

Table 2.1. Format of DPM after Whitman (1974)

Damage state	Structural Damage	Non-structural damage	Damage ratio (%)	Intensity of Earthquake				
				V	VI	VII	VIII	IX
0	None	None	0-0.05
1	None	Minor	0.05-0.3
2	None	Localized	0.3-1.25
3	Not noticeable	Widespread	1.25-3.5
4	Minor	Substantial	3.5-4.5
5	Substantial	Extensive	7.5-20
6	Major	Nearly total	20-65
7	Building Condemned		100
8	Collapse		100

Eight damage states with qualitative description were assigned at corresponding ranges of DRs. The qualitative determination of damage is useful for visual assessment purposes.

Empirical vulnerability curves were also derived by a number of other researchers such as Scawthorn (1981) for Japan, Schierle (2000) based on the Northridge earthquake and vulnerability data from Steinbrugge and Algermissen (1990) from experience in California. Several other examples can be found of curves derived based on local data from single or a small number of events. These curves can only be proved reliable based on the repetition of similar events. In addition they are derived using a small number of data that depend on local characteristics.

A more general attempt using data from different countries and earthquakes was conducted by Spence (1992). Five damage grades were considered. The scatter of earthquake intensity at which each damage threshold was assumed to be normally distributed. This implies that the damage potential at a particular earthquake intensity is equally spread around the mean value of the corresponding damage. Although this assumption may be reasonably accurate for buildings with flexural behaviour it can not represent the possibility of sudden failure from brittle failure modes, which cause a corresponding sudden increase in the vulnerability that can not be predicted by a normal distribution.

The most general database for the derivation of empirical vulnerability curves was compiled by Rossetto (2002) in an attempt to derive empirical vulnerability curves for European-type RC structures. The majority of data were obtained from recent European destructive earthquakes in Greece, Italy and Turkey. The database was completed using

data from Algeria, Chile, Japan, Mexico, Philippines and the USA in order to cover a wider spectrum of building types. Initially, the database was compared with the empirical curves from Orsini (1999) and the non-empirical ones from Spence (1992) and Singhal (1997). Rossetto (2002) stated that although the non-empirical curves show a better fit to the observations the correlation is still poor and the calculated errors in prediction are significant.

The database included in Rossetto (2002) study was divided into six classes based on the height of the building (low, medium and high-rise) and the seismic design code used in the design process (Pre, Old and New-Code). Six damage grades were used ranging from slight damage to collapse. The distribution of damage for a particular damage grade and earthquake intensity level is assumed to vary log-normally. This type of variability is unlikely to adequately capture the sudden increase in vulnerability from brittle modes of failure and it is questionable that any pre-assigned type of variability is necessary or correct. The spectral displacement is used as the earthquake intensity parameter, which was shown in the study to simulate better the damage potential, but makes it difficult to compare them with curves using PGA as the intensity parameter. This is reasonable since damage in buildings in the inelastic range is in general a function of displacement (Priestley, 1997) and the effect of the local spectrum is accounted for directly (Rossetto, 2002). Although this database can be regarded as the most complete in Europe, it seems from the data points plotted on the derived curves that very little data exist for high earthquake hazard levels (Figure 2.1) and most of these correspond to moderate or less damage. Rossetto (2002) also concludes to the same. It should also be pointed out that a more refined classification of the buildings by combining the six building classes (for example curves for pre-seismic and low-rise) would be more meaningful for vulnerability assessment purposes since it would remove the large variability of using a single classification for all construction periods.

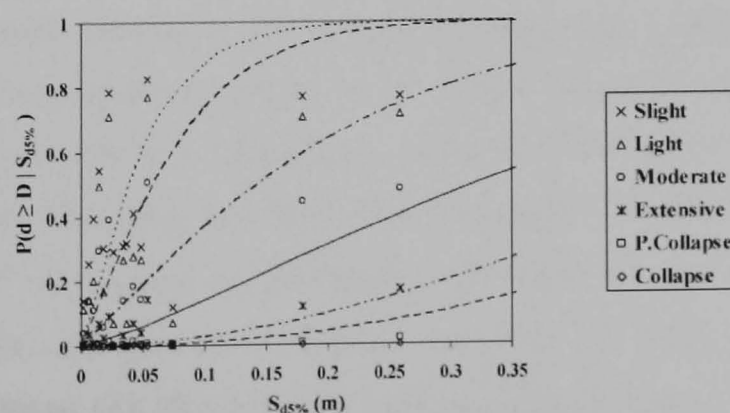


Figure 2.1. Weighted observational damage statistics (after Rossetto, 2002)

In the case of reinsurance companies, earthquake risk assessment is in general undertaken based on the loss database. Premium values are determined based on the expected annual average loss. This form of empirical assessment can be risky since it is based on the repetition of previous claims and can be biased by isolated events. However, overall it can be considered a safe and easy way for insurance companies to ensure a net gain.

Although post-earthquake building inspection is the best method for determining empirical vulnerability curves and is relatively simple to apply, the following should be considered when adopting such a method:

- Very few data exist on non-standard constructions.
- Only building types in affected areas can be used thus only curves for limited building classes can be derived.
- Relatively few buildings have been subjected to extreme seismic forces and for many of them no sufficient data from post-earthquake damage inspection are available. There is difficulty in developing a reliable scenario for events that lead to collapse.
- There is uncertainty in determining earthquake intensity.
- There is uncertainty due to the high variability of damage data.

2.3.2 Expert judgment

This method is an effective alternative to the empirical technique, since it is less affected by the unavailability of data. The main disadvantage of this method is in its subjectivity, i.e. the opinion of the experts, and this uncertainty is compounded by the inherent uncertainties in building performance.

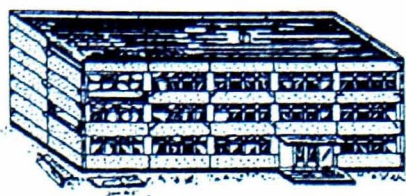
The first complete attempt to identify the damage state of a wide variety of building classes at various ground motion levels based primarily on expert judgment was conducted by the Applied Technology Council, primarily for the state of California (ATC-13, 1985). The study was funded by the Federal Emergency Management Agency (FEMA). MMI was used as the earthquake hazard parameter and the DR as proposed by Whitman (1974) was used as the damage indicator. The damage assessment was based on expert judgment (58 experts) with experience from past earthquakes in a variety of areas. Buildings were classified into 40 types along with an additional number of 38

non-building structures (such as bridges, pipelines and tunnels). RC buildings were classified into four main categories according to the resisting system type (dual system, ductile and non-ductile frames and precast structures). Furthermore each main category was divided into three subcategories to account for the number of storeys i.e. low rise (1-3 storeys), medium rise (4-7 storeys), and high rise (≥ 8 storeys) whereas there was an extra category for 'tilt-up' low-rise buildings. The derived curves were also used later on for the risk assessment of the state of Utah (ATC-36, 1997) and by Chin-Hsiung (2001) to evaluate the damage after the 1999 "Chi-Chi" Taiwan earthquake.

In 1998 the European Seismological Commission combined the expertise of a number of researchers from around Europe (such as UK, Germany, Italy, etc.) to produce the European Macroseismic Scale (EMS, 1998), which since then comprises the most comprehensive reference point for the derivation of vulnerability curves based on expert opinion for any region in Europe. EMS includes fifteen buildings types and six vulnerability classes (Table 2.2). The most likely vulnerability class and a probable range for each class can be assigned for each building type. Five damage grades both for RC and Masonry buildings are used to describe the damage potential. The qualitative description of each damage grade is the most comprehensive found in the literature and helps assign a grade for damaged buildings (example in Figure 2.2). The probability of occurrence of each damage grade at every MMI level is obtained from an additional document included in EMS (1998) referred to as "Definitions of intensity degrees" (example in Table 2.3). The description of "few", "many" and "most" buildings corresponds to 0%-20%, 20%-50% and 50%-100% of buildings, respectively.

Table 2.2. Differentiation of building types into vulnerability classes (EMS, 1998)

Type of Structure	Vulnerability Class					
	A	B	C	D	E	F
MASONRY	rubble stone, fieldstone					
	adobe (earth brick)					
	simple stone					
	massive stone					
	unreinforced, with manufactured stone units					
	unreinforced, with RC floors					
	reinforced or confined					
REINFORCED CONCRETE (RC)	frame without earthquake-resistant design (ERD)					
	frame with moderate level of ERD					
	frame with high level of ERD					
	walls without ERD					
	walls with moderate level of ERD					
	walls with high level of ERD					
STEEL						
steel structures						
TIMBER						
timber structures						



Grade3: Substantial to heavy damage

(moderate structural damage, heavy non-structural damage)

Cracks in columns and beam column joints of frames at the base and at joint of coupled walls. Spalling of concrete cover, buckling of reinforcement rods. Large cracks in partition and infill walls, failure of individual infill panels.

Figure 2.2. Qualitative description of RC buildings for damage grade 3

Table 2.3. Definition of intensity degrees for MMI=8

Intensity VIII. Heavily damaging

- a) Many people find it difficult to stand, even outdoors.
- b) Furniture may be overturned. Objects like TV sets, typewriters etc. fall on the ground. Tombstones may occasionally be displaced, twisted or overturned. Waves may be seen on very soft ground.
- c) Many buildings of vulnerability class A suffer damage of grade 4; a few of grade 5. Many buildings of vulnerability class B suffer damage of grade 3; a few of grade 4. Many buildings of vulnerability class C suffer damage of grade 2; a few of grade 3. A few buildings of vulnerability class D sustain damage of grade 2.

For the case of Cyprus, an attempt was conducted by Schnabel (1987) to derive vulnerability curves based on damage data from similar seismotectonic environments and expert judgment. The derived curves are shown in Figure 2.3. Both the lower and upper bound are shown for superior and substandard construction. Since this constitutes the only attempt for the whole area of Cyprus, it provides a reference point for comparison with the results of this study.

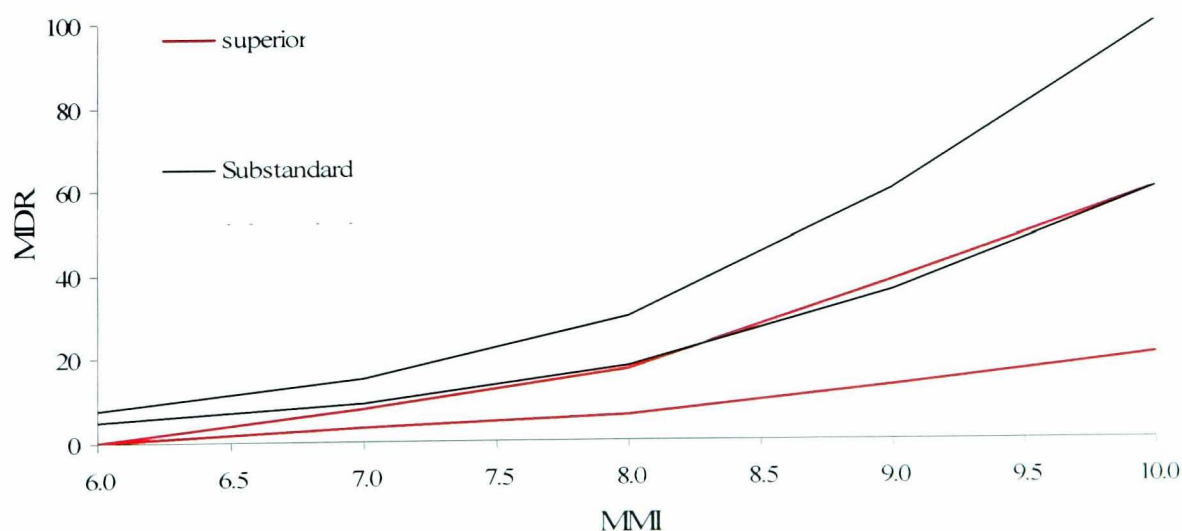


Figure 2.3. Vulnerability curves for Cyprus (after Schnabel, 1987).

2.3.3 Analytical

Both simple and detailed analytical methods exist in the literature for the derivation of vulnerability curves. The main difference lies on the sophistication used for the modelling of the building. Simple methods do not require the analysis of the structure but rely on simple equations to derive its capacity. Simple analytical methods were derived with the objective of analysing a large number of buildings in a rather short period of time. Therefore, structural modelling is based on a few input parameters such as the period of construction, the number of storeys and the construction material. In contrast, for detailed analysis methods capacity is defined through analysis of the structural model, the sophistication of which varies based on the required accuracy.

2.3.3.1. Simple analytical procedures

A simple analytical procedure was proposed recently by Calvi (1999) and is based on the ratio between the displacement capacity of a building corresponding to several limit states and the displacement demand from an earthquake event as obtained from the corresponding displacement spectrum. Four limit states (LS) are considered ranging from slight non-structural damage to collapse. A set of minimum and maximum drift limits is provided for each damage state. Each building type is idealised as a single degree of freedom system (SDOF). The capacity curve (force versus displacement) of the SDOF system is defined based on simple equations for yield and ultimate capacity. The following steps are then applied (see also Figure 2.4):

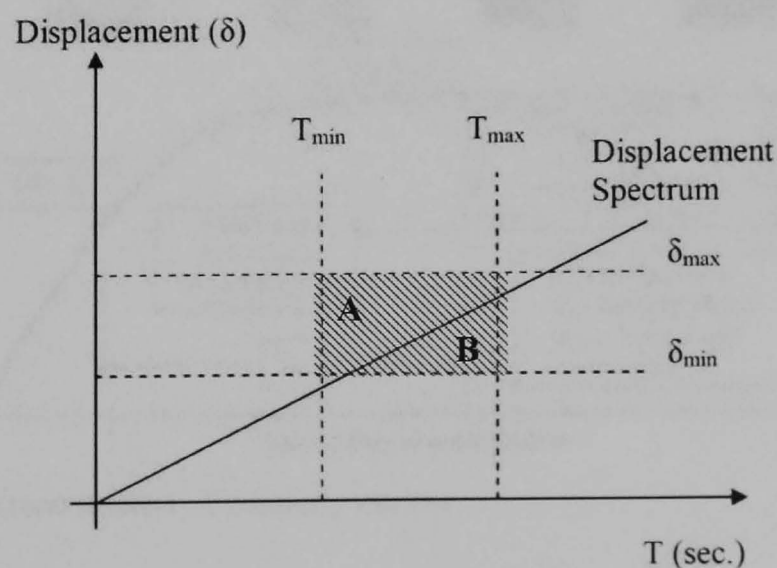


Figure 2.4. Comparison of displacement demand and capacity for LS2 at PGA=0.5g

- The secant periods and corresponding displacements at minimum and maximum drifts are obtained using a specific equation for each damage state. These equations were derived based on drift limits.
- The lines corresponding to these threshold points are drawn on the displacement demand spectrum.
- The resulting rectangle defined by the intersection points of these lines denotes the capacity of the building. The ratio between the areas of the rectangle above and below the displacement spectrum corresponds to the probability of occurrence of the specific damage state for the particular building type ($\frac{A}{B}$ in Figure 2.4).

A more thorough attempt to produce simple analytical methods was undertaken by the National Institute of Building Science (NIBS) funded by FEMA (1997). After being updated in 1999 the project resulted in an interactive software for risk assessment referred to as HAZUS99 (NIBS, 1999). Thirty-six building types are considered. The damage potential is expressed through four damage grades for slight, moderate, extensive and complete damage. For each building type, the threshold value and variation of all damage grades are provided using spectral displacement (SD) as the earthquake hazard parameter. Threshold values and variation distributions were assigned by experts.

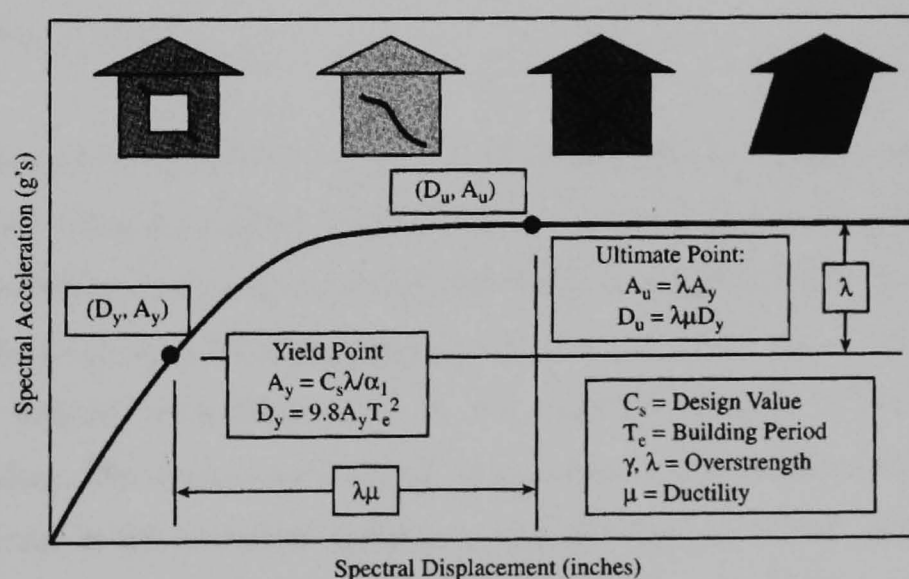


Figure 2.5. Determination of capacity curves

As in the Calvi procedure, the capacity of the structure is defined using 2 control points; yield and ultimate. The equations for the calculation of yield and ultimate capacity are shown in Figure 2.5 as obtained from HAZUS99 (NIBS, 1999). In this case though, the earthquake demand is expressed through highly damped response spectra. The performance of the structure is defined using the capacity-demand method. A detailed discussion on the capacity-demand method is given in Chapter 6 but in brief, the performance point (PP) is defined by superimposition of the capacity curve and the highly damped demand spectrum (see Figure 2.6). The percentage of buildings in each damage grade for the corresponding PP is then extracted from the threshold values and variation of the damage states.

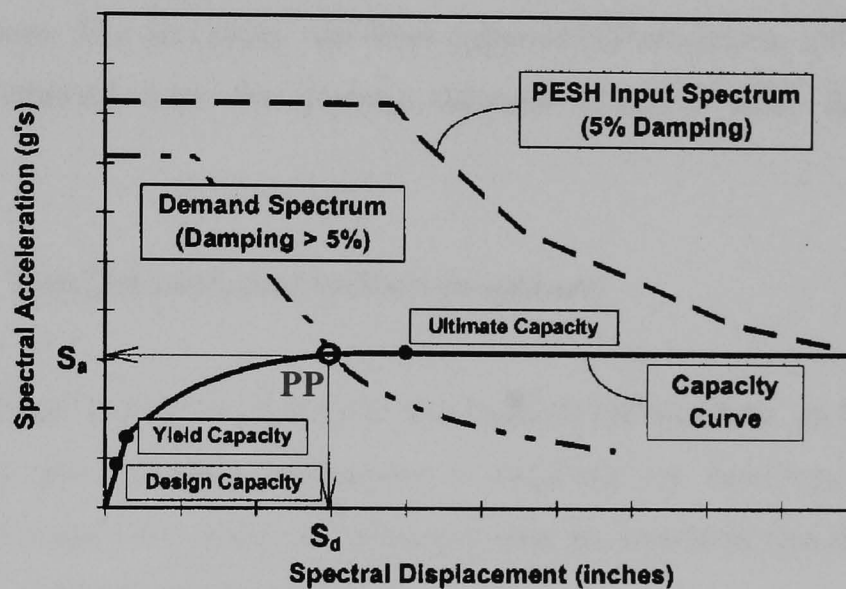


Figure 2.6. Example of capacity curve and demand spectrum

Rapid Visual Screening

Simple analytical procedures have also been developed for rapid visual screening purposes. Such procedures form the first step of a multi-step procedure for identifying vulnerable buildings that need to be analysed using detailed analytical procedures. The first comprehensive rapid screening procedure was included in ATC-14 (1987) and was intended to identify vulnerable areas in the structural system, which could cause structural failure. The evaluation is based on a number of statements related to potential vulnerable areas in the structural system. A simple “true” or “false” response to each statement must be provided by an expert. The former response implies adequate structural capacity in the specific area of the structural system whereas the latter suggests that further detailed evaluation is required. An updated procedure was recently

released by FEMA (FEMA 154, 2001), which requires detail representation of the structural system through detailed drawings and destructive tests.

A more sophisticated alternative representation method towards rapid screening assessment was developed by Mandas and Dritsos (2004) using fuzzy logic. Visual inspection is used to define the vertical regularity and the geometry of the structure. whereas a large number of parameters (such as behaviour factor, deterioration factor etc.) are used to define three additional variables related to the earthquake hazard potential, the structural strength of the building and the construction characteristics of the building. A specific combination of these variables provides the damage rate for the specific structure. The procedure was later enhanced (Demartinos, 2006) based on the information obtained from the damage database compiled after the 1999 Athens earthquake.

2.3.3.2. Detailed analytical method procedures

Detailed analytical procedures are more thorough and demanding, and are intended to be used when more detailed information is required, i.e. buildings with particular importance, structures for which no empirical data are available (innovative structural designs). In general these methods rely on:

- the determination of earthquake hazard parameter,
- the structural modelling and analysis for the determination of the structural response,
- correlation of structural response with damage.

Initially issues involved with the determination of earthquake hazard, structural modelling and analysis methods are examined. Damage analysis is examined in detail in the subsequent section.

Hazard

The determination of earthquake hazard parameter in general follows the use of site-specific response spectra as for the simple analytical procedures. In some cases though, where the objective is to simulate the behaviour of a building in detail (exact

displacement profile, the propagation of cracks, the distribution of stresses and the shape of the hysteretic curve) several time-history records are used as the earthquake hazard parameter.

Structural modelling

Modelling of the structure should be able to accommodate a number of failure modes such as flexure, shear, local buckling and debonding of reinforcement. It should be noted that most analytical vulnerability studies concentrate primarily on the flexural and, to a smaller extent, shear failures at the member level (Dymioti, 2000, Rossetto, 2005, Ahmed, 2007). It can be argued that the modelling issue is not addressed at a satisfactory level in these studies, which show a discrepancy between sophisticated structural analytical methods and vulnerability studies. In particular, no attention is paid in most vulnerability studies to damage in the joint region. Observations of damage patterns from recent earthquakes in the Mediterranean region clearly show that severe damage occurs in joints such as shear failure due to limited or no shear reinforcement. In addition, slip of reinforcement in the joint due to inadequate anchorage length or lack of confinement in the anchorage region, can cause bar debonding and result in large cracks in the region around the joint. Besides the joint region, inadequate link spacing especially in sub-standard constructions can lead to local buckling of the column reinforcement bars and subsequently to severe loss in column capacity. Illustrative examples of the effects of such failures are shown in Figure 1.1 (from field observations) and Figure 2.7 (from experimental testing). Structural modelling issues are discussed in further detail in Chapter 4.

Structural analysis

Most existing procedures for detailed analytical methods use nonlinear static analysis procedures for the estimation of the structural response. Various analytical procedures based on nonlinear static analysis were initially proposed in a number of design and assessment codes such as ATC-40 (1996) and FEMA 356 (2000). In both cases, the capacity of the structure is expressed through the push-over curve (base shear versus top displacement). In the former, the performance displacement is computed through highly damped spectra (capacity-spectrum method shown in Figure 2.6), whereas in the latter the displacement coefficient method is used as a simple alternative. An attempt to

improve these methods was conducted in FEMA 440 (2005). Especially in the case of the ATC-40 (1996) method, considerable improvement was achieved and eventually the method was substituted by the Modified Acceleration-Displacement Response Spectrum (MADRS) procedure.

Modern assessment codes (EC-8 Part 3, 2004 and GRECO, 2004) provide detail models for the assessment of RC member capacities for a variety of failure modes.



Figure 2.7. Shear failures in joints (Pagni, 2004, Dhakal, 2005 and Pantelides 2000)

The definition of the damage potential can be assessed at three limit states corresponding to the threshold of damage limitation (prior to reinforcement yielding), significant damage, and near collapse. It should be noted though that the complication of these models makes them impractical for large vulnerability assessment studies.

Irrespective of the procedure used, in static analysis, the seismic demand is approximated by an equivalent lateral force distribution. EC-8(2004) proposes the use

of either a uniform or inverted triangular distribution. The latter is estimated based on the fundamental mode of vibration of the structure.

An adaptive static analysis method was proposed by Antoniou (2002), in which the lateral applied load distribution is updated at each load increment based on the instantaneous structural stiffness, modal properties and consequent ground motion demand. This method was implemented within the framework of the INDYAS (Elnashai, 2000) finite-element package and was adopted in the analytical vulnerability study conducted by Rossetto (2005). Although this method yields representation of the seismic force distribution it can only be adopted in the context of INDYAS (Elnashai, 2000), which is not commercially available software.

Simpler procedures that account directly for the influence of higher modes of vibration and can be implemented irrespective of the software used were proposed by a number of researchers and assessment codes. Chopra (2002) proposed the use of modal static analysis in which static analysis on the structure is repeated using modal shapes from all credible modes of vibration (contributing to 90% of the modal mass). The peak modal responses are combined according to the square-root-of-sum-of-squares (SRSS) or the complete quadratic combination (CQC) rules. The drawback of the method lies on the fact that a number of analyses, one for each mode shape, are required.

In FEMA 356 (2000), a simplified model is included for the definition of the of the lateral force distribution, which is suggested to account for higher modes of vibration. The calculation of the modified vertical distribution factor is shown in eq.2-1. The modification is applied on the height of each floor which is raised to the power of k. This value is defined based on the natural period of the fundamental mode of vibration.

$$C_{vx} = \frac{W_x (h_x)^k}{\sum_{i=1}^n W_i (h_i)^k} \quad \text{eq.2-1}$$

Where:

C_{vx} vertical distribution factor for floor x

k 2 for $T > 2.5$ seconds

	1 for $T < 0.5$ seconds
	Linear interpolation used in-between
W_i	weight at each floor i
W_x	weight at floor x
h_i	height of each floor i
h_x	height of floor x

In a comparison study conducted by Kalkan (2004), it was shown that top storey displacement results for a 4 storey RC building, using both the modal static analysis proposed by Chopra (2002) and the FEMA 356 (2000) procedure, are very close to the corresponding “exact” displacements computed using time-history analysis. The correlation though decreases for the FEMA 356 (2000) procedure for higher buildings. Based on the above discussion, it is concluded that the FEMA 356 (2000) approach provides a simple, fairly accurate and easily implementable alternative for the derivation of the lateral force distribution for static analysis.

Further to the code guidelines a number of individual analytical vulnerability studies use the capacity-spectrum method for the estimation of the structural response (Rossetto, 2005, Ahmed, 2007, Kappos, 2007). Although analytical vulnerability curves based on PGA as the hazard parameters were derived in (Kappos, 2007) it is emphasized in the paper that these curves are intended for Thessaloniki buildings since they have been developed using a combination of analysis and statistical data. A large portion of the statistical data used is from the 1978 Thessaloniki earthquake, which makes them inapplicable for the region of Cyprus.

2.4. Structural Damage Indicators

A number of structural damage indicators found in the literature can be used for the correlation of the structural response with the expected damage potential. Timchenko (2002) clustered the variety of damage indicators (DI) in the following three categories based on the structural parameters required for their calculation.

- Dynamic parameters of the structure
- Displacement parameters
- Displacement and cumulative damage

2.4.1 Dynamic parameters assessment

The most widely used analytical damage indicators using the dynamic parameters of the structure are discussed below.

1. Maximum Softening

DiPasquale and Cakmak (1989) developed a damage index (eq.2-2) based on the evolution of the natural period of a time-varying linear system equivalent to the actual non-linear system. This global damage index depends on a combined effect of stiffness degradation and plastic deformation (Ghobarah, 1999). Although it is a global index, the complexity in the calculation of the maximum period as well as the fact that it does not account for the dissipated hysteretic energy and strength deterioration are its main disadvantages.

$$\delta_M = 1 - \frac{T_0}{T_{\max}} \quad \text{eq.2-2}$$

Where:

T_0 initial natural period,

T_{\max} maximum natural period of the equivalent linear system.

2. Final Softening

In the same paper, DiPasquale and Cakmak (1989) utilised the concept of the final softening as a damage indicator. They used the change in the fundamental period of the structure as a measure of the change in the stiffness caused by the earthquake. The advantage of final softening method is that it can be evaluated from the initial natural period and the final period determined from vibration field-testing after the earthquake. On the other hand, it does not provide any information about local and storey damage. The period calculation at the final time step of the excitation may be affected by the randomness of the instantaneous tangent stiffness at the end of the dynamic load (Ghobarah, 1999). Nevertheless, it is a reliable method for rapid field assessment.

The proposition that damage is related to the increase in period (or decrease in frequency) was recently verified by using experimental data. Calvi et al. (2006) concluded from results of experimental tests on RC frames that *a significant period elongation occurs during strong ground motion and this can be attributed to the accumulation of damage in the structure*. Zembaty et al. (2006) moved a step forward by producing a damage scale that can be used for the definition of the degree of damage from the recorded decrease in the natural frequency (Figure 2.7).

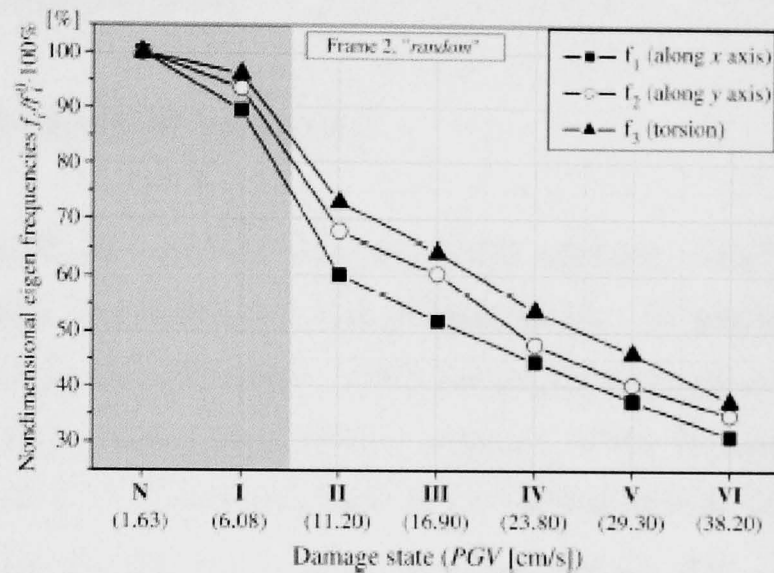


Figure 2.8. Normalised natural frequency drop with progressive damage states (after Zembaty et al.,2006)

3. Stiffness Index

A more recent approach, using the dynamic parameters of the building for seismic damage evaluation, was conducted by Ghobarah et al (1999) and resulted in a global stiffness index. Ghobarah (1999) proposed a methodology in which two nonlinear static analyses are conducted before and after subjecting the structure to an earthquake. The earthquake is applied with the use of time-history analysis. The stiffness damage index $(DI)_K$ of the whole structure is calculated as shown in equation 2-3.

$$(DI)_K = 1 - (K_{\text{final}}/K_{\text{initial}}) \quad \text{eq.2-3}$$

Where:

K_{initial} initial slope of the base shear-top deflection relationship resulting from the pushover analysis before the time-history analysis

K_{final} initial slope of the same relationship after the time-history analysis

Since this DI can be derived only after time-history analysis, it is regarded as being computationally very demanding.

2.4.2 Displacement parameters

Displacement parameters are the most commonly used for vulnerability assessment purposes since they can easily be obtained analytically. In addition, it is generally accepted (Ambraseys, 2002, Priestley, 1997) that displacement parameters such as drift and ductility simulate better the structural response in the inelastic range. Priestley (2003) argued that seismic damage is related to material strains, which are related to maximum response displacements rather than accelerations. Xue (2000) pointed out that, when the inelastic behaviour of a structure is used in the assessment, displacement rather than force is recognised as the most suitable indicator of structural damage. A detailed discussion follows on the appropriateness of such DI.

- **Ductility Ratio (DR):** Ductility ratio is defined as the ratio of maximum deformation to yield deformation. As a DI it can be shown to be unsatisfactory, especially when shear distortion in joints and bar pullout are anticipated (Ghobarah, 1999). Additionally the ductility ratio fails to take into account the damage induced by repeated loading cycles of inelastic action (O'Connor and Ellingwood, 1986) leading to the underestimation of cumulative damage. It is commonly assumed that failure occurs when the ductility demand exceeds the structural ductility capacity.
- **Interstorey drift (ISD):** It is defined as the maximum relative displacement between two storeys, normalised to the storey height. It was chosen as a damage indicator for structural and non-structural damage by Elenas and Meskouris (2001), Gunturi and Shah (1992) and Rossetto (2005). An initial attempt was conducted by Culver (1975) to estimate the threshold ISD values at different

levels of damage using results from damaged buildings. It was suggested that a value of interstorey drift equal to $h/100$ corresponds to damage to non-structural components, while $h/25$ corresponds to severe structural damage or collapse. Napetvaridze (1984) concluded that the threshold values of interstorey drift for a variety of building types i.e. moderate damage on RC buildings at $IDS = h/250$. Elenas (2001) suggested the values of $ISD = h/200$ for low damage, $h/83$ for medium and $h/58$ for great damage. The most recent attempt to provide ISD limits for RC buildings (Table 2.1) was conducted by Rossetto (2005) based on an extended database of damaged buildings from a number of earthquakes, mainly European.

Table 2.4. ISD (%) for RC buildings (Rossetto, 2005).

ISD (%)					
Slight	Light	Moderate	Extensive	Partial collapse	Collapse
$h/2000$	$h/1250$	$h/330$	$h/87$	$h/36$	$h/23$

2.4.3 Displacement and cumulative damage

Damage models were also developed to take both energy dissipation and peak displacement into account. The most popular DI of this category was derived by Park and Ang (1985) and is shown in eq.2-4. The ductility level at each displacement increment is superimposed on the hysteretic energy dissipated in the structure up to the specific displacement. The calibration of this DI is rather demanding since laboratory or field data are required to calibrate the constant β and, as with most of the cumulative damage indices, depends strongly on the hysteretic model of the elements.

$$D = \frac{\delta_m}{\delta_u} + \frac{\beta}{Q_y \delta_u} \int dE \quad \text{eq.2-4}$$

Where:

- δ_m Maximum experienced deformation
- δ_u Ultimate deformation
- Q_y Yield force
- β Constant determined by experimental calibration

As stated by Ghobarah (1999), the model is based on the following two controversial assumptions,

- The contribution to damage of the extreme deformation and the dissipated energy can be superimposed linearly,
- The related evolution in time of these components can be disregarded.

In addition, it has been suggested by Kappos and Xenos (1996) that, in general, cumulative indices are dominated by the ductility term and are only marginally affected by the energy term.

2.5. Conclusions

Empirical vulnerability assessment curves though easy to derive when the data are available suffer from a number of drawbacks in particular relating to the determination of high vulnerability values and in describing modern or unusual buildings. Since some empirical data have been made available for the island of Cyprus, it is worth making an attempt to see how vulnerability curves derived from these data compare with the existing curves based on expert opinion.

It has to be mentioned that at least a comparison with some analytically developed curves may be required especially for modern buildings for which no vulnerability data exist.

Chapter 3

EMPIRICAL RISK

ASSESSMENT

3.1. Introduction-background to empirical risk assessment

Despite the scientific value of using analytical models for seismic hazard and vulnerability assessment it is widely accepted that empirical models are essential for both hazard and vulnerability assessment for comparison purposes. The single most important feature of empirical assessment in each case is the databank, since it determines the accuracy of the derived assessment models. The formulation of each databank requires careful selection of the input parameters so as to capture the local effect. To demonstrate and assess the capabilities and limitations of this type of assessment the island of Cyprus is used as a case study. Cyprus was chosen because raw data were readily available to the author.

Empirical studies on risk assessment were conducted in the past mainly from reinsurance companies (Swiss Re, Munich Re etc) for insurance premium calculation purposes. The initial studies used the Modified Mercalli Intensity (MMI) scale to describe the hazard parameter and expert opinion damage indices such as ATC-13 (1985) for the vulnerability parameter of risk assessment. Intensity based hazard definition is derived using historical seismicity and knowledge of the geological structure of the region. By having enough data the determination of the probability of events of specific magnitude can be determined for a specific location. With the introduction of accelerometers, peak ground acceleration (PGA) data were used to

derive attenuation equations describing the spatial characteristics of earthquake hazard for a particular area (Ambraseys 1975, Joyner and Boore, 1981 etc.).

A recent work on ERA was conducted by Kythreoti (2001) at the University of Sheffield, which provided a framework for earthquake risk assessment (EQ-RACY) using Cyprus as a case study based on empirical models for both hazard and vulnerability assessment. The historical seismicity data for the island compiled by Ambraseys were enhanced by data from the Israel Seismological Bulletin (1995), Solomi (1998) and Gajardo et. al. (1998). Therefore a more refined earthquake catalogue was created and a recurrence relationship (RR) showing the frequency of occurrence of earthquake events of specific magnitudes was derived. Since no major events took place since that study, no improvements can be made on the RR. In addition, RRs are only useful in macro ERA. As far as the spatial determination of hazard in terms of intensities and PGA Kythreoti (2001) used the well-known PGA attenuation laws of Theodulidis and Papazachos (1992), which are based on empirical data from Greece. Kythreoti (2001) stated that a considerable enhancement of the existing PGA attenuation models based on data from local accelerometers is vital to increase the accuracy of the risk assessment framework.

For the vulnerability of the local building stock Kythreoti (2001) used Schnabel's (1987) mean damage ratio curves which were at the time the only vulnerability curves for the types of buildings found in Cyprus. Kythreoti (2001) pointed out that Schnabel's vulnerability curves are based on very limited data and are a result of theoretical loss forecasts which possibly makes them highly unreliable. Previous experience is always valuable but when new data are available conclusions need to be re-evaluated.

In 1995 accelerometers were installed in various areas around the island by the local Seismological Centre, and those started to provide data after the destructive Paphos 1996 earthquake. Following this earthquake, a governmental authority called "Earthquake Rehabilitation Service" (ERS) was established with responsibility to assess the damage levels and prepare repair strategies. ERS was assigned the role of evaluating the level of damage in each area by site inspections soon after the events. Following these developments, the author was granted access to information on both PGA and damage data. The scope of the first part of the research is to use these data in an attempt

to develop new models and examine whether these models can help enhance the level of accuracy of the risk assessment of the island.

Initially, the available strong motion PGA data are presented and analyzed to produce new PGA attenuation curves specific for Cyprus. These models are used together with damage data from the corresponding events to produce empirical vulnerability curves. A discussion on the applicability and accuracy of the derived curves follows which will influence the next steps of the research.

3.2. Description of Acceleration Data

The majority of data used for the derivation of an enhanced PGA attenuation law were provided by Mr K. Solomis (Solomis K., 2002), director of the Cyprus Seismological Centre, to whom the author is extremely grateful. Briefly, the databank includes data for,

- The location and soil characteristics at the accelerometer stations
- The magnitude of the events and the number of PGA readings from each event
- The PGA recordings at each station from all the events

Table A-1 in Appendix A provides the location, coordinates and description of the geological conditions of the eleven stations considered in this study. The locations of the instruments were selected to cover the most seismically intense zones of Cyprus. Most of them are located in the basements of low-rise reinforced concrete (RC) buildings to avoid spectral amplification due to the structural response.

The instruments are placed on locations with different geological conditions ranging from soft soils to hard rock. The classification of soil conditions, shown in the last column of Table A-1, follows the simple procedure proposed by Theodulidis and Papazachos (1992) which uses a dummy variable S with values in the range of $S=0$ (soft soils) and $S=1$ (hard rock).

To get a more refined classification for the intermediate geological formations, a table was produced based on expert engineering judgment (Cripps, 1999). Table A-2 includes

the majority of the geological conditions present in Cyprus as defined by the geological map of Constantinou (1997) and an S-value was assigned according to the concentration of rock and soft soil in each formation.

Table A-3 includes the epicentral locations and magnitude of recorded data of earthquakes with $M_s \geq 4$ occurring after 1995, for which acceleration readings were available. The magnitude data were obtained in local magnitude M_L and were transformed to surface magnitude M_s using equation 3-1 proposed by Kythreoti (2001),

$$M_s = 0.7M_L + 1.33 \quad \text{eq.3-1}$$

The use of M_s for the magnitude parameter is in line with Ambraseys (2002) and Theodulidis and Papazachos (1992) for low seismicity areas.

The number of readings recorded by accelerograms per earthquake is also shown in the last column. All of the events are utilised in the attenuation study, but only data from the two most destructive events (marked with *) are used for damage assessment later on. Only data from earthquakes of $M_s \geq 4$ are included in the study to avoid overestimation of small magnitude earthquakes (Theodulidis and Papazachos, 1992 and Ambraseys and Bommer, 1991).

Table A-4 provides data for the maximum horizontal component of PGA recorded at each station and the corresponding Modified Mercalli Intensity (MMI) at the recording station as estimated by the local Seismological Centre for the various events. The first column relates the readings to the corresponding events in Table A-3. Additionally, the epicentral distance and depth of the earthquakes are provided since they are key parameters for PGA attenuation relationships.

Before undertaking regression analysis of the data the suitability of the existing attenuation relationship developed by Theodulidis and Papazachos (1992) for Greece and used by Kythreoti (2001) for Cyprus is examined. The data for the independent variables (M_s , R and S-value) and dependent (PGA) variables of the regression are listed at Table A-4.

3.3. PGA attenuation relationship by Theodulidis

The data are used to test the relevance of the existing attenuation relationship for shallow earthquakes (eq.3-2) derived by Theodulidis and Papazachos (1992) for the area of Greece.

$$\ln \text{PGA} = 3.88 + 1.12M_s - 1.65 \ln(R + 15) + 0.41S + 0.71P \quad \text{eq.3-2}$$

Where:

PGA	Peak Ground Acceleration,
M_s	Surface Magnitude,
R	Epicentral distance,
S	Surface geology parameter,
P	Error parameter

The data sets for each earthquake event, listed in Table A-4 (M_s , R and S-value), were substituted into equation 3-2 to obtain the predicted values for PGA (in cm/sec^2). The variable P in the equation represents the standard error of the logarithm of the PGA and, if it is set to zero, the equation outputs the mean value of the logarithm of the PGA. At the extremes of the distribution, P takes the value of ± 1 , which correspond to $\pm 1\sigma$ accuracy level of the normal distribution of the residual error. In this study, only the mean values ($P=0$) of the logarithm of the PGA are calculated and used in the comparison with the observed values. Figures 3.1 and 3.2 show the results of the comparison. The first two figures indicate an increase of the residual error (observed PGA-calculated PGA), with regards to the surface magnitude and the distance. The influence of the two earthquake parameters (M_s , R) on the residual error is significant to deserve some attention. Therefore, since the mathematical model of the relationship is sound there is a need only for a minor modification of the relationship to reflect better the local geology of Cyprus.

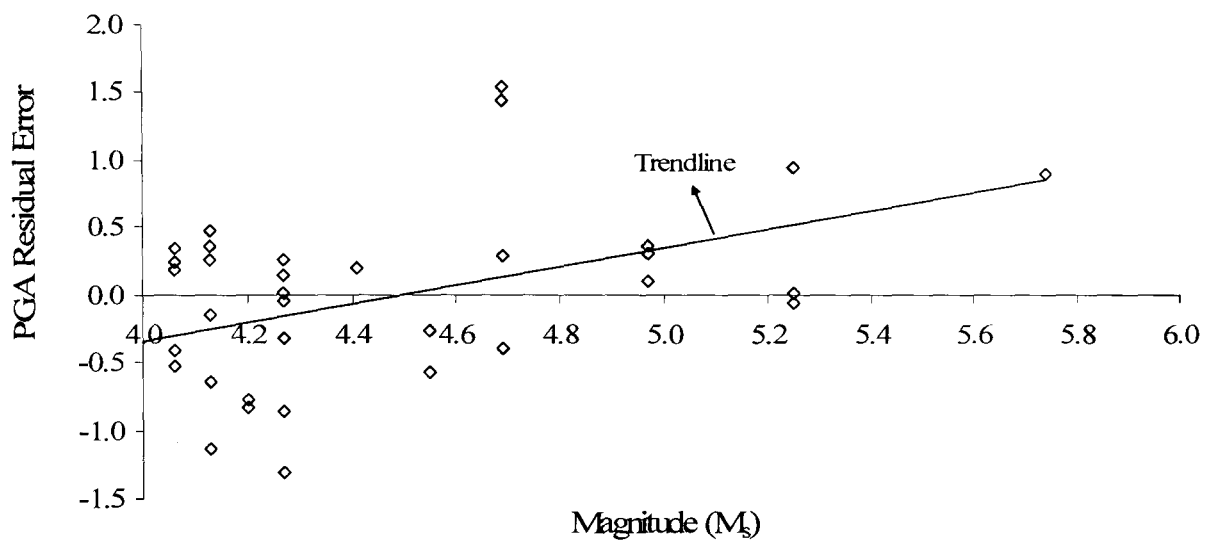


Figure 3.1 Error in PGA (cm/sec^2) with increased magnitude

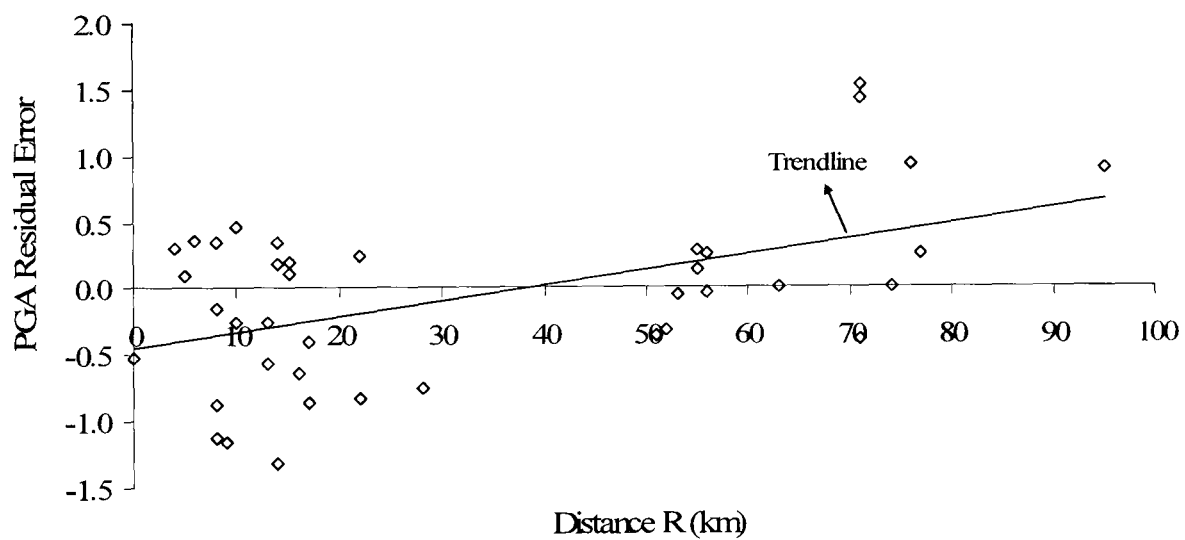


Figure 3.2 Error in PGA (cm/sec^2) with increased epicentral distance

3.4. Derivation of enhanced PGA relationship

The mathematical model used by Theodulidis and Papazachos (1992) for regression analysis for the derivation of PGA attenuation relationship is shown below.

$$SI = c_1 + c_2 M + c_3 \ln(R + c_4) + c_5 S + \sigma_{\ln Y} P \quad \text{eq.3-3}$$

Where:

SI the ground parameter, such as intensity, peak ground acceleration, velocity or displacement, spectral values of the ground motion and the duration of the motion,

M	the surface magnitude (M_s),
R	the epicentral or hypo-central distance,
S	the soil classification parameter (zero for alluvial site and 1 for hard rock),
$\sigma_{\ln Y}$	the residual error,
P	zero for the mean value and ± 1 for standard deviation values
c_1 to c_5	the regression constants.

All data (M_s , R, and S-value) to be used in the regression procedure are shown in Table A-4. The value of C_4 is treated deterministically as prescribed by Theodulidis and Papazachos (1992) who proposed the value of 15 after a parametric study in an attempt to minimise the residual error ($\sigma_{\ln Y}$) in PGA. This value was found to be close to the mean depth of earthquakes in the region. The same value is used in this study since, according to Table A-4, it is a good approximation of the mean depth observed from past seismicity in Cyprus (16km). Hence, the final regression equation is shown in equation 3-4.

$$\ln \text{PGA} = C_1 + C_2 M_s - C_3 \ln(R + 15) + c_6 S + \sigma_{\ln Y} P \quad \text{eq.3-4}$$

The regression analysis for the scaling coefficients c_1 , c_2 , c_3 , and c_6 is based on a simple and effective procedure developed by Theodulidis and Papazachos (1992). The two independent variables of magnitude and distance are regressed against PGA separately in two stages. This is to decouple the determination of the magnitude dependence from the determination of the distance dependence. The coefficient of geometrical attenuation rate (c_3), and the scaling coefficients of magnitude (c_2) and soil conditions (c_6) are recalculated twice at four steps aiming to minimise the residual error in PGA.

The rest of the section provides a detailed description of the steps involved in Theodulidis and Papazachos (1992) regression procedure which is outlined in Figure 3.3.

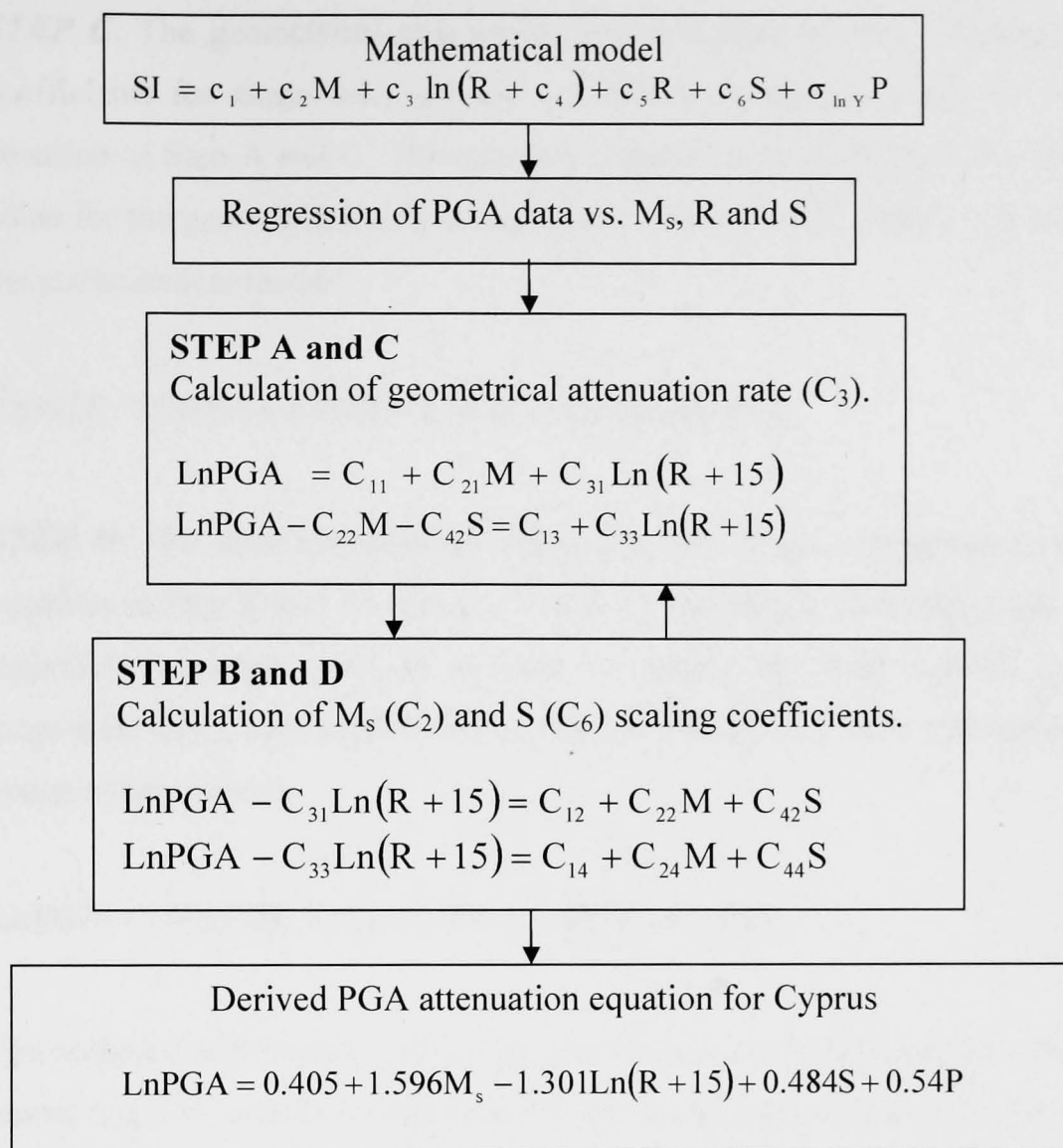


Figure 3.3 Summarised schematic of the methodology for PGA attenuation equation.

STEP A. The data in Table A-3 are initially substituted into the first equation in Step A and C to obtain the regression equation 3-5. The first estimation of the geometrical attenuation rate ($C_{31} = -1.228$) is obtained from this equation.

$$\ln PGA = -0.124 + 1.685 M - 1.228 \ln(R + 15) \quad \text{eq.3-5}$$

STEP B. The value of C_{31} (-1.228), obtained in Step A, is substituted into the first equation in Step B and D which is regressed against the same data. The resulting regression equation (eq.3-6) is used to obtain an initial estimation of the scaling coefficients of magnitude ($C_{22} = 1.567$) and soil conditions ($C_{42} = 0.444$).

$$\ln PGA - 1.228 \ln(R + 15) = 0.273 + 1.567 M + 0.444 S \quad \text{eq.3-6}$$

STEP C. The geometrical attenuation rate is recalculated by substituting the scaling coefficients for magnitude and soil conditions calculated in Step B into the second equation of Step A and C. The resulting regression equation (eq.3-7) provides the final value for the geometrical attenuation rate ($C_{33}=C_3=-1.301$), which will be substituted in the mathematical model.

$$\text{LnPGA} - 1.567M - 0.444S = 0.543 + -1.301\text{Ln}(R + 15) \quad \text{eq.3-7}$$

STEP D. The final geometrical attenuation rate (C_{33}) is substituted into the second equation in Step B and D, which is regressed against the same databank. The resulting regression equation (eq.3-8) is used to obtain the final scaling coefficients for magnitude (C_{24}), soil conditions (C_{44}) and constant C_{14} , which corresponds to C_1 in the mathematical model.

$$\text{LnPGA} - 1.301\text{Ln}(R + 15) = 0.405 + 1.596M + 0.484S \quad \text{eq.3-8}$$

The scaling coefficients C_{14} , C_{24} , C_{33} , and C_{44} are now substituted into the mathematical model (eq.3-3) and the predictions of the model are compared to the corresponding observed values of PGA (see section 3.4.2) to obtain the residual error for each prediction ($\sigma_{\text{ln}Y}$). The standard deviation of the residual error is added in the attenuation model as a fraction of a dummy variable P, which is equal to zero for mean values and $P=\pm 1$ for $\pm 1\sigma$ (standard deviation). Thus, the refined attenuation equation is shown below,

$$\text{LnPGA} = 0.405 + 1.596M_s - 1.301\text{Ln}(R + 15) + 0.484S + 0.54P \left(\frac{cm}{s^2}\right) \quad \text{eq.3-9}$$

3.4.1 Comparison of predicted to observed PGA

In this section, the predicted PGA values for all earthquakes in the databank (Table A-4) are compared with the corresponding observed data to obtain the distribution of the residual error defined as the difference between observed and predicted PGA's. The residual error in the predicted PGA values is plotted against the magnitude (M_s) and the distance of the corresponding earthquake (Figure 3.4). In both cases the trend-line as

expected coincides with the x-axis indicating that the error does not increase with increased magnitude or distance. In addition the peak values are slightly smaller than the ones obtained using the Theodulidis and Papazachos (1992) relationship developed for Greece. The frequency of the residual error is approximated by a normal distribution with mean (μ) equal to zero and a standard deviation (σ) equal to 0.54 (Figure 3.5), which is substituted in the final attenuation equation (eq.3-9).

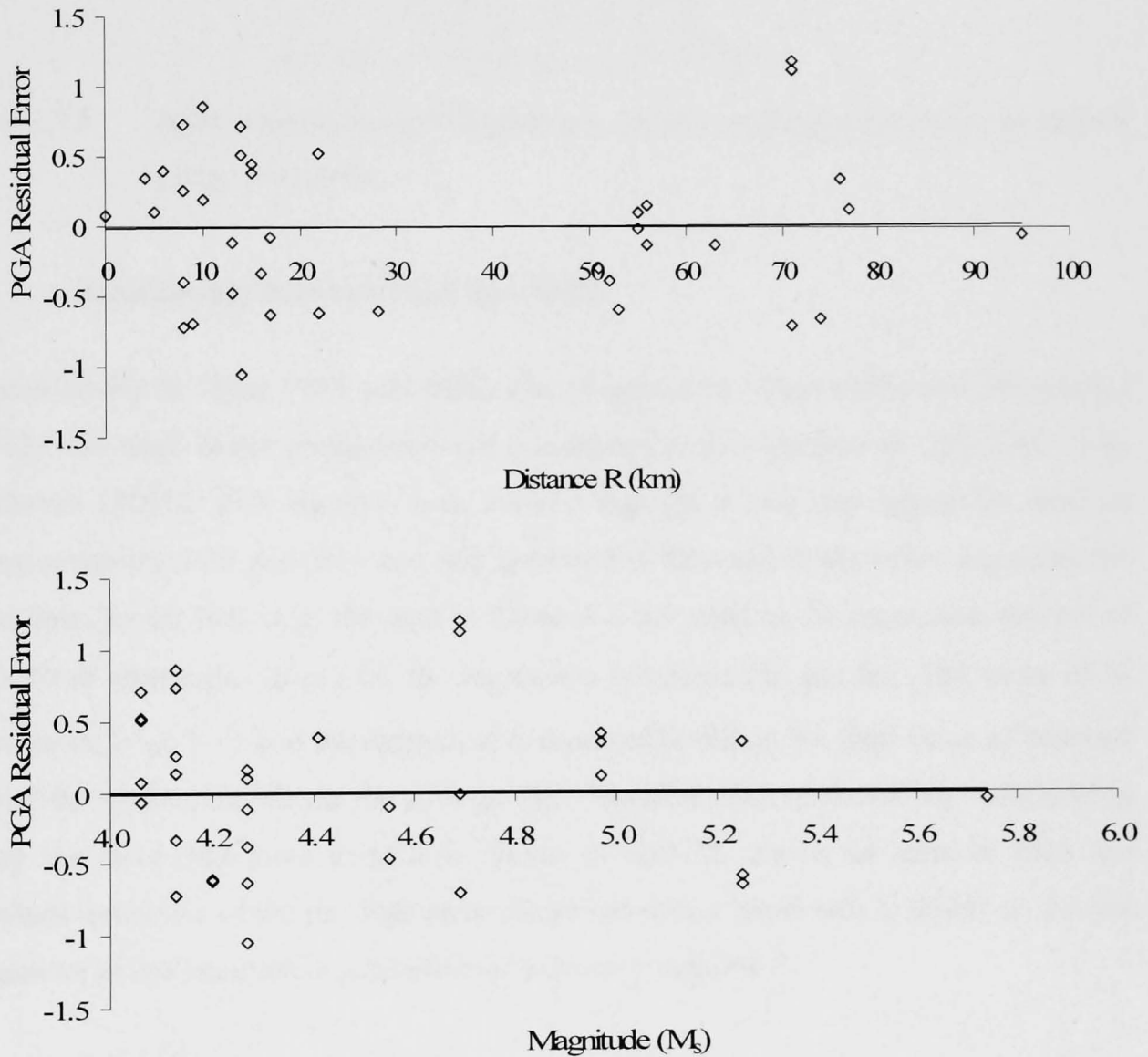


Figure 3.4 Residual error (cm/sec^2) in the predictions of eq-3-9 for increasing M_s , and R .

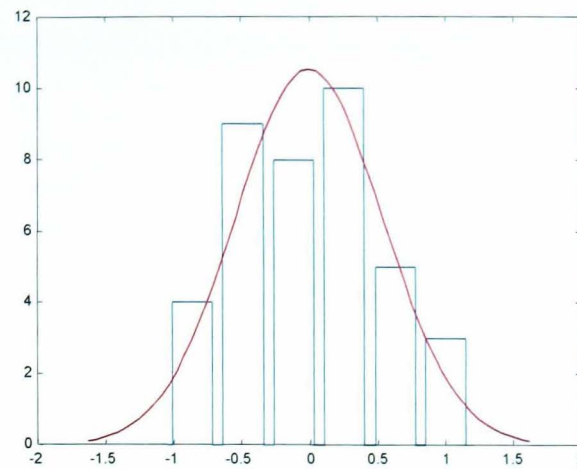


Figure 3.5 Approximate normal distribution for the residual error in the prediction of eq. 3-9 ($\mu=0$).

3.5. Relationship between PGA and MMI

A relationship between PGA and MMI also proposed by Theodulidis and Papazachos (1992) was used in the earthquake risk assessment (ERA) framework (EQ-RACY) by Kythreoti (2001). This equation was derived through a two step regression analysis using equations 3-10 and 3-11 and this approach is followed in the following using the field data. In the first step, the data in Table A-4 are used in the regression process of eq.3-10 to obtain the values for the regression constants (b'_1 and b_2). The value of b_2 substituted in eq.3-11 and the regression is repeated to obtain the final value of constant b_1 and the scaling coefficient for geology (b_3). The final form of the derived relationship using the field data from Cyprus is shown in eq.3-12. As in the case of PGA the standard deviation of the residual error (observed minus predicted) is added as the last parameter in the equation as a function of a dummy variable P.

$$\text{LnPGA} = b'_1 + b_2 \text{MMI} + \sigma_{\text{LnPGA}} P \quad \text{eq.3-10}$$

$$\text{LnPGA} - b_2 \text{MMI} = b_1 + b_3 S + \sigma_{\text{LnPGA}} P \quad \text{eq.3-11}$$

$$\text{LnPGA} = 0.18 + 0.63 \text{MMI} + 0.31 S + 0.27 P \quad \text{eq.3-12}$$

The comparison of the predictions of equation 3-12 with the observed data is shown in Figure 3.6. It can be seen that the derived equation (eq.3-12) agrees with the field data in a satisfactory manner. The derived equation is a slight improvement on the mean predictions of the relationship proposed by Theodulidis and Papazachos (1992) for Greece and used by Kythreoti in the ERA framework for Cyprus.

The new equation 3-12 together with eq.3-9 will be adopted for use in the ERA framework for the estimation of seismic risk for Cyprus.

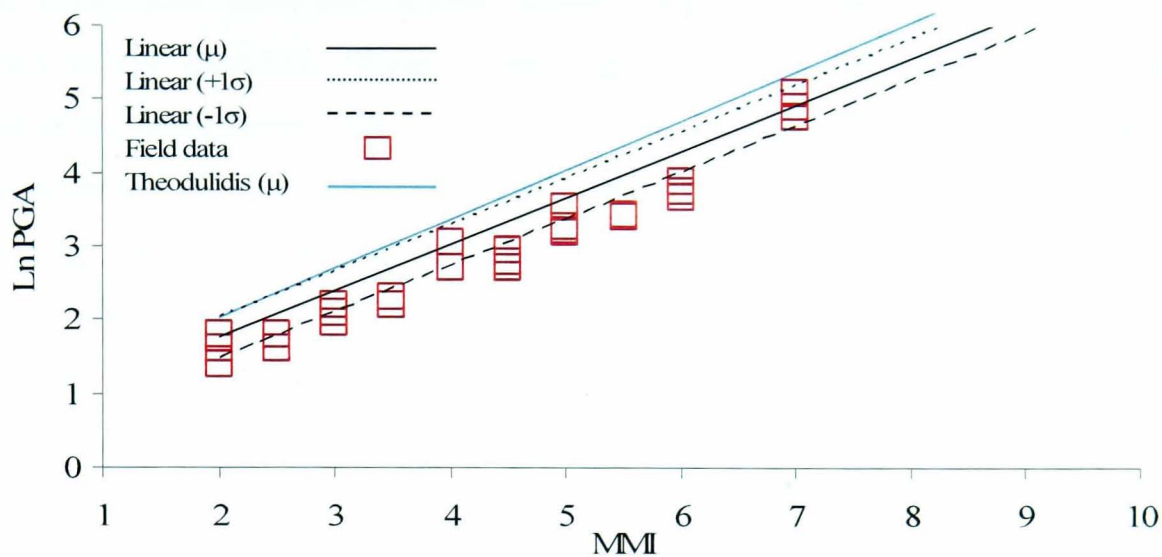


Figure 3.6 Relationship between PGA (in cm/sec^2) and MMI

3.6. Empirical vulnerability -Introduction

The second part of this study will focus on the assessment of existing damage data from the two most recent destructive earthquakes in Cyprus (No.1 and 4 in Table A-3) for use in the derivation of empirical vulnerability curves for buildings in Cyprus. Table A-5 shows a representative sample of the data used for this purpose. The data were collected by the ERS during site inspections, and cover the district areas of Limassol and Paphos. All damage data are expressed in Cypriot Pounds per square metre ($\text{CY}\text{£}/\text{m}^2$) in 1997 and 2000 for earthquakes 1 and 4, respectively.

The magnitude and epicentral locations of the two earthquakes are shown in Table A-3. Data from the first event cover both the affected areas of Paphos and Limassol, whereas data from the latter were from the affected area of Limassol.

The following section presents the format of the damage data and the classification scheme of the building inventory.

3.7. Data classification

The information about the location, building type, and repair cost is provided for the whole of the databank, whereas data regarding the dynamic properties (number of floors) and construction year are only provided for a limited number of data. Therefore, the building stock is grouped in a rather simplistic manner using the single criterion of building type. The influence of the construction material is the single most important factor affecting the vulnerability of a structure mainly because of the variation in structural capacity, weight and stiffness. A more refined classification scheme accounting for the height of the buildings and level of design practice was not possible due to the lack of data.

3.8. Identification of damage grade

The vulnerability of the building stock is expressed using the ratio of repair to replacement cost denoted by Whitman (1974) as the damage ratio (DR). A previous study funded by UNOPS and conducted by the Technical Chamber of Cyprus (2003) used the damage databank from recent seismicity in Cyprus to assign repair cost per square meter to each damage grade (DG) as defined in the European Macroseismic Scale (EMS, 1998). The description of each damage grade for both RC and Masonry buildings is shown in Figures A-1 and A-2 respectively. The resulting cost of repair per square meter for RC and Masonry buildings in Cyprus is shown in Tables 3.1 and 3.2, respectively. These values are based on repair costs based on 1997 values. Unfortunately, it has not been possible to obtain information on the number of buildings used to derive these repair values, but in the absence of more refined data, they will be adopted for the derivation of empirical vulnerability curves.

Table 3.1 Repair costs/m² for each DG for RC buildings in Cyprus (1997 prices)

Damage Grade	1	2	3	4	5
CY£/m ²	2	10	30	50	400

Table 3.2 Repair costs/m² for each DG for Masonry buildings in Cyprus (1997)

Damage Grade	1	2	3	4	5
CY£/m ²	5	11	50	80	300

The corresponding average replacement cost per square meter for RC buildings for the same year was CY£312 as obtained from data of the Statistical Service of Cyprus through a personal communication with Kypridakis (2003). It is interesting to observe the fact that for RC buildings the replacement value is less than the repair value at damage grade 5 (Table 3.1), which corresponds to collapse of the structure. In the case of masonry buildings the maximum repair was considered to be CY£300/m² and this value was adopted as the replacement value since most collapsed masonry buildings had to be repaired since replacement can not be achieved. The corresponding DRs for each damage grade are shown in Tables 3.3 and 3.4.

Table 3.3 DR for each damage grade for RC buildings (account for 1997)

Damage Grade	1	2	3	4	5
DR (%)	0.63	3.2	9.6	16	128

Table 3.4 DR for each damage grade for masonry buildings (account for 1997)

Damage Grade	1	2	3	4	5
DR (%)	1.67	3.67	16.67	26.7	100

The DR of each damage grade can now be used for the derivation of empirical vulnerability curves.

3.9. Empirical Vulnerability curves

The first step towards the derivation of empirical vulnerability curves requires the determination of the hazard level (PGA) at each location in the damage databank. For this step, the previously derived PGA attenuation model is utilised. The Cartesian coordinates of the centre point of the all villages and municipalities were provided by Kythreoti (2001), along with the corresponding ground conditions expressed in an S-value. It is assumed that the same PGA applies for the whole village or municipality.

In the second step, the repair cost per square metre is computed for each building in the databank. Based on the threshold values (Tables 3.1 and 3.2) for each damage grade, the percentage of damaged buildings in each damage grade is calculated for each PGA level. The matrix of the percentage of buildings in a particular damage grade and PGA

level is referred to as Damage Probability Matrix (DPM). The DPMs as computed herein for Cyprus for RC and Masonry buildings are given in Tables 3.5 and 3.6. The recorded PGA values at the areas with damage data are listed on the first row of the matrix. Each column represents the percentage of damaged buildings at the corresponding damage grade.

Table 3.5 DPM in % values for RC buildings in Cyprus

Damage Grade	Peak Ground Acceleration (g)					
	0.11	0.12	0.13	0.15	0.17	0.25
1	0.43	0.3	0.23	0.21	0.14	0.09
2	0.51	0.6	0.65	0.65	0.65	0.45
3	0.09	0.1	0.12	0.14	0.21	0.45
4	-	-	-	-	-	0.01
MDR	2.78	3.08	3.38	3.56	4.19	5.99

Table 3.6 DPM in % values for Masonry buildings in Cyprus

Damage Grade	Peak Ground Acceleration (g)					
	0.11	0.12	0.13	0.15	0.17	0.25
1	0.4	0.285	-	0.125	-	0.145
2	0.4	0.4	-	0.33	-	0.36
3	0.2	0.3	-	0.51	-	0.45
4	-	0.015	-	0.033	-	0.03
5	-	-	-	-	-	0.017
MDR	5.47	7.34	-	10.80	-	12.74

The percentage of buildings in each damage grade for the range of PGA values can be plotted directly from the DPM. The results for RC buildings are shown in Figure 3.7.

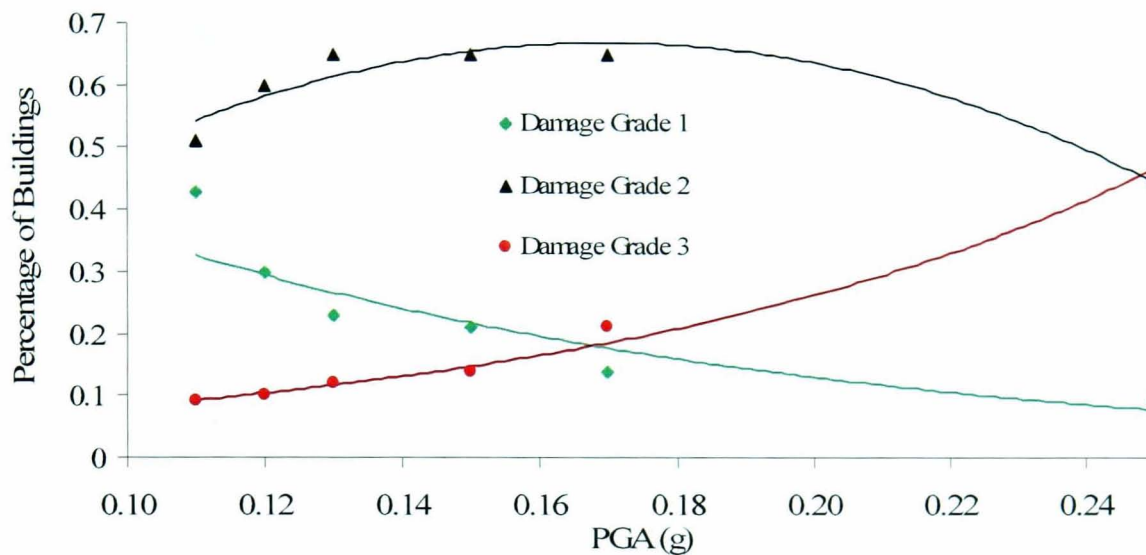


Figure 3.7 Percentage of buildings for each damage grade (DG) for the range of PGA values.

The vulnerability (Mean Damage Ratio) of each building type for the range of PGA values obtained can also be derived from the DPM as shown in eq.3-15.

$$\text{MDR/PGA} = \sum_{i=1}^4 \text{DR}_i = \text{DR}_i \times (\% \text{ of damaged buildings}) \quad \text{eq.3-15}$$

Where:

DR_i damage ratio of damage grade i (found in Table 3.3 and 3.4)

The derived empirical vulnerability curves for RC and Masonry buildings in Cyprus are shown in Figure 3.8.

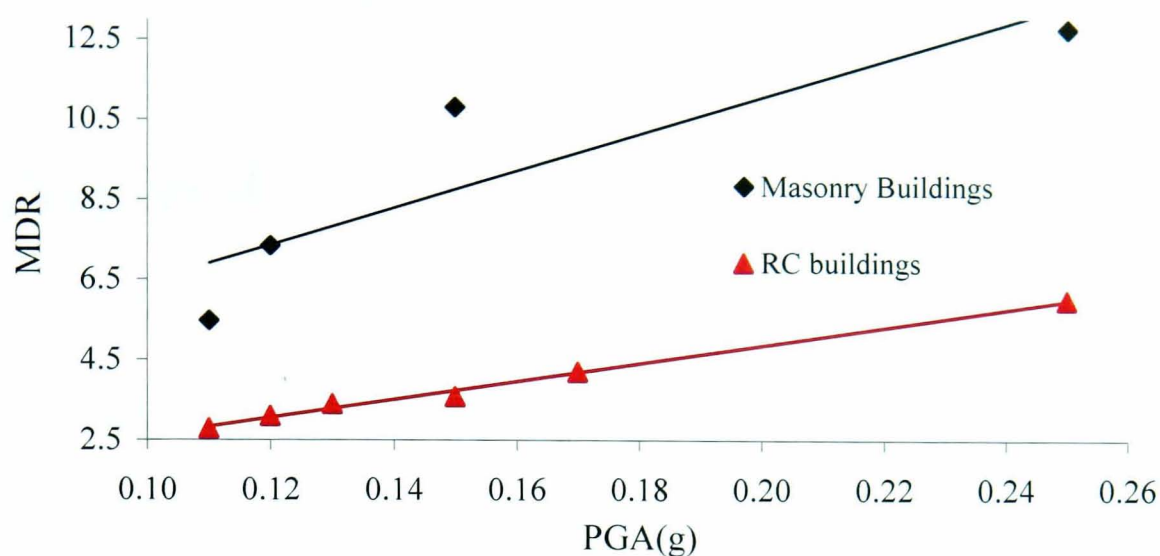


Figure 3.8 Empirical vulnerability curves for RC and masonry buildings for Cyprus

3.10. Discussion on the Vulnerability Results

It should be pointed out that the newly derived vulnerability curves were obtained from a limited data set and cover mainly a small range of PGA levels (0.11g-0.17g) since only one set of data is available for moderate PGA levels (PGA=0.25g). It is obvious from Figure 3.8 that masonry buildings are more vulnerable than RC ones. However, it is not possible to tell from Figure 3.7 how structural damage (DG3) will progress after 0.25g since the curve could climb rapidly. Therefore an analytical investigation of the behaviour of buildings at higher PGA levels needs to be undertaken to complete the distribution of the vulnerability curves. The rest of the work will aim to derive analytical vulnerability curves for several classes of RC buildings.

Chapter 4

Structural Modelling

4.1 Introduction

The initial objectives of the research relating to improving the attenuation and vulnerability models using empirical data was completed in the previous chapter. Though a considerable enhancement was attained in the hazard model based on the seismic data, very limited conclusions were drawn from the damage data regarding vulnerability. To enhance the risk assessment procedure, it is therefore necessary to focus on the vulnerability models by adopting a more theoretical and thus more challenging approach through analytical vulnerability. The outcome of this work should lead to MDR curves at different PGA levels.

The framework for the derivation of analytical vulnerability curves presented herein requires the determination of the following:

- Appropriate structural analysis modelling.
- Suitable analytical tool able to simulate all the anticipated failure modes.
- A procedure capable of determining the damage potential for various seismic scenarios and that takes into account the probabilistic nature of the problem.

This chapter will focus on selecting an appropriate structural analysis tool with suitable element models in order to assess and verify their capability against experimental data obtained from full-scale seismic tests.

4.2 Background on Analysis and Modelling

Following the development of capacity-spectrum method in the mid 1970s (Freeman, 1975) static nonlinear analysis has become the main alternative for performance evaluation purposes since it provides a simple and effective alternative to complicated non-linear time-history analysis. This method is discussed in a subsequent chapter, but in brief, it compares the nonlinear capacity of the structure with the reduced force-based demand from a seismic event to evaluate the performance of the structure for the particular event.

The most important parameter for the accurate simulation of the nonlinear seismic behaviour of RC frames is the modelling of the structural elements. To address the modelling deficiencies of previous work in this field it is necessary to select element models that can simulate any possible damage potential. A brief outline of possible damage on RC frames includes:

- Cracking of concrete in tension
- Plastic hinge formation through yielding of reinforcement
- Slip of the reinforcement due to excessive bond deterioration
- Shear failure due to
 - inadequate shear reinforcement
 - inadequate spacing of the shear links
 - diagonal compressive failure
 - cumulative deterioration
- Local buckling of the reinforcement
- Concrete deterioration and crushing

It is obvious from the above and from the discussion in 2.3.3.2 that realistic RC modelling should cover flexural, shear and bond failures in members and joints. The remaining part of this section discusses the issues concerning each failure mode and proposes the corresponding requirements for their appropriate modelling.

4.2.1 Lumped plasticity constitutive models

In most frame analysis tools nonlinearity is added to the element through finite hinges at the element ends with lumped plasticity moment-rotation models that accounts for the:

- formation of plastic hinges at member ends
- dissipation of energy in the hinges
- ductility of the members

An example of a simple lumped plasticity element as introduced by Clough and Johnson (1965) is shown in Figure 4.1, which consists of two parallel sub-elements, an elastic-perfectly plastic element to represent yielding and a perfectly elastic one to represent strain hardening. The response envelop is formed by the addition of moments from the two sub-elements for every increase in rotation.

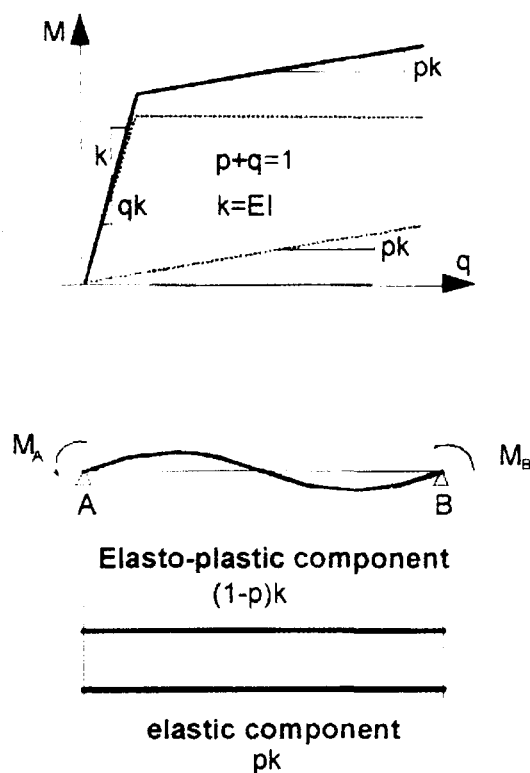


Figure 4.1. Clough and Johnson lumped plasticity element

Considerable improvements in lumped plasticity constitutive models have been proposed to date accounting for cyclic stiffness degradation and pinching in flexure and shear (Takeda et al., 1970 and Brancaleoni et al., 1983) shown in Figure 4.2 and fixed end rotations at the beam-column joint interface due to bar pullout (Taucer, F., 1991, Deng Chang-Gen et al., 2000 etc.).

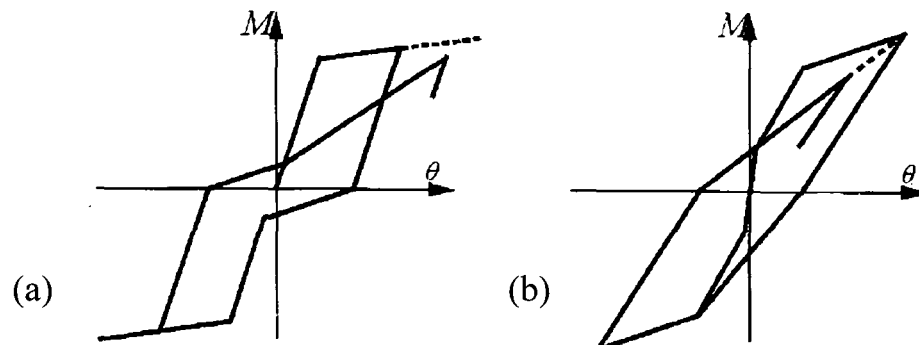


Figure 4.2. (a) Stiffness degradation with shear deterioration, and (b) Takeda hysteretic model

Ghobarah et al (1999) moved a step further by producing separate lumped plasticity constitutive models accounting for several softening effects, which can be used both for element and joint modelling (Figure 4.3).

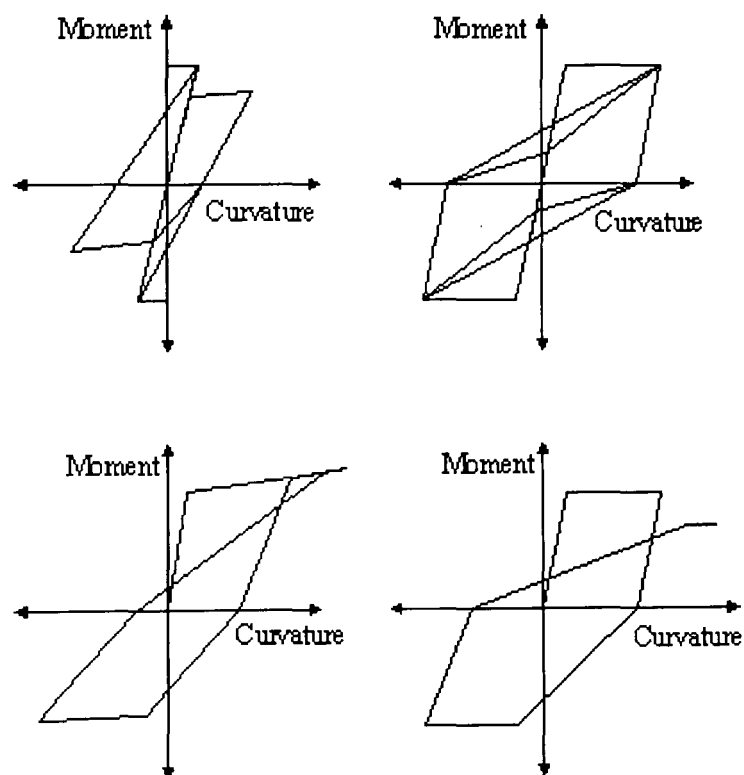


Figure 4.3. Hysteretic modelling of the moment-curvature relationship (Ghobarah, 1999)

However, even sophisticated constitutive moment-rotation models such as the above are insufficient since they need to be calibrated against experimental cyclic testing data. The analytical definition of these constitutive models becomes difficult due to the combination of different effects such as flexure, shear and bond. Therefore though they provide direct control on the strength capacities, initiation of degradation and

degradation rate at the global level, the question is how to obtain this information. An additional limitation is that lumped plasticity at element ends is just an approximation of the true plastic hinge zone, which may distribute considerably both in the member and in the joint.

4.2.2 Resistance models

Another approach for determining element behaviour is to utilise resistance models for each potential failure type.

4.2.2.1 Flexure

To increase the accuracy of flexural behaviour modelling a multi-section (fibre) analysis element which enables distributed plasticity needs to be introduced. The element should be able to produce the moment-curvature envelopes and interaction diagrams using only the cross-section details and material properties. In addition, the element should provide the user with the capability of decoupling the effects of various failure modes.

4.2.2.2 Shear

Most studies treat shear deformations in an elastic manner and assume abrupt shear failure when the shear capacity is reached in members (Dymiotis, 1999). Although this is a conservative assumption, it is not a realistic one since shear failure may exhibit different post-peak characteristics. In particular, shear failure in joints is not discussed in any of the recent vulnerability studies although it is a very common failure mode for sub-standard construction. This is due to the fact that in most cases no shear links were placed in the joint region (due to practical reasons), and also due to the fact that in most cases the joint capacity is less than that of the corresponding of the beam.

Experiments in joints conducted by numerous researchers show that the degradation rate can lead to gradual strength loss for up to considerable deformations as shown in Figures 4.4 (Biddah and Ghobarah, 1997) and Figure 4.5 (Walker, 2001). Even in the case of no shear reinforcement as in the case of Figure 4.4 (b) degradation is not immediate and there is some level of residual strength.

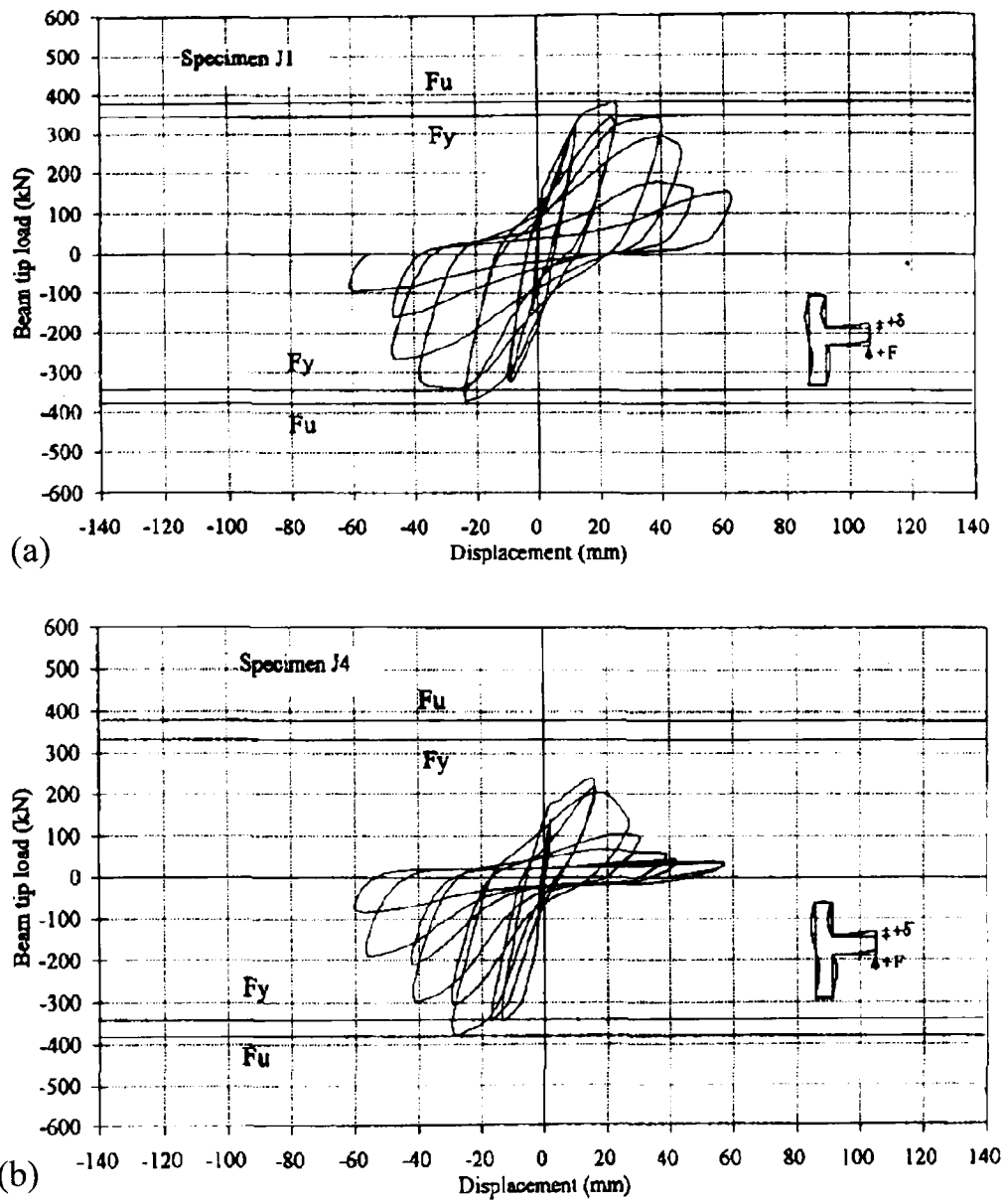


Figure 4.4. (a) Shear failure after reinforcement yielding and (b) no shear in joint and poor anchorage of reinforcement (from Biddah, 1997).

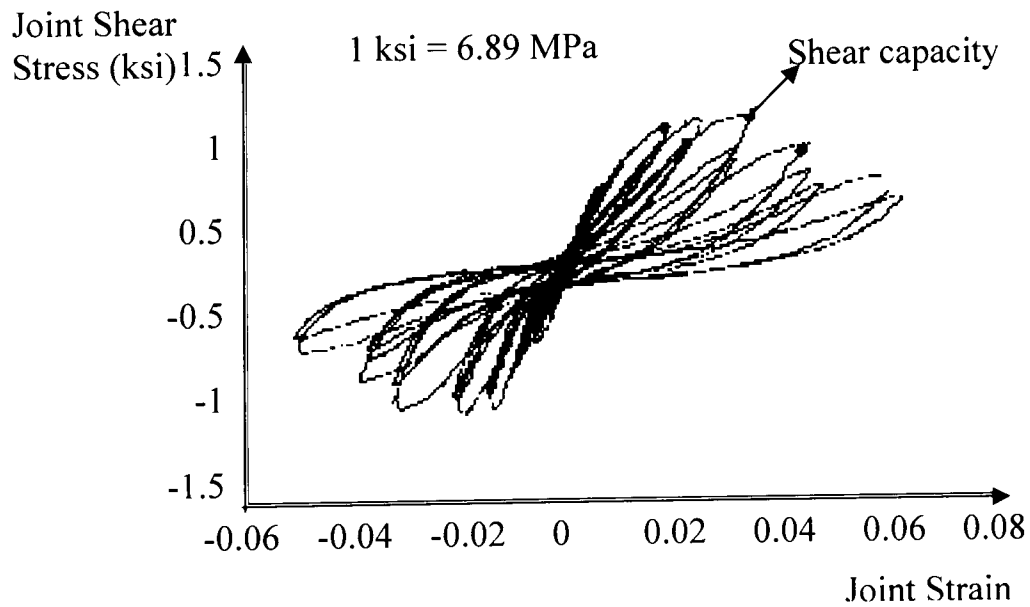


Figure 4.5. Hysteretic response of damaged joint (after Walker, 2001)

4.2.2.3 Bond

Most studies fail to address bond issues at all, mainly due to lack of suitable models, but also due to underestimation of its importance. The flexural forces from beams and columns cause tension and compression forces in the longitudinal reinforcement passing through the joint. Bond stresses increase as the force in the bar increases up to the yield level. When the longitudinal bars passing through the joint are stressed beyond yielding, debonding along the bar can cause the deterioration of bond between steel and concrete. This deterioration may cause slip which can contribute to additional apparent flexural deformations. A typical steel stress versus slip behaviour for column bars with inadequate anchorage length is shown in Figure 4.6. Kwak and Filippou (1990) analysed the deformations on an interior joint and concluded that bond-slip of the reinforcing bars in the joint contributed approximately 33% of the total deformation near the ultimate load. Sezen (2002) also monitored slip deformations on columns and concluded that these contribute between 25-40% of the total lateral displacement (Figure 4.7). Slip of the reinforcement is only prevented by providing adequate development length and confinement detailing in the lapping regions placed outside the yield penetration zone, which is defined as the length of the reinforcement bar expected to reach yielding.

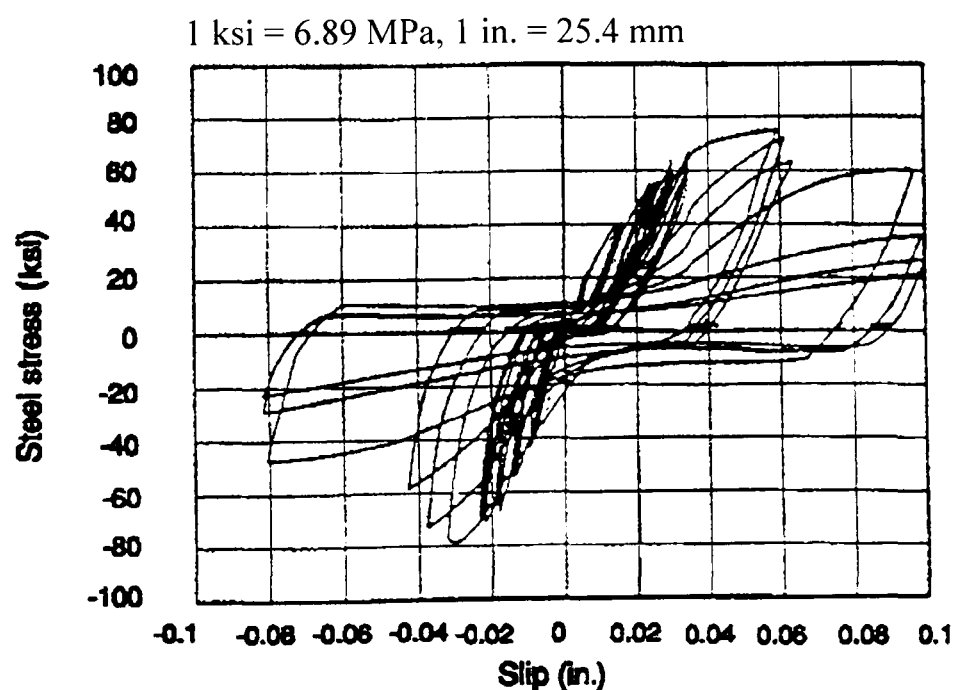


Figure 4.6. Experimental stress-slip response of anchored reinforcing bar under cyclic push-pull (Viathanatepa, 1979)

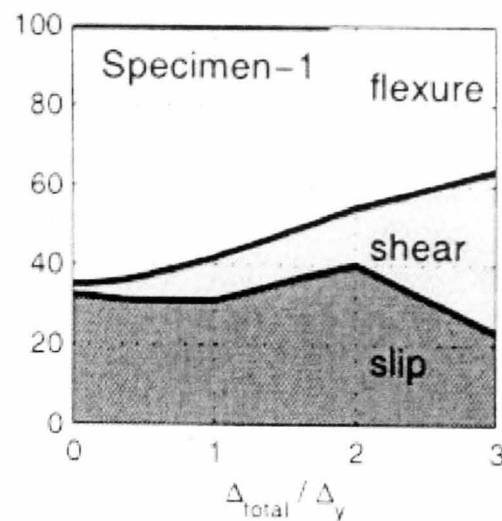


Figure 4.7. Contribution of flexure, shear and slip deformations to total column displacements (from Sezen, H., 2002).

4.3 Choice of Analytical Tool

The issues addressed in the previous paragraphs regarding the member and joint response lead to the conclusion that sophisticated modelling needs to be used in order to improve the estimation of structural performance. After a wide literature search and consideration of available resources it was decided to use DRAIN-3D frame analysis FE software (Prakash, 1994) as it includes local elements with degradation characteristics fulfilling the requirements discussed above. It should be noted that the 3D version is preferred to the 2D since it includes a cyclic shear element. Besides having an extensive element library (Powell, 1994) and accessible source code it has been widely used for both dynamic and static analyses (Dymiotis, 1999, Deng, 2000, Rubiano, 2001, Shin, 2004, Karayannis, 2005, etc.) and proven to have a reliable solver (good convergence). Its main drawback is that it lacks a user friendly visual interface, which makes it difficult to work with.

The following paragraphs describe the elements used both for member and joint modelling based on the requirements set above.

4.3.1 Drain-3D (Flexure)

The element library of DRAIN-3D includes a section analysis element (element 15), which is used to model the flexural behaviour of beams and columns. This element can have rigid zones (to simulate joints) and deformable regions. Within the length of the deformable region the element has distributed plasticity accounting for the spread of the

inelastic behaviour both over the cross section and along the member length (Powell and Campbell, 1994). It also accounts automatically for the interaction between axial force and bending in columns (M-N interaction).

A schematic representation of the element is shown in Figure 4.8. Each cross-section comprises of a number of concrete and steel fibres. The location of each fibre depends on a local axis system defined at the beginning of the analysis. The cross-section characteristics are defined by assembling these fibres based on their coordinates and sectional area. The response of each fibre is concentrated at its centre of gravity. As a result, the stiffness and strength of the section depends on the number and location of the fibres. A dense rectangular grid discretization increases the accuracy in the flexural capacity predicted by the section analysis routine of DRAIN-3D, but is computationally more intensive.

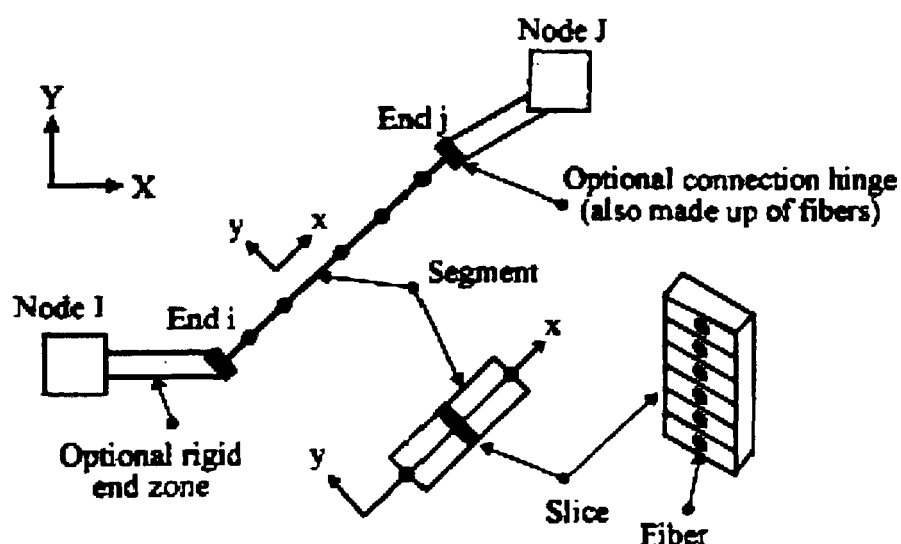


Figure 4.8. Section analysis element (Prakash, 1994)

The deformable part of the element can be divided into a number of segments. The cross-section properties are assumed to be constant within each segment, but can vary from segment to segment if required. The behaviour is monitored at the mid point of each segment and accounts for the spread of the inelastic behaviour both over the cross section and along the member length (Powell and Campbell, 1994). A study conducted by Isakovic and Fischinger (1998) investigated the effect of the number and length of segments required to accurately simulate the distribution of rotations along the element length and concluded that the plastic hinge regions at member ends could be modelled as separate single segments. Division of the plastic hinge in a number of smaller

segments seems to have little effect on the element response. It has also suggested the use of one segment that can even be elastic for the length of the element outside the plastic hinge regions.

4.3.1.1 Material Modelling

The material library includes both concrete and steel models. The backbone curves for both models are shown in Figure 4.9. In both cases, the element allows for the use of up to 5 stress-strain points for the curve definition. In the case of concrete, two additional points can be added to account for its tensile strength. As far as the “post-yield” behaviour is concerned, kinematic strain hardening can be assumed for steel and strength deterioration for concrete. Although the concrete model allows for intermediate and full degradation in unloading stiffness it was proven by Isakovic and Fischinger (1998) that only the full degradation option actually works. However, stiffness degradation can also be modelled through connection hinges as discussed later.

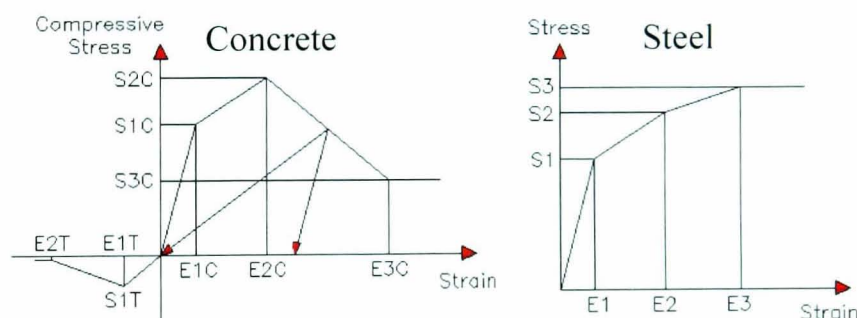


Figure 4.9. Concrete and steel stress-strain envelopes

4.3.2. Drain-3D (Anchorage)

Element 15 (used above for flexural behaviour) is also capable of modelling slip deformations at connection hinges at element ends. These connection hinges are defined as fibres having both pullout and gap characteristics. Pullout fibres can model slip movement of the reinforcement bars whereas gap fibres are used to account for gap opening of concrete. Therefore, pullout and gap fibres replace steel and concrete fibres at member ends, and are modelled based on the connection hinge properties as explained in more detail below.

4.3.2.1 Pullout Fibres

This section starts with the description and calibration of the bar pullout hysteretic behaviour model included in DRAIN-3D. The monotonic stress-displacement envelope consists of trilinear tensile and compressive portions representing the relationship between slip in bar reinforcement with increased bar stress (as shown in Figure 4.10).

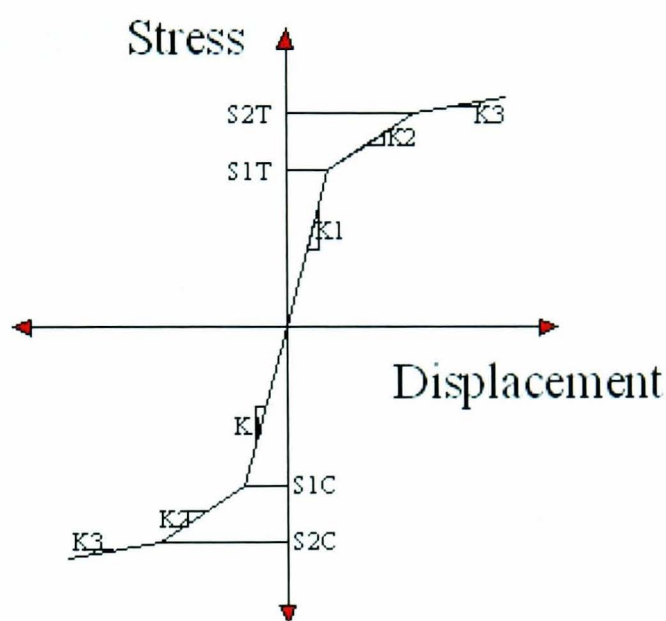


Figure 4.10. Trilinear backbone curve of pullout fibre

The stiffness of the trilinear portion is the same in both tension and compression while the strength may vary. The calibration of the trilinear envelope is discussed in detail later in the section.

Further to the monotonic envelope, the complete hysteretic behaviour of the fibre can be modelled with the definition of degradation parameters accounting for the effects of repeated loading and unloading cycles. These parameters are capable of capturing degradation in strength, stiffness and pinching behaviour in the unloading branch of each cycle.

The process for applying degradation starts with the decomposition of the trilinear curve (Figure 4.10) into two bilinear curves and an elastic curve acting in parallel as shown in Figure 4.11a. Stiffness degradation factor (SDF) controls the unloading/reloading stiffness of the bilinear curves (see Figure 4.11b). A value between zero and one is specified for the degradation. No degradation of stiffness occurs if a value of zero is given (unloads at initial stiffness) while a value of one causes the curve to unload along

a line passing through the point where the curve last crossed the zero stress axis (Figure 4.11b). Values between zero and one cause a linear interpolation of the stiffness between the two extremes.

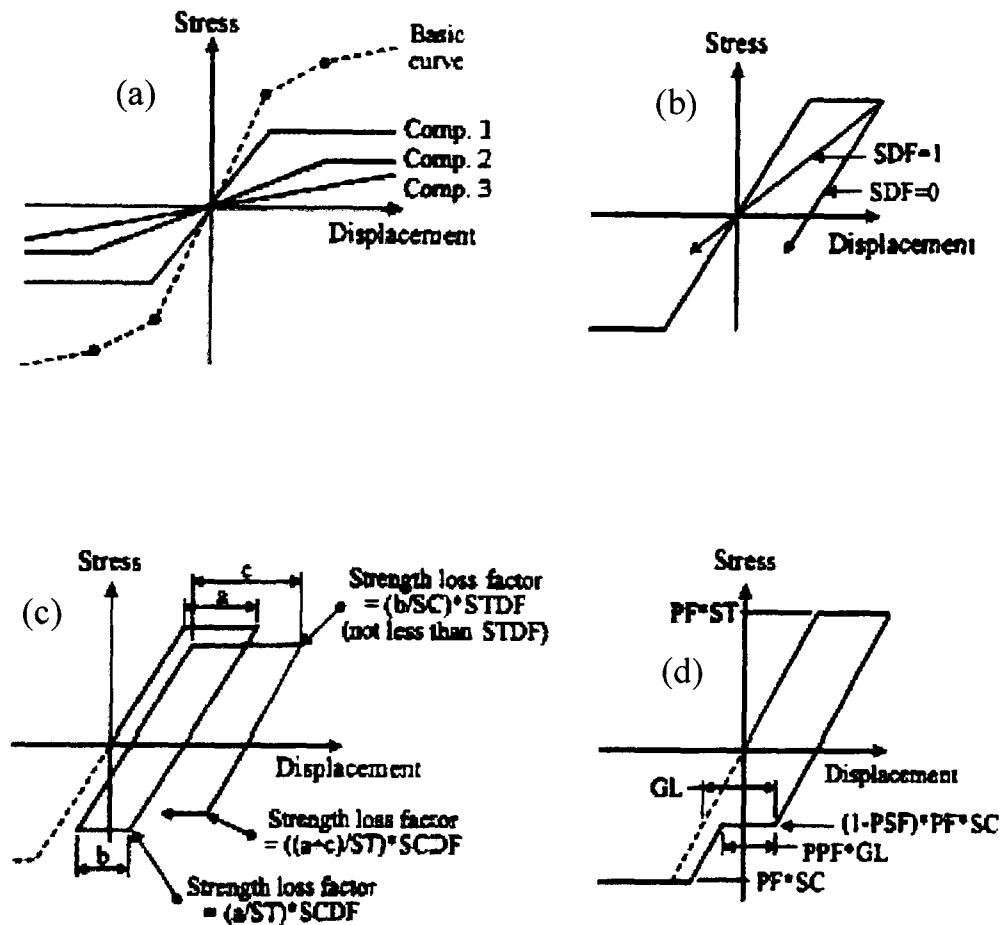


Figure 4.11. Pullout fibre degradation properties (a) Basic trilinear curve decomposed in three parallel components, (b) Stiffness degradation factor (SDF), (c) Strength loss in each component depends on strength degradation factor (STDF or SCDF) and the ratio of accumulated plastic displacement to saturated displacement (ST or SC), and (d) Pinch factor (PF), pinch strength factor (PSF) and plateau factor (PPF).

Strength loss in each component depends on the strength degradation factor (STDF or SCDF) and the ratio of accumulated plastic displacement to saturated displacement (ST or SC) (Figure 4.11c). STDF is treated as a dummy variable in the model taking values of 0 and 1 for no and full degradation. Thus, degradation rate is controlled only with the ST and SC values, which correspond to bar slip in tension and compression at full debonding conditions. Tensile plastic slip causes compressive strength degradation and vice versa. The strength degrades linearly between zero loss below capacity stress to full

loss at saturated plastic slip (ST or SC). Despite the wide spectrum of pullout tests in the literature it was decided that the most comprehensive set of slip values for the definition of ST and SC can be found in the CEB (1993) model, which account both for confinement conditions in the anchorage region and quality of bond conditions.

Pinching behaviour is controlled by three parameters (see Figure 4.11d). The first is the pinching factor (PF) that determines how much of the fibre strength undergoes pinching. The strength at which pinching occurs is controlled by the pinch strength factor (PSF) whereas, after pinching begins, the pinch plateau factor (PPF) determines the length of the plateau. A value of one indicates that the plateau extends until it meets the last unloading curve. Since no extensive experimental data could be found, full pinching degradation is modelled in subsequent analysis, which is in line with various models proposed by researchers in the field of bond (Eligehausen, 1983, Filippou, 1983, CEB, 1993 etc.).

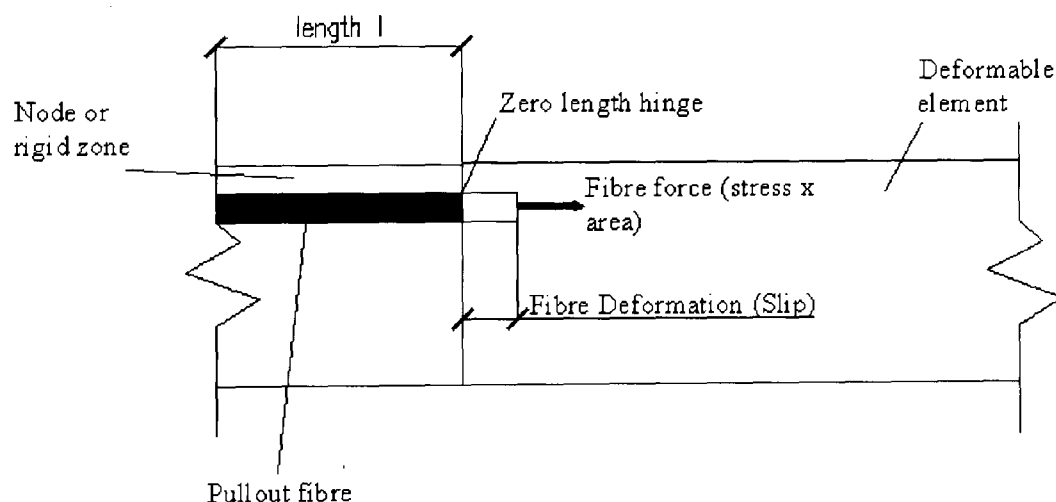


Figure 4.12. Fibre deformation (reproduced from Prakash, 1994)

The following key parameters need to be defined for the calibration of the trilinear backbone curve shown in Figure 4.10 for use in subsequent analysis:

1. The initial stiffness (K_1 in Figure 4.10) defines the bond conditions prior to yielding of the reinforcement (S_{IT} in Figure 4.10) and it is defined as the ratio between steel yield strength (S_{IT}) and elastic bar slip (see Figure 4.12). For the calculation of elastic slip the equilibrium of forces acting on the bar is assumed. Therefore, the normal force at the bar end (Figure 4.12) is balanced by the bond force acting on the bar circumference, which is assumed uniform, as shown in

equation 4-1 below. The slip caused by the normal force is assumed to be a function of the steel strain distribution along the bar (eq.4-2), which can be found by substituting $f_s = E_s \varepsilon_s$ and $A_s = \pi \frac{d^2}{4}$ into equation 4-1 and rearranging. Thus, by integrating the strain for the whole anchorage length (eq.4-3) the elastic slip up to yielding can be computed.

$$f_s A_s = \tau_e d \pi l \quad \text{eq.4-1}$$

$$\varepsilon_s = \frac{4\tau_e}{dE_s} x \quad \text{eq.4-2}$$

$$\text{Slip} = \int_0^l \frac{4\tau_e x}{dE_s} dx = \frac{f_s^2 d}{8\tau_e E_s} \quad f_s < f_y \quad \text{eq.4-3}$$

Where:

- f_s bar stress
- d bar diameter
- τ_e bond strength for elastic steel
- ε_s steel strain
- E_s Elastic steel modulus
- l anchorage length as shown in Figure 4.12
- x distance from zero strain in the bar

Therefore, K1 is calculated as

$$K1 = \frac{SIT}{\text{elastic slip}} \quad \text{eq.4-4}$$

In cases where anchorage failure occurs before bar yielding, due to inadequate anchorage length, SIT is defined as the maximum stress that can be achieved in the bar for the provided anchorage length as shown in eq.4-5.

$$SIT = \frac{4\tau_e l}{d} \quad \text{eq.4-5}$$

2. In cases where anchorage failure precludes yielding, stiffness K_2 is set to zero whereas a model needs to be adopted for the slip in reinforcement loaded beyond yielding. For that purpose the distribution of bond stress in yielded steel (τ_y) needs to be assumed. Existing nonlinear models for stress-slip found in the literature (Lowes et al., 2003 and Sezen et al., 2003) assumed a piecewise constant bond distribution for reinforcement in the strain hardening region, with bond strength lower than τ_e used previously for steel in the elastic region (see Figure 4.13).

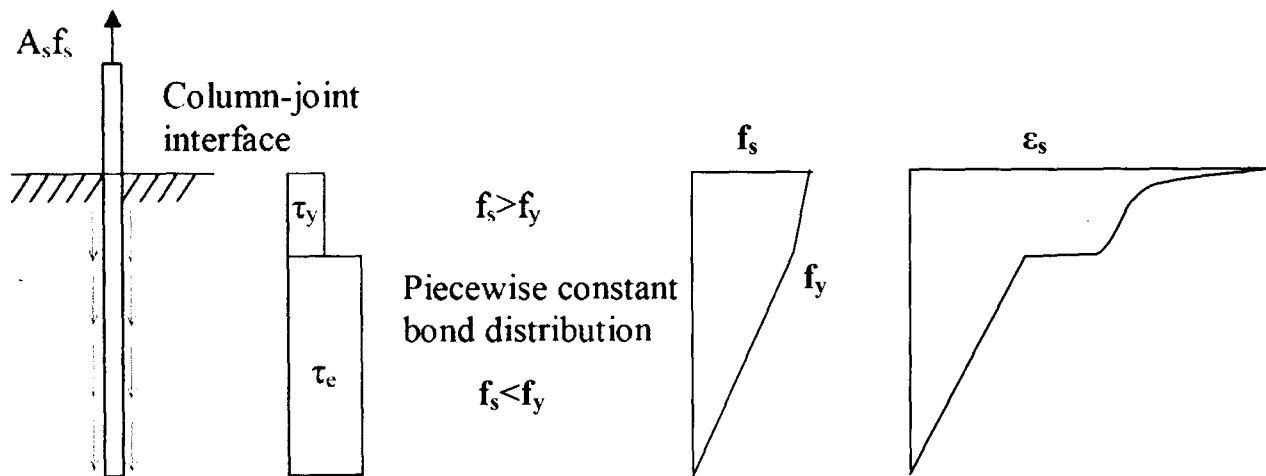


Figure 4.13. Piecewise constant bond distribution for yielded steel.

Based on this assumption eq.4-1 is rearranged into:

$$A_s E_h (\epsilon_s - \epsilon_y) = \tau_y \pi d l \quad \text{eq.4-6}$$

Where:

- A_s area of steel bar
- E_h steel hardening modulus
- ϵ_s steel strain in the hardening region

The nonlinear slip model, based on eq.4-6, used in Lowes et al. (2003) and Sezen et al. (2003) studies is shown in eq.4-7.

$$\text{Slip } (f_s > f_y) = \frac{f_y^2 d}{8E_s \tau_e} + \frac{(f_s - f_y) f_y d}{4\tau_y E_s} + \frac{(f_s - f_y)^2 d}{8\tau_y E_h} \quad \text{eq.4-7}$$

Where:

τ_y bond strength in yielded steel

E_h steel hardening modulus

For the definition of the uniform elastic (τ_e) and yielded (τ_y) bond strength required in equations 4-3 and 4-6, proposals from various researchers are examined. Eligehausen et al. (1983) experimentally defined the peak and average value of $2.5\sqrt{f_c}$ and $1.8\sqrt{f_c}$ for steel moderately confined that remains in the elastic region. Shima et al. (1987) arrived at average bond strength of $0.4\sqrt{f_c}$ for yielded steel. Lehman (2000) used the values of $1.0\sqrt{f_c}$ and $0.5\sqrt{f_c}$ respectively, which were also adopted in Sezen (2003) study. The CEB (1993) bond model shown in Figure 4.14 proposes $1.0\sqrt{f_c}$ as the ultimate value of bond strength for unconfined concrete in poor bond conditions and $1.25\sqrt{f_c}$ for confined concrete in similar bond conditions. In cases of good bond conditions these values are doubled in the model. EC-2 (2004) design model for ultimate bond strength yields approximately a value of $0.75\sqrt{f_c}$ for good bond conditions, which is lower than the CEB (1993) since it is used for design purposes.

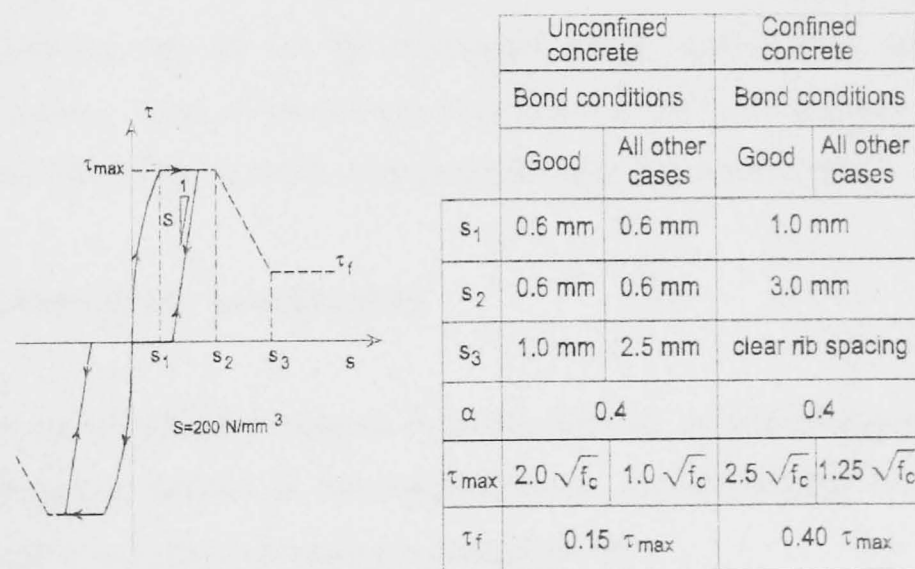


Figure 4.14. Bond-slip model in CEB (1993)

From the above it can be concluded that the elastic bond strength proposed by Lehman (2000) is in agreement to the ultimate value proposed in CEB (1993) and the yielded bond strength proposed in the same study is similar to the findings

from Shima et al. (1987). In addition, the ultimate design bond strength in EC-2 lies in between of the two values proposed in the same study. As far as confined concrete is concerned, there is a good agreement between elastic bond strength values calculated by Eligehausen et al. (1983) and the peak value proposed in CEB (1993) for good bond conditions ($2.5\sqrt{f_c}$). The average value proposed in the same study ($1.8\sqrt{f_c}$) also lies in-between the values for good and poor bond conditions proposed in CEB (1993), which can be assumed to simulate moderate bond conditions.

In light of the above it is concluded that in this study the values proposed by Lehman (2000) are used in subsequent analysis for cases of unconfined concrete. In cases of moderate confinement the average value proposed by Eligehausen (1983) for elastic bond strength will be used since it is very close to the average between the two values in the CEB (1993) model for good and poor bond conditions. In the latter case, the bond strength for yielded steel is assumed to be half the strength of the elastic following the pattern found in Lehman (2000) and the CEB (1993) model for unconfined concrete.

In addition threshold slip values (s_3) for unconfined and confined concrete, as shown in Figure 4.14 (CEB, 1993), are used to define the saturated slip (ST or SC) deformations required for the calibration of the pullout fibre model. As mentioned earlier, these deformations correspond to the ultimate slip prior to complete bar debonding and thus control the strength degradation rate.

4.3.2.2 Reinforcement local buckling

The pullout fibre model shown in Figure 4.10 provides an additional capability for modelling local buckling failures in steel reinforcement. Local buckling reduces the capacity of the steel in compressive loading and depends on:

1. shear link spacing
2. shear link diameter
3. longitudinal bar diameter

The reduction in compressive bar strength (S1C in Figure 4.10) is assumed to be linearly correlated with the ratio between the required and provided spacing (eq.4-8) of confinement reinforcement as prescribed by Penelis (1997).

$$s \leq \frac{100d_{bw}^2 f_{yw}}{(0.25d_{bl})^2 f_{ys}} \quad \text{eq.4-8}$$

Where:

- s shear link spacing
- d_{bw} shear link diameter
- d_{bl} longitudinal bar diameter
- f_{yw} shear link yield strength
- f_{ys} bar yield strength

In sub-sequent analysis a check for the required spacing is included and the compressive strength of the bar is reduced accordingly.

4.3.2.3 Gap Fibre

Gap fibres can be used to simulate crack opening at the joint interface, which cause additional deformations of the joint. Gap deformations for various levels of compressive stress can be modelled in DRAIN-3D through the model in Figure 4.15.

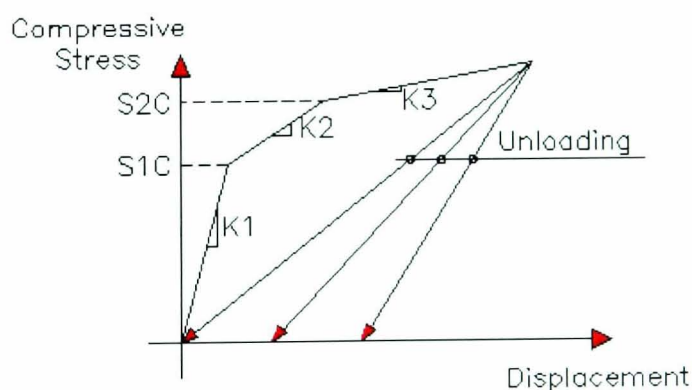


Figure 4.15. Model for gap fibres

For the purpose of this study, elastic gap deformations are assumed to be included in the elastic pullout model whereas after the attainment of elastic bond stress capacity it is assumed that bar slip dominates the additional deformations at the column interface.

Thus, in all subsequent analysis the values for stiffness K_1 , K_2 and K_3 are set at very high values so as not to include any deformations due to gap openings and closings.

4.3.3. Drain-3D (Shear)

The nonlinear shear behaviour of members and joints can be modelled using element 8 in DRAIN-3D with the use of shear “hinges” distributed along the element length. These “hinges” account for additional elastic and inelastic shear deformations. The backbone curve of the element is in the form of shear force versus shear deformation as shown in Figure 4.16.

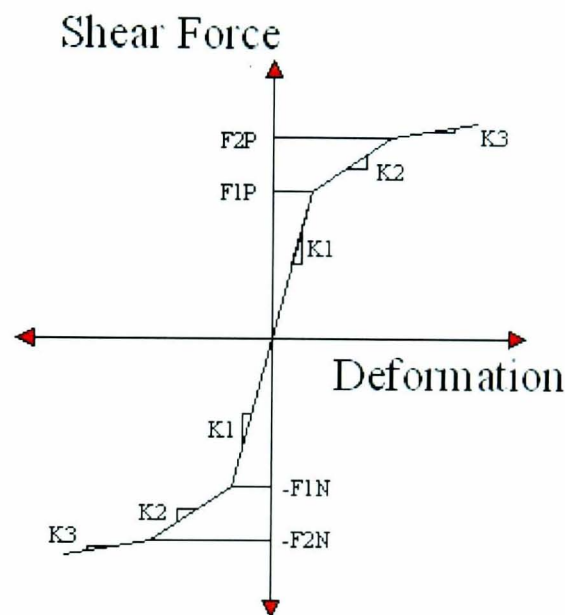


Figure 4.16. Backbone curve of inelastic shear element.

The inelastic shear model in DRAIN-3D is used in parallel to a linear elastic model accounting for the elastic flexural deformations prior to the attainment of the shear capacity. There can be up to two shear hinges, for shear deformations in the two local y and z axes (Figure 4.17). The calibration of the model requires the definition of the shear capacity values (F_{1P} and F_{2P} in Figure 4.16) and the corresponding elastic and post elastic stiffness (K_1 and K_2 in Figure 4.16).

Similarly to the pullout model defined in 4.3.2.1, degradation in strength (F_{1P} in Figure 4.16), stiffness and pinching can be defined based on the hysteretic rules of shear behaviour. Degradation parameters are applied using the same process as in the pullout hysteretic model shown in Figure 4.11. In this case though, strength capacity is

expressed in the form of shear force FIP (Figure 4.16) and displacements represents additional shear deformations.

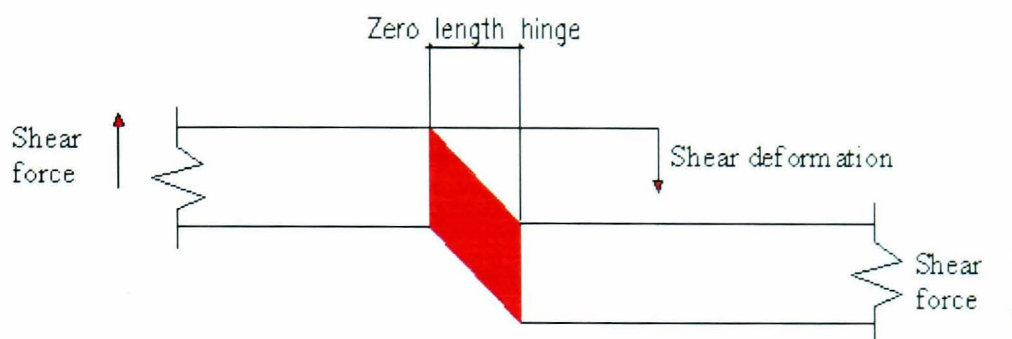


Figure 4.17. Shear hinge deformation

Based on the experiments from Biddah (1997) and Walker (2001) full pinching behaviour is assumed for the unloading curve. As in the pullout model, strength degradation at each cycle varies linearly with the ratio between accumulated to saturated shear deformations (ST and SC). Therefore, the rate of decrease in shear strength of a member after the attainment of ultimate shear capacity depends on the ultimate deformation at full shear strength loss (ST and SC). For a column in a frame, this saturated deformation corresponds to the storey displacement at which the shear capacity of the column approaches zero. This value depends primarily on the amount of shear reinforcement and on the anchorage of shear reinforcement. Inadequate anchorage of shear links produces abrupt shear failure, whereas detailing according to EC-8 (2004) allows for a more soft post-capacity degradation rate (as shown in Figures 4.4 and 4.5). For the purpose of subsequent analysis, this parameter is treated deterministically as discussed later in Chapter 6.

4.3.3.1 Calibration of shear model

The monotonic envelop in Figure 4.16 provides the possibility of defining bilinear shear behaviour prior to the attainment of ultimate shear capacity accounting for the change in stiffness between uncracked and cracked conditions. Nevertheless for the purpose of this study it is deemed possible to disregard uncracked conditions and assume cracked stiffness up to the attainment of the ultimate shear capacity. Shear force capacity (FIP, see Figure 4.16) of RC members can be obtained directly from design codes. In most codes such as ACI (1999), BS8110 (1985) and EC-2 (2000) the main parameters included in the calculations are concrete strength, flexural reinforcement, axial force and size effect. Although shear capacity models in the above codes differ they are all

based on the assumption that concrete strength contribution can be added to the shear reinforcement contribution. The latest version of EC-2 (2004) uses a different approach, based on the strut and tie method, and uses only the shear reinforcement contribution after the concrete capacity is exceeded. It is believed that the latter procedure underestimates the shear capacity and yields unrealistic results. Great concerns were expressed by various researchers such as Cladera, A. and Mari, A. (2004) suggesting that EC-2 (2004) approach leads to considerable underestimation of the shear capacity for lightly shear reinforced members compared with experimental results.

Further to the code provisions more advanced models exist in the literature accounting for the reduction in shear strength with increased ductility. Sezen (2004) compiled a database of 51 test columns having inadequate and poorly detailed transverse reinforcement obtained from experiments conducted by a number of researchers cited in Sezen (2004) to develop a shear strength model for lightly reinforced columns. The study also compared experimental results with analytical ones computed using FEMA 273 (1997), ACI 318-2002 and Priestley et al. (1994) models. It was concluded by Sezen (2004) that although these models address most variables influencing shear strength, a refined model should be derived including considerations for ductility-related strength degradation and degradation due to increase in aspect ratio that are evident from the experimental results. The refined model proposed in the above mentioned study is shown in eq.4-9. The value of k accounts for the ductility-related strength degradation. A value between 1 and 0.7 is attributed linearly for ductility levels 2 to 6. The ratio $\frac{\alpha}{d}$ is also assumed to cause a linear decrease on the shear strength,

which is verified against experimental results with $\frac{\alpha}{d}$ ratios from 2 to 4.

$$V_n = V_s + V_c = k \left(\frac{A_v}{s} f_y d \right) + k \left(\frac{0.5\sqrt{f_c}}{\alpha/d} \sqrt{1 + \frac{P}{0.5\sqrt{f_c} A_g}} \right) 0.8A_g \quad \text{eq.4-9}$$

Where:

- P axial force
- k ductility-related strength degradation value
- a/d aspect ratio
- A_g cross-sectional gross area
- A_v shear link area

Although this model may serve as a powerful tool for design calculations it can not be used as a capacity estimation model since it depends on the ductility undergone by the structure. The definition of the ductility at shear capacity is not a trivial decision, which requires the coupling of the flexure and shear models. In order to bypass the uncertainties and complications related with modern code provisions (EC-2, 2004) and advanced model calibration (Sezen, 2004), it is decided to use the well-known and verified EC-2 (2000) model (similar to BS8110) shown in equations 4-10 and 4-11, in combination with the provision in EC-8 (2000) for increased ductility. As a result, only 40% of concrete contribution for DC “M” RC buildings is accounted for in the calculation of the ultimate shear capacity of a member (eq.4-12).

$$V_{rd1} = [\tau_{rd} k(1.2 + 40\rho_1) + 0.15\sigma_{cp}]bd \quad \text{eq.4-10}$$

$$V_{wd} = \frac{A_{sw}}{s} 0.9d f_{ywd} \quad \text{eq.4-11}$$

$$V_{rd3} = 0.4V_{cd} + V_{wd} \quad \text{eq.4-12}$$

Where:

V_{rd1} design shear resistance without shear reinforcement

ρ ratio of longitudinal reinforcement

σ_{cp} ratio of axial force to cross-sectional area

V_{wd} shear link contribution

V_{cd} concrete contribution

V_{rd3} design shear force of a member with shear reinforcement (FIP in Figure 4.16)

Further to the definition of the shear capacity, the calibration of the monotonic envelope in Figure 4.16 requires the calculation of stiffness $K1$. The shear stiffness of a member depends on the shear modulus (G) of the material, the shear area of the cross-section and the shear span of the member. As it was stated earlier in the section, cracked shear area is assumed for the definition of $K1$, which is a realistic simplification since the magnitude of shear deformations prior to the attainment of ultimate shear capacity is very small.

At this point the calibration procedure for each capacity model is established. In the next chapter an attempt is conducted to verify the effectiveness of these models and the applicability of DRAIN-3D based on the results obtained from a full-scale shaking table testing of an RC frame.

Chapter 5

VERIFICATION of ANALYTICAL TOOL

5.1. Data for Verification of Analytical Tool

Drain-3D has been used extensively by many researchers in the field of seismic analysis (Deng, 2000, Rubiano, 2001, Shin, 2004, Karayannis, 2005, etc.). However, few researchers have examined the accuracy of the degradation models by using full-scale data, and most work has been done at the element level (Deng, 2000, Shin, 2004 and Karayannis, 2005). In order to address this issue the Construction Innovation research group at the University of Sheffield received support from the European Union (ECOLEADER PROJECT N° 2 - SEISMIC TESTS ON A REINFORCED CONCRETE BARE FRAME WITH FRP RETROFITTING, 2004) to participate in the full-scale seismic testing of a two storey full-scale RC frame. The testing was conducted at the mechanical seismic studies laboratory EMSI (d'Etudes De Mecanique Sismique) at CEA research centre (Commissariat à l'Energie Atomique) in Saclay, Paris (Chaudat, 2005). The aim of the project was to assess different strengthening strategies and techniques on a damaged RC frame. Therefore, the frame was intentionally designed for low seismic loading, with poor detailing and no capacity design considerations. Tests were initially conducted on the bare frame and were repeated after the damaged frame was retrofitted using FRP sheets.

For the purpose of the verification of the degradation models in DRAIN-3D the results obtained during the testing of the bare frame are used. The following section gives details of the frame and the results of the tests.

5.1.1. Design Details of the frame

The geometry of the frame is summarised as follows:

- Total height of the specimen: 6.87m
- 4 square columns: 260mm section
- 2 square slabs: 120mm thickness and 4.26m width
- 4 beams per slab: 400mm thickness and 260mm width

The self-weight of the structure is around 20 tons. Additional masses were provided to the building for the testing in the form of two steel plates, with mass equal to 9 tons each, fixed under each slab. The detailing of the connection between the masses and the slabs was designed to enable the free rotation of the slab as shown in figure 5.1. In this way the stiffness of the plate does not prevent the slab and subsequently the beams from deforming.

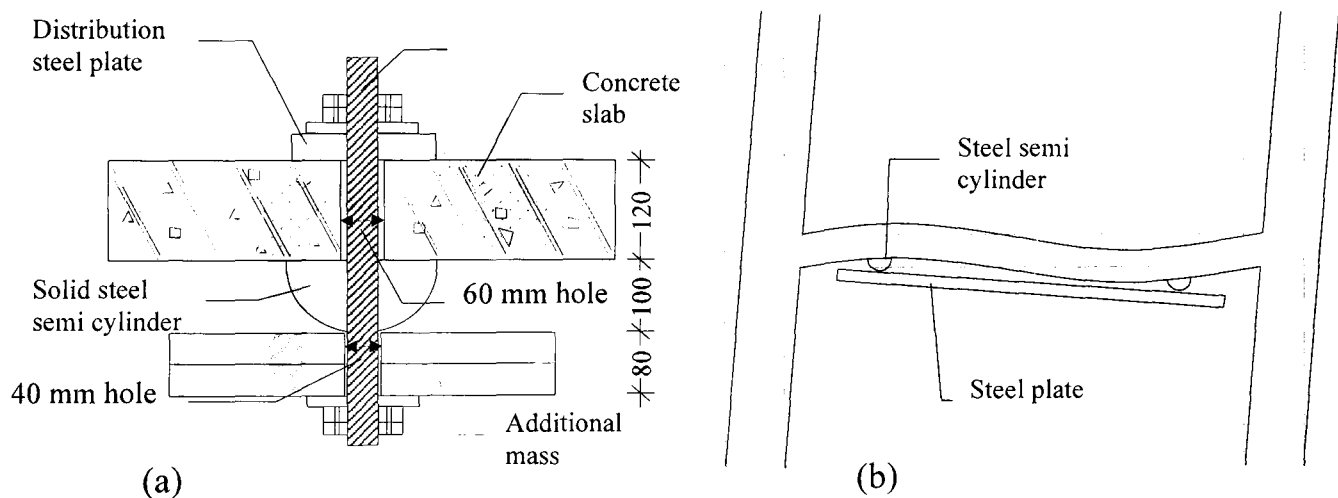


Figure 5.1. a) Connection detail of steel plate, and b) free rotation of the slab (reproduced from Chaudat, 2005)

The reinforcement details of the members are summarised below and can be seen in Figure 5.2 along with a plan view of the frame.

- Longitudinal reinforcement:
 - Columns: 1st floor: $3\phi 14 + 2\phi 14 + 3\phi 14$
2nd floor: $2\phi 14 + 2\phi 14$
 - Beams: top and bottom: $4\phi 14$
- Transverse reinforcement:
 - Columns: $\phi 6/200$ stirrups

- Beams: ϕ 8/300 stirrups
- Slab Reinforcement: steel mesh top and bottom: ϕ 9 mm – 100x 100mm
- Distance to the centre of reinforcement: 30 mm

The reinforcement consists of Fe500-3 (equivalent to Class C in EC-2, 2004) bars. Tests were performed to determine the mechanical properties of 8mm and 14mm diameter bars. The results are shown in Table 5.1. Conventional elongation (A%) refers to the elongation at mid-point of the bar where necking occurs. It is suggested that this strain is 2.5 times higher than the ultimate steel strain (Dritsos, 2008) which is required for subsequent analysis. In addition, the design compressive strength of concrete was 20MPa. To assess the properties of concrete, 12 cylindrical concrete specimens from each floor were sampled during pouring and tested. The results are shown in Table 5.2.

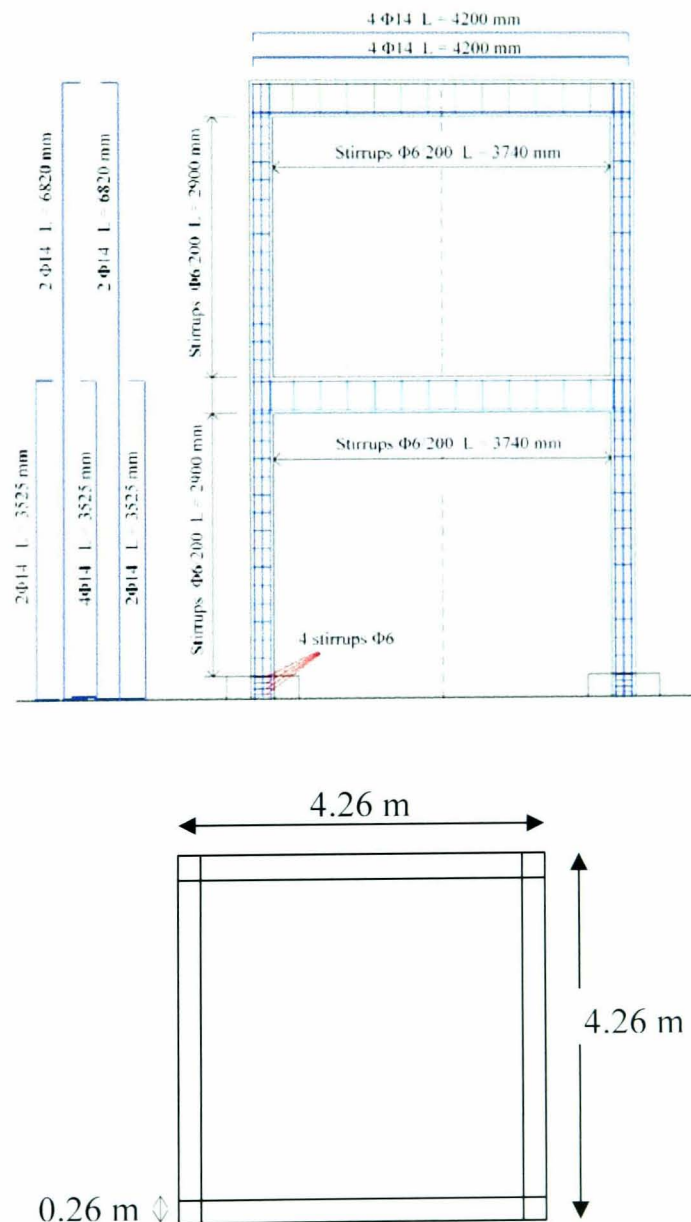


Figure 5.2. Reinforcement details of the elements (Chaudat et al., 2006) and plan view of the frame.

Table 5.1. Steel Mechanical Properties (Chaudat et al., 2005).

Diameter (mm)	Yielding Limit (MPa)	Tensile Strength (MPa)	Conventional Elongation A%
8	582	644	25
14	551	656	23.6

Table 5.2. Concrete Mechanical Properties (Chaudat et al., 2005).

	Mean Compressive resistance (MPa)	Tensile Resistance (MPa)	Elastic Modulus E (MPa)
Floor 1:	22.1	2.1	25590
Floor 2:	19.6	2.07	23500

5.1.2. Reinforcement detailing

The significance of proper anchorage of longitudinal bars for seismic design is emphasised in modern design codes EC-8 (2004). Adequate anchorage is regarded as the most important detailing provision in order for the reinforcement to yield and the element to achieve ductility.

In the case of the Saclay frame the detailing of the columns was supposed to simulate detailing provided by old codes. A very short anchorage length was initially used, but that led to disproportional damage to the joints. As a result, the details were modified for the column reinforcement bar; anchorage bars were welded on short re-bar lengths. The beam reinforcement anchorage was provided in accordance to BS8110. The spacing of the links was 200mm in the columns and 300mm in the beams in accordance to old construction practice.

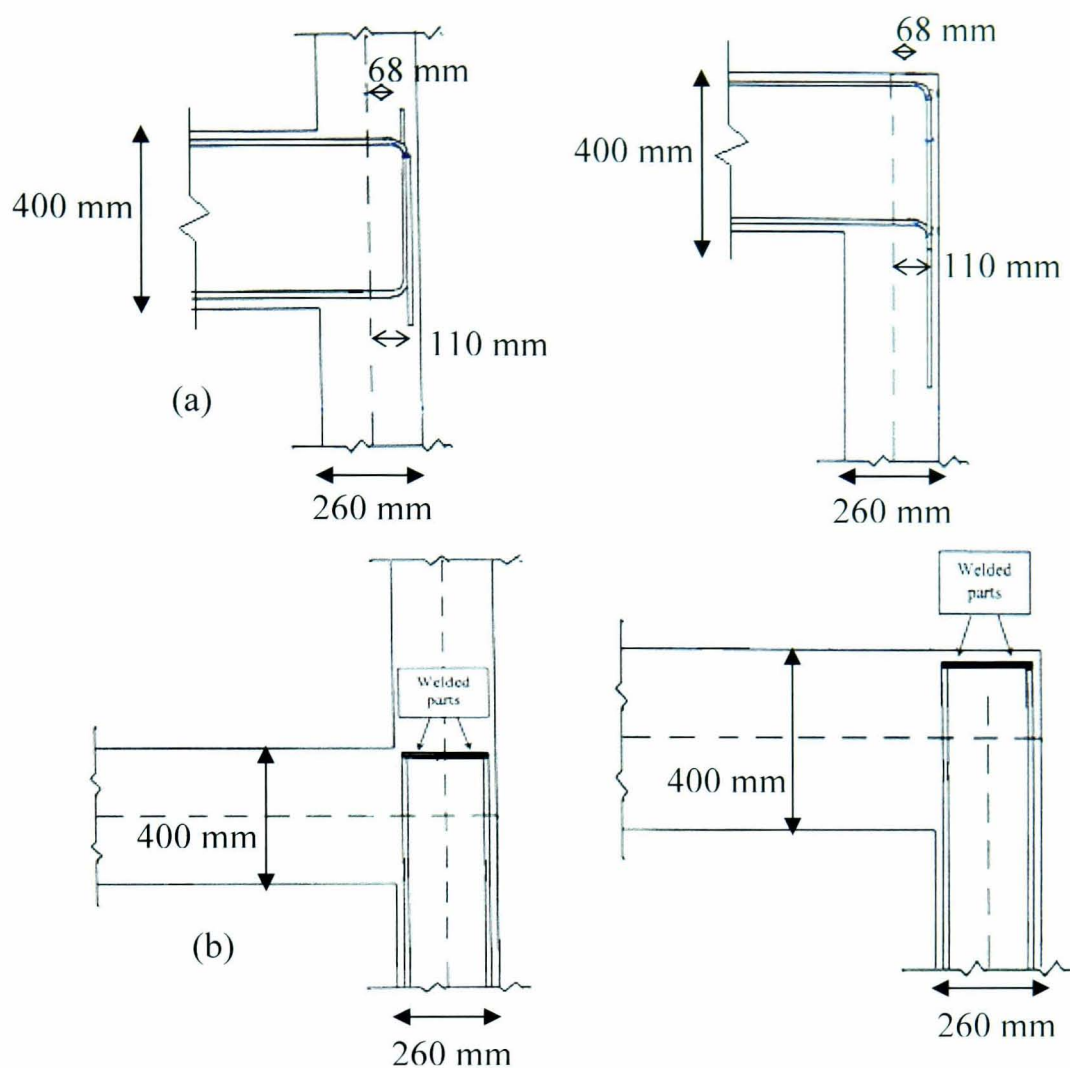


Figure 5.3. Anchorage details of 1st and 2nd storey (a) beams, and (b) columns (Chaudat et al., 2006).

The detailed drawings and in place arrangement of the anchorage arrangement at the top of the 1st and 2nd storey joints are shown in Figures 5.3 and 5.4.



Figure 5.4. Detail of anchorage of column bars at the top of the storey joints (Chaudat, 2005).

At the base of the column the aim was to ensure fully fixed support conditions. The column reinforcement was anchored by welding at the base of a steel box, which served as a foundation. The steel box was 270mm deep and 700mm square in plan and was anchored with the use of 30mm bolts onto the shaking table platform. An additional measure to ensure no rotation at the column ends was the placement of a horizontal tie bars ($\Phi 16$) welded at the sides of the steel box as shown in Figure 5.5.

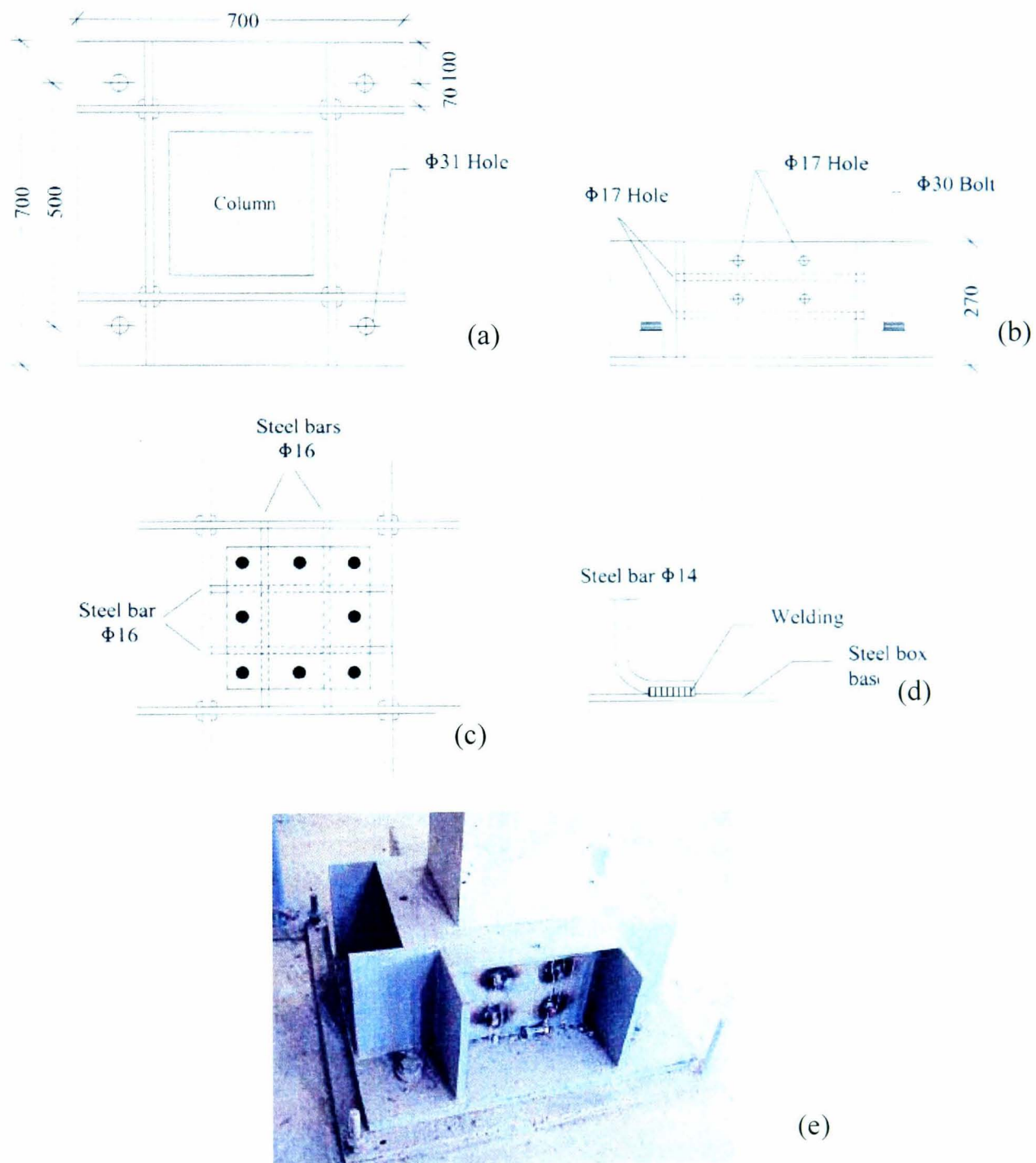


Figure 5.5. (a-d) reproduced from Chaudat, 2005), a) Plan view of the steel box, b) Side view of the steel box, c) Cross-section of a typical steel box, d) Column bar welding detail into the steel base and e) Isometric view of the foundation (obtained from Chaudat, 2005).

5.1.3. Instrumentation

The behaviour of the frame members was monitored both globally and locally. Both force and displacement readings were taken at all nodes. The force at the nodes was computed with the use of capacitive accelerometers whereas the corresponding displacements were read from the LVDT (Linear Variable Differential Transformer) displacement transducers fitted on a retaining wall at one side of the frame. The exact locations of all the transducers are shown in Figure 5.6.

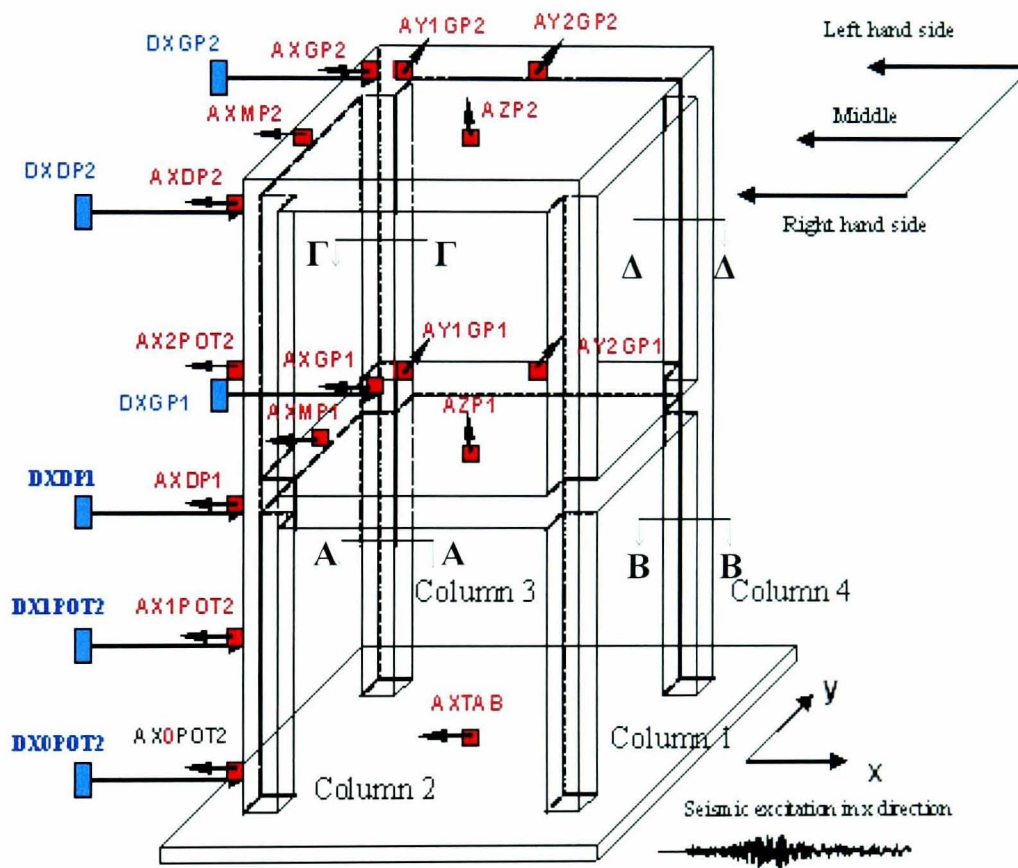


Figure 5.6. Location of Displacement and Acceleration transducers (Chaudat, 2005).

All accelerometers and displacement transducers have a specific code which identifies their measuring direction and position. The general form is **IDPF** and the description for each letter is the following:

- I** stands for type of instrumentation
[D = displacement transducer and A =accelerometer]
- D** measuring direction [X,Y,Z = x, y and z direction respectively]
- P** position of the instrumentation [G = left, M = middle, D = right] (Figure 5.6)
- F** floor level [P1 = floor 1, P2 = floor 2 and if it is an intermediate level
POT(number); where number is the number of the column]

For example, DXGP2 is a displacement transducer, in the x direction, bonded on the left hand side and located on the second floor (level of the slab) of the building. It should be mentioned that the nomenclature was based on the French vocabulary, hence G stands for *gauche* (left), M for *moyen* (middle), D for *droite* (right), P for *plancher* (floor) and *Pot* for column.

As far as the local response of steel bars is concerned, strain gauges were placed on steel bars at locations close to the joint where plastic behaviour is expected to take place (Figures 5.7 and 5.8). The sections in Figure 5.7 refer to Figure 5.2. These gauges also serve as a means to identify slip of the reinforcement. They were placed on selected bars with inadequate development length at a distance of 130mm from the column-joint interface thus they were expected to be close to the middle of a possible plastic hinge (Figure 5.8).

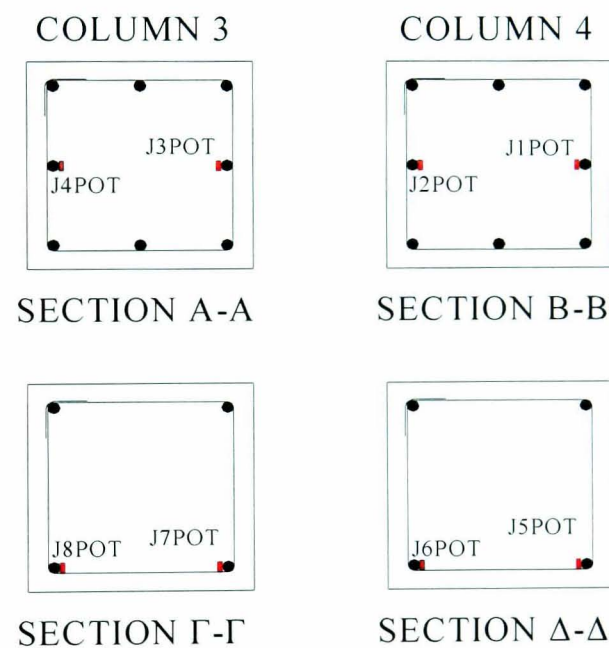


Figure 5.7. Location of strain gauges on steel bars (reproduced from Chaudat, 2005)

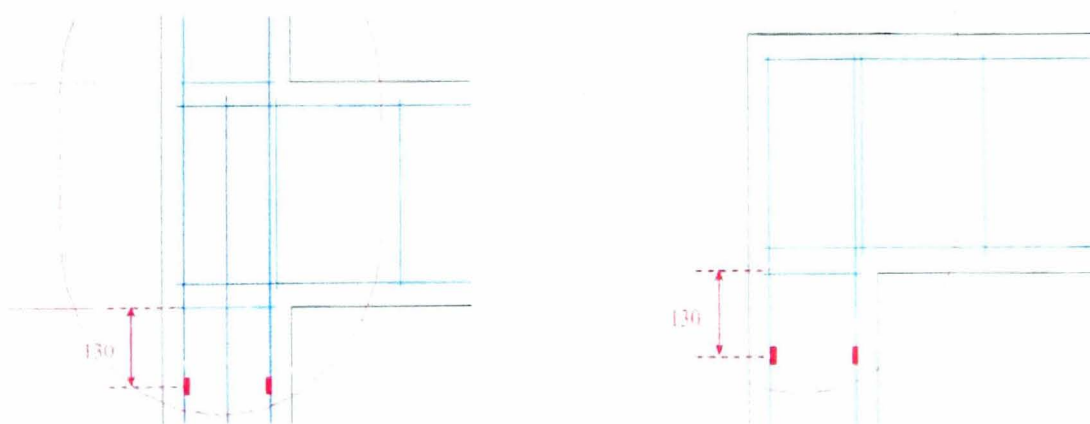


Figure 5.8. Location of strain gauges relative to the column-joint interface (Chaudat, 2005).

5.2. Shaking Table Tests

During the tests on the bare frame 5-uni-axial seismic tests with artificial acceleration records and increasing peak ground acceleration (PGA) levels from 0.05g to 0.4g were applied on the structure. The natural frequencies of the frame were measured before and after each test by white noise tests. The first and second natural frequencies of the frame before testing were measured as 1.9Hz and 5.6Hz respectively.

The artificial acceleration signal used as input on the shaking table, was generated using as a target the EC8 elastic response spectrum corresponding to a medium soil category (type C), which simulates the magnitude of the input on a structure located on medium dense sand. The excitation acceleration signal had a duration of 40 seconds with a frequency rate of 100 Hz and the spectrum of this signal, calculated with a damping of 5%, is given in Figure 5.9.

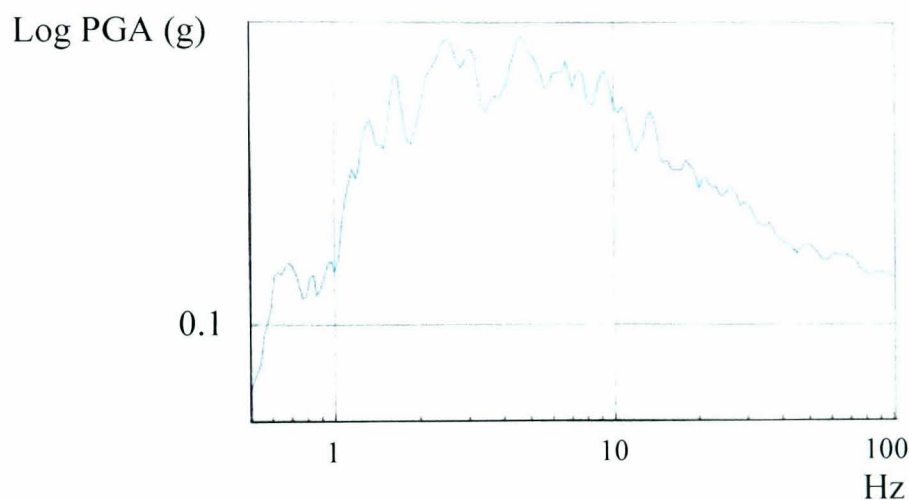


Figure 5.9. Spectrum of the acceleration signal (Chaudat, 2005).

A more detailed description of the experiment can be found in Chaudat (2005).

5.3. Observed Damage

Five tests were conducted corresponding at each PGA level shown in Table 5.3. The recorded natural periods of vibration of the frame after each seismic test, obtained by low level white noise excitation, are also shown in the same table.

The damage after each test was marked on the frame elements with the use of marker lines to represent cracking patterns. In this way it is easier to see the level at which

cracks are formed and how they developed as the shaking strength increased. A general conclusion drawn from the damage observation is that most cracks are located close to the joints and very few in beams. The damage history after each test is discussed below.

Cracking of the concrete was observed after the first two seismic tests (0.05g and 0.1g) as evident by the drop in frequency. During the 0.2g PGA test, diagonal cracking appeared on the 1st floor joints along with horizontal cracking at the top interface of the 1st floor joint. Also, horizontal cracking was observed at the interface below the 2nd floor joint. Figure 5.10 shows the damaged areas after 0.2g PGA seismic test. From the increase in period of the structure the equivalent reduction in stiffness is around 75%, which indicates severe cracking and possible yielding.

Table 5.3. Frequency change after each test (Chaudat, 2006)

PGA (g)	0	0.05	0.1	0.2	0.3	0.4
Frequency (Hz)	1.9	1.66	1.36	1.07	.88	.68
Natural Period (sec.)	0.526	0.6	0.74	0.93	1.14	1.47



Figure 5.10. Damage at the column-joint interface and column length after the 0.2g and 0.4g tests (Chaudat, 2005).

At 0.3g some new horizontal cracks were added at the top interface of the 1st floor joint, at the mid span of 1st floor columns and at the base of a single column. Finally, during the last test (0.4g PGA), cracking was visible on a column between the base and the first level. In addition, spalling of concrete at the base of the column, where horizontal cracks were formed during the previous test (0.3g PGA), was observed (Figure 5.10).

By the last test, the structure experienced a 64% frequency decrease (245% period elongation), which according to damage scales included in Russian (International Building Codes of NIS, 2001) and Armenian (Building Codes of Armenia, 1995) codes indicates severe damage (Timchenko I., 2002). A similar damage scale compiled from experimental results (Zembaty, 2006) quantitatively categorises this level of period shift in damage state five, which qualitatively corresponds severe damage at the columns and joints.

5.4. Capacity-Demand

Although the elongation in period calculated above agrees with the severity of damage observed, a closer examination of displacement and accelerations is expected to increase the understanding of the buildings' actual behaviour. For that purpose, the demand on the structure is compared to the capacity of its members to identify two key points:

1. the capacity of the structure based on modern design codes
2. the response of the structure at post-capacity demand

In order to establish the capacity of the structure, the design moment of resistance of the 1st floor column section is calculated based on the assumptions included in EC-2, (2004) concerning material safety factors ($\gamma_c=1.5$ and $\gamma_s=1.15$) and the area of the concrete compressive stress block. The factored axial load on the column was 135kN as a result of 18kN imposed and 20kN dead loading. In addition section analysis was used to calculate the yield and ultimate moment capacity of the same column cross-section with an unfactored axial load of 95kN. Using these values, the corresponding maximum shear force demand for each column is calculated by means of eq.5-1, which is based on the assumption of zero moment at the column mid-point. Therefore, the maximum base shear force demand for the whole frame can be found by adding the demand from the four columns. The capacity values for 1st and 2nd storey columns are shown in Table 5.4. The considerable reduction in flexural capacity of the 2nd floor columns is due to the severe reduction in flexural reinforcement.

$$F = \frac{2 \times M}{l} \quad \text{eq.5-1}$$

Table 5.4. Strength capacities for 1st and 2nd floor columns.

	M _d (kNm)	M _y (kNm)	M _{ult} (kNm)	F _d (kN)	F _y (kN)	F _{ult} (kN)
Floor 1	41	60	80	100	145.5	194
Floor 2	25	37	46	61	90	111.5

A backwards analysis using the Eurocode 8 (2004) relationship between base shear and PGA (eq.5-2) is used to calculate the design PGA based on modern design codes. According to Eurocode 8 (EC8:2004, equation 4.5), the base shear force is calculated as follows:

$$F_b = S_d(T_1) \cdot m \cdot \lambda \quad \text{eq.5-2}$$

Where:

T_1 fundamental period (0.526 sec)

m total mass of the building (38 tons)

λ correction factor ($\lambda=1$ for less than three-storey buildings)

$S_d(T_1)$ ordinate of the design spectrum

The ground is classified as ground type C and a type 1 elastic response spectrum is used following the relationship in eq.5-3.

$$S_d(T_1) = \alpha_g \cdot S \cdot \frac{2.5}{q} \quad \text{eq.5-3}$$

Where:

α_g design ground acceleration

q behaviour factor ($q=1.0$ for elastic design) .

S soil parameter ($S=1.15$ for soil type C)

Therefore,

$$S_d(T_1) = \alpha_g \cdot S \cdot \frac{2.5}{q} \Rightarrow S_d(T_1) = \alpha_g \cdot 1.15 \cdot \frac{2.5}{1.0} \Rightarrow S_d(T_1) = 2.875 \cdot \alpha_g$$

$$F_d = S_d(T_1) \cdot m \cdot \lambda \Rightarrow F_d = 2.875 \cdot \alpha_g \cdot 38,000 \text{kg} \cdot 1 \Rightarrow F_d = 109,250 \cdot \alpha_g \quad \text{eq.5-4}$$

By substituting F_d into eq.5-4 the design seismic demand is equal to,

$$\alpha_g \approx 0.1g$$

Since F_d (design base shear force) ≈ 100 kN as calculated before the building is expected to remain in the elastic range up to a PGA=0.1g. Its post-elastic behaviour depends on material overstrength, design safety factors and ductility of the reinforcement steel. The next section examines its post-elastic behaviour by comparing the capacity-demand after each test.

5.4.1 Post-elastic behaviour

In this section the maximum shear force demand (Table 5.4) as calculated using the flexural capacity of columns is compared with the shear demand on columns expressed by the shear force time-histories at each floor. Initially, the demand values of the 0.2g test, at which point visible structural damage has occurred and post-elastic behaviour is expected to take place, are compared with the yield demand time-histories of the two floors (Figures 5.11 and 5.12). The shear demand on the second floor is around 110kN (Figure 5.11), which is in the range of the column yield shear force capacity. Similarly, the base shear force on each column is around 160kN, which exceeds the 1st floor column yield capacity of 145kN. In light of the above results it is safe to assume that steel reinforcement in columns was close to reaching its yielding capacity at the 0.2g test.

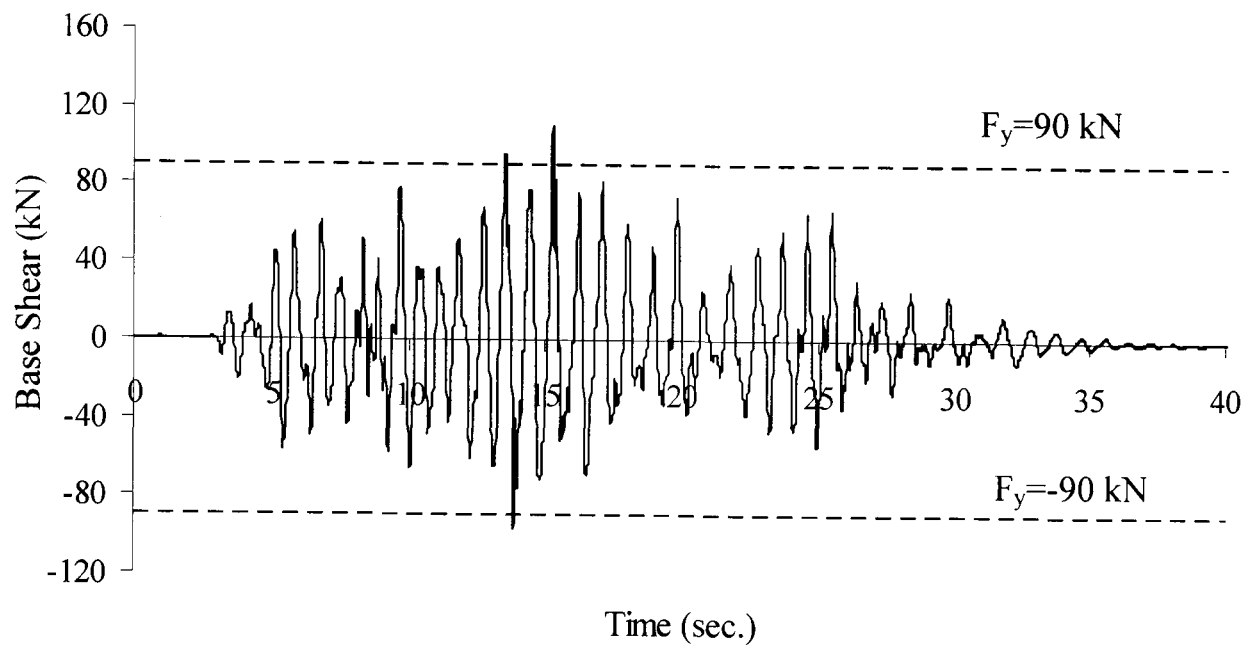


Figure 5.11. Time-history of shear force at 2nd floor after the 0.2g test.

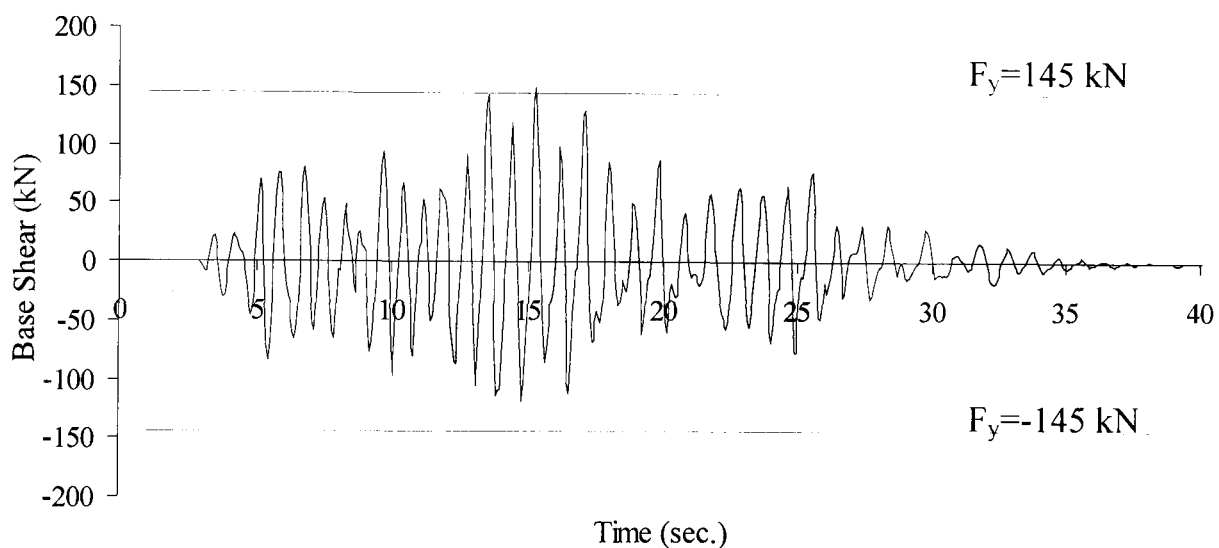


Figure 5.12. Time-histories of base shear force after the 0.2g test.

Similarly the ultimate shear force demand of the 1st floor columns is compared to the shear demand imposed during the final test (0.4g). In this case though, the column has not reached its ultimate flexural capacity (Figure 5.13) as it was expected due to strain hardening of the steel reinforcement, but remained close to its yielding capacity. Thus, a further investigation into this softening behaviour of the building after yielding needs to be conducted to identify any possible effects from failure modes other than flexure. For that purpose it is required to move a step further and examine local recordings from strain gauges, which may enlighten what happens after strain at yielding is achieved in the bars.

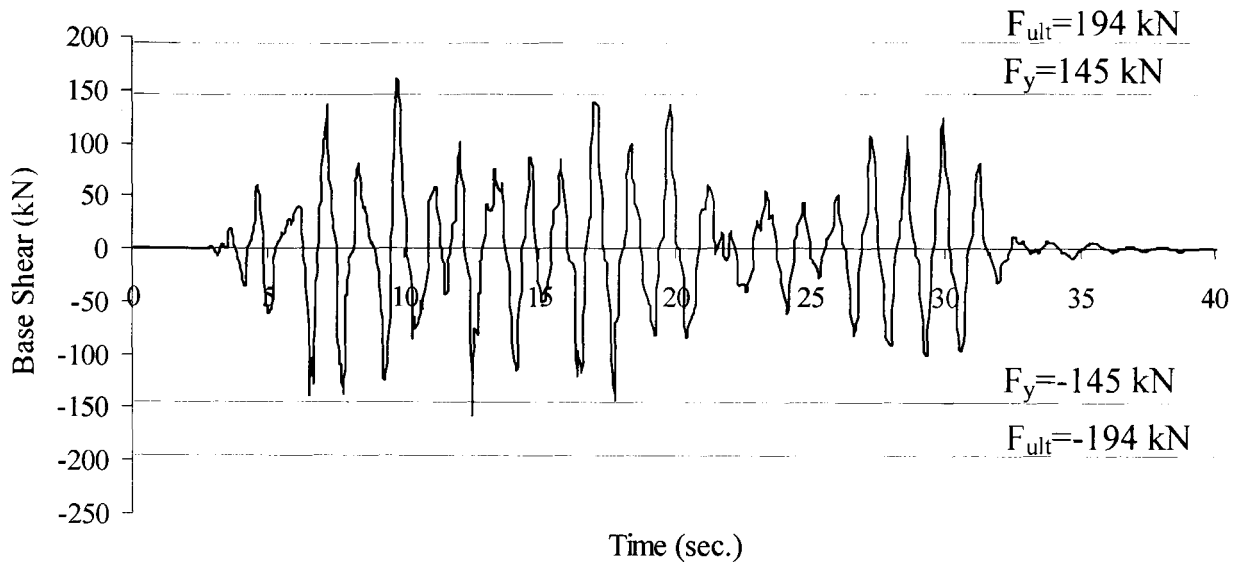


Figure 5.13. Time-histories of base shear force after the 0.4g test.

5.5. Strain histories

The investigation of the local response uses the strain histories of columns after the 0.2g test where, yielding of the reinforcement is likely to initiate. The consistency between strain results and displacements is checked for each test, using green and red circles to graphically indicate whether results are consistent or not.

5.5.1 First storey response

Unfortunately, only results from the 1st storey column (strain gauge code j3pot in Figure 5.7) were considered reliable (Figure 5.14).

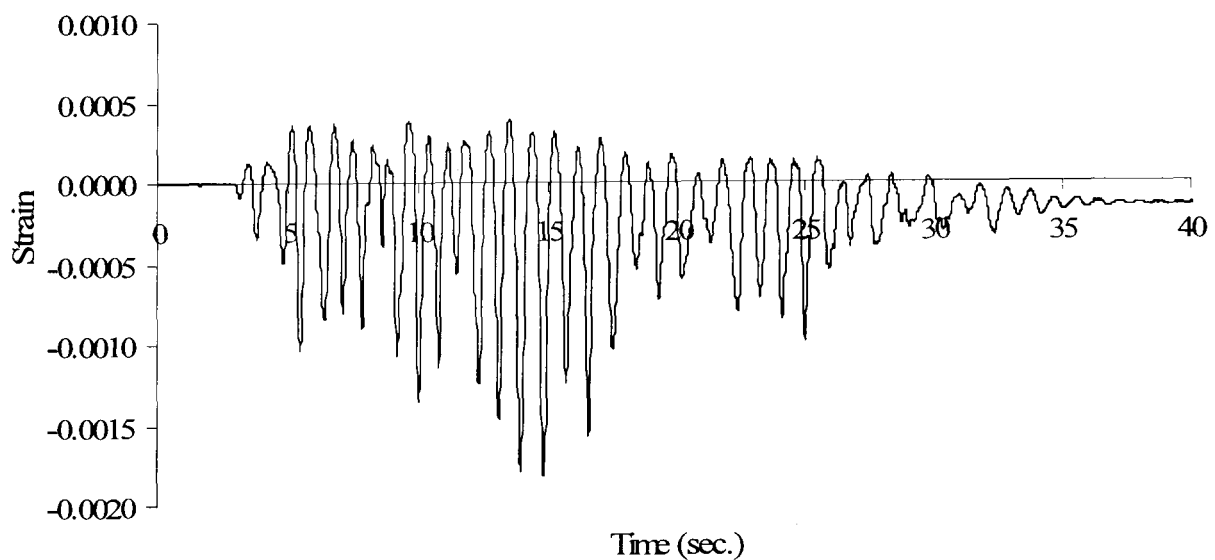


Figure 5.14. Strain history of 1st storey columns (j3pot).

These show that the maximum tensile strain is still in the elastic range (less than yield strain). Even at higher intensity seismic excitations (Figure 5.15), no yielding of the reinforcement appears to happen on this side of column 3 (see in Figure 5.7). In contrast, yielding is attained in the reinforcement as seen from results obtained in strain gauge j2pot (Figure 5.16) located in the opposite side of column 4 (see Figure 5.7), which is expected to be in tension when j3pot is in compression.

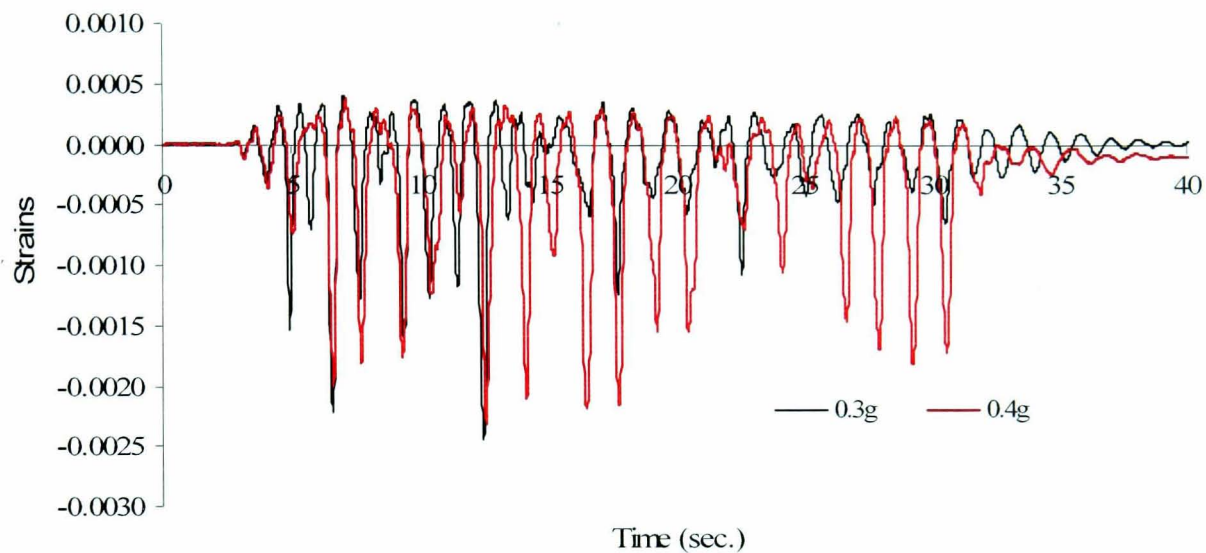


Figure 5.15. Strain histories of 1st floor column 3 for 0.3g and 0.4g (j3pot).

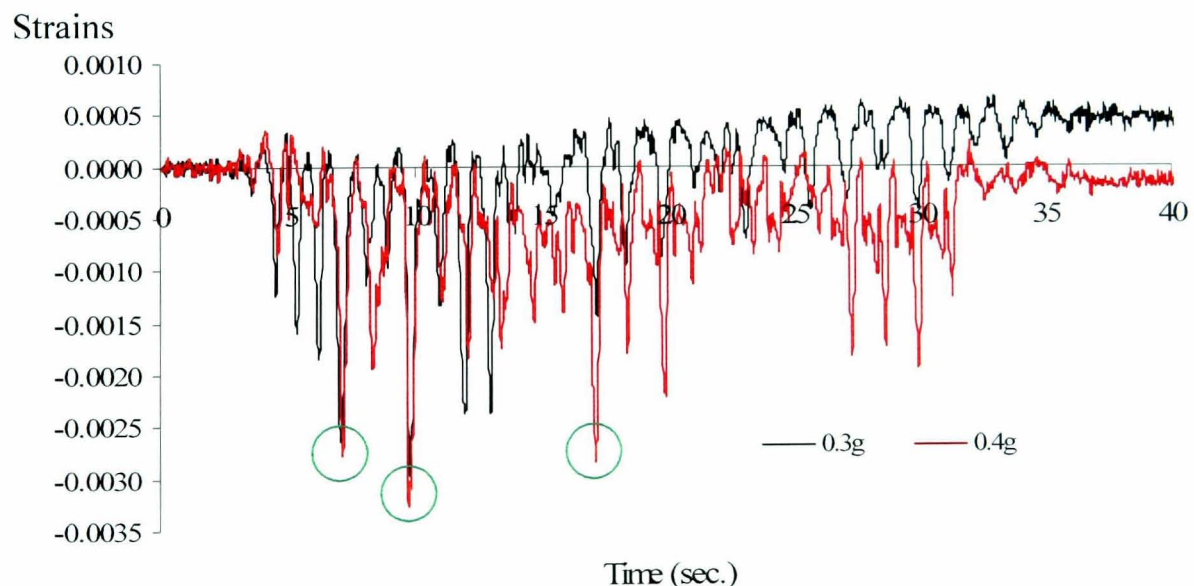


Figure 5.16. Strain histories of 1st floor column 2 for 0.3g and 0.4g (j2pot).

The ultimate strain in the yielded bars though is just above the yield strain indicating that no considerable strain hardening took place. To conclude the discussion on the 1st storey strain results, their consistency is checked against the corresponding storey displacement results for the two PGA levels shown in Figure 5.17. The peak displacement values circled in green colour in Figure 5.17 can be traced in the

corresponding green circles of Figure 5.16. Hence, without further analysis it is difficult to conclude that there were any significant problems in this storey.

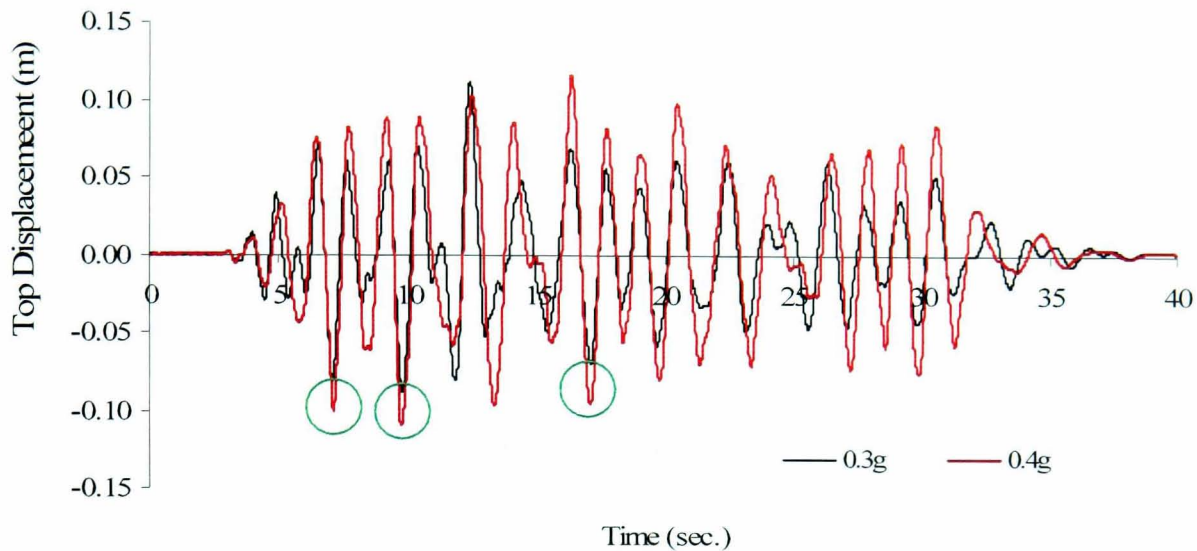


Figure 5.17. 1st storey displacement records.

5.5.2 Second storey response

In the absence of reliable strain results for the 2nd storey columns at 0.2g, the investigation focuses on the two remaining tests. Strain history of j8pot (Figure 5.18), which is located on column 3 that undergoes higher tensile excitation (at the level of reinforcement above j4pot) shows yielding of the reinforcement at $t=6.6$ seconds, and further yielding at $t=12.4$ seconds

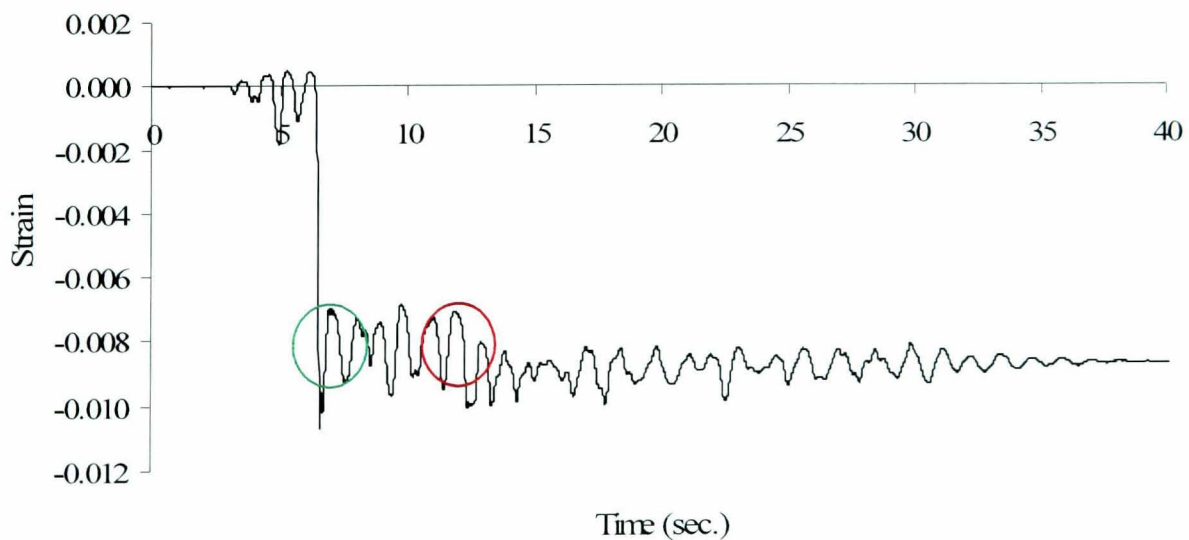


Figure 5.18. Strain history of 2nd floor column 3 (j8pot) for 0.3g.

By examining the corresponding top displacement history, a peak displacement (green circle in Figure 5.19) appears to occur at the time of first yielding $t=6.6$ seconds. A

second peak at 12.4 seconds also coincides with the second yielding of the bar (red circle in Figure 5.19).

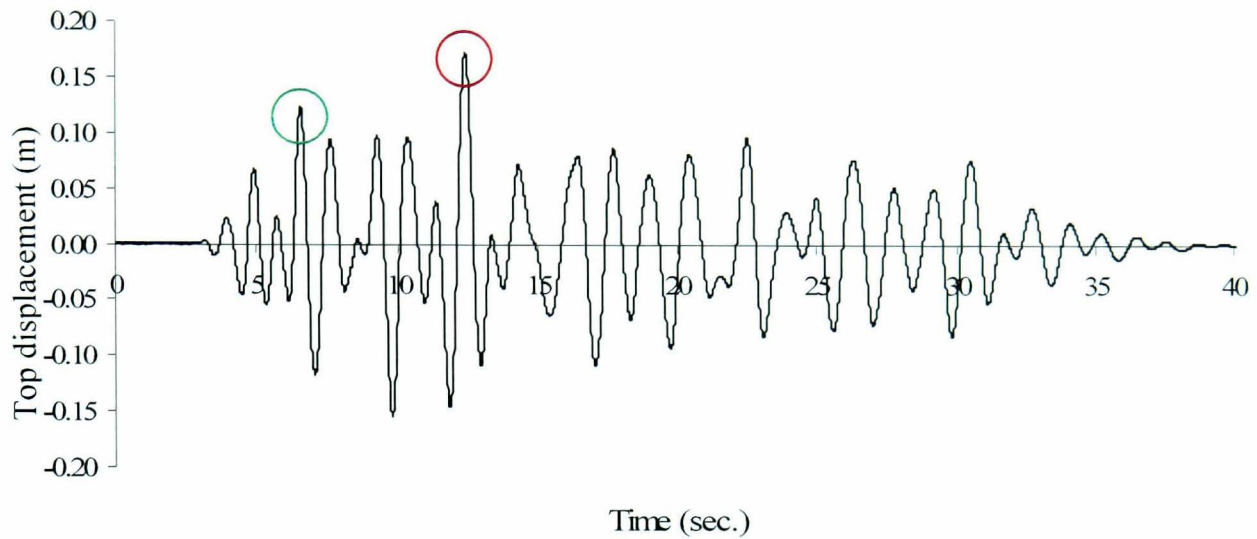


Figure 5.19. Top storey displacement history at 0.3g.

Although the second yield displacement is higher than the first, lower extra yield strains were added. In addition, the strain cycles after this point are smaller than expected from the displacement levels observed. The combination of these observations leads to the conclusion that some kind of softening of the building occurs after yielding.

The strain history of the same strain gauge at 0.4g (Figure 5.20) shows the yielding of reinforcement also consistent with the peak displacement (Figure 5.21). However, the residual strain levels at subsequent yielding (red circles in Figures 5.20 and 5.21) are considerably lower than expected from approximately equal displacement levels as the first yielding, which may indicate loss of bond.

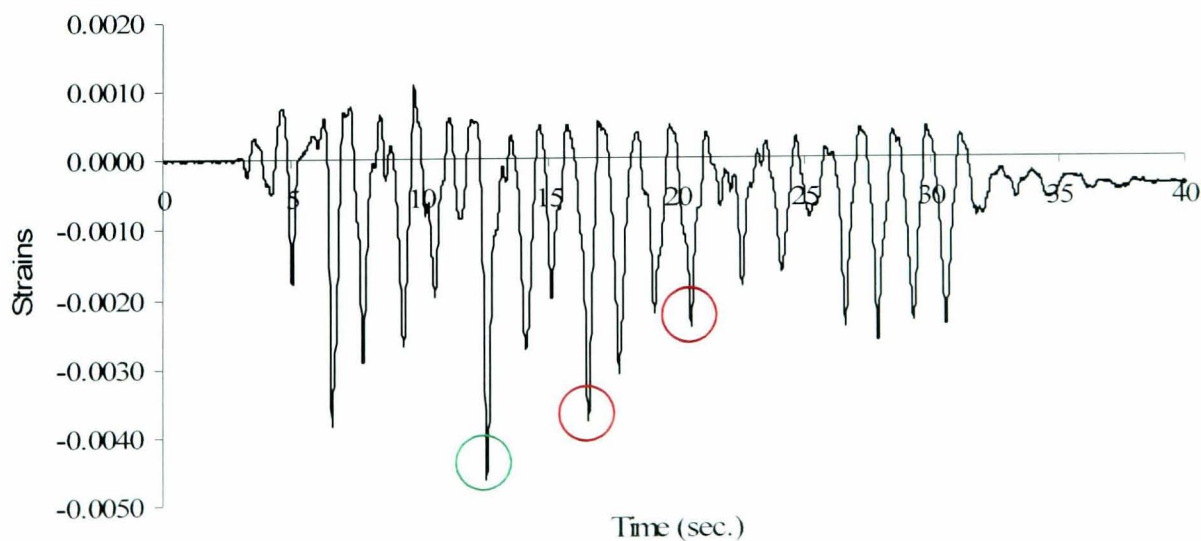


Figure 5.20. Strain history for j8pot at 0.4g.

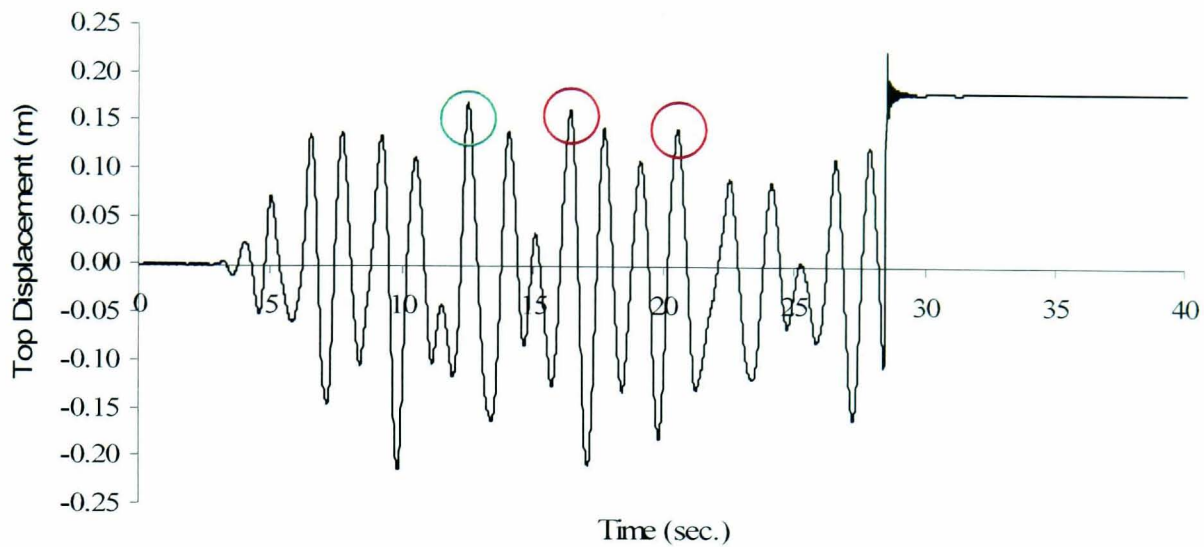


Figure 5.21. Top storey displacement history at 0.4g.

In order to determine if softening behaviour took place in the columns, it is necessary to undertake global time-history analysis with the incorporation of sophisticated models such as the ones discussed in Chapter 4.

5.6. Modelling of the Saclay frame in DRAIN-3D

The remaining of the chapter discusses the simulation of the shaking table results obtained from the Saclay frame testing. Due to symmetry, 2D time-history analysis is conducted on half the frame. This section addresses all issues involved with the modelling of the structural and dynamic characteristics of the frame based on the whole spectrum of modelling capabilities provided by DRAIN-3D. The final section of the chapter includes the comparison of the experimental recordings with the analytical results and the final conclusions regarding the frame response.

5.6.1 Section modelling

Section geometrical properties follow the dimensions given in 5.1.1. An example of the section discretization process is given in Figure 5.22 for the 1st floor column of the Saclay frame. The cross-section is divided into 4 concrete and 8 steel fibres. This discretization pattern of concrete fibres was determined after a small parametric study to simulate accurately the flexural behaviour of the section. Thus a finer grid, which would be more time consuming, was avoided.

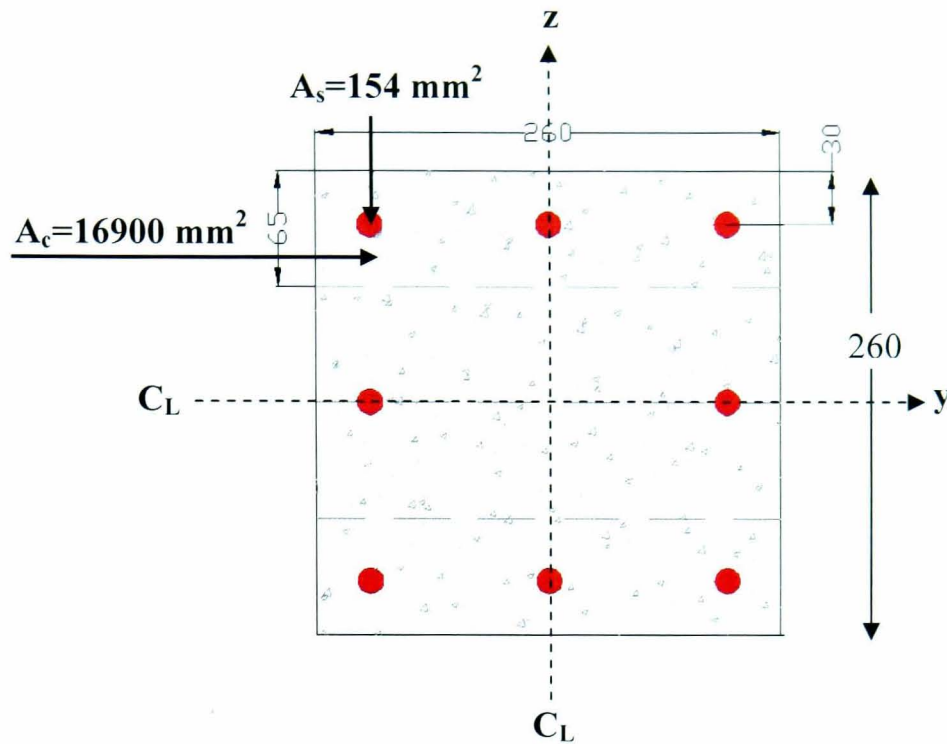


Figure 5.22. Layout of the fibre element for the 1st storey columns

5.6.2 Material modelling

The stress-strain envelopes of concrete and steel strength are shown in Figure 5.23. Five stress-strain coordinates are used to define the concrete compressive envelope in the input file, whereas two points are needed to represent the trilinear tensile (and compressive) properties of steel bars. Both models are derived using EC-2 models and ultimate strength values based on the material results given in Tables 5.1 and 5.2.

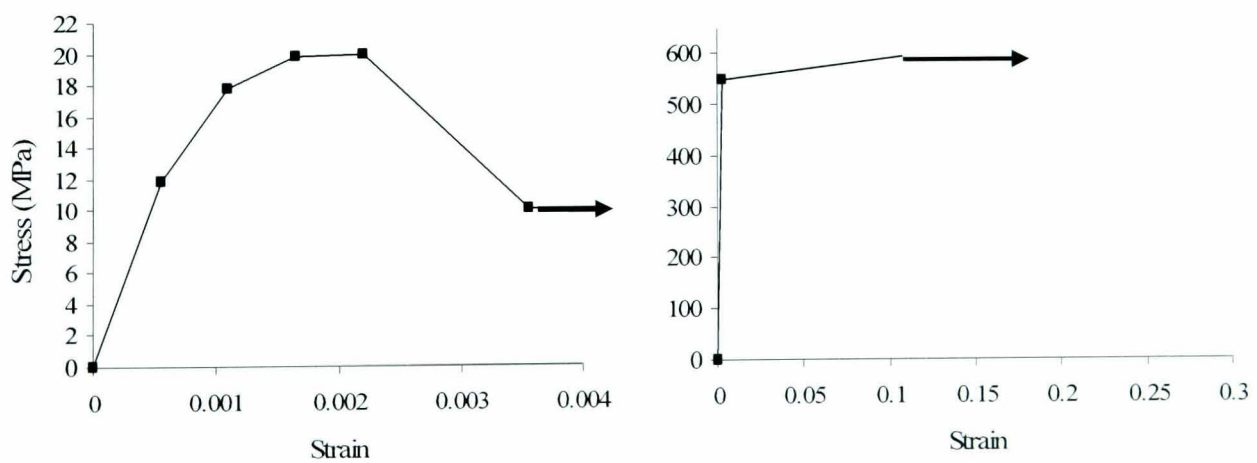


Figure 5.23. Stress-strain envelopes of concrete and reinforcement steel.

Concrete compressive stress value at ultimate strain depends on the level of confinement and on the axial load (Pilakoutas, 2007). The exact crushing stress due to flexure can be obtained from section analysis hence a lower stress value was used to

account for all possibilities and to eliminate numerical instability problems. In addition, modelling of the tensile properties of concrete is neglected since their effect at high seismic excitation levels is regarded as minimal.

5.6.3 Moment-curvature relationships

To verify the effectiveness of the section discretization described in 5.6.1 the moment-curvature results obtained by DRAIN-3D for the corresponding column section are compared to results given by a widely used fibre section analysis software XTRACT (Imbsen, 2002) and manual section analysis calculations based on EC-2 models. The cross-section characteristics are as shown in Figure 5.22. The $M - \phi$ curves show exact agreement with DRAIN-3D (Figure 5.24), which verifies the accuracy of the section analysis element in DRAIN-3D in predicting member flexural response.

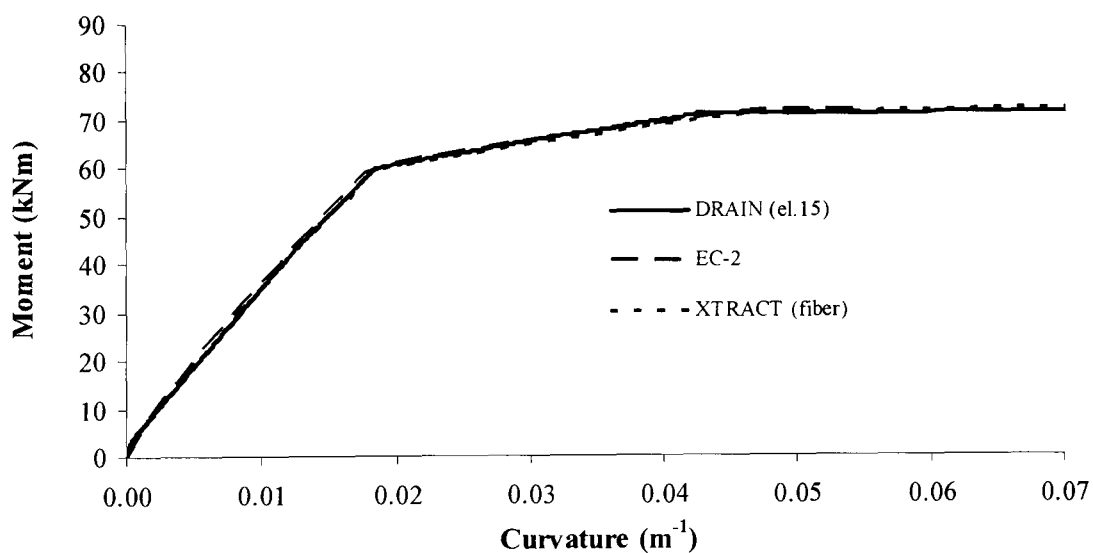


Figure 5.24. Comparison of moment-curvature curves for 1st floor columns.

5.6.4 Modelling slip deformations

The need to include additional deformations due to bar slip was identified in 5.5. Based on the findings from the local strain response analysis, softening of the structure due to bond slip was suspected in the columns of the 2nd storey. The softening effects were activated after the yielding of the reinforcement, and contributed to additional deformations.

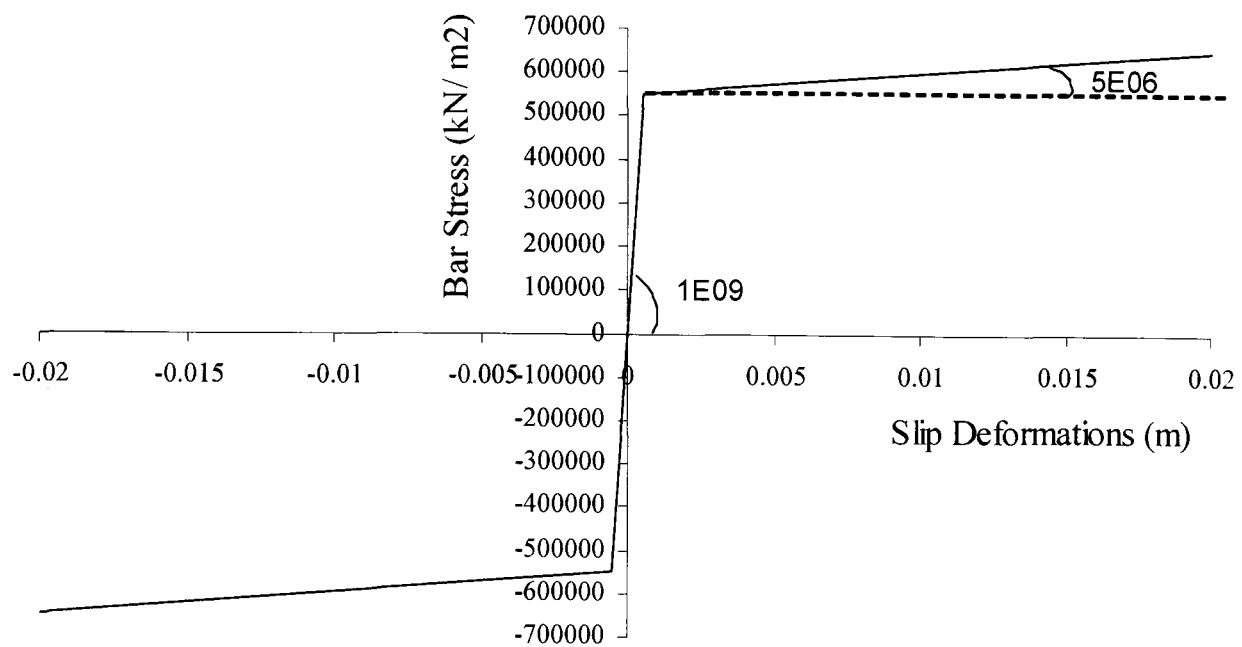


Figure 5.25. Backbone curve of pullout hinge.

Slip deformations at yielding and ultimate stress values are calculated using the models given in 4.3.2.1 for unconfined concrete. The resulting backbone curve is shown in Figure 5.25. The model is completed by applying the hysteretic rules for the simulation of degradation in loading and unloading cycles. Based on the findings of the strain analysis no strength degradation below f_y is applied in the model since the yield strength was achieved. Unloading stiffness is set equal to the initial stiffness based on the CEB (1993) cyclic bond model whereas full pinching degradation is assumed in the unloading curve based on findings from cyclic experimental pullout tests conducted by various researchers, such as, Viwathanatepa et al. (1979). In addition, unloading stiffness and pinching behavior is consistent with cyclic bond models derived by Tassios (1979), Balazs (1991), Monti et al. (1997), Filippou (1999) and Elmorsi et al. (2000).

5.6.5 Modelling of joints

Joints are modelled using a combination of a linear element to account for the elastic joint deformations, and a nonlinear shear element, described in 4.3.3 to account for additional shear deformations. The joint is modelled to behave linear elastically with stiffness equal to EI_{cr} up to the attainment of its shear capacity. In the case of the Saclay frame $E=29\text{GPa}$ and $I_{cr}=0.5*I_g=0.0019$. Elastic shear deformations in this joint are

modelled using the cracked shear stiffness $\frac{GA_{cr}}{l}$ of the column (Figure 5.26). The shear capacity of the joint is calculated using equation 4.12.

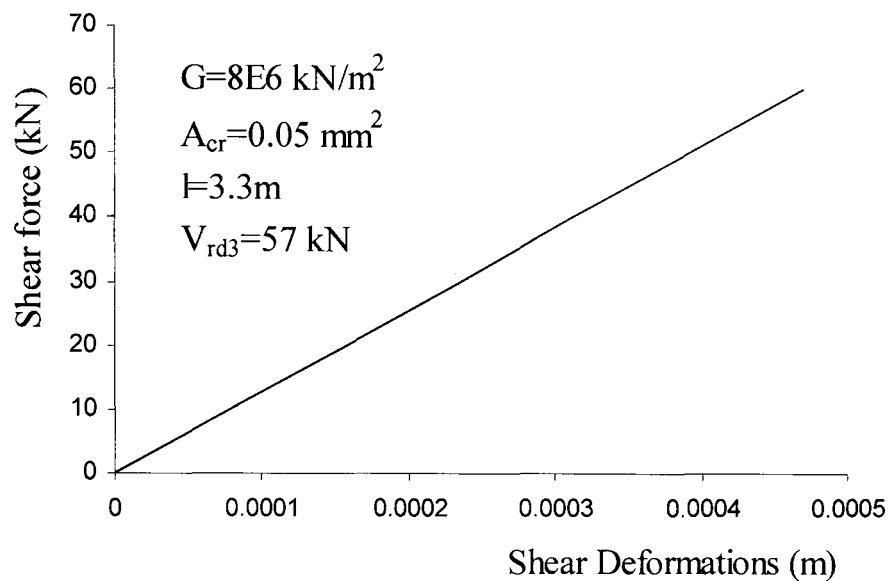


Figure 5.26. Model for elastic shear deformations

Since the shear column capacity (V_{rd3}) is higher than the shear force demand observed in Figure 5.13 (around 150kN for 4 columns) the shear model is calibrated only for elastic response.

5.6.6 Segment distribution

Each member is divided in three segments to account for the spread of plasticity. Two segments at the member ends having a length of 10% of element length are used to model the plastic hinge region based on the guidelines of Isakovic and Fischinger (1998). This segment distribution leads to accurate results with the least computational effort.

5.6.7 Frame Mass

The mass of the structure is modelled in DRAIN-3d with the use of lumped masses at each floor. In order to calculate the total mass at each floor, the mass of each structural element at the floor is added to the imposed load of the steel plates (4.4.1). Detailed mass calculations are shown below:

- **Mass of the slab:** $(4m \cdot 4m \cdot 0.12m) \cdot (24kN / m^3) / g = 4.6tons$
- **Mass of beam:** $(4m \cdot 0.4m \cdot 0.26m) \cdot (24kN / m^3) / g = 0.99tons$
- **Mass of column:** $(3.3m \cdot 0.26m \cdot 0.26m) \cdot (24kN / m^3) / g = 0.54tons$
- **Mass of Steel plate (imposed loading):** 9 tons

Half of the floor mass is carried by each frame. Therefore the mass at each level is calculated by adding half the slab weight, the beams connected on the frame, and half the column weight above and below the floor. Consequently, the floor masses are calculated as in eq.5-5 and 5-6. :

- $m_1 = \left(\frac{1}{2} M_{slab}\right) + (2M_{beam}) + 4\left(\frac{1}{2} M_{column}\right) + \left(\frac{M_{plate}}{2}\right) \Rightarrow m_1 = 9.8tons$ eq.5-5

- $m_2 = \left(\frac{1}{2} M_{slab}\right) + (2M_{beam}) + 2\left(\frac{1}{2} M_{column}\right) + \left(\frac{M_{plate}}{2}\right) \Rightarrow m_2 = 9.2tons$ eq.5-6

5.6.8 Damping

DRAIN-3D accounts for the effect of linear damping through Rayleigh damping coefficients for mass and viscous element related damping. The damping matrix is assembled together by adding the effects of each damping coefficient.

$$c = \alpha_0 m + \alpha_1 k \quad \text{eq.5-7}$$

Where:

α_0 mass damping coefficient

α_1 element viscous damping coefficient.

Based on the above equation, the damping ratio of mode n is calculated as follows:

$$\zeta_n = \frac{\alpha_0}{2} \frac{1}{\omega_n} + \frac{\alpha_1}{2} \omega_n$$

The coefficients α_0 and α_1 can be calculated for the corresponding damping ratios ζ_i and ζ_j of the i th and j th mode by solving the following matrix equation

$$\frac{1}{2} \begin{bmatrix} 1/\omega_i & \omega_i \\ 1/\omega_j & \omega_j \end{bmatrix} \begin{Bmatrix} \alpha_0 \\ \alpha_1 \end{Bmatrix} = \begin{Bmatrix} \zeta_i \\ \zeta_j \end{Bmatrix}$$

Where:

ω_i, ω_j angular frequencies of each mode of vibration ($\omega = 2\pi f$)

The initial natural frequencies for the 1st and 2nd mode of vibration of the building are 1.9Hz and 5.6Hz ($\omega_1 = 11.94\text{rad/s}$ and $\omega_2 = 35.18\text{rad/s}$), respectively. Damping ratios of 5% and 2.5% for the two modes of vibration are assumed for the determination of α_0 and α_1 for elastic analysis (up to 0.1g). For higher PGA levels the effect of Rayleigh damping is reduced linearly with the reduction in frequency since hysteretic damping dominates the response.

5.7. Correlation of experimental and analytical dynamic results

The correlation of the experimental shaking table results with the analytical predictions described in 5.6 is examined in this final section of the chapter. The cumulative damage caused by each successive exposure to the various levels of seismic excitation is accounted for in the analysis by continuing the analysis after each event. Bond-slip deformations are included in the analysis when shown to be necessary to capture the frame behaviour. A comparison of the recorded results versus the predictions for the first two tests (0.05g and 0.1g) shown in Figures 5.27 and 5.28 indicates an excellent correlation both as far as the peak displacement and response frequency change is concerned.

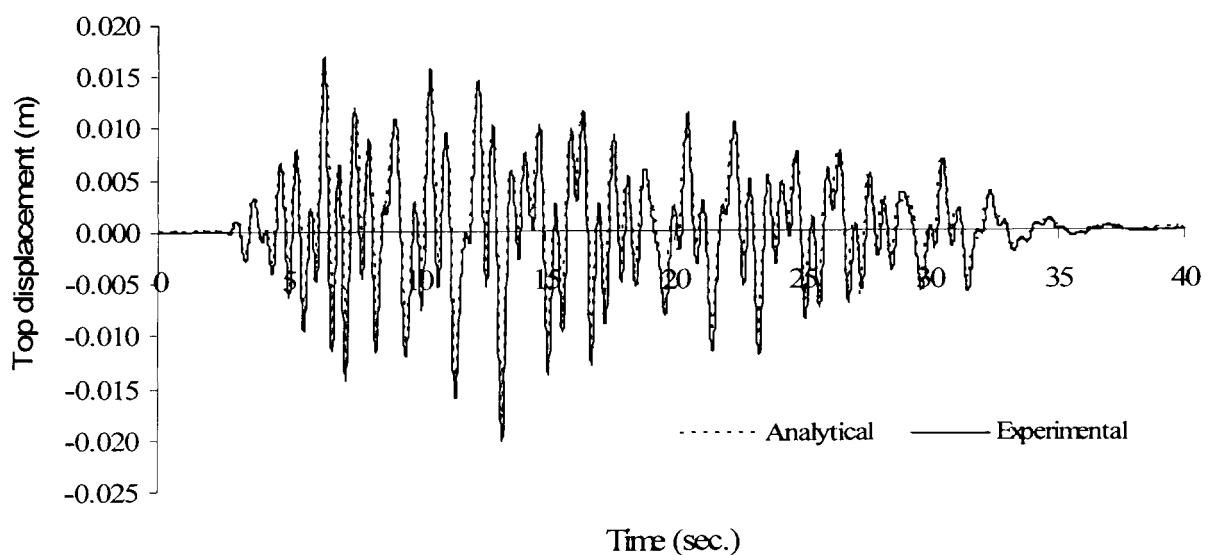


Figure 5.27. Analytical vs. experimental top storey displacements (0.05g)

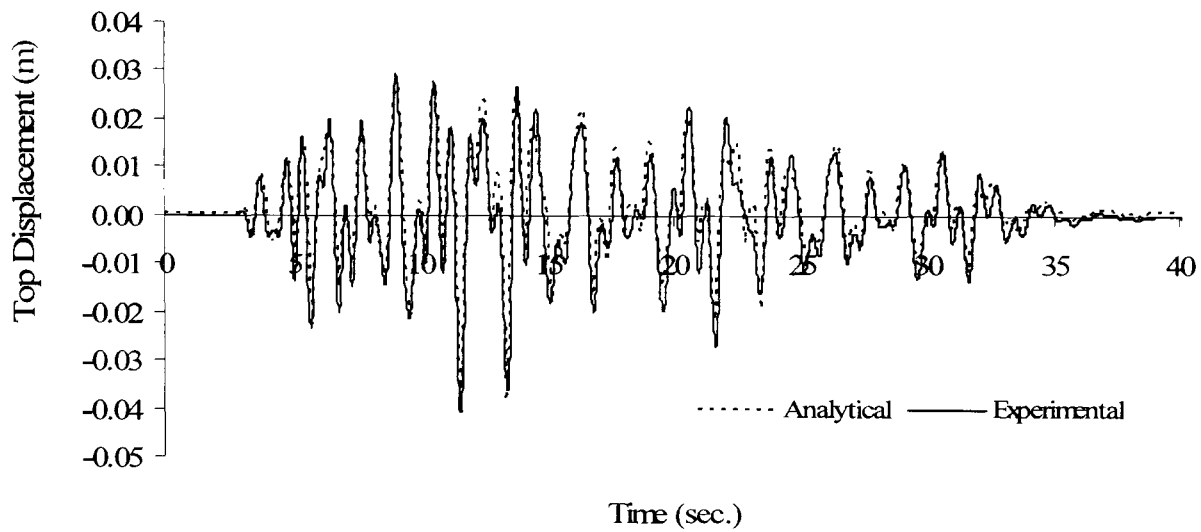


Figure 5.28. Analytical vs. experimental top storey displacements (0.10g)

The very good correlation ceases to exist at the 0.2g test as can be seen in Figure 5.29; a small difference (between recorded and predicted top displacements) begins early, after about 7 seconds, but a more considerable difference is obvious in the two peaks occurring in the negative direction just after 14.84 seconds. The initial difference in recorded results can be attributed to an underestimation of the structural damping which is expected to increase with concrete cracking. The predicted 2nd floor relative displacements (Figure 5.30) show a peak displacement in the positive direction at $t=13.84$ seconds, which according to the analytical strain results (Figures 5.31) causes yielding of the reinforcement. Given that the analysis underestimates damping and predicts yielding of the reinforcement at $t=13.84$ seconds it is very surprising that it underestimates massively the negative displacements after $t=13.84$ seconds. One possible explanation is that bond-slip starts after yielding of the reinforcement. Therefore, analysis is repeated including bond-slip deformations at 2nd storey column ends. The comparison of the revised analysis results (Figure 5.32) shows considerable improvement in simulating the displacement behaviour, which provides fairly good evidence that bond-slip deformations play a role in these tests. Further confirmation of this will be needed from the next test at 0.3g.

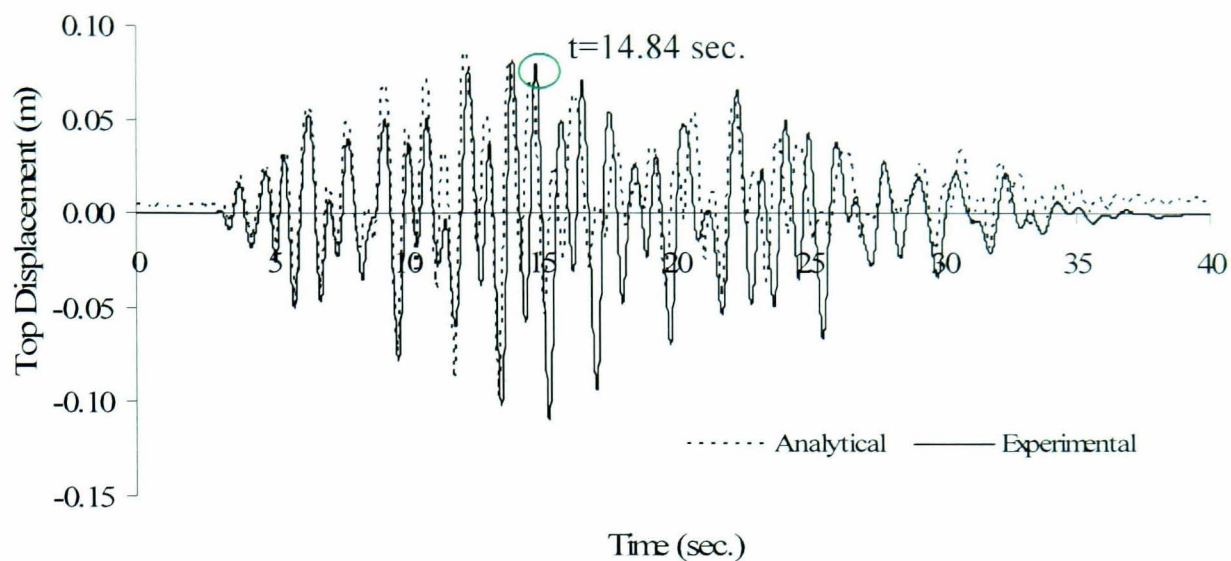


Figure 5.29. Analytical vs. experimental top storey displacement at 0.20g with no bond slip.

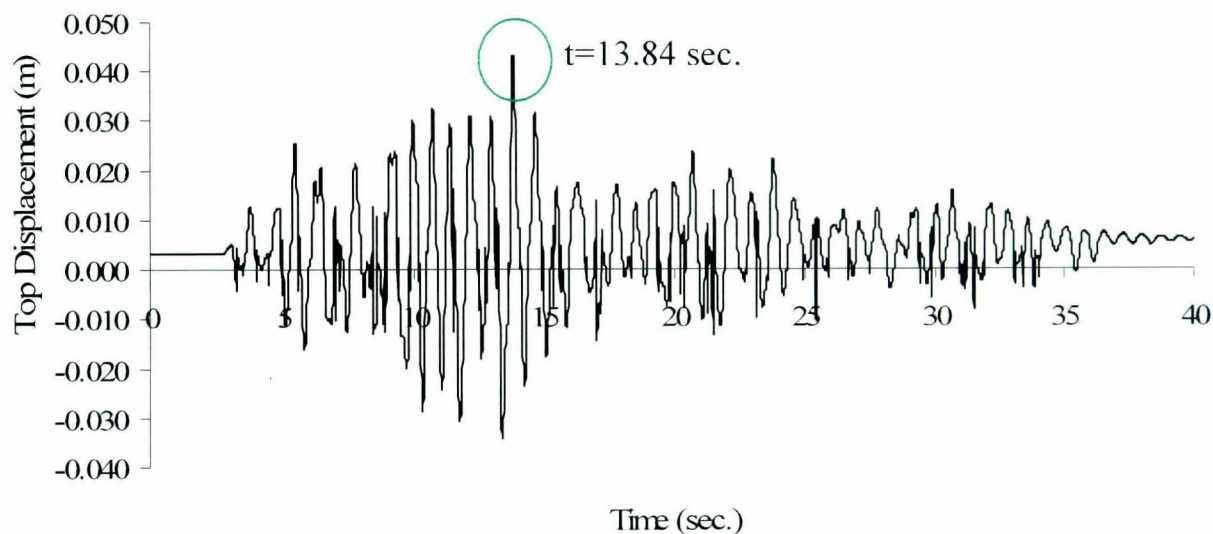


Figure 5.30. Analytical relative displacement history of 2nd storey at 0.20g with no bond slip.

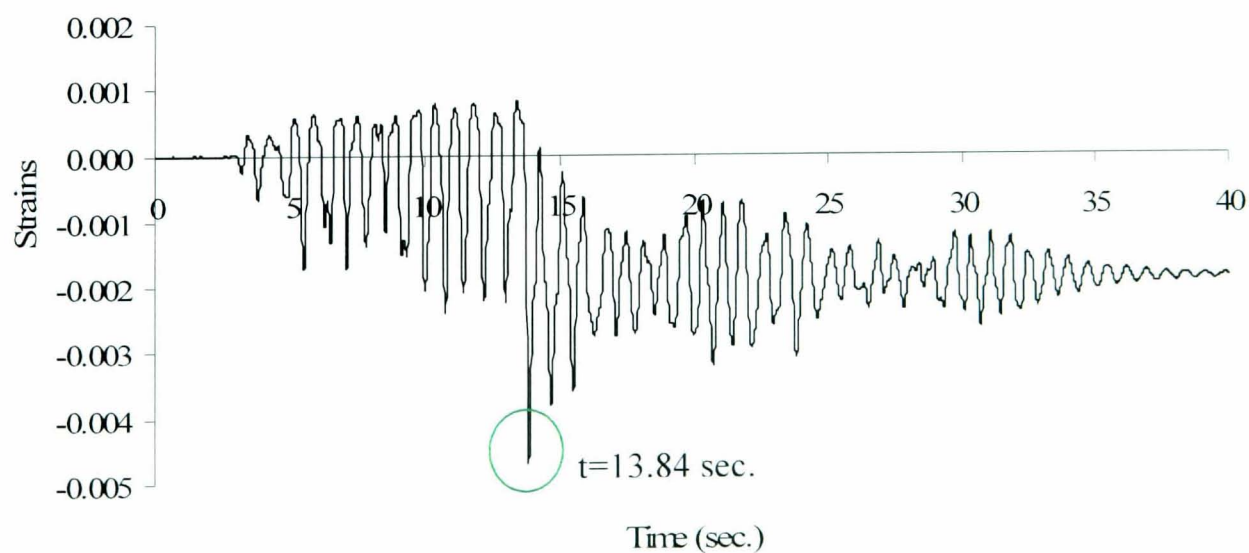


Figure 5.31. Analytical positive strain results of 2nd floor (0.2g test).

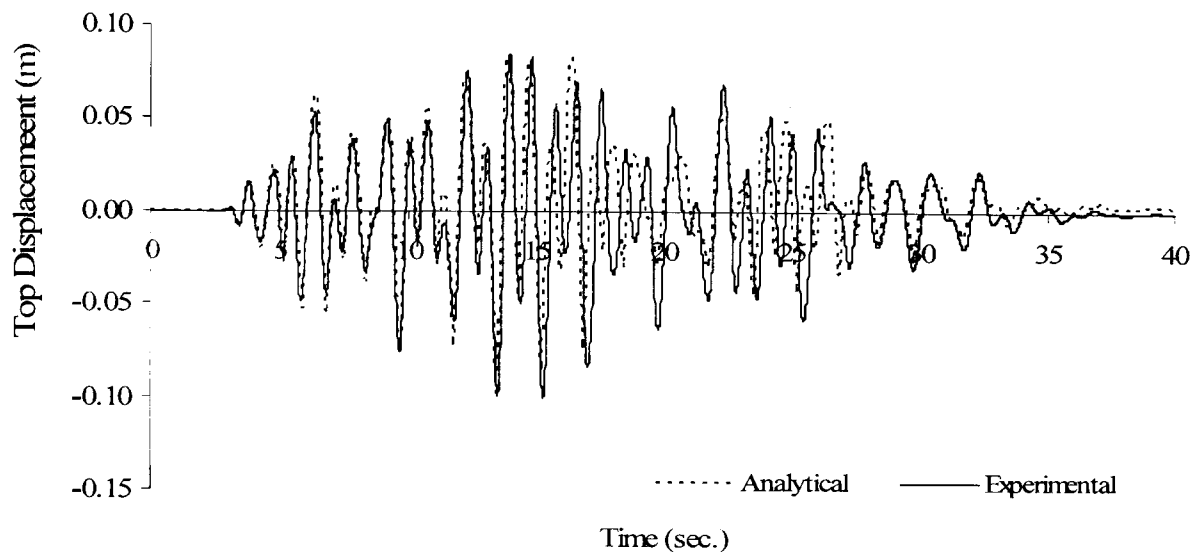


Figure 5.32. Analytical vs. experimental top storey displacements at 0.20g with bond slip.

The results for the 0.3g test are shown in Figure 5.33. Although the analysis simulates the initial positive and negative displacement peaks at $t=6.6$ and $t=9.8$ seconds respectively, significantly lower displacement values are predicted for peaks at $t=11.5$ and $t=12.4$ seconds. In addition, the change in response frequency observed in the experimental results does not appear in the analytical predictions. By checking the consistency between the displacement history results (Figure 5.33) and the available strain results for j8pot (tension in positive displacement) (Figure 5.34) it is concluded that, as in the 0.2 g test, only the first yielding (green circle) is predicted by the analysis. The next displacement peak at $t=12.4$ seconds fails to reach the same magnitude in the analysis since lower strains are observed at that instant (see Figure 5.34). This leads again to the suspicion that some kind of softening mechanism altered the post-yield displacement response. Hence, the analysis is repeated including the bond-slip model described before. This increases the accuracy of the prediction substantially both as far as displacement magnitude and response frequency change are concerned (Figure 5.35). This provides firm evidence that bond-slip takes place soon after yielding.

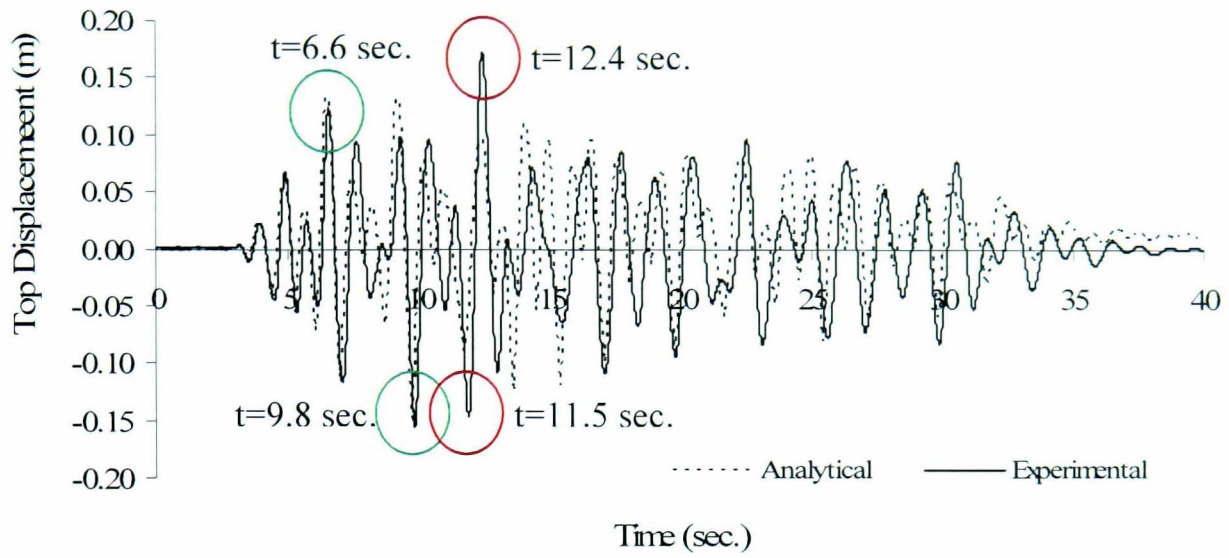


Figure 5.33. Analytical vs. experimental at 0.30g with no bond slip.

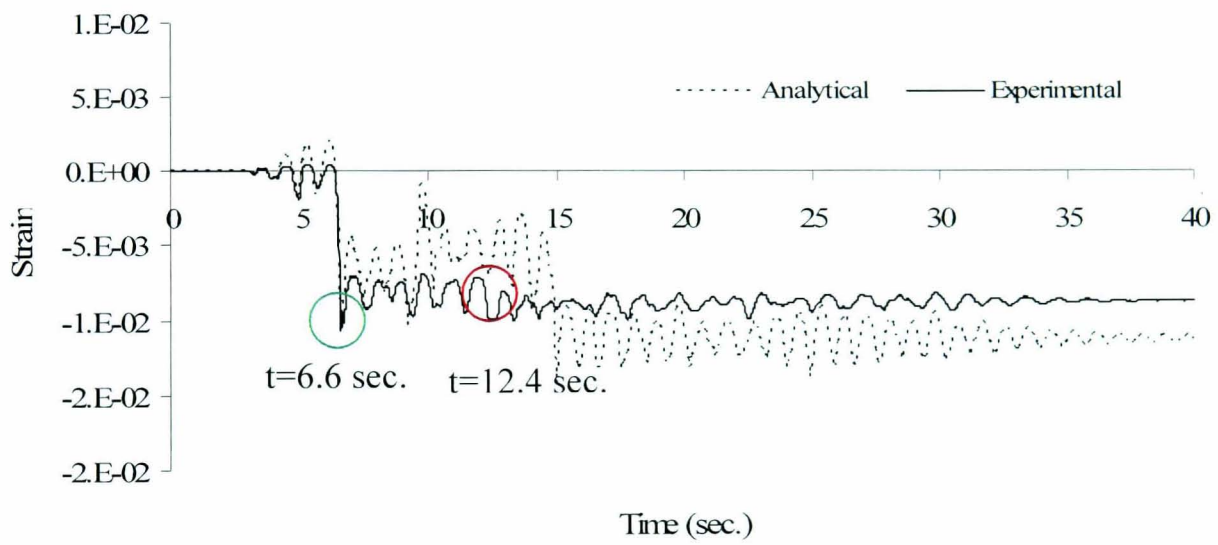


Figure 5.34. Analytical strain results (j8pot) of 2nd floor (0.3g test) without bond slip.

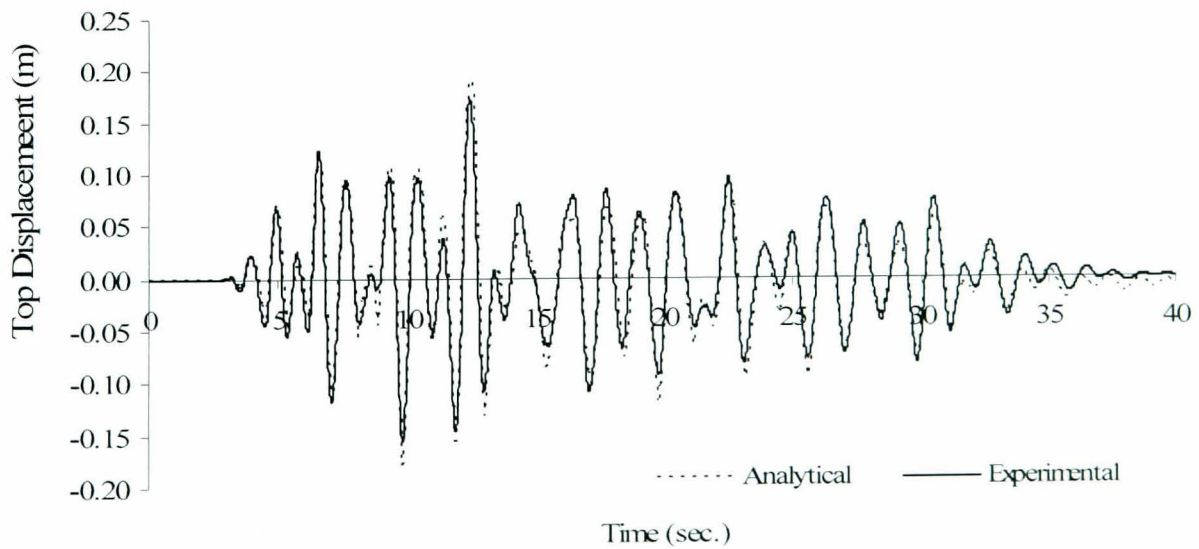


Figure 5.35. Analytical vs. experimental at 0.30g with bond slip

In the same way, excluding slip deformations leads to unrealistic results for the prediction of the 0.4g test. In this case the displacement predictions at a number of displacement cycles are considerably lower while an underestimation of the response frequency change is also evident (Figure 5.36). These variations in response diminish with the inclusion of the bond-slip model as shown in Figure 5.37.

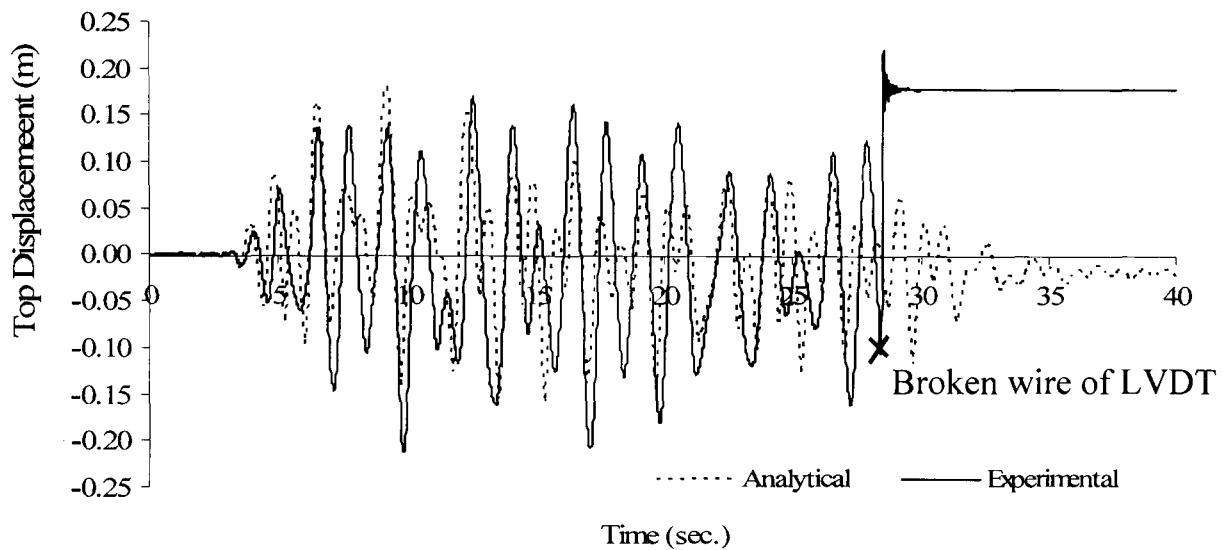


Figure 5.36. Analytical vs. experimental at 0.40g with no bond slip

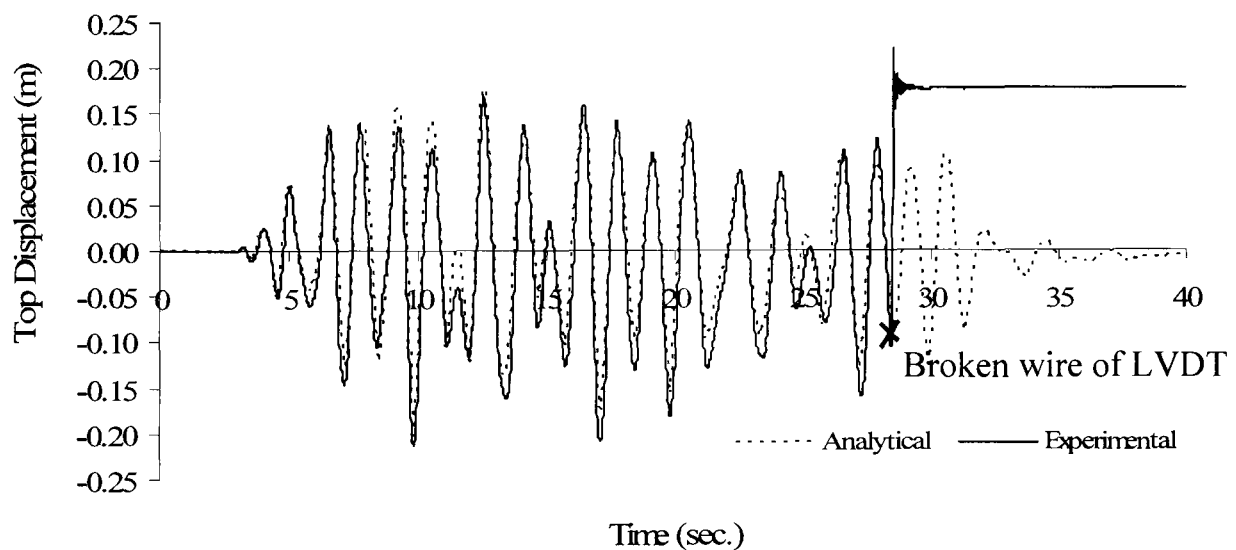


Figure 5.37. Analytical vs. experimental at 0.40g with bond slip

5.8. General Discussion

This chapter dealt with the analytical tool and its modelling capabilities and made comparisons with a structure which exhibited deteriorating behaviour. The analytical tool (DRAIN-3D) was shown to predict the behaviour very well prior to structural softening. Structural softening was attributed in this case to bond-slip after bar yielding

and the analytical tool was able to predict the structural response successfully after modelling bond-slip in a relatively simple manner. Bond deterioration may be a result of deficiencies in the anchorage detailing of the bars shown in Figure 5.4. Most likely this caused the crushing of concrete between the column bars and welded “anchors” due to the sharp angle between them allowing for some amount of slip. On the other hand though, full debonding of the bars was avoided, thus no complete degradation in strength leading to pullout failure was observed.

Given that the analytical tool performed so well in predicting the behaviour of this difficult weak structure and since it includes the modelling capabilities for the calibration of failures other than flexural (mainly shear and pullout failures) it is thus considered appropriate for modelling the range of deficiencies that are likely to be encountered in structures in Mediterranean countries. Therefore it will be adopted in the following vulnerability analysis.

Chapter 6

ANALYTICAL VULNERABILITY ASSESSMENT

6.1 Introduction

The first two steps of the framework for the derivation of analytical vulnerability curves (as stated in 4.1) dealing with structural modelling and the verification of the analytical tool were completed in the previous chapter. This chapter deals with the final step, which is to develop a procedure capable of using the analysis results for the derivation of analytical MDR vulnerability curves at different PGA levels and examine their probabilistic nature. To develop this procedure the following three tasks are required:

1. To predict the structural response (ultimate deformation) on the force-displacement envelope for various PGA levels for a range of typical Mediterranean RC buildings
2. To quantify the damage potential for the predicted structural response
3. To produce the statistical distribution of damage at each PGA level

The following sections will provide reliable ways to meet each of the three tasks.

6.2 Prediction of structural response

In the case of the Saclay frame, the overall response was obtained by using the results of time-history analysis at 5 PGA levels. Time-history analysis is supposed to lead to “exact” solutions provided the input data are accurate. It is widely accepted though that

significant variation in peak values may be obtained if different records are used for the same PGA due to,

1. Frequency content of the signal
2. Variations in soil conditions
3. Duration of the excitation
4. Type of elastic response spectrum (defined as Type 1 and 2 in EC-8, 2004)

Thus, to obtain a complete view of damage potential for a specific excitation level, a number of records are required accounting for the above parameters. For example, EC-8 (2004) prescribes the use of the mean value obtained from analyses of at least 7 records both for design and assessment purposes. Therefore an average “exact” solution, for each excitation level, is required to define the response envelope of a structure. Clearly, such level of analysis is extremely time-consuming. In addition to the complications of defining the appropriate records for each PGA level and the amount of time required for the analysis, a further issue involving the definition of the dynamic characteristics (e.g. damping values) of the structure also needs to be chosen for every analysis case. In light of the issues associated with time-history, a more efficient yet reliable alternative for performance evaluation can be achieved through Capacity-Spectrum method (CSM).

The Capacity Spectrum Method (CSM) can trace its roots to John A. Blume’s Reserve Energy Technique (RET) (Blume et al. 1961), which estimates the inelastic displacement by equating elastic energy (or work) with inelastic energy (Freeman, 2004). It was originally developed and implemented by Freeman in 1975 as part of a pilot program on establishing the seismic vulnerability of the Puget Sound Naval Shipyard (PSNSY). After the PSNSY project was completed the process was used for several case studies including two high-rise 7-storey hotel buildings (Freeman, 1978). The philosophy behind this method is based on the assumption that the performance of a Multi-degree of freedom (MDOF) system under a particular earthquake event can be estimated by comparing the demand from the earthquake event with the capacity of an equivalent SDOF system. This capacity is defined by the transformation of the force-displacement envelope of the MDOF system into that of an equivalent SDOF system. The earthquake demand is expressed in the form of a representative response spectrum, which is similarly transformed for an elastic SDOF system to enable their direct comparison by superposition. The response spectrum is obtained by reducing the elastic

spectrum to account for the nonlinear behaviour of the force-displacement envelope. A number of procedures for the reduction of the elastic spectrum have been proposed in the literature and will be examined later. This section will deal with the issues regarding the determination of the capacity and demand envelopes and the applications of CSM.

6.2.1. Capacity Envelope

For the purpose of this study, the force-displacement envelope of each MDOF system is obtained from push-over analysis using DRAIN-3D models discussed in Chapter 4. The transformation of the force-displacement relationship of a MDOF system into that of an equivalent SDOF system requires the definition of the modal participation factor (Γ) and the equivalent mass of the SDOF system (m^*) calculated as shown in equations 6-1 and 6-2.

$$\Gamma_1 = \frac{\sum_{j=1}^N m_j \phi_{j1}}{\sum_{j=1}^N m_j \phi_{j1}^2} \quad \text{eq.6-1}$$

$$m^*_1 = \frac{\left(\sum_{j=1}^N m_j \phi_{j1} \right)^2}{\sum_{j=1}^N m_j \phi_{j1}^2} \quad \text{eq.6-2}$$

Where:

- m_j lumped mass at the j th floor
- ϕ_{j1} is the j th floor element of the fundamental mode ϕ_1
- N number of floors
- m^*_1 is the effective modal mass for the fundamental vibration mode

The transformation process, shown in Figure 6.1, results in a capacity envelope in the Spectral Acceleration versus Spectral Displacement (SA-SD) space.

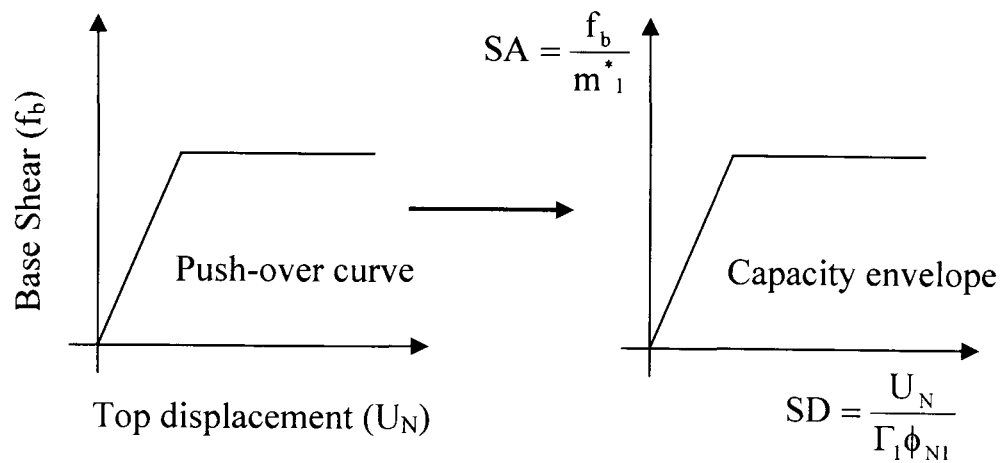


Figure 6.1 Transformation of push-over curve to capacity diagram

In the context of CSM, the transformed capacity envelope is required to be idealised into an elastic-perfectly plastic form. This is necessary so as to enable the establishment of the ductility levels at each displacement. This form is universally accepted and even the latest variation of CSM, included in FEMA 440 (2005), assumes an elasto-plastic (E-P) approximation. However, this assumption means that the energy of the elasto-plastic (E-P) system is not necessarily equal to the energy of the capacity envelope at all displacements. This may cause inaccuracies in degrading structures.

In the context of this work, the use of the E-P approximation is considered insufficient to model the more complex degrading behaviour encountered in sub-standard constructions. Therefore, in order to maintain the special characteristics of the capacity curve it is proposed that the shape of the curve is approximated by a number of different elastic-perfectly plastic systems with zero post-yield stiffness. Each SA_i - SD_i coordinate on the capacity curve is treated as the strength and ultimate displacement of an equivalent elastic-perfectly plastic system (ES) defined using the equal energy rule. However, after degradation, energy dissipated above the current force level is considered unrecoverable and is excluded from the energy balance calculation. An example of the idealisation process for a specific capacity curve is shown in Figure 6.2. The example illustrates the idealised curve for the point on the capacity curve with coordinates $SA=0.25g$ and $SD=0.2m$. The bold dotted line corresponds to the equivalent elastic-perfectly plastic system for the point on the capacity curve with coordinates $SA=0.25$ and $SD=0.2$. Unrecoverable energy above this point is filled in yellow colour. Negative energy (-ve), filled with green colour, corresponds to the additional energy dissipated in the equivalent system and is balanced by positive energy (+ve) filled with red colour, which is not dissipated under the elastic part of the equivalent system.

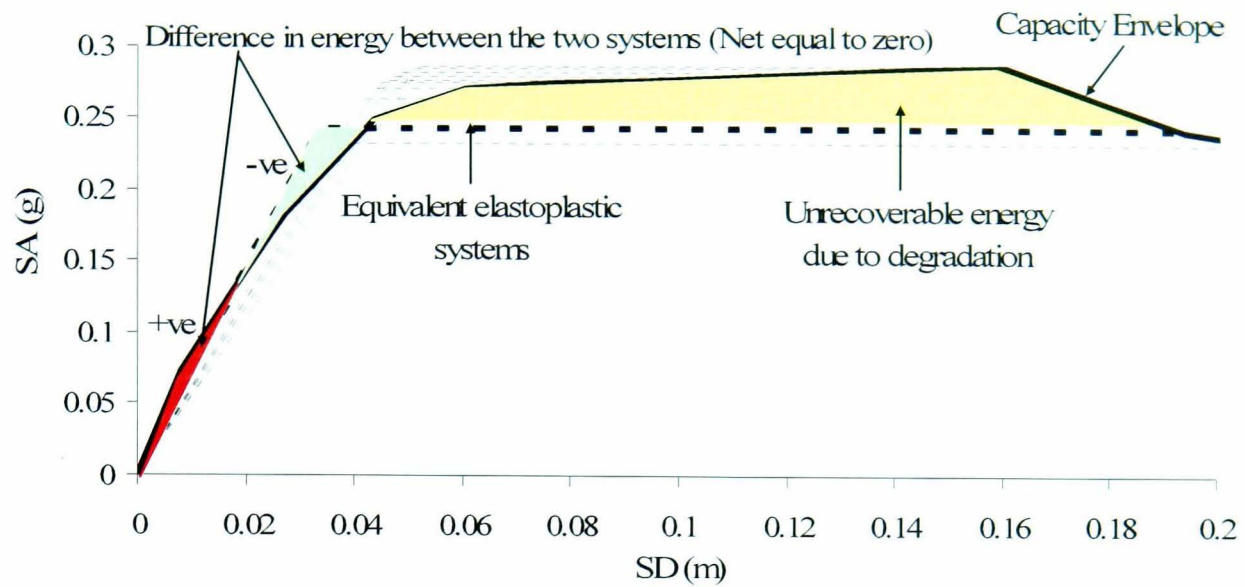


Figure 6.2 Idealisation of capacity curve using the ES approximation

This process is repeated for every point on the capacity curve. Thus, a single capacity curve is divided into a number of equivalent elastic-perfectly plastic systems. For CSM calculations, the ductility at a certain point on the capacity curve is obtained from the equivalent system corresponding to that point. The accuracy of this idealisation technique in the context of CSM is assessed herein in a small simulation study.

The Saclay frame is used as a reference frame in this simulation study. The frame details (member sizes, member reinforcement and frame geometry) are treated deterministically as presented in the previous chapter. Material parameters f_c and f_y are treated probabilistically with $\mu_{f_c}=20$ MPa, $\sigma_{f_c}=6$ MPa and $\mu_{f_y}=550$ MPa, $\sigma_{f_y}=20$ MPa. Latin Hypercube Sampling (LHS) technique is used to derive 25 simulation values, which are shown in Table 6.1. LHS technique is explained in detail later in this chapter. The same number of random values were also derived for the shear link spacing (s) and the bar development length (l) based on the corresponding statistical distributions for Pre-Seismic buildings found in Table 6.5. The corresponding joint shear and bar pullout capacity for each simulation was calculated based on the simulated values by using the models discussed in chapter 4. Besides the first four simulations, both strength (depending on saturated deformations as defined in 6.4.1) and full pinching degradation is assumed after the attainment of these capacities.

Each simulated frame (25 simulated frames) was subjected to the same cumulative time-histories as the original Saclay frame (from $PGA=0.05g-0.4g$). The maximum top displacement at the end of the final test ($PGA=0.4g$) was recorded and is shown at the

last column of Table 6.1. The recorded results were compared with the performance point predictions at $PGA=0.4g$ for the same frames using the revised CSM included in FEMA 440 (2005). A detailed discussion on the FEMA 440 (2005) CSM and the specific application for performance point prediction is given in subsequent sections. Displacement-based cyclic push-over analysis is used for the derivation of the capacity curve. The details regarding the displacement step and the force distribution are discussed later in the chapter. The same recorded time-history results were compared with performance point predictions, obtained using a simpler idealisation technique for the capacity curve. In this case, the curve is idealised by a single elastic-perfectly plastic system based on the equal energy assumption at the final displacement (FD). The final displacement is assumed to be at a top drift of 4.5%, which is shown later in the chapter to be the threshold for complete damage for low-rise buildings designed according to basic code provisions. The capacity of the idealized curve is assumed equal to the maximum capacity of the original capacity curve.

The recorded time-history spectral displacements at $PGA=0.4g$ are shown in Table 6.1 whereas a plot of the residual error between the recorded values and the performance point predictions using the two idealisation techniques is shown in Figure 6.3. The residual error in the performance point prediction in the first 4 simulation cases where no softening was included is approximately the same for both idealisation techniques. This consistency ceases to exist for all subsequent simulation cases where strength degradation effects due to bar pullout or shear deterioration took place. In all these simulation cases the residual error using the proposed ES technique is considerably lower with a mean residual error value equal to $\mu=1.38\%$ and $\sigma=4.94\%$. The mean residual error for FD is $\mu=-4.08\%$ and $\sigma=11.96\%$.

Table 6.1. Values used in simulation study

No	f_c (MPa)	f_y (MPa)	Shear Capacity (kN)	Bar pullout capacity (fs in MPa)	Comments	Recorded from time-history (m)
1	14.3	532	49	610	Strain hardening-No degr.	0.153
2	21.0	572	44	608	No hardening-No degr.	0.180
3	16.2	580	44	611	No hardening-No degr.	0.172
4	15.3	564	44	594	No hardening-No degr.	0.172
5	10.6	550	41	575	No hardening-Shear degr.	0.209
6	10.8	564	39	588	No hardening-Shear degr.	0.206
7	10.5	527	41	551	No hardening-Shear degr.	0.209
8	16.4	554	42	585	No hardening-Shear degr.	0.168
9	23.1	557	46	596	Strain hardening-Pullout degr.	0.171
10	16.5	536	48	569	No hardening-Pullout degr.	0.194
11	21.0	542	49	580	Strain hardening-Pullout degr.	0.227
12	13.1	523	43	552	No hardening-Pullout degr.	0.158
13	22.3	533	46	573	Strain hardening-Pullout degr.	0.167
14	19.7	515	47	551	Strain hardening-Pullout degr.	0.169
15	18.5	558	47	592	Pullout degr.	0.169
16	22.6	537	51	576	Strain hardening-Pullout degr.	0.165
17	17.8	500	50	535	Strain hardening-Pullout degr.	0.175
18	21.4	519	44	558	Strain hardening-Pullout degr.	0.198
19	19.9	546	46	582	Strain hardening-Pullout degr.	0.173
20	22.0	554	49	592	Strain hardening-Pullout degr.	0.192
21	24.1	506	52	548	Strain hardening-Pullout degr.	0.159
22	18.5	559	45	593	Pullout degr.	0.170
23	14.4	516	42	546	Pullout degr.	0.202
24	22.7	571	49	609	Strain hardening-Pullout degr.	0.161
25	18.8	545	45	580	Pullout degr.	0.167

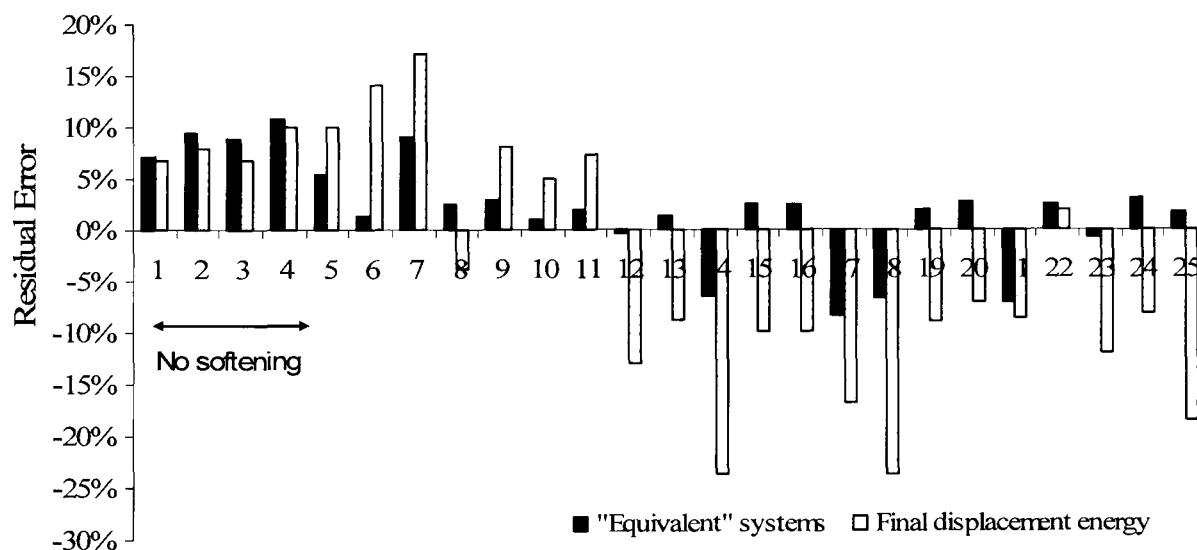


Figure 6.3 Comparison of the residual error using the two idealization techniques

Since the ES increased significantly the accuracy in the predictions, this idealization technique will be adopted in the analytical vulnerability procedure.

6.2.2. Response Spectrum

In the context of this study the response spectrum models (elastic or design) of EC-8 (2004) will be used as the earthquake demand for any subsequent analysis. These spectra represent the envelopes of recorded earthquake events in the European region

and are regarded as representative of the expected seismic activity in Cyprus since they are adopted in the local seismic code (Cyprus Civil Engineers and Architects Association, 1991). Equations 6-3 to 6-6 and 6-7 to 6-10 are defined in EC-8 (2004) for the calculation of the Type 1 elastic and design spectrum respectively.

$$SA(T) = a_g S \left[1 + \frac{T}{T_B} (2.5\eta - 1) \right] \quad 0 < T < T_B \quad \text{eq.6-3}$$

$$SA(T) = 2.5 a_g S \eta \quad T_B < T < T_C \quad \text{eq.6-4}$$

$$SA(T) = 2.5 a_g S \eta \left(\frac{T_C}{T} \right) \quad T_C < T < T_D \quad \text{eq.6-5}$$

$$SA(T) = 2.5 a_g S \eta \left(\frac{T_C T_D}{T^2} \right) \quad T_D < T < 4 \text{sec.} \quad \text{eq.6-6}$$

$$SA(T) = a_g S \left[\frac{2}{3} + \frac{T}{T_B} \left(\frac{2.5}{q} - \frac{2}{3} \right) \right] \quad 0 < T < T_B \quad \text{eq.6-7}$$

$$SA(T) = a_g S \frac{2.5}{q} \quad T_B < T < T_C \quad \text{eq.6-8}$$

$$SA(T) = a_g S \frac{2.5}{q} \left(\frac{T_C}{T} \right) \quad T_C < T < T_D \quad \text{eq.6-9}$$

$$SA(T) = a_g S \frac{2.5}{q} \left(\frac{T_C T_D}{T^2} \right) \quad T_D < T \quad \text{eq.6-10}$$

Where:

- T period of vibration of an elastic SDOF system
- a_g design ground acceleration
- T_B lower limit for the period of the constant spectral acceleration branch
- T_C upper limit for the period of the constant spectral acceleration branch
- T_D value defining the beginning of the constant displacement response branch
- S_{EC} soil factor
- η damping correction factor with a reference value of 1 for 5% viscous damping
- q behaviour factor

The values for S_{EC} , T_B , T_C , and T_D are obtained from Table 6.2 (as obtained from EC-8, 2004).

Table 6.2. Values of the parameters used in elastic and design response spectra

Ground Type	S_{EC}	T_B (sec.)	T_C (sec.)	T_D (sec.)
A (Rock)	1	0.15	0.4	2
B (Dense sand, very stiff clay, gravel)	1.2	0.15	0.5	2
C (Medium dense sand)	1.15	0.2	0.6	2
D (Loose cohesionless soil)	1.35	0.2	0.8	2
E (alluvium)	1.4	0.15	0.5	2

Either the elastic or the design spectrum described above is used as the demand parameter in all proposed CSM procedures as will be discussed later. In order to enable their comparison with the capacity curve defined in the previous section, a transformation into the SA-SD space is needed using the relationship for an elastic SDOF system (eq.6-11). Both the design and transformed design spectra are shown in Figure 6.4.

$$SD = \left(\frac{T}{2\pi} \right)^2 SA \quad \text{eq.6-11}$$

Where:

SD displacement ordinate of the elastic spectrum

SA acceleration ordinate of the elastic spectrum

T corresponding period of vibration

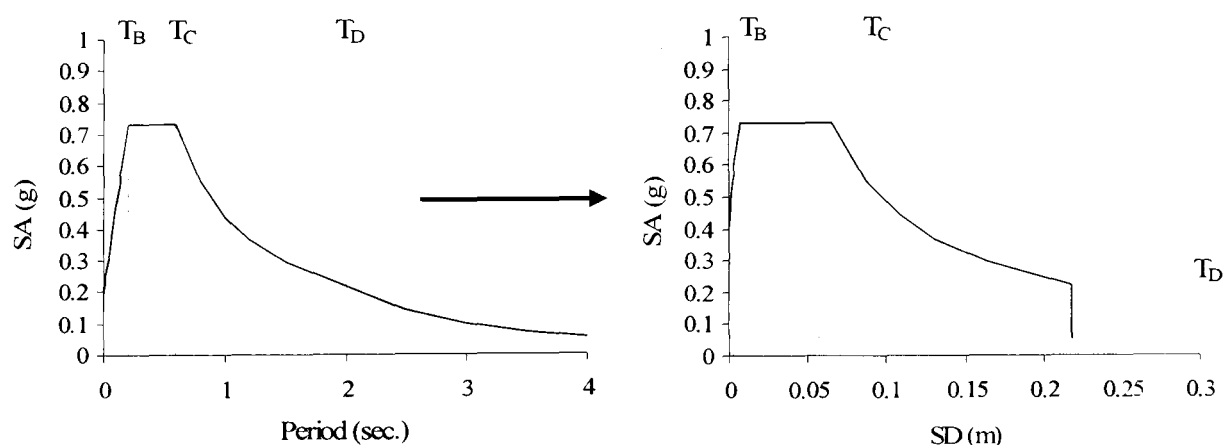


Figure 6.4 Transformation of elastic spectrum based on EC-8 (2004) model for $PGA=0.25g$ and ground type C.

In the case of SDOF systems with nonlinear behaviour, various procedures are used to account for the resulting strength reduction in the demand spectrum (either elastic or design). The initial codified CSM procedures, included in ATC-40 (1996), used the elastic spectrum with increased viscous damping to account for the reduction in strength due to hysteretic damping introduced during nonlinear behaviour. Increased damping is introduced in the elastic spectrum through parameter η which decreases with increased viscous damping ratio. The relation between the increase in viscous damping and ductility is provided in ATC-40. The procedures included in ATC-40 (1996) have been proven by Chopra (1999) to yield large errors in the prediction of performance point and are considered as inadequate for the scope of this study.

More recent CSM procedures such as the “N2” method proposed by Fajfar (1999) use the design spectrum and account for the reduction in strength through the behaviour factor. A number of researchers have examined the effect of ductility (μ) on the strength reduction (R) for the three branches of the design spectrum (for different T values). In the “N2” procedure the three parameters are related through R - μ - T relationships as proposed by Vidic et al. (1994) shown in equations 6-12 to 6-14.

$$R_{\mu} = (\mu - 1) \frac{T}{T_0} + 1 \quad T < T_0 \quad \text{eq.6-12}$$

$$R_{\mu} = \mu \quad T > T_0 \quad \text{eq.6-13}$$

$$T_0 = 0.65\mu^{0.3}T_c \quad \text{eq.6-14}$$

Fajfar (1999) allows for a simplification by assuming $T_0 = T_c$. The application of this procedure for structural performance assessment is schematically shown in Figure 6.5. The intersection of the radial line corresponding to the elastic stiffness of the idealised bilinear system and the design spectrum defines the strength required for elastic behaviour and the corresponding elastic displacement demand. If the elastic period lies in the constant displacement region of the spectrum (eq.6-13) the inelastic displacement demand (SD) is equal to the elastic one. The ductility (μ in Figure 6.5) is equal to the reduction factor (R_{μ}) and can be obtained directly from the graph. Therefore, the SA coordinates of the performance point are defined by dividing the strength of the elastic system with R_{μ} . In cases where the elastic stiffness lays in the constant acceleration region of the design spectrum ($T < T_c$) the reduction factor R_{μ} is similarly determined as

the ratio between the elastic to the yield SA. In this case though, the corresponding ductility demand is calculated using eq.6-12.

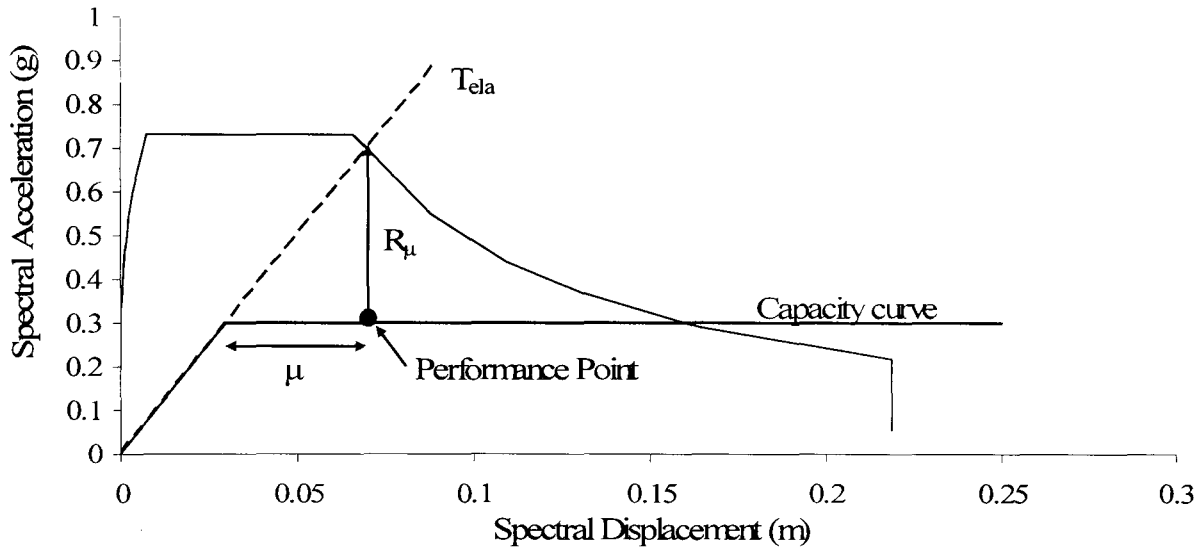


Figure 6.5 Graphical application of N2 method after Fajfar (1999)

The latest attempt to improve the accuracy of CSM, included in FEMA 440 (2005), uses an iterative procedure to arrive at the performance point. The displacement response of the nonlinear SDOF system is computed using an “equivalent” linear system with effective period T_{eff} and damping β_{eff} . The procedure is explained in the following steps:

1. Select a representative elastic spectrum denoted as ADRS (β_0) in Figure 6.6.
2. Assume a performance point (PP in Figure 6.6) on the capacity envelope and calculate the corresponding ductility and secant period T_{sec} using eq.6-11.
3. Calculate T_{eff} and β_{eff} for the particular ductility level using the corresponding equations in sections 6.2.1 and 6.2.2 of FEMA 440 (2005).
4. Substitute β_{eff} in the elastic spectrum equations to adjust the ADRS (β_0) into ADRS (β_{eff}).
5. Multiply the SA ordinates only of the ADRS (β_{eff}) by the modification

$$\text{factor } M = \left(\frac{T_{eff}}{T_{sec}} \right)^2 \text{ to generate the Modified Acceleration-Displacement Response}$$

Spectrum denoted as MADRS (β_{eff} , M) in Figure 6.6. This factor corresponds to the difference in ductility between the nonlinear (T_{sec}) and “equivalent” linear (T_{eff}) SDOF systems.

6. The intersection of the MADRS (β_{eff} , M) with the capacity envelope corresponds to the estimated performance point (PP). The estimated performance point is

adopted if it is within acceptable limits to the assumed one in step 2. Otherwise, the process is repeated with a refined assumed performance point.

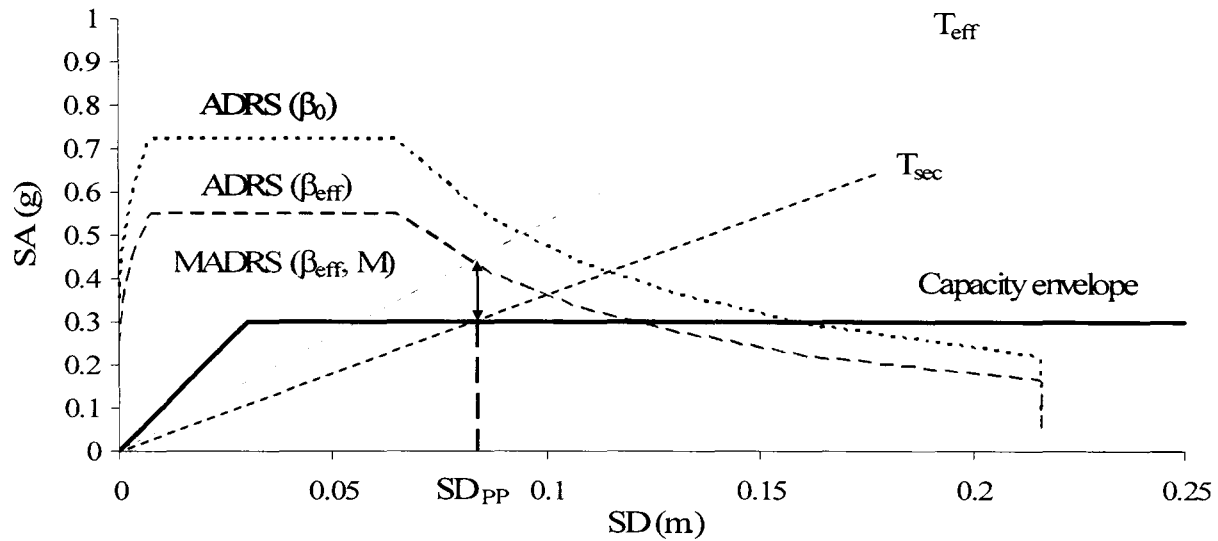


Figure 6.6 MADRS in FEMA 440 (2005) for use in CSM

The simulation study on the Saclay frame conducted in 6.2.1 is repeated here to assess the accuracy of the two procedures (N2 and MADRS) for performance point prediction. The corresponding predictions were compared with the recorded time-history spectral displacements shown in Table 6.1. The residual error in the displacement predictions of the two procedures is shown in Figure 6.7 and provides enough evidence to assume that an increase in accuracy can be achieved through the MADRS procedure. Thus, it is decided to use this procedure for the determination of the structural response for analytical vulnerability assessment purposes.

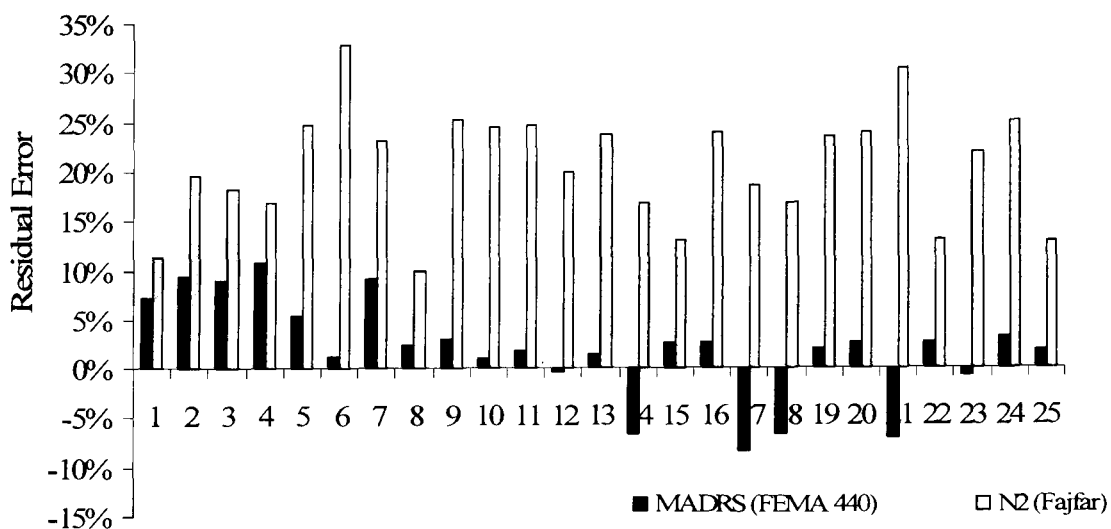


Figure 6.7 Residual error of the simulation study

At this point the initial objective set in 6.1 is completed by establishing and verifying an efficient and fairly accurate alternative to time-history analysis for the prediction of the structural response.

6.2.3. Applications of CSM

In the previous section the most recent variations of CSM were evaluated for performance assessment purposes. Although this is the most widely used application of CSM it is not the only one since it can also be used for:

1. performance based seismic design (PBSD) and,
2. to find the correlation between earthquake ground motion level and building performance.

For modern displacement-based design purposes, as proposed by Priestley (1997), the displacement and ductility (Figure 6.8) need to be known to determine the elastic stiffness and corresponding strength, whereas for conventional force-based design the elastic stiffness and ductility are fixed to determine the strength and, possibly, performance displacement. In both design and performance assessment applications though, the peak ground ordinate of the elastic spectrum is obtained a-priori from design codes for the specific area and soil conditions.

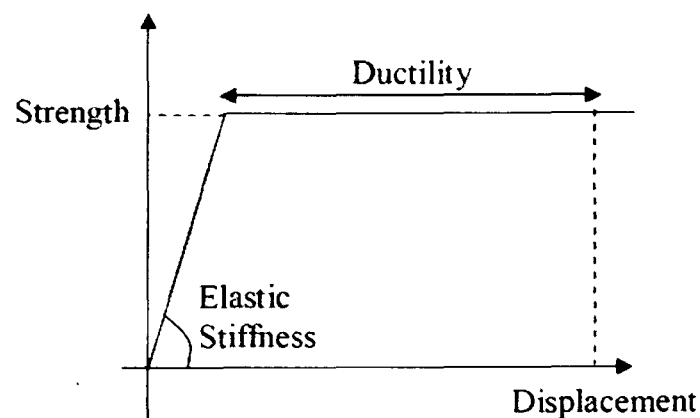


Figure 6.8 Quantities required to define structural behaviour

For the scope of this study though, the PGA ordinate of the elastic spectrum, at every displacement step (SD1-2 shown in Figure 6.9) on the force-displacement envelope, is the required output for the formulation of the vulnerability curves. This application of CSM was initially used in ATC-10 (1982). It requires that all parameters characterising

the structural response (capacity envelope) should be known at every displacement step in order to predict the PGA level required to bring the structure at a specific displacement. In effect this is the reverse procedure of calculating the PP. Each SD_i point on the capacity envelope is treated as a PP, with known ductility (μ), strength (SA_i) and initial period (T) as obtained from the capacity envelope (an example is shown in Figure 6.9 for two performance points). Thus, the MADRS procedure is reversed deterministically to define the peak ground ordinate (PGA) of the corresponding ADRS (β_0) spectrum.

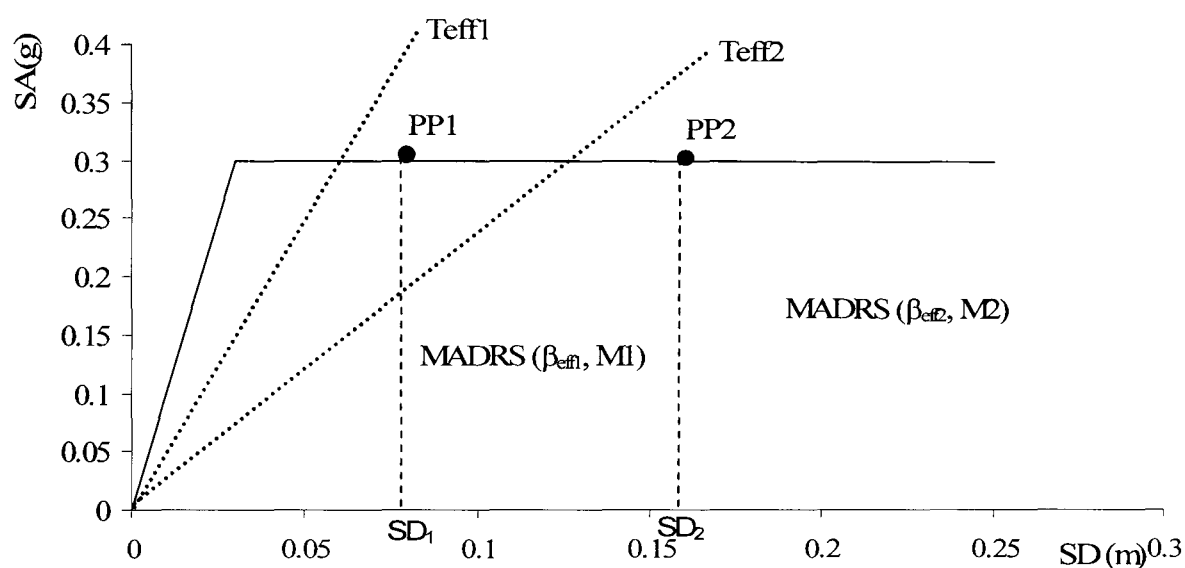


Figure 6.9 Schematic of the application to determine PGA using CSM (colouring based on Figure 6.6)

6.3 Quantification of damage potential

The quantification of damage potential at the estimated structural response is the second task en route to the derivation of analytical vulnerability curves. A number of damage indices (DIs) were presented in the literature review and could be used at this stage to predict damage potential. For the purpose of this framework, the following criteria need to be satisfied by the chosen DI:

1. It should account for the residual strength and safety of a damaged structure as a whole (global DI)
2. It should be easily calibrated against simply recorded data from damaged buildings
3. It should be correlated to the capacity envelope

4. It should be able to account for critical damage thresholds such as cracking, yielding and softening due to local and cumulative damage.

In light of the above criteria set in this study, it emerges that the most appropriate quantification of damage potential is through a direct correlation with the increase in the natural period of vibration of the structure since:

1. An increase in the natural period is a global effect emerging from localised damage.
2. The increase in period can be easily measured after the earthquake using relatively simple recording equipment.
3. The increase in period can be easily extracted from the capacity envelope using equation 6-16.
4. Any alteration in the increase rate of the natural period signifies critical structural damage such as yielding and strength loss (softening).

The proposition that damage is related to the increase in period was recently verified by Calvi et al. (2006) using experimental data. Zembaty et al. (2006) moved a step forward by producing a damage scale that can be used for the definition of the degree of damage from the recorded drop in natural frequency of a structure (Figure 2.7). Similar damage scales are included in Russian (International Building Codes of NIS, 2001) and Armenian (Building Codes of Armenia, 1995) codes of practice.

The DI defined based on the above proposition, normalised for the initial condition of zero damage at initial period T_{initial} is given in equation 6-15.

$$DI = \frac{T_{\text{sec}}}{T_{\text{initial}}} - 1 = \frac{T_{\text{sec}} - T_{\text{initial}}}{T_{\text{initial}}} \quad \text{eq.6-15}$$

Where T_{sec} is the secant period at each SA_i - SD_i coordinate given by equation 6-16.

$$T_{\text{sec}} = 2\pi \sqrt{\left(\frac{SD_i}{SA_i} \right)} \quad \text{eq.6-16}$$

This DI is bound by an additional condition (DI=100) for the value of period at complete damage defined herein as T_{100} . The value of T_{100} is defined later on in the chapter (see Table 6.9). Therefore a final adjustment is applied to equation 6-15 to produce the final relationship for the DI (standardised for no damage at DI=0 and collapse at DI=100) at each SA_i, SD_i coordinate.

$$DI = 100 \left(\frac{T_{sec} - T_{initial}}{T_{100} - T_{initial}} \right) \quad \text{eq.6-17}$$

In order to use the adopted DI for the scope of this work its predictions should be correlated to MDR's (eq.6-18). Thus, the shape of the function relating DI with MDR needs to be defined.

$$MDR = f(DI) \quad \text{eq.6-18}$$

For that purpose, the empirical results from chapter 3 (section 3.8, Table 3.3) are used as reference. It is observed that a linear increase in the damage grade causes an exponential increase in the DR. Since the adopted DI increases exponentially with an increase in damage grade (due to the exponential increase in period) it is decided to assume that the DI is linearly correlated to the MDR with a correlation coefficient equal to 1. For example, the increase in the period of vibration of the Saclay at $PGA=0.4g$ was around 70% and the frame was close to complete damage. Future work needs to be conducted for the verification of this assumption.

At this point, the tools for the derivation of analytical vulnerability curves are established, since a procedure to predict the structural response (described in 6.2.3) and a DI to compute the MDR's (damage potential) has been established. To take into account the probabilistic nature of analytical vulnerability assessment the key parameters involved in the procedure that need to be treated probabilistically are discussed in the next section.

6.4 Probabilistic vulnerability assessment

The key parameters involved in the derivation of the capacity curve are assumed to control the probabilistic nature of analytical vulnerability curves. These key parameters, which are used for the calibration of flexural, bond, buckling and shear capacity models,

are shown in Table 6.3. Geometrical parameters such as section and reinforcement dimensions and positioning are not considered as key parameters since it is considered that their mean value is close to the nominal value and their variability is low. The overall effect on variability of such parameters could be accounted for at a later stage.

Table 6.3. Calibration parameters for capacity models

Capacity model	Key Parameters	Deterministic Parameters	Design Parameters
Flexure:	f_c, f_y	$b, d, k = \frac{f_{ult}}{f_y}, \epsilon_{su}$	ρ
Shear:	f_c, s	$b, d, f_{yw}, \text{saturated displacements (SC and ST)}$	A_{sw}, s
Bond:	f_{ct}, s, l	Saturated slip (SC and ST)	s, l, d_b
Buckling:	s, f_y	f_{yw}, d_{bw}	d_b

Where:

- f_c concrete compressive strength
- f_y steel yield strength
- s shear link spacing
- f_{ct} concrete tensile strength
- l anchorage length
- d_b longitudinal bar diameter
- d_{bw} shear link bar diameter
- f_{yw} shear link yield strength
- b, d section dimensions
- ρ longitudinal reinforcement ratio
- ϵ_{su} strain in steel at ultimate steel stress
- f_{ult} ultimate stress capacity of a steel bar

The probability distribution functions (PDF) for the key parameters are defined based on statistical studies and professional judgment in accordance with the typical construction and design practice (CDP) at the assumed time of construction. To cover the whole spectrum of CDP in the area under consideration, the simulation study will be divided in three well-defined periods as shown in Table 6.4.

Table 6.4. Qualitative description of CDP for the selected periods

Description	Period	Construction and Design Practise (CDP)
Pre-seismic	early 70's to mid 80's	Rapid and in general uncontrolled CDP with no seismic design provisions. The most widely used design guidelines had the sophistication level of CP110 (BSI, 1972).
Basic seismic	mid 80's to mid 90's	Minimum requirements for earthquake resistant structures (1985) are introduced in Cyprus and are used in addition to BS8110 (1985) for RC design. Thus, design is enhanced with the inclusion of the seismic demand in a rather simplistic manner. Minor improvement in construction practise.
Modern seismic	mid 90's-	The introduction of the Seismic Code for RC structures in Cyprus (Cyprus Civil Engineers and Architects Association, 1991) raised the design practise to a higher level. The seismic hazard is identified in more detail and capacity design has been introduced. Construction practise has also been improved considerably due to compulsory quality assurance checks.

6.4.1 CDP considerations

In order to account for the variations in CDP per period, two basic frames (low-rise and mid-rise) for each period will be designed using the corresponding design codes of the reference period. In that way, the probabilistic nature of vulnerability will be assessed for each period by assigning different PDF for the key parameters for each period. Most of the statistical data for the PDF of key parameters per period are given in Table 6.5.

Table 6.5. Statistical data of PDF for the four key parameters per period

Key Parameter	f_c (MPa)				
	(normal distribution)				
	Design	Mean (μ)	σ	min	max
Pre-seismic	20	30	8	$\mu-3.1\sigma$	$\mu+3.1\sigma$
Basic seismic	25	35	7	$\mu-3.1\sigma$	$\mu+3.1\sigma$
Modern seismic	35	45	6	$\mu-3.1\sigma$	$\mu+3.1\sigma$

Key Parameter	f_y (MPa)				
	(log-normal distribution)				
	Design	Mean (μ)	σ	min	max
Pre-seismic	350	420	32	$\mu-80$	$\mu+80$
Basic seismic	460	530	32	$\mu-80$	$\mu+80$
Modern seismic	500	570	32	$\mu-80$	$\mu+80$

Key Parameter	s (mm)			
	(normal distribution)			
	Mean (μ)	σ	min	max
Pre-seismic	250	30	$\mu-100$	$\mu+100$
Basic seismic	design	30	$\mu-50$	$\mu+50$
Modern seismic	design	30	$\mu-25$	$\mu+25$

Key Parameter	$l_f(d)$			
	(normal distribution)			
	Mean (μ)	σ	min	max
Pre-seismic	30	6	$\mu-2\sigma$	$\mu+2\sigma$
Basic seismic	design	4	$\mu-2\sigma$	$\mu+2\sigma$
Modern seismic	design	3	$\mu-2\sigma$	$\mu+2\sigma$

The statistical data for the key material parameters are obtained from Neocleous (1999), whereas in the case of the key detailing parameters the standard deviation, minimum and maximum values are defined based on the opinion of expert designers in Cyprus (Pilakoutas, 2007, Kyriakides, 2007 and Demetriou, 2007). The mean values for the key detailing parameters (s , l) are obtained from the relevant design.

The key material parameters (f_c and f_y) along with deterministic parameters (for the corresponding period) as shown in Tables 6.6 and 6.7 (for each frame) are used for the structural design.

Table 6.6. Values for deterministic design parameters for LR (per period)

Deterministic Parameters	b, d (mm)		k	ϵ_{su}	f_{yw} (MPa)	d_{bw} (mm)
	Columns	Beams				
Pre-seismic	200x200	200x400	1.15	0.1	250	6
Basic seismic	250x250	250x400	1.15	0.075	250	8
Modern seismic	300x300	250x400	1.20	0.075	500	10

Table 6.7. Values for deterministic design parameters for MR (per period)

Deterministic Parameters	b, d (mm)		k	ϵ_{su}	f_{yw} (MPa)	d_{bw} (mm)
	Columns	Beams				
Pre-seismic	250x250	250x400	1.15	0.1	250	6
Basic seismic	300x300	250x500	1.15	0.075	250	8
Modern seismic	400x400	250x600	1.20	0.075	500	10

For saturated slip deformations (SC and ST) the values for $s_3 = 2.5\text{mm}$ and $s_3 = 1\text{cm}$ (clear rib spacing) in the CEB (1993) model (Figure 4.14) are used for unconfined concrete (Pre and Basic seismic) and confined (Modern seismic) respectively. The definition of saturated shear deformations is more trivial since no specific model was found in the literature for this purpose. From the experimental tests on RC joints conducted by Biddah (1997) it was observed that members with no shear reinforcement undergo approximately 2% drift deformation before full strength loss, which increases to 3% for members with nominal shear reinforcement. In a similar experiment conducted by Clyde (2000) on an RC frame with no shear reinforcement it was observed that failure of the joint occurred approximately at 2% drift. Results from joint testing conducted by Shiohara (2001) concluded that, in the case of joints designed

based on early 90s code provisions, failure was observed on average at 4.5% drift. This observation is verified from Pagni (2004) results on similar joints. In light of the above discussion and based on expert judgment (Pilakoutas, 2007) it was concluded that a 3% and 4.5% storey drift limits (saturated deformation) will be used for Pre and Basic seismic design in subsequent analysis.

Two loading combinations are used for each period are shown in Table 6.8. Gravity loading combination is used as prescribed in the corresponding codes, whereas an additional horizontal load combination is also used for each period based on the standard practice of the period. During the pre-seismic design it was of standard practice to account for wind loading through the load combination in CP110 (1972) using a value of around 0.2 MPa per m^2 as the horizontal force uniformly distributed on the structure. During the basic seismic design period, basic seismic zonation was introduced and seismic loading was accounted for in design using simple equivalent static techniques. "Minimum requirements for earthquake resistance structures" (1985) were also introduced in Cyprus. In this document it was proposed to apply a horizontal force equal to 10% of total weight at each floor, which corresponds to using a design seismic coefficient of 0.1 in the equivalent static analysis included in EC-8 (2004). In modern seismic design period it is of common practice to use the modal analysis procedure for design purposes. The regional seismicity is obtained from an updated seismic hazard map included in the Seismic Code for Reinforced Concrete Structures in Cyprus (Cyprus Civil Engineers and Architects Association, 1991).

Table 6.8. Loading combinations used in design (per period)

Loading Combinations	G_k	Q_k	Seismic loading
Pre-seismic	1.4	1.6	-
	1.2	1.2	± 1.2 (0.2 MPa per m^2)
Basic seismic	1.4	1.6	-
	1.2	1.2	± 1.2 (10% of base shear)
Modern seismic	1.35	1.5	-
	1	0.3	EC-8 design spectrum

Two example buildings (low and mid-rise, based on the (NIBS, 1999) categorisation), are chosen to illustrate the proposed probabilistic framework. The low-rise (LR)

consists of two storeys of equal height and one bay and the mid-rise (MR) of four storeys and two bays. The layout and dimensions of both frames are shown in Figure 6.10. As far as the MR is concerned, it is of common practice in Cyprus to be constructed using the “pilotis” system, thus not including infill walls in the ground floor. In effect the ground floor or 1st storey is less stiff than the rest of the storeys, which may lead to “soft storey” failure. In order to account for the likely stiffness variation in elevation, it was decided to increase the height of the 1st storey. It is anticipated that this arrangement can simulate the “pilotis” system but future work using wall panels is required to verify this assumption.

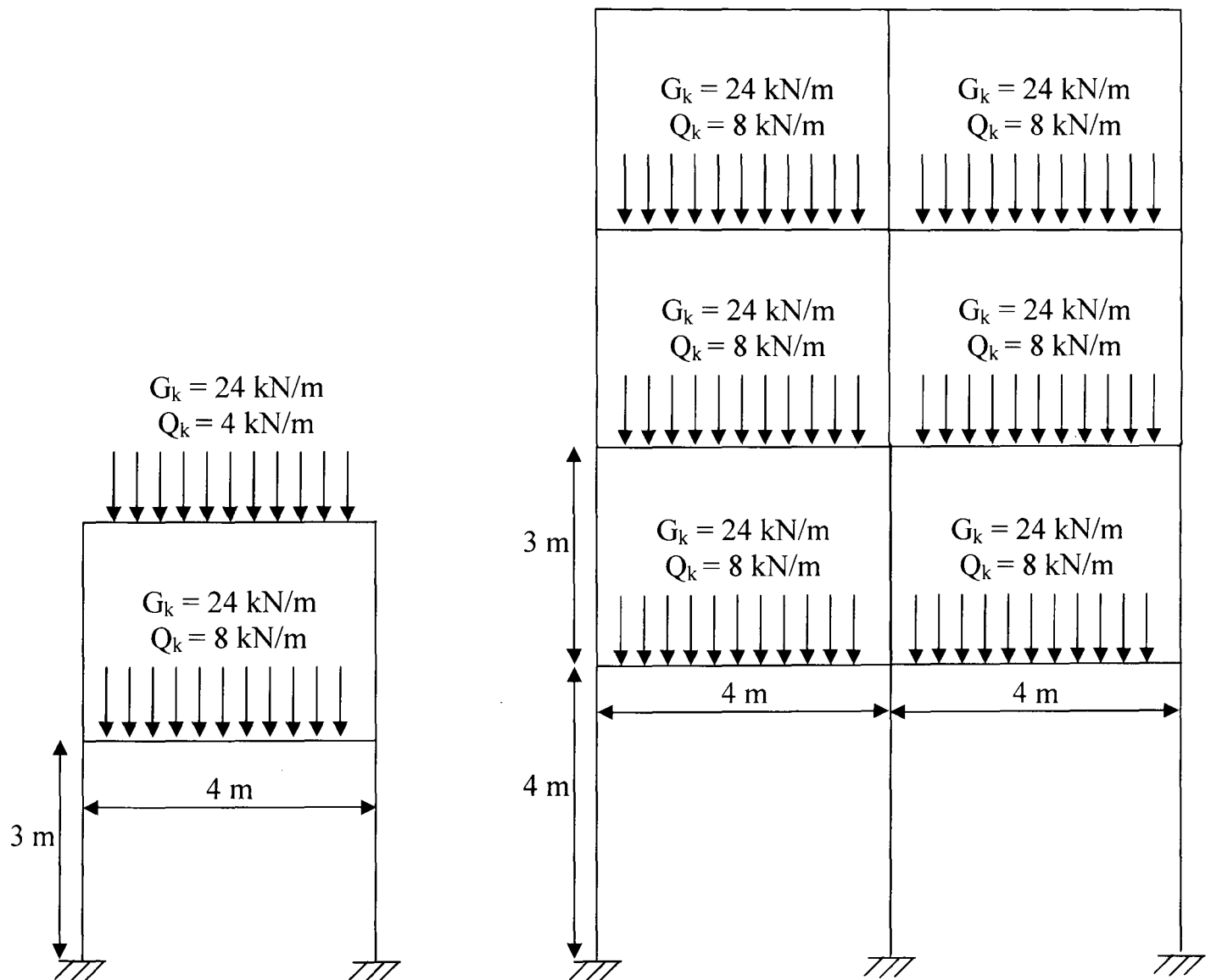


Figure 6.10 Layout of LR and MR simulation frames

Both frame geometries are defined deterministically and are shown in Figure 6.10 along with the design dead and live loads. Design for the three periods in Table 6.4 is conducted using the CP110 (BSI, 1972), BS8110 (1985) and the Seismic Code for RC structures in Cyprus (Cyprus Civil Engineers and Architects Association, 1991) respectively.

6.4.2 Analytical determination of capacity envelope

Both frames will be analyzed in DRAIN-3D to determine their capacity envelopes using cyclic push-over analysis to simulate better the repetitive nature of seismic loading. The load cycles are applied at increasing levels of displacement well into the inelastic range. One load cycle is applied at each displacement step. The hysteretic response of the simulated frames (6.2.1) from time-history analysis (PGA=0.4g) described in 6.2.1 is compared to the corresponding cyclic envelope obtained using three different displacement steps. The cyclic envelope for each simulated frame is obtained by using 0.15%, 0.3% and 0.6% top drift (Δ) as the displacement step. The comparisons of the hysteretic time-history (dynamic) and cyclic envelope response for two different degradation levels (simulation 14 and 19 in Table 6.1) are shown in Figure 6.11. It is evident from the figure that the 0.3% top drift displacement step simulates well the envelope of the 40 second artificial record used.

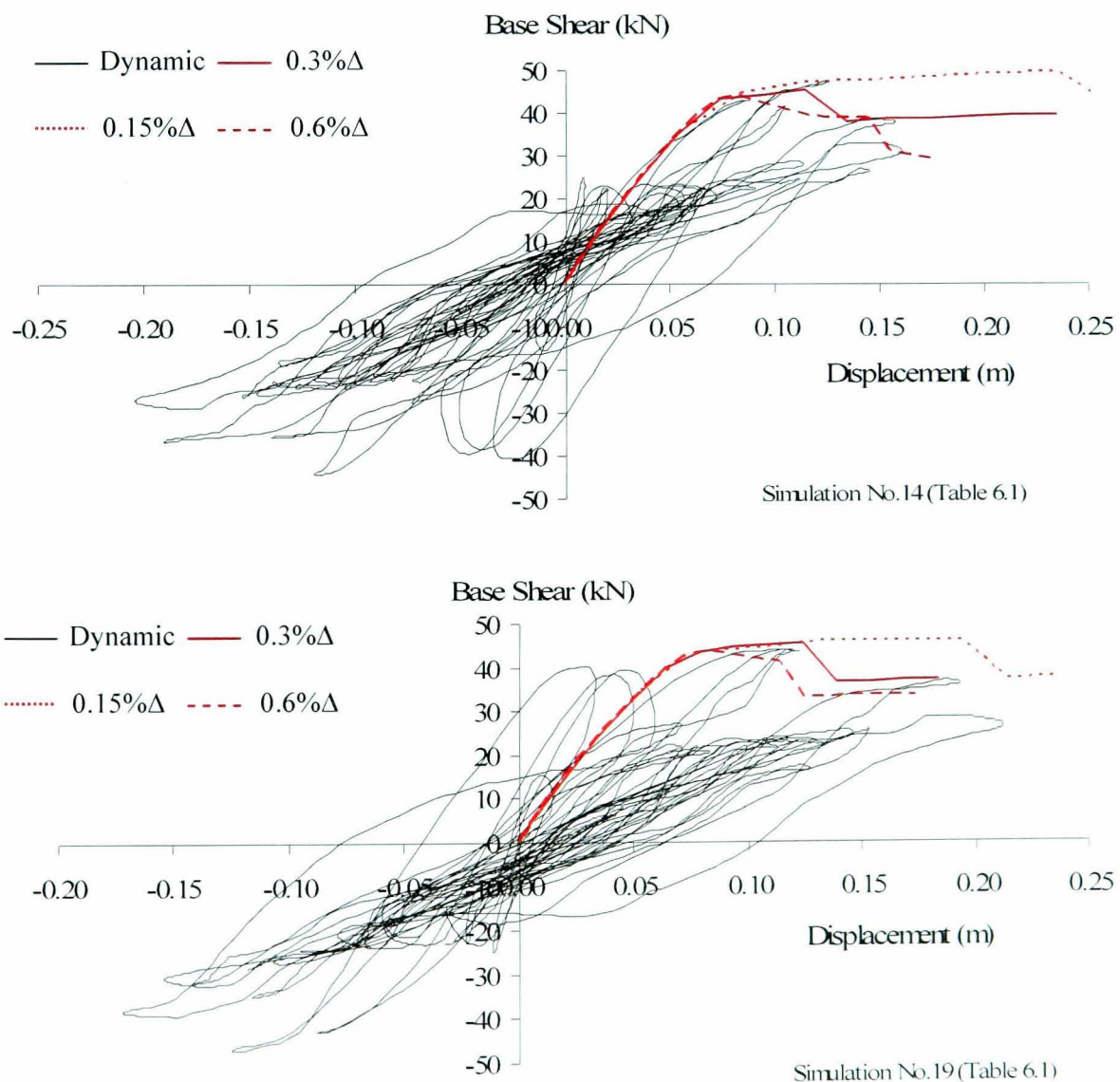


Figure 6.11 Comparison between time-history and cyclic push-over for different displacement step

For brevity, a 2D analysis on a single frame will be conducted in one direction. Irregularities in plan are not accounted for and should be taken into account in a more comprehensive study. The force distribution along the height of the structure is determined as proposed by the lateral force method of EC-8 (2004). The seismic demand at each storey is calculated from eq.6-19.

$$F_i = F_b \frac{h_i m_i}{\sum h_j m_j} \quad \text{eq.6-19}$$

Where:

- F_i horizontal force acting on storey i
- F_b base shear
- h_i, h_j height of masses m_i and m_j from the base of the building
- m_i, m_j storey masses

In the case of the MR frames, the horizontal storey force distribution accounts for the effect of higher modes of vibration through the modification of the lateral force distribution (eq.6-19) as proposed in FEMA 356 (2000) and discussed in detail in 2.3.3.2. The sum of the effective modal mass for the first two modes taken into account amounts to at least 90% of the total mass of the structure, as required in EC-8 (2004).

6.4.3 Definition of complete damage

The threshold values for top storey drift corresponding to the collapse of the building are obtained from HAZUS99 (NIBS, 1999) for each combination of construction period and building height (Table 6.9). The failure plane for each combination in Table 6.9 is defined by the radial line corresponding to the limit value of SD for a non-degradating building with strain-hardening (black envelop in Figure 6.12). This radial line corresponds to T_{100} in equation 6.17. Any capacity envelope crossing the corresponding failure plane is regarded as collapsed.

Table 6.9. Top storey drift at complete damage (as obtained from SD values in HAZUS99 (NIBS, 1999) for an h=6m and h=13m building)

Top drift (%)	High-Code (Modern seismic)	Low-Code (Basic seismic)	Pre-Code (Pre-seismic)
Low-rise (1-3 storeys)	7	4.5	3.6
Mid-rise (4-7 storeys)	5.5	3.5	3

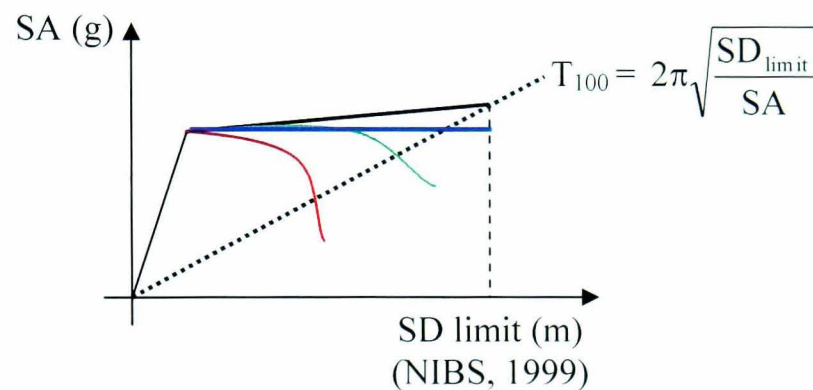


Figure 6.12 Definition of the failure plane

At this point the formulation of the framework for the derivation of analytical vulnerability curves is completed since:

1. An analytical tool is verified for the simulation of the structural behavior
2. A reliable procedure is established for the prediction of the structures response
3. A DI is adopted for the quantification of the damage potential at the predicted structural response
4. The probabilistic nature of vulnerability curves is addressed through the statistical distributions of the key parameters.

The final step before the derivation of analytical curves for the example structures involves the definition of the required number of simulations.

6.4.4 Process for choosing the simulation values

For the derivation of probabilistic analytical vulnerability curves a number of simulation values have to be chosen from the statistical distributions of the key parameters. These simulation values will be used to formulate the corresponding number of LR and MR

frames for each period. The simulation values from each statistical distribution are obtained using the Latin Hypercube Sampling algorithm. This technique, proposed by McKay (1979), enables the reduction in the number of simulations compared to the Monte Carlo technique (Ayyub, B. and McCuen, R., 1995) by adopting a stratified approach in selecting the simulation values from the PDF. Initially it is assumed that each key parameter is uniformly distributed in the space between 0 and 1. The uniform distribution is divided into a number of non-overlapping sub-intervals equal to the number of simulations. A uniform value U_i is then selected at random from each sub-interval (eq.6-20) and the inversion method is applied to transform them into values that correspond to the cumulative distribution function (CDF) of each key parameter.

$$U_i = \frac{(\pi - 1) + u_i}{N} \quad \text{eq.6-20}$$

Where:

- N the number of simulations
- π_i random permutations of the integers $i=1, \dots, N$
- u_i uniform random numbers on $[0,1]$ generated independently from π_i

An example is given to describe the procedure for the determination of the simulation values for concrete compressive strength f_c ($\mu=25$ and $\sigma=8$ MPa) using Latin Hypercube sampling (for 9 simulation values). Initially, the uniform distribution is divided into 9 sub-intervals and a random number (u_i) is chosen from each sub-interval (values in the 1st column of Table 6.10). Next, a random arrangement of the integers between “0” and “9-1” is computed and hence, an integer $(\pi-1)$ corresponds to each u_i value. Each combination of $[(\pi-1), u_i]$ is substituted into eq.6-20 to provides a probability value (U_i). The values in the last column of Table 6.10 are at obtained at $U_i\%$ on the cumulative distribution function of f_c .

Table 6.10. Latin hypercube sampling procedure using 9 simulation values

u_i	$\pi-1$	U_i	Value at $U_i\%$ of the inverse normal cumulative distribution function with $\mu=25$ and $\sigma=8$ MPa.
0.01	0	0.10%	6.53
0.16	4	46.17%	24.42
0.25	7	80.57%	30.17
0.42	8	93.58%	34.12
0.49	3	38.80%	23.29
0.66	2	29.52%	21.77
0.69	6	74.30%	28.92
0.81	5	64.52%	27.23
0.91	1	21.17%	20.20

$\mu=24.07$ and $\sigma=7.91$

In order to define the required number of simulations a small study was conducted to assess possible variations in analytical vulnerability curves using 10, 25 and 50 simulations. The framework was applied using the data from the simulation study described earlier in section 6.2.1 to derive probabilistic vulnerability curves using 25 simulations. Using the same statistical distributions as in 6.2.1 (for f_c , f_y , s and l) revised sets of simulation values were derived (10 and 50 simulation values). The framework was applied twice using 10 and 50 simulation values and the comparison of the results is shown in Figure 6.13. Although a very good correlation exists between 25 and 50 simulations a smaller number of 10 simulations overestimate the MDR. This conclusion is consistent with the findings of similar studies conducted by Ahmed (2007) and Rossetto (2005). Therefore, 25 simulations will be used for the derivation of the analytical vulnerability curves.

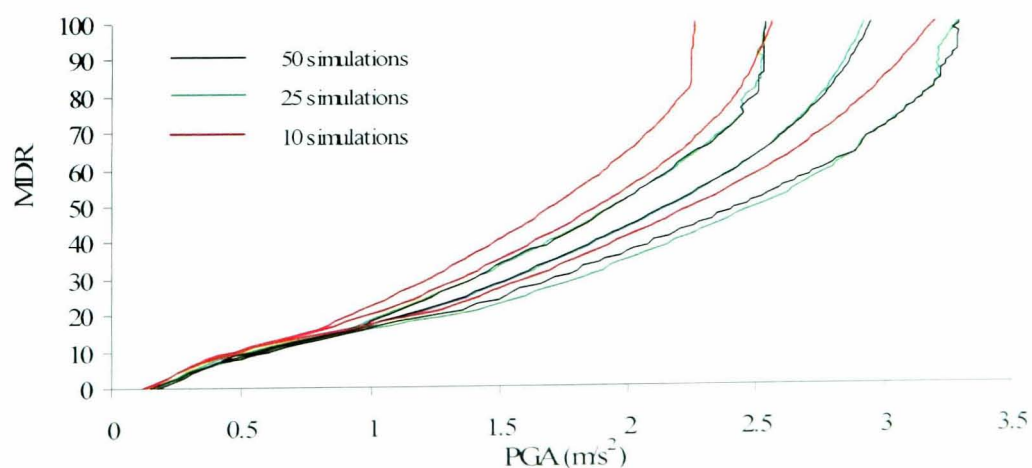


Figure 6.13 Comparison of analytical curves using 10, 25 and 50 simulations

6.4.5 Probabilistic vulnerability curves

The final section of this chapter deals with the derivation of the analytical vulnerability curves for the two building classes for different types of CDP. The models for different failure types as described in 4.3.1-3 are determined based on the key and deterministic parameters shown in Tables 6.5-7. The simulation values for the key deterministic parameters are tabulated in Appendix B. The design member cross-sections for both LR and MR for the three periods are shown in Appendix C.

Zero damage (MDR=0) is assumed prior to cracking. The derived curves are compared to the predictions based on the guidelines included in HAZUS99 (NIBS, 1999) for each period.

6.4.5.1. LR buildings

The three sets of curves for LR buildings (corresponding to Pre, Basic and Modern seismic design) are shown in Figures 6.14 to 6.16. In all cases, the mean, 95% and 5% probability of exceedance (POE) curves are derived.

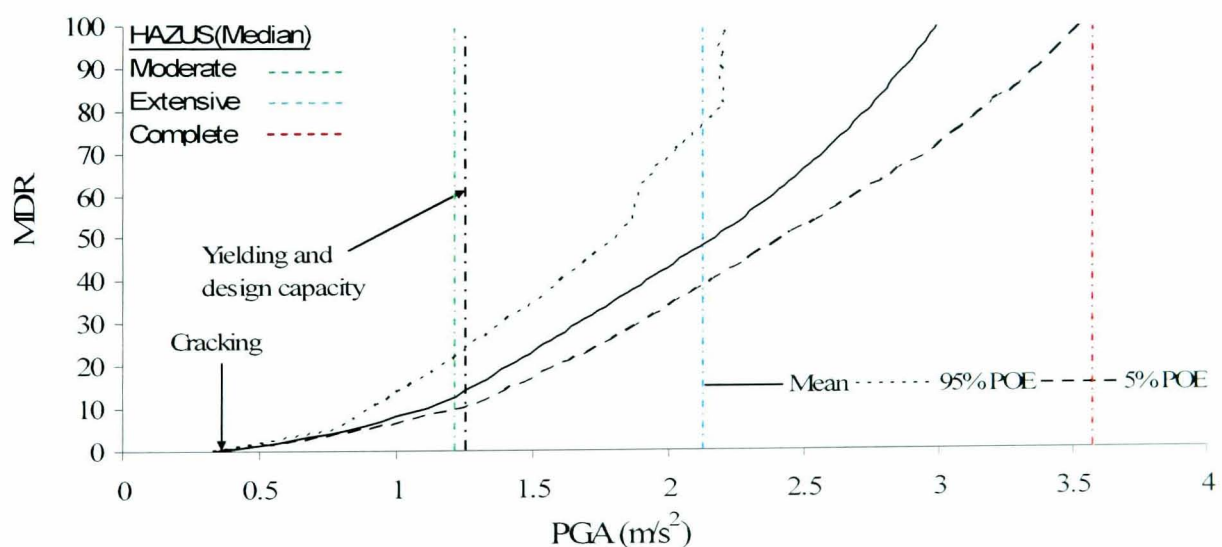


Figure 6.14 Analytical vulnerability curves for LR Pre-seismic buildings

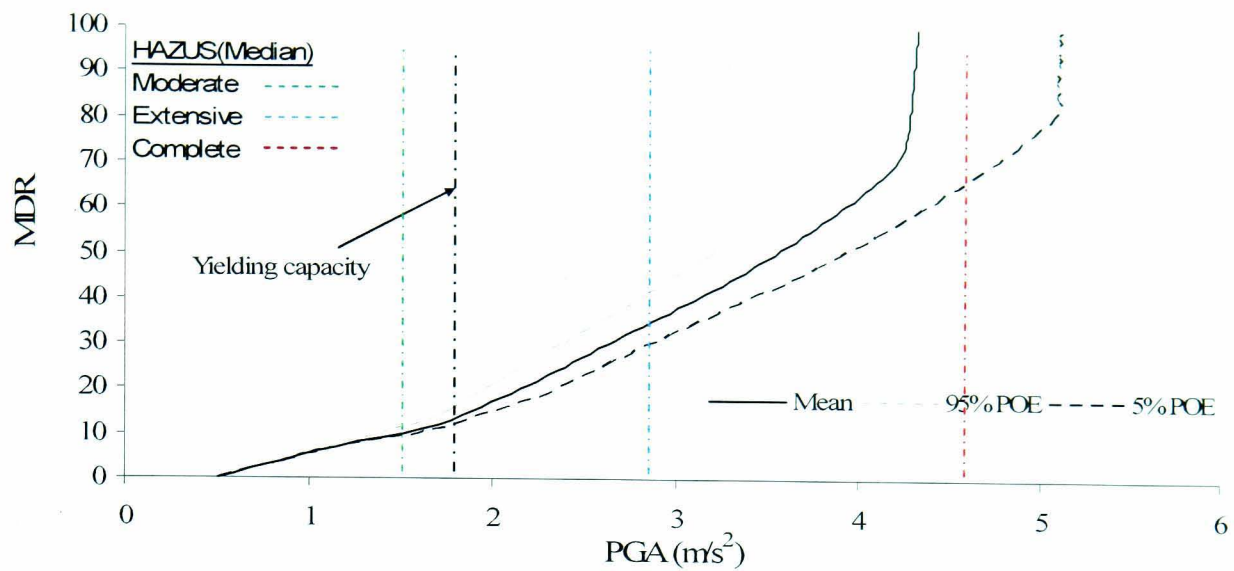


Figure 6.15 Analytical vulnerability curves for LR Basic seismic buildings

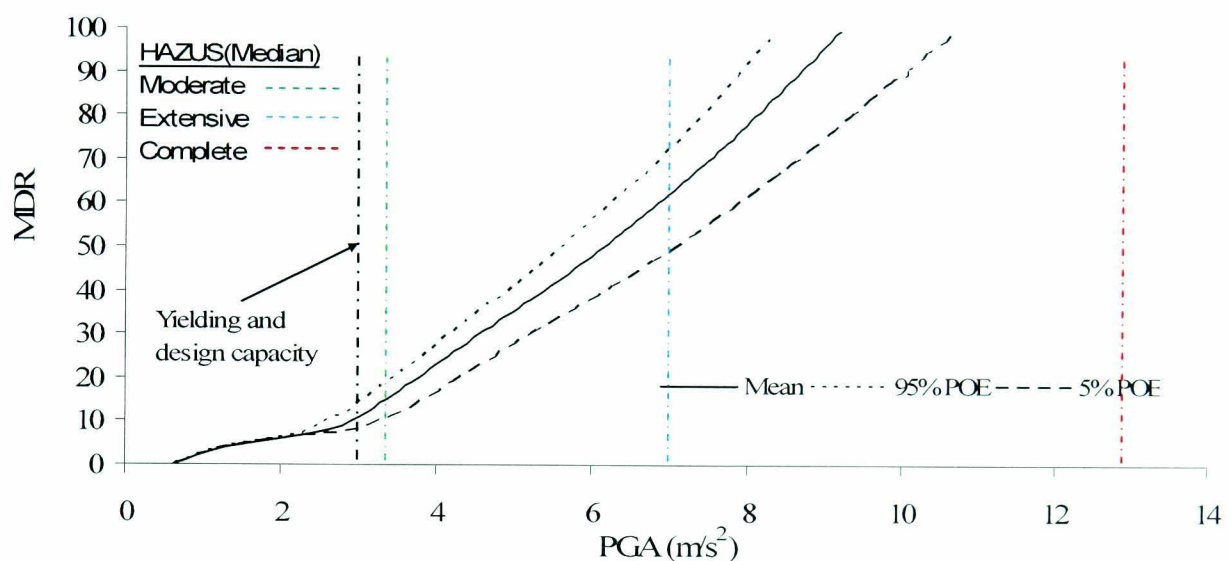


Figure 6.16 Analytical vulnerability curves for LR Modern seismic buildings

In the first two figures it can be seen that at $MDR=100\%$ there is a considerable difference between the lower (95% POE) and the upper (5% POE) bound curves. This variation can be attributed to severe damage of the structure due to failures initiated from bar pullout or shear deterioration. The lower bound curve (95% POE) of the Pre-seismic buildings (Figure 6.14) indicates that around 25% damage occurs before yielding. In addition, the same curve shows rapid failure of the structure at around $PGA=0.22g$. In contrast, the mean and 5% POE curves do not show similar rapid increase in damage. This can be attributed to the fact that the flexural capacity of the columns is lower in most cases than the corresponding shear and bond capacities. It can be clearly seen though that the threshold median value in HAZUS99 (NIBS, 1999) for complete damage accounts solely for flexural failures and overestimate the mean

response of such structures since it coincides with the 5% POE curve. Using the HAZUS99 (NIBS, 1999) value in this case can be unconservative.

In the case of the curves for basic design (Figure 6.15) rapid failure of the buildings is obvious in all three curves at 0.33g, 0.42g and 0.51g, respectively. This shows that most buildings suffer severe damage initiated by local failures and this is again underestimated by the HAZUS99 (NIBS, 1999) median value for complete damage.

In the last case, modern seismic designed buildings are shown not to exhibit any softening behaviour due to brittle modes and the damage is due to the spread of plasticity. The buildings on average fail at approximately 3x times the design capacity. Even in this case the HAZUS99 (NIBS, 1999) guidelines appear to overestimate the capacity and underestimate the damage.

6.4.5.2. MR buildings

The vulnerability curves for the MR buildings are shown in Figures 6.17 to 6.19. As in LR buildings, most Pre-seismic buildings do not exhibit rapid failure due to brittle modes due to their low flexural capacity. However they are affected by local deficiencies as suggested by their large variability in response. Such variability can not arise purely from material variability.

The limit for complete damage in HAZUS99 (NIBS, 1999) is relatively high and may account to some extent for structures dominated by flexural response but does not come close to accounting for softening behaviour from brittle modes. As in LR buildings, most MR Basic design buildings fail due to abrupt failure modes. These modes are not accounted by the median complete damage limit given in HAZUS99 (NIBS, 1999). In the case of the Modern design buildings, damage is dominated by the spread in plasticity and the small variation in the derived curves is attributed to material strength variability. Although the response is dominated by the flexural mode, HAZUS99 (NIBS, 1999) median limit for complete damage again underestimates the damage potential.

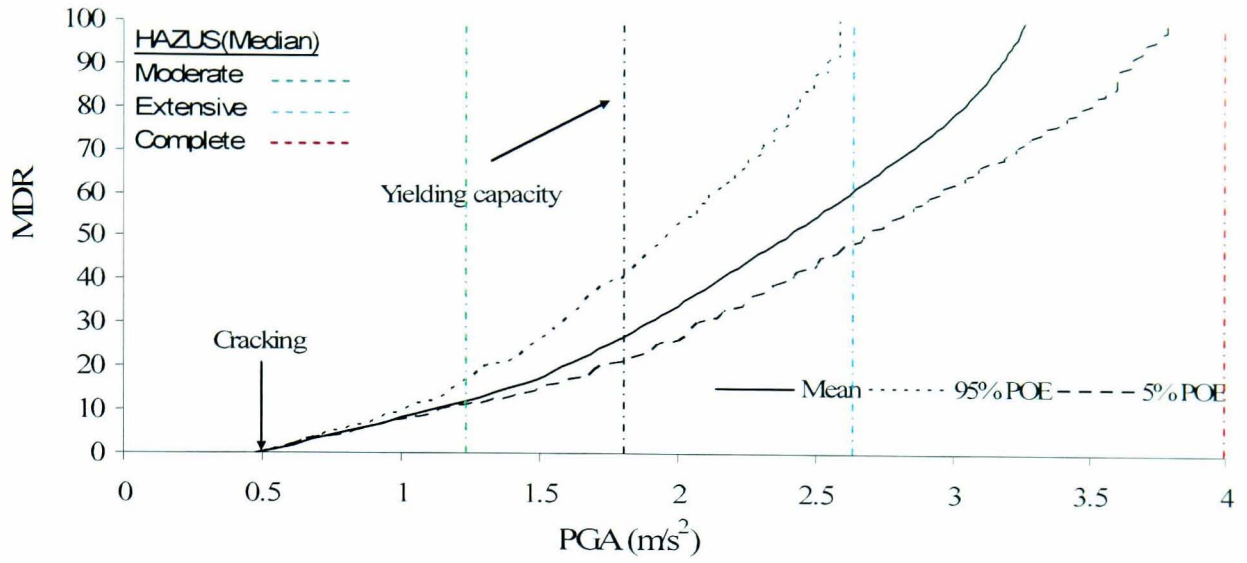


Figure 6.17 Analytical vulnerability curves for MR Pre-seismic buildings

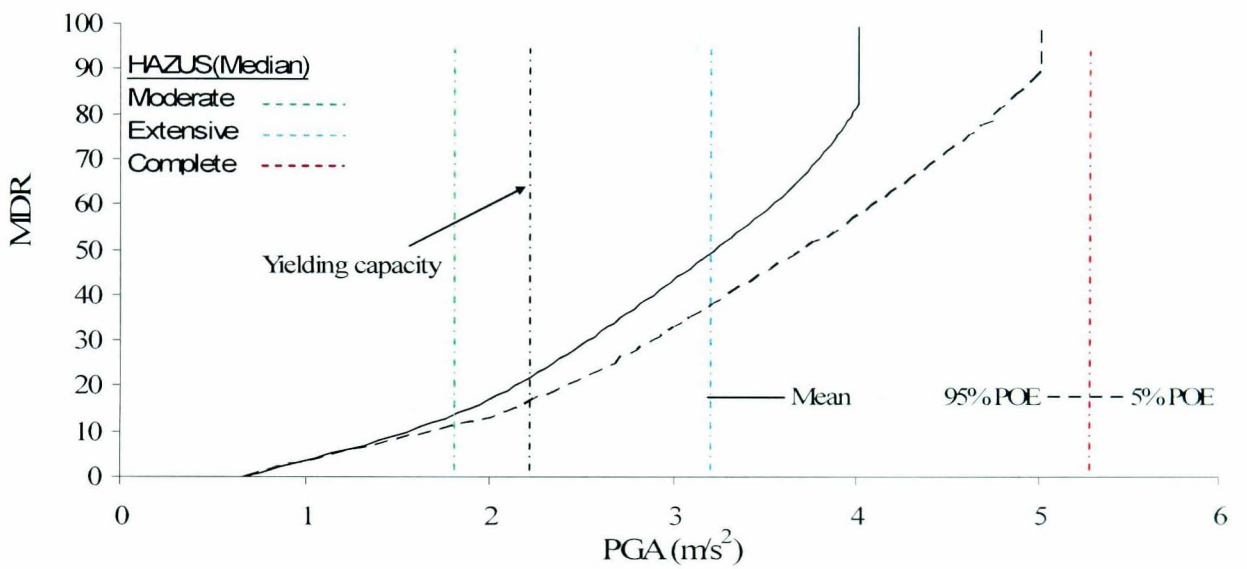


Figure 6.18 Analytical vulnerability curves for MR Basic seismic buildings

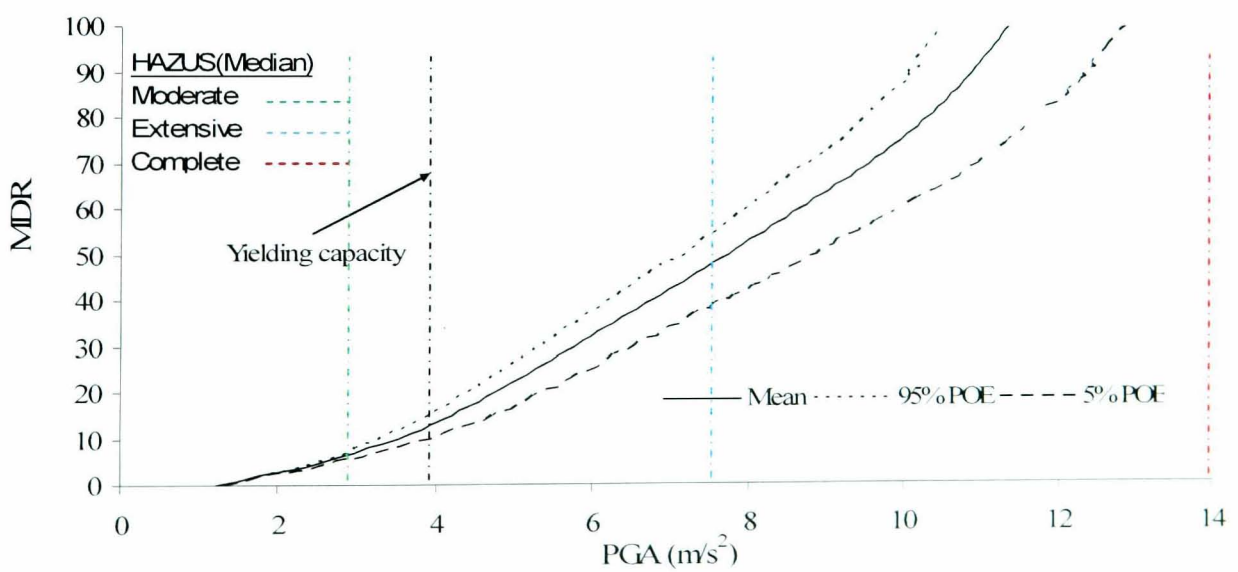


Figure 6.19 Analytical vulnerability curves for MR Modern seismic buildings

It should be noted that the HAZUS99 (NIBS, 1999) limits are probably intended for the seismic region of California for which the design ground acceleration may be higher than the ones used for Cyprus. These limits were derived from threshold SD values, and are based on the combination of available drift/damage information from a number of published sources from researchers in the US (NIBS, 1999). This information, which relies heavily on US expert opinion and may be based on US practice and a building stock that in general complies with code guidelines, may overestimate the characteristics of buildings in other regions and with less stringent code compliance. Nonetheless it is fairly clear that such universal limits, as given by HAZUS99 (NIBS, 1999), are neither adequate for all places nor for all building classes. For example, a Pre-seismic building in Pakistan is very different from one in Cyprus which is very different from the one in California. In addition, Modern design buildings may well exceed the HAZUS99 (NIBS, 1999) limit for complete damage if the buildings are designed accordingly.

6.4.5.3. Comparison with other empirical vulnerability curves

The curves for LR buildings are compared with the empirical vulnerability curves (for superior and substandard construction) derived by Schnabel (1987) based on experience from similar regions and observed damage data from the region of Cyprus (Kyriakides, 2007). These curves are the only ones proposed for the specific region, and were also used by Kythreoti (2001) in an Earthquake Risk Assessment framework (EQ-RACY). The curves cover two types of construction practice, Substandard and Superior (for buildings less than 4 storeys). Since the curves were derived in 1987, the Substandard buildings correspond to buildings in the Pre-seismic period and the superior buildings to Basic designed buildings. Upper and lower limit curves are provided for each type of construction. The original curves used MMI as the earthquake demand parameter. For comparison purposes the derived vulnerability curves, which were developed using PGA, are modified using the previously derived equation (eq.3-12) to convert PGA to MMI. The comparison of the Substandard with the Pre-seismic vulnerability curves is shown in Figure 6.20. Although the corresponding predictions for MDR agree at the very early stages the derived curves show a much more rapid increase in MDR and predict considerably lower MMI level at complete damage. The same conclusion can be drawn from the comparison of the Superior with the Basic design buildings curves shown in Figure 6.21.

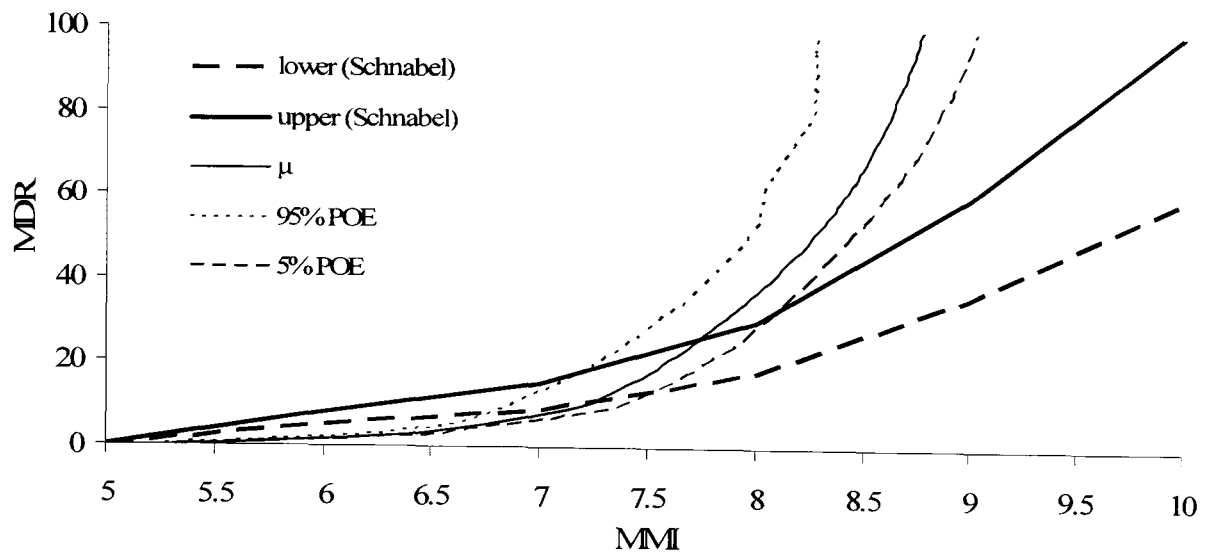


Figure 6.20 Comparison of vulnerability curves for substandard construction

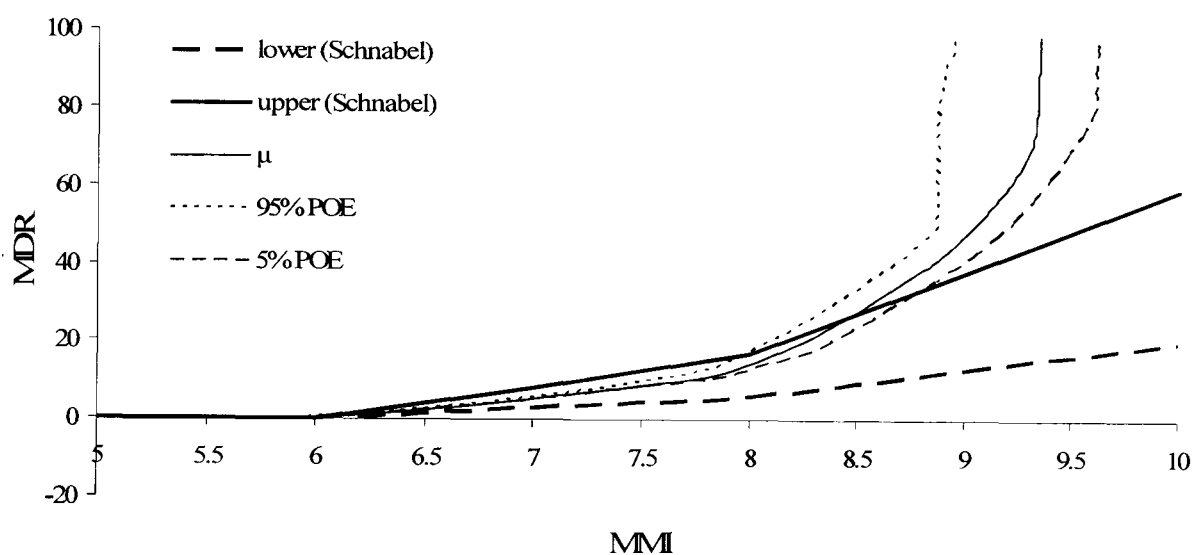


Figure 6.21 Comparison of vulnerability curves for superior construction

It is clear that the derived curves for LR buildings overestimate the damage potential compared to the empirical observations used in the derivation of Schnabel's curves. This may be attributed to the fact that in the reverse MADRS procedure the EC-8 (2004) Type 1 elastic spectrum is used, which is widely accepted that it overestimates the earthquake potential in Cyprus. This type of elastic spectrum can be used as the envelope of seismic records in regions with high seismicity and most importantly with long duration events. In such regions, buildings undergo several cycles at the high PGA levels. Cyprus is located in a moderately seismic region, in which case most damaging events constitute of a single spike. Therefore, it is anticipated that for the specific case of Cyprus, the EC-8 (2004) Type 2 elastic response spectrum may be more appropriate to simulate the seismic activity. It is also suggested by EC-8 (2004) that *if the earthquakes that contribute most to the seismic hazard defined for the site for the*

purpose of probabilistic hazard assessment have a surface-wave magnitude, M_s , not greater than 5.5, it is recommended that the Type 2 spectrum is adopted. Therefore, to address the specific classes of buildings in Cyprus, the probabilistic vulnerability curves are re-calculated using the Type 2 elastic spectrum as the earthquake demand parameter.

The comparison of the revised curves (Type 2 spectrum) for Pre-seismic and Basic designed buildings with Schnabel’s curves for substandard and superior construction is shown in Figures 6.22 and 6.23, respectively.

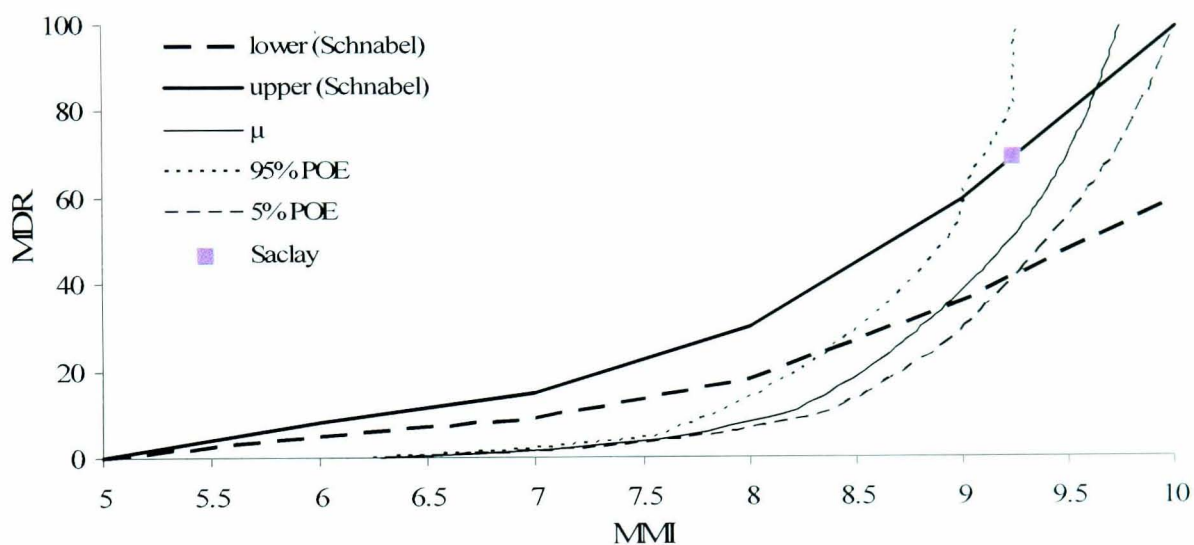


Figure 6.22 Comparison of vulnerability curves for Substandard construction (Type 2 spectrum)

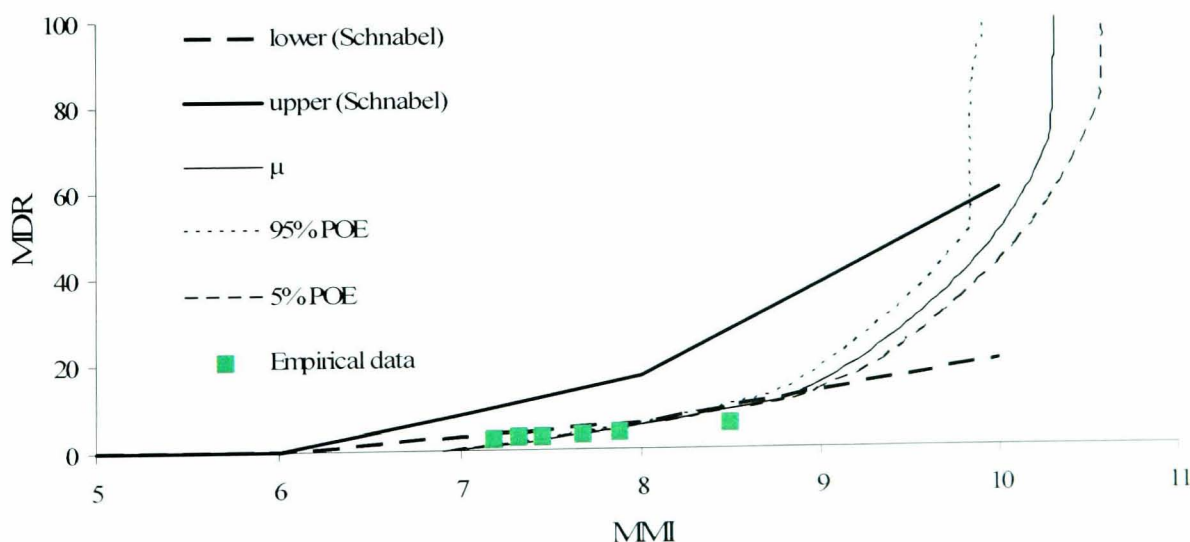


Figure 6.23 Comparison of vulnerability curves for superior construction (Type 2 spectrum)

In both cases a close correlation is observed up to an MDR of around 50%. The curves for Basic design buildings are also compared with the limited damage data obtained

from recent seismic activity in Cyprus (see chapter 3) showing very good correlation with the derived vulnerability curves. Beyond MDR=50% Schnabel's curves seem to underestimate the rapid increase in damage observed in the proposed curves. Since no previous experience exists for such buildings subjected to high levels of excitation, reference can be made to the Saclay frame (see Chapter 5). The MRD for the Saclay frame computed based on the DI in equation 6.17 is shown in Figure 6.21. Though no much visible damage was observed at PGA=0.4g the frame was severely damaged and was considered to be close to collapse. Hence, it is unlikely that the frame would have resisted much higher intensity levels, contradicting the Schnabel's curves in this region.

Based on the above discussion it is concluded that the revised curves using the Type 2 elastic spectrum are more representative of the distribution of damage for buildings in Cyprus. It should be noted though, that the initially derived vulnerability curves (using Type 1 elastic spectrum) should be used for vulnerability assessment purposes in high seismicity regions. The analytical vulnerability curves adopted for the region of Cyprus for LR and MR buildings for the three CDP periods are shown in Figures 6.24 to 6.29.

It should be pointed out that what is proposed here is that vulnerability curves are not just a function of the structural characteristics, but they are also a function of the response spectrum. Hence, for the same type of building different vulnerability curves should be derived, based on the local seismic hazard.

The objective set in Chapter 1 for the enhancement of the existing vulnerability curves for Cyprus is now completed. The derived curves will be substituted into the earthquake risk assessment framework produced by Kythreoti (EQ-RACY, 2001) to improve the estimation of the earthquake risk for Cyprus.

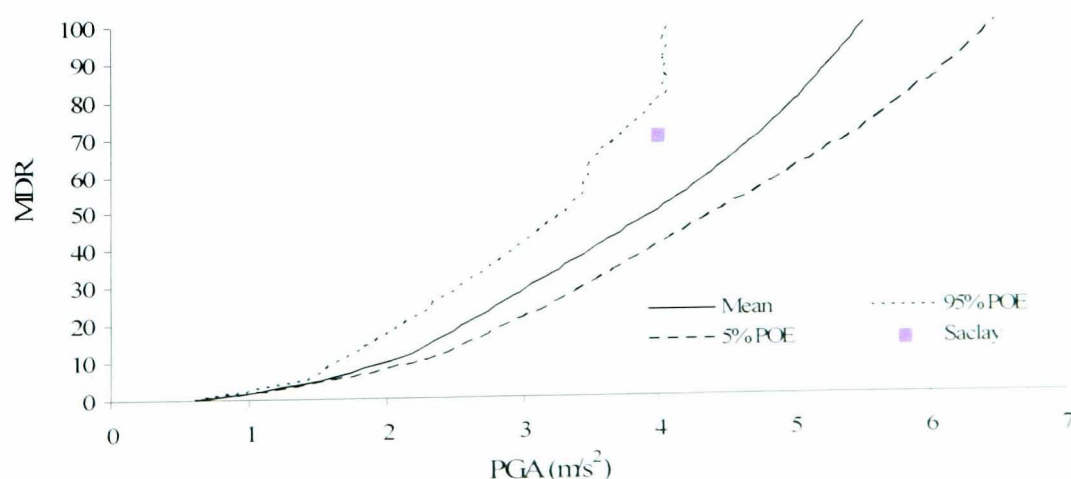


Figure 6.24 Analytical vulnerability curves for LR Pre-seismic buildings in Cyprus

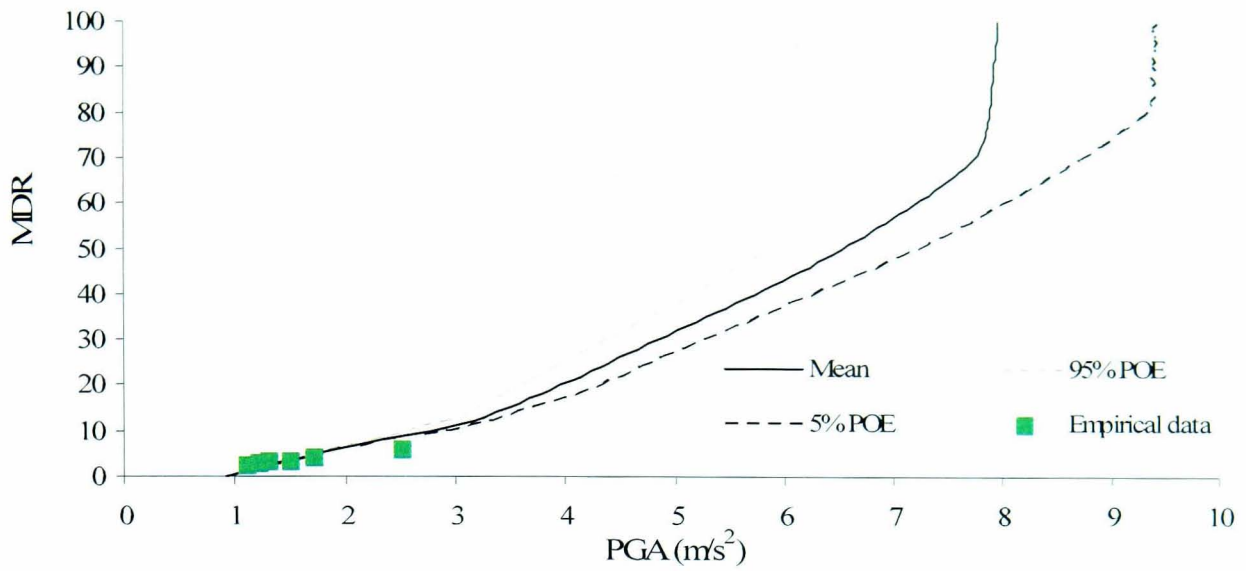


Figure 6.25 Analytical vulnerability curves for LR Basic designed buildings in Cyprus

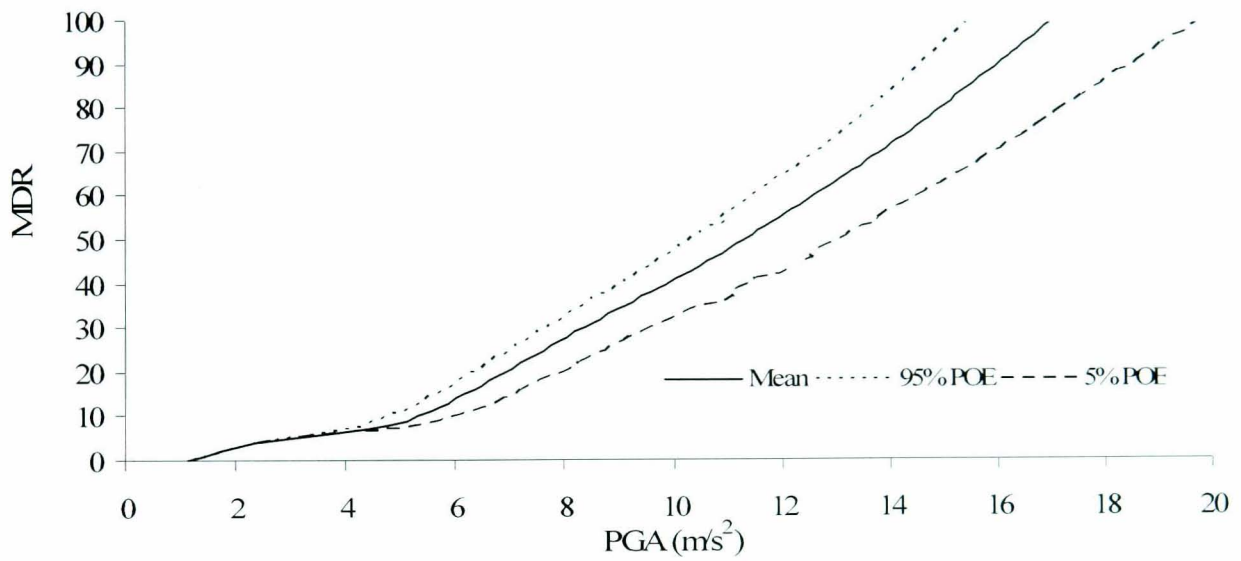


Figure 6.26 Analytical vulnerability curves for LR Modern seismic buildings in Cyprus

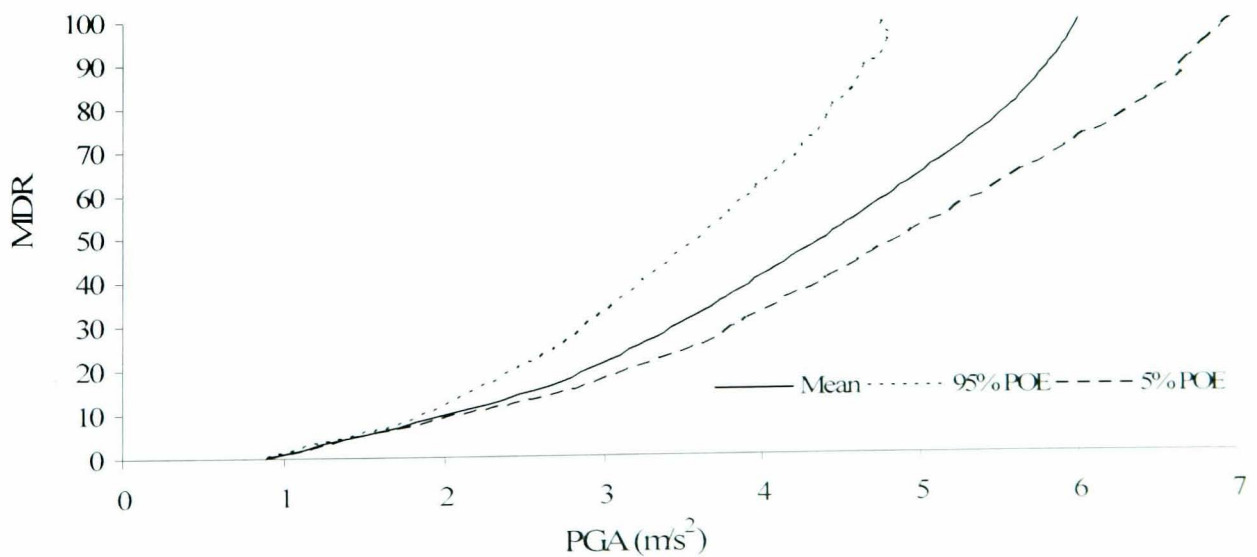


Figure 6.27 Analytical vulnerability curves for MR Pre-seismic buildings in Cyprus

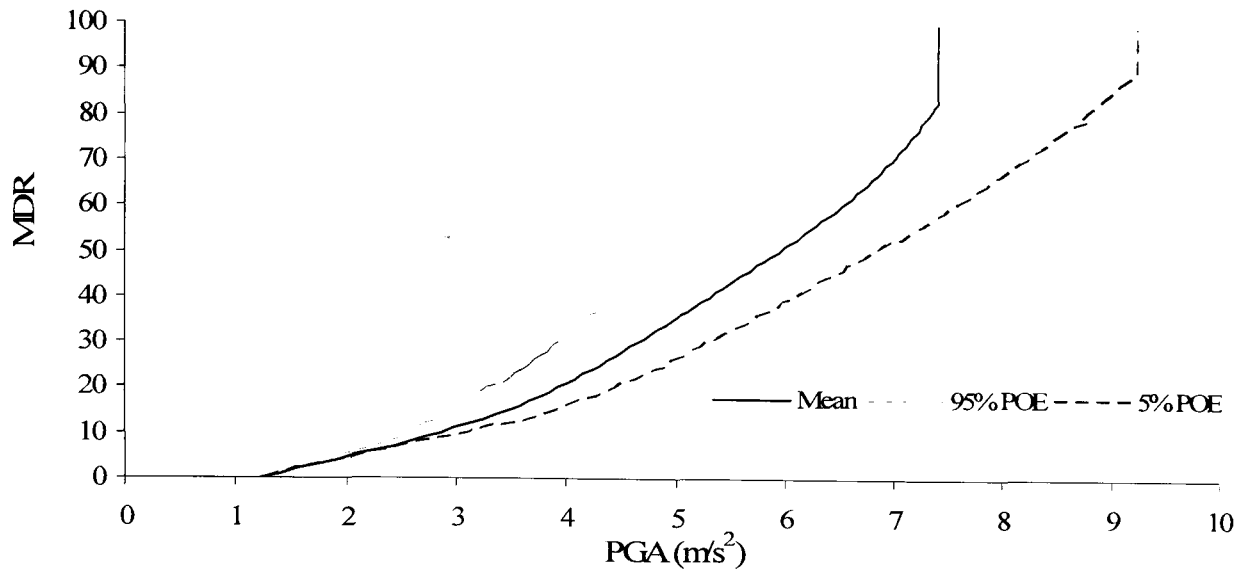


Figure 6.28 Analytical vulnerability curves for MR Basic designed buildings in Cyprus

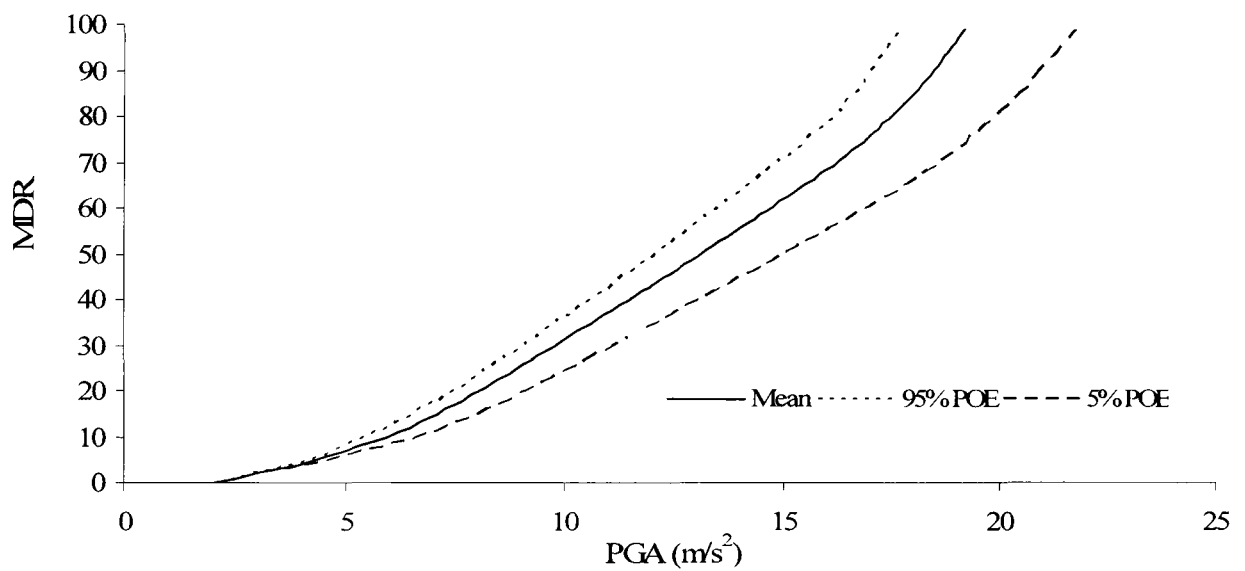


Figure 6.29 Analytical vulnerability curves for MR Modern seismic buildings in Cyprus

Chapter 7

EARTHQUAKE RISK

ASSESSMENT

7.1. Introduction

In this chapter, the enhanced models developed for PGA attenuation and vulnerability are used in the Earthquake Risk Assessment framework “EQ-RACY” (Kythreoti, 2001) to compute the seismic risk for the region of Cyprus.

7.2. Background on EQ-RACY

The Earthquake Risk Assessment framework “EQ-RACY” was initially developed by Kythreoti (2001) to predict the earthquake risk for the region of Cyprus. Both parameters constituting the earthquake risk (hazard and vulnerability) were treated probabilistically. The hazard is based on an earthquake catalogue compiled for past seismicity in the region for a period of 103 years. The variability of future seismic events is introduced by varying spatially the epicentral location ($\pm 15\text{km}$), depth ($\pm 20\text{km}$) and magnitude (± 0.2) of past events.

The coordinates of the all cities and villages in Cyprus were introduced in the framework in small geographical units which include amongst other, information on geology and type and number of buildings. The hazard at each location from each earthquake was calculated using Theodulidis and Papazachos (1992) attenuation laws as derived for Greece. The soil conditions at each location were also treated probabilistically ($\pm 0.25S$). The vulnerability (MDR) of the building stock was obtained from Schnabel’s empirical curves and was also treated probabilistically ($\pm 20\%$). The

estimated hazard and vulnerability at each location was combined with cost and integrated to arrive at the total risk.

The main recommendations for future research included the enhancement of the hazard attenuation laws based on data from Cyprus and the derivation of new vulnerability curves representative of the building stock in Cyprus. These recommendations have already been addressed in this thesis and the enhanced models were used in EQ-RACY to arrive at the seismic risk for Cyprus.

7.3. Estimation of earthquake risk for the region of Cyprus

The average total risk using the previous models was found to be CY£802m for a return period of 103 years, which corresponds to an annual risk of CY£7,8m (1996 replacement values).

After substituting the newly derived PGA attenuation law (chapter 3) and the analytical vulnerability curves (chapter 6) into EQ-RACY (Kythreoti, 2001) the probabilistic analysis of the framework (EQ-RACY) was repeated using 100 simulations (using the inherent variability discussed in 7.2) of the 103 years earthquake catalogue. This simulation study resulted in average annual risk prediction (average of 100 earthquake catalogues x 103 years for each catalogue) of CY£8,9m (1996 values). This value increases to CY£13m for the same building stock using 2007 prices. The increase can be attributed to the rapid increase in damage observed in 6.4.5.3 for Pre and Basic design buildings.

Based on data from the Statistical Service of Cyprus, Kythreoti (2001) concluded that the total number of buildings used as living quarters up to 1996 was 294,563. By dividing the average annual risk with the total number of buildings the annual risk per building (with a 1996 average construction cost of CY£44,490) is equal to CY£30. The insurance premium value allocated to seismic risk in 2007 by insurance companies (Hatzijortsis, 2007) in the island range between 0.06-0.08%. Hence, the average annual insurance premium allocated to seismic risk per building (using 1996 values) is CY£31. which is very close to the annual risk per building estimated value using the new models and EQ-RACY. Therefore, it appears that insurance companies estimate the overall earthquake risk accurately as far as the whole of the island is concerned.

Since the framework (EQ-RACY) provides risk estimates for every location and different buildings types around the island, it was decided to examine the risk results only for Pre-Seismic buildings since it is regarded as the most vulnerable construction period. The analysis of the risk results concluded that the average annual risk per building in this construction period is equal to CY£98, which is three times the average annual premium value. Therefore for Pre-seismic construction, it appears that the insurance companies underestimate this risk considerably. However, this is compensated by the fact that the number of these buildings is reducing with time.

Finally the spreading of risk around the island was assessed using the risk estimates from the simulations for each city. The spread of risk in the island was also assessed by Kythreoti (2001) (Figure 8.1), concluding that existing premium values are:

- Conservative for Nicosia and Larnaca
- Unconservative for Limassol and Famacusta
- Unrealistically low for Paphos

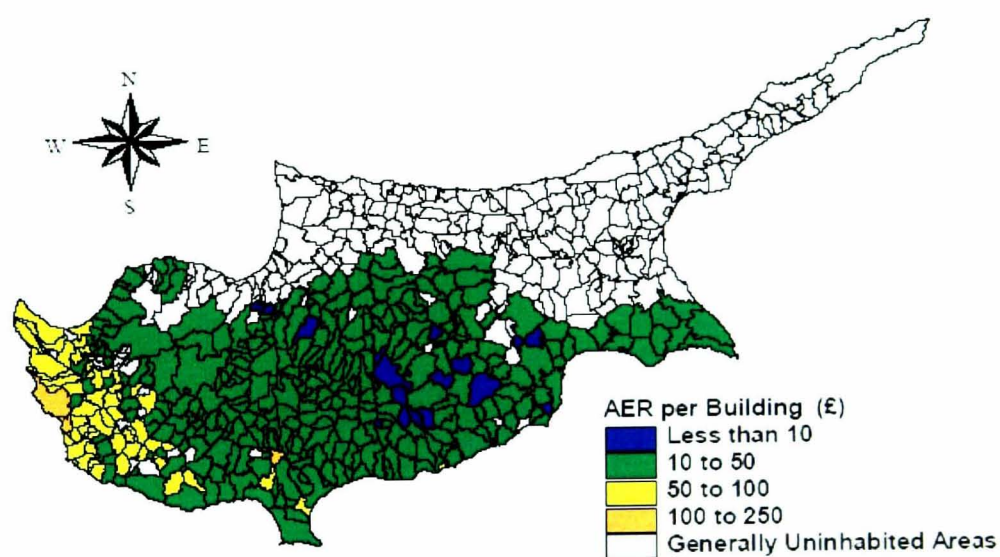


Figure 7.1 Spreading of risk around the island (Kythreoti, 2001).

The results from the simulation study conducted herein verified Kythreoti's (2001) observations resulting in a maximum annual risk of CY£150 for Pre-seismic construction in Pegeia (Paphos municipality).

Chapter 8

SUMMARY AND CONCLUSIONS

8.1 Introduction

The aim of this study was to combine empirical damage data and analytical techniques and develop a framework for improved earthquake vulnerability assessment. The framework was intended to be demonstrated using the island of Cyprus as a case study. Early in the study it was realised that due to limited empirical data the framework should rely entirely on analytical techniques, and empirical data should only be used for comparison purposes. Thus, the bulk of the work concentrates on the derivation of analytical vulnerability curves.

This chapter presents a summary and main conclusions followed by a list of the recommended topics for future work.

8.2 Summary and main conclusions

The derivation of analytical vulnerability curves is a multidisciplinary problem, whose accomplishment is dependent on many issues. It is concluded that the single most important issue is the definition of an appropriate structural model, which requires sophisticated modelling capabilities to simulate brittle failure modes, something which has not been done in detail in the past. It was shown in the vulnerability curves in chapter 6 that such failure modes influence the shape of the vulnerability curves in a great degree by causing sudden increase in MDR's.

From the review of existing vulnerability assessment methods it is concluded that:

- Empirical vulnerability curves in the literature are derived based on limited data especially at high vulnerability levels, and disregard the effect of a combination between construction type and period.
- Curves based on expert opinion are biased towards the types and age of buildings of the expert experience.
- Analytical vulnerability curves provide the most reliable alternative but, in order to be examined in detail, require sophisticated modelling and analysis techniques.

From the processing of field data it was concluded that:

- A new PGA attenuation law (based on the mathematical model and derivation procedure proposed by Theodulidis and Papazachos, 1992) is proposed and this leads to improved predictions for the region of Cyprus.
- Very limited information can be drawn from the processing of the damage data from Cyprus since they cover only low vulnerability values.

From the review on modelling it was concluded that:

- Sophisticated modelling needs to be adopted in order to obtain results on the structural response for a variety of typical failure modes. The models in DRAIN-3D were found to be appropriate for this study.
- The calibration of the capacity models, available in DRAIN-3D, for each anticipated failure mode was undertaken using data from the literature and expert judgment.
- The analytical tool was verified both on the global and local level against recorded data from shaking table tests.

From the derivation process of analytical vulnerability curves:

- A modified capacity-spectrum procedure was adopted for the estimation of structural response and verified against time-history results. This procedure includes the bilinearisation of strain softening capacity curves so as to simulate structural deterioration due to a variety of local brittle modes of failure.
- A reverse capacity-spectrum procedure was assembled for the estimation of structural response for exposure to specific PGA levels.
- A damage index was adopted based on fundamental period shift and this was linked to MDR's.
- The selected key probabilistic parameters were chosen from the capacity models of all credible failure modes.
- The probability distribution functions of the key parameters are defined based on experimental results and expert judgment.
- The simulation values used in probabilistic analysis can be obtained using the Latin Hypercube Sampling method.
- Analytical vulnerability curves were derived for two example buildings and three design levels.

From the derived analytical vulnerability curves

- A rapid increase in damage well before the anticipated flexural failure threshold is observed in "Pre" and "Basic" design buildings. This occurs due to the dominance of brittle failure modes. Such behaviour is not currently anticipated by any simple analytical vulnerability curves or existing curves for Cyprus.

- The effect of the local spectrum on the vulnerability curves was found to be considerable and should be taken into account when developing regional vulnerability curves.
- In the case of Cyprus, Type 2 spectra (EC-8, 2004) were found to simulate better the earthquake hazard potential.
- The average annual earthquake risk for Cyprus is CY£9.8m (1996 values) and CY£13m for the same building stock for 2007 values.
- Annual insurance premiums allocated for seismic risk range between 0.06-0.08% and as such predict the overall risk accurately. However, the use of a single premium for all building types and the entire island leads to an underestimation of seismic risk in Pre-seismic buildings by up to three times. This underestimation is more profound in regions along the southwest coast of the island.

8.3 Recommendations for future work

- The derived PGA attenuation law needs to be verified against an extended PGA database.
- The derived analytical vulnerability curves should be compared with future local damage data and data from experimental results on these types of buildings.
- The calibration of the capacity models in DRAIN-3D needs to be undertaken in more detail using more experimental data. More sophisticated models are still required to capture all the anticipated failure modes.
- The damage index used should be calibrated against field data so as to improve the link to damage limits.
- The effect of semi-rigid foundations on structural response needs further examination.

- The effect of infills was beyond the scope of this study but should be considered in future similar work.
- The probabilistic distribution functions of the key parameters should be verified against experimental data.
- A larger number of deterministic design parameters should be treated probabilistically.
- A larger number of building types and configurations need to be considered.
- Statistical data in EQ-RACY need to be updated.
- EQ-RACY framework should be implemented in GIS.

REFERENCES

ACI 318-99/318r-99 (1999) Building code requirements for structural concrete and commentary, ACI Committee 318.

Ahmed M. (2006) Earthquake loss estimation and structural vulnerability assessment for Greater Cairo. Department of Civil and Environmental Engineering. Imperial College, PhD Thesis.

Ambraseys N. (1975) Trends in engineering seismology in Europe, Fifth European Conference on Earthquake Engineering, 3, 39-52.

Ambraseys N. (2002) Engineering Seismology in Europe. 12th European Conference on Earthquake Engineering. Elsevier Science Ltd.

Ambraseys N., and Bommer J. (1991) The attenuation of ground accelerations in Europe, *Earthquake Engineering & Structural Dynamics*, 20, 1179-1202.

Antoniou S. (2002) Advanced inelastic static analysis for seismic assessment of structures. Department of Civil and Environmental Engineering. Imperial College of Science, Technology and Medicine, PhD Thesis.

Armenia, Building Codes Of (1995) Seismic resistant construction, SNRA II-2.02.94. Yerevan.

ATC Applied Technology Council (1982) An investigation of the correlation between earthquake ground motion and building performance (ATC-10), Publication of the Applied Technology Council, Redwood City, California.

ATC Applied Technology Council (1985) Earthquake damage evaluation data for California (ATC-13), Publication of the Applied Technology Council. Redwood City, California.

ATC Applied Technology Council (1987) Evaluating the seismic resistance of existing buildings (ATC-14), Publication of the Applied Technology Council, Redwood City, California.

ATC Applied Technology Council (1996) Seismic evaluation and retrofit of concrete buildings (ATC-40), Publication of the Applied Technology Council, Redwood City, California.

ATC Applied Technology Council (1997) Earthquake damage and loss estimation methodology and data for Salt Lake County (ATC-36), Publication of the Applied Technology Council, Utah.

Ayoub A., and Filippou F. (1999) Mixed Formulation of Bond-Slip Problems under Cyclic Loads, *Journal of Structural Engineering*, 125, (6), 661-671.

Ayyub B., and McCuen R. (1995) Chapter 4 – Simulation-based Reliability Methods in Probabilistic Structural Mechanics Handbook-Theory and Industrial Applications, Ed. Sundararajan C. R., Chapman & Hall, 53-69.

Balazs G. (1991) Fatigue of bond, *ACI Materials*, 88, (6), 620-629.

Bardakis V., and Dritsos S. (2007), Evaluating assumptions for seismic assessment of existing buildings. *Journal of Soil Dynamics and Earthquake Engineering*, 27, 223-233.

Biddah A., Ghobarah A., and Tarek A. (1997) Upgrading of nonductile reinforced concrete frame connections, *Journal of Structural Engineering*, 123, (8), 1001-1010.

Blume J., Newmark N., and Corning L. (1961) Design of Multi-storey RC buildings for earthquake motions, Portland Cement Association, Chicago, U.S.A.

Brancaleoni F., Ciampi V., and Di Antonio R. (1983) Rate-type models for nonlinear hysteretic structural behaviour, *EUROMECH Colloquium*, Palermo, Italy.

- BS8110-3 (1985) Structural use of concrete, British Standard Institution, London.
- BSI (CP110) (1972) The structural use of concrete, Part 1, British Standards Institution, London.
- Calvi G.M. (1999) A displacement-based approach for vulnerability evaluation of classes of buildings, *Journal of Earthquake Engineering*, 3, (3), 411-438.
- Calvi G.M., Pinho R., and Crowley H. (2006) State-of-the-knowledge on the period elongation of RC buildings during strong ground shaking, First European Conference on Earthquake Engineering and Seismology, Geneva, 3-8 September 2006, Paper No. 1535.
- Chaudat T., Garnier C., and Poupin S. (2005) Ecoleader project No.2-Seismic tests on an RC frame with FRP retrofiting-Tests report. SEMT/EMSI/RT/05-006/A.
- Chaudat T., Pilakoutas K., Papastergiou P., and Ciupala A. (2006) Shaking Table tests on RC retrofitted frame with FRP. First European Conference on Earthquake Engineering and Seismology, Paper Number: 996.
- Chin-Hsiung L., and Ching T. (2001) Response of the earthquake engineering research community to the Chi-Chi (Taiwan) earthquake, *Journal of Earthquake Spectra*, 17, (4), 625-656.
- Chopra A., and Goel R. (1999) Capacity-Demand diagram methods based on inelastic design spectrum, *Earthquake Spectra*, 15, (4), 637-656.
- Chopra A., and Goel R. (2002) A modal pushover analysis procedure for estimating seismic demands for buildings., *Earthquake Engineering & Structural Dynamics*, 31, (3), 561-582.
- Cladera A., and Mari A. (2007) Shear strength in the Eurocode 2. A step forward? *Structural Concrete*, 8, (2).

Clough R., Benuska K., and Wilson E. (1965) Inelastic earthquake response of tall buildings, Proceedings of the 3rd World Conference on Earthquake Engineering, New Zealand, 2, 68-89.

Clyde C., Pantelides C., and Reaveley L. (2000) Performance-Based Evaluation of Exterior Reinforced Concrete Building Joints for Seismic Excitation, PEER 2000/05, 3, (1), 1-5.

Coburn A., and Spence R. (1992) Earthquake Protection, John Wiley & Sons, Chichester.

Comite Euro-International Du Beton (Ceb). (1993) CEB-FIP Model Code 1990, CEB Bulletin d'Information 213-214.

Comite Europeen De Normalization (Cen). (2000) Eurocode (EC) 2: Design of concrete structures-Part 1 General rules and rules for buildings (prEN-1992-1-1).

Comite Europeen De Normalization (Cen). (2004) Eurocode (EC) 2: Design of concrete structures-Part 1 General rules and rules for buildings (prEN-1992-1-1).

Comite Europeen De Normalization (Cen). (2004) (EC) 8: Design of structures for earthquake resistance-Part 1 General rules, seismic actions and rules for buildings (EN 1998-1).

Constantinou G. (1997) Introduction to the Geology of Cyprus. Ministry of Agriculture and Natural Resources, Geology Department. Nicosia, Cyprus.

Cripps J. (1999) S-values for attenuation relationships, Personal Communication with Dr. Stella Kythreoti, cited in Kythreoti, (2001), Department of Civil Engineering, University of Sheffield, UK. PhD Thesis.

Culver C. (1975) National hazards evaluation of existing buildings. Journal of Building Science, 61, (3), 142-166.

Cyprus Civil Engineers and Architects Association (1991) Seismic code for RC structures in Cyprus, Streets and Buildings Regulations authority.

Demartinos K., and Dritsos S. (2006), First Level Pre-Earthquake Assessment of Buildings Using the Fuzzy Logic Method” Earthquake Spectra Journal, 22, 4, p.p.865-885.

Deng C., Oreste B., and Zandonini R. (2000) A hysteretic connection element and its applications, Computers and Structures, 78, (1), 93-110.

Department of Town Planning and Housing. (1985) Minimum requirements for aseismic design of buildings in Cyprus.

Dhakai R., Pan T-C., Irawan P., Tsai K., Lin K-C., and Chen C-H. (2005) Experimental study on the dynamic response of gravity-designed RC connections, Engineering Structures, 27, (1), 75-87.

Dipascuale E., and Cakman A.S. (1988) Identification of the serviceability limit state and detection of seismic structural damage. Report NCEER-88-0022, National Centre for Earthquake Engineering Research. State University of New York at Buffalo, NY.

Dritsos S. (2008) Personal communication.

Dymiotis C. (2000) Probabilistic seismic assessment of reinforced concrete buildings with and without masonry infill walls. Department of Civil and Environmental Engineering. Imperial College of Science, Technology and Medicine, PhD Thesis.

Demetriou T. (2007) Personal communication. Cyprus Rehabilitation Service.

Elenas A., and Meskouris K. (2001) Correlation study between seismic acceleration parameters and damage indices of structures. Journal of Engineering Structures, 23, 698-704.

Eligehausen R., Popov E., and Bertero V. (1983) Local bond stress-slip relationships of deformed bars under generalized excitations, Report No. UCB/EERC-83/23. Earthquake Engineering Research Center, College of Engineering, University of California, Berkeley, CA.

Elnashai A. (1999) The North Athens (Greece) Earthquake of 7 September 1999. Analytical Studies of Structural Response, Report No. ESEE 99-4.

Elnashai A., Pinho R., and Antoniou S. (2000) INDYAS-A program for inelastic dynamic analysis of structures. ESEE report 00-2, Imperial College, London.

European Macroseismic Scale (Ems). (1998) Centre Europeen de Geodynamique et de Seismologie, Luxembourg.

Fajfar P. (1999) Capacity spectrum method based on inelastic demand spectra, *Earthquake Engineering & Structural Dynamics*, 28, 979-993.

FEMA 273. NEHERP (1997) Guidelines for the seismic rehabilitation of buildings, Federal emergency management agency report no.273, Applied Technology Council, Washington, USA.

FEMA 310. NEHERP (1998) Handbook of the seismic evaluation of existing buildings – a Pre-standard, Federal emergency management agency report no.310, Applied Technology Council, Washington, USA.

FEMA 356. NEHERP (2000) Prestandard and Commentary for the Seismic Rehabilitation of Buildings, Federal emergency management agency report no.356, Applied Technology Council, Washington, USA.

FEMA 154. NEHERP (2001) Report on the Rapid Visual Screening of Buildings for Potential Seismic Hazards, Federal emergency management agency report no.154, Applied Technology Council, Washington, USA.

FEMA 440 (2005) Improvement of nonlinear static seismic analysis procedures. Applied Technology Council (ATC-55 Project), Redwood City, California.

Filippou F., Popov E., and Bertero V. (1983) Modeling of Reinforced Concrete Joints under Cyclic Excitations, *Journal of Structural Engineering*, 109, (11).

Freeman S. (1978) Prediction of response of concrete buildings to severe earthquake motion, Proceedings of Douglas McHenry International Symposium on concrete and concrete structures, Publication SP-55, American Concrete Institute, Detroit, Michigan, US.

Freeman S. (2004) Review of the development of the capacity spectrum method, *Journal of Earthquake Technology*, 41, (1), 1-13.

Freeman S., Nicolletti J., and Matsumura G. (1984) Evaluation of existing buildings for seismic risk-A case study of Puget Sound Naval Shipyard, Bremerton, Washington, Proceedings of U.S National Conference on Earthquake Engineering, Berkeley, U.S.A, 113-122.

Gajado E., Franke M., and Quijada P. (1998) Seismic microzonation of Larnaca, Cyprus, Ministry of Agriculture, Natural Resources and Environment, Geological Survey Department.

Ghobarah A., Abou-Elfath H., and Biddah A. (1999) Response-based damage assessment of structures, *Earthquake Engineering & Structural Dynamics*, 28, (1), 79-104.

Greek Ministry for Environmental Planning and Public Works. GRECO (draft version). (2004) Greek Retrofitting Code, Greek Organization for Seismic Planning and Protection, Athens, [in Greek].

Gunturi S., and Shah K. (1992) Building specific earthquake damage estimation. Department of Civil Engineering. Stanford University, Stanford, CA, PhD Thesis.

Hatzijortsis (2007) Personal Communication. Superintendent of Insurances.

Imbsen and Associates, Inc. XTRACT (2002) – Cross-section analysis program for structural engineer, ver. 2.6.2, California.

International Building Codes of Nis (2001) Seismic resistant construction, Moscow.

IPRG (1995) Seismological Bulletin of Israel 1900-1994, Institute for Petroleum Research and Geophysics, Holon, Israel.

Isakovic T., and Fischinger M. (1998) Analysis of fibre beam-column element in DRAIN-3D (Type 15), Report IKPIR, EE 2/98, University of Ljubljana.

Joyner W., and Boore D. (1981) Peak horizontal acceleration and velocity from strong motion records including records from 1979 Imperial Valley, California, earthquake. Bulletin of the Seismological Society, 71, 2011-2038.

Kalkan E., and Kunnath S. (2004) Method of modal combinations for pushover analysis of buildings. 13th World Conference on Earthquake Engineering. Vancouver, B.C., Canada.

Kappos A., and Xenos A. (1996) A distributed shear flexibility model for seismic damage assessment for reinforced concrete structures. Proceedings of the 11th European Conf. on Earthquake Engineering. Paris.

Kappos A., Panagopoulos G. And Penelis G. (2007) Development of a seismic damage and loss scenario for contemporary and historical buildings in Thessaloniki, Greece, Journal of Soil Dynamics and Earthquake Engineering, doi:10.1016/j.soildyn.2007.10.017.

Kwak H., and Filippou F. (1990) Finite element analysis of reinforced concrete structures under monotonic loads. Report No. UCB/SEMM-90/14. University of California, Berkeley.

Kypridakis I. (2004) Personal communication. Statistical Service of Cyprus.

Kyriakides C. (2007) Existing vulnerability curves and design practise for Cyprus. Personal Communication.

- Kythreoti S. (2001) Earthquake risk assessment and management. Case Study: Cyprus. Department of Civil and Structural Engineering. University of Sheffield, PhD Thesis.
- Mandas A., and Dritsos D. (2004) Vulnerability Assessment of RC Structures Using Fuzzy Logic., Proceedings of the International Conference on Risk Analysis IV. Rhodes, WIT Press, p.p.51-62.
- Lehman D., and Moehle J. (2000) Seismic performance of well-confined concrete bridge columns, PEER-1998/01, University of California, Berkeley.
- Lowes L., Mitra N., and Altoontash A. (2003) A beam-column joint model for simulating the earthquake response of reinforced concrete frames, PEER-2003/10, University of California (400/P33/2003-10).
- McKay M., Conover W., and Beckman R. (1979) A comparison of three methods for selecting values of input variables in the analysis of output from a computer code, *Technometrics*, 21, 239-245.
- Monti G., Filippou F., and Spacone E. (1997) Finite element for anchored bars under cyclic load reversals, *Journal of Structural Engineering*, 123, (5), 614-623.
- Napetvaridze S.G. (1985) Probability Problems of Engineering Seismology and Theory of Seismic Stability [in Russian]. Metsniereba, Tbilisi.
- National Institute of Building Science (NIBS). (1999) Earthquake loss estimation methodology, HAZUS 99 Technical manual, Report prepared for the Federal Emergency Management Agency, Washington D.C.
- Neocleous K. (1999) Design and safety philosophy for concrete structures reinforced with fibre reinforced polymers (FRP). Department of Civil and Structural Engineering. University of Sheffield, PhD Thesis.

- O'Connor J., and Ellingwood B. (1987) Reliability of nonlinear structures with seismic loading, *Journal of Structural Engineering*, 113, (5), 1011-1027.
- Orsini G. (1999) A model for buildings' vulnerability assessment using the Parameterless Scale of Seismic Intensity (PSI), *Earthquake Spectra*, 15, 463-483.
- Pagni C., and Lowes L. (2004) Predicting earthquake damage in older RC beam-column joints, PEER 2003/17.
- Park R., Ang A., and Wen Y. (1985) Seismic damage analysis of RC buildings., *Journal of Structural Engineering*, 111, (4), 740-757.
- Penelis G., and Kappos A. (1997) *Earthquake-resistant concrete structures.*, E&FN Spons, London.
- Pilakoutas K. (2007) Meeting.
- Powell G., and Campbell S. (1994) Drain-3D element description and user guide for element type 01, 04, 05, 08, 09, 15, 17 version 1.10, Report No. UCB/SEMM-94/08, Department of Civil Engineering, University of California, Berkeley.
- Prakash V., Powell G., and Campbell S. (1994) Drain-3D base program description and user guide, version 1.10, Report No. UCB/SEMM-94/07, Department of Civil Engineering, University of California, Berkeley.
- Priestley, M. J. N. (2003) Myths and fallacies in earthquake engineering. revisited: The Malley-Milne lecture, Rose School, Collegio Alessandro Volta, Pavia, Italy.
- Priestley M.J.N, Verma R., and Xiao Y. (1994) Seismic shear strength of RC columns, *Journal of Structural Engineering*, 120, (8), 2310-2329.
- Priestley M.J.N. (1997) Displacement-based seismic assessment for reinforced concrete buildigns, *Journal of Earthquake Engineering*, 1, (1), 157-192.

Rossetto T., and Elnashai A.S. (2002) Derivation of vulnerability functions for European-type RC structures based on observational data, *Engineering Structures*, 25, (10), 1241-1263.

Rossetto T., and Elnashai A.S. (2005) A new analytical procedure for the derivation of displacement-based vulnerability curves for population of RC structures, *Engineering Structures*, 27, (3), 397-409.

Rubiano N. (2001) A comparison of nonlinear models for RC frames, *Advances in Earthquake Engineering, Earthquake Resistance Engineering Structures III*, 9, 327-336.

Schnabel W.E. (1987) The Accumulation of potential in Cyprus. Paper presented at the Number 13: Earthquake risk and insurance - e.g. in Cyprus. Nicosia, Cyprus.

Scawthorn C. (1981) Seismic damage estimation for Low- and Mid-Rise buildings in Japan. *Journal of Earthquake Engineering and Structural Dynamics*, 9, 93-115.

Schierle G. (2000) Northridge Earthquake Field Investigations: Statistical Analysis of Woodframe Damage, CUREE Publication No. W-02, Consortium of Universities for research in Earthquake Engineering, Richmond, CA.

Shiohara H., (2001) New model for shear failure of RC interior beam-column connections. *Journal of Structural Engineering*, 127, (2), 152-160

Stenbrugge K., and Algermissen S. (1990) Earthquake losses to single family dwellings: California experience. U.S. Geological Survey, Reston, VA, 162-213.

Sezen H. (2002) Seismic behaviour and modelling of RC building columns. University of California, PhD Thesis.

Sezen H., and Moehle J. (2003) Bond-slip behaviour of reinforced concrete members. Proceedings, fib Symposium, Concrete Structures in Seismic Regions. Athens, Greece.

Sezen H., and Moehle J. (2004) Shear strength model for RC columns, *Journal of Structural Engineering*, 130, (11), 1692-1703.

Shima H., Choo L., and Okamura H. (1987) Bond characteristics in post-yield range of deformed bars., *Concrete Library of JSCE*, 10, 113-124.

Singhal A., and Kiremidjian A. (1997) A method for earthquake motion-damage relationships with application to reinforced concrete frames. NCEER report, NCEER-97-0008. State University of New York at Buffalo, USA.

Solomis K. (1998) Personal Communication with Dr. Stella Kythreoti, cited in Kythreoti, (2001), Department of Civil Engineering, University of Sheffield, UK. PhD Thesis.

Solomis K. (2002) Personal Communication. Geological Survey Department, Ministry of Agriculture and Natural Resources, Cyprus.

Takeda T., Sozen M., and Nielsen N. (1970) Reinforced concrete response to simulated earthquakes, *Journal of Structural Division (ASCE)*, 96, (12), 2557-2573.

Tassios T. (1979) Properties of bond between concrete and steel under load cycles idealizing seismic actions, *Comite Euro-International De Beton*, Bulletin No.131.

Taucer F., Spacone E., and Filippou F. (1991) A fibre beam-column element for seismic response analysis of RC structures, Report No. UCB/EERC-91/17, Earthquake Engineering Research Centre, University of California, Berkeley.

Technical Chamber of Cyprus (2003) Nicosia seismic risk assessment. A vulnerability study for a UNOPS project.

Theodulidis N. P., and Papazachos B.C. (1992) Dependence of strong ground motion on magnitude-distance, site geology and macroseismic intensity for shallow earthquakes in Greece: I, Peak horizontal acceleration, velocity and displacement, *journal of Soil Dynamics and Earthquake Engineering*, 11, 387-402.

Timchenko I. (2002) Seismic vulnerability assessment of buildings on the basis of numerical analyses. 12th European Conference on Earthquake Engineering. London.

Viawanthanatepa S., Popov E., and Bertero V. (1979) Effect of generalised loadings on bond of reinforcing bars embedded in confined concrete blocks, Report UCB/EERC-79/22. Berkeley, EERC, University of California.

Walker S. (2001) Seismic performance of existing RC beam-column joints. Civil and Environmental Engineering. Seattle: University of Washington, M.S Thesis.

Whitman R., Reed J., and Hong S. (1974) Earthquake damage probability matrices. Proceedings of the fifth World Conference on Earthquake Engineering, pp. 2531. Rome.

Xue Q. (2000) Assessing the accuracy of the damping models used in displacement-based seismic demand evaluation and design of inelastic structures., *Journal of Earthquake Engineering and Engineering Seismology*, 3, (2), 37-44.

Zembaty Z., Kowalski M., and Pospisil S. (2006) Dynamic identification of an RC frame in progressive states of damage, *Engineering Structures*, 28, (5), 668-681.

Appendix A

DATA FOR EMPIRICAL RISK ASSESSMENT

Table A-1. Location and surface geology at the recording stations (Solomis, 2002)

CODE	LOCATION	COORDINATES		BUILDING	GEOLOGY	s
YER	Yermasoya Dam	34.73	33.08	1-st RC small warehouse at the edge of the dam	Marly chalk	0.75
LMS	Limassol	34.67	33.04	1-st prefabricated building	Sands, clays, gravels	0
PSR	Pissouri	34.65	32.72	1-st RC building	Sandstones, marly limestone	0.5
ARM	Arminou Dam	34.87	32.73	1-st RC small warehouse at dam basement	River deposits, over pillow lavas	1
EVR	Evretou Dam	34.98	32.47	1-st RC small warehouse at dam basement	Marly chalk	0.75
LWP	Limassol Water Refinery	34.70	33.00	2-st RC building	Sandstones, marly limestone	0.5
VAS	Vasilikos	34.71	33.32	2-st RC building	Sands, clays, gravels	0
KAL	Kalavassos Dam	34.8	33.26	Dam Crest	Sandstones, marly limestone	0.5
KOU	Kouris Dam	34.73	32.92	Dam Crest	Marly chalk	0.75
KPF	Kato Pafos	34.69	32.44	1-st stone building	Sands, clays, gravels	0
PAF	Pafos	34.77	32.42	3-st RC building	Sands, clays, gravels	0

Table A-2. Main geological formations of Cyprus (after Kythreoti, 2001)

NO	CODE	LITHOLOGY	FORMATION	EPOCH	PERIOD	INFLUENCE ON MMI	S VALUE
1	H	Sands, silts, clay and gravels	Alluvium-Colluvium	Holocene	QUATERNARY	+2	0
2	Mi-Mu	Chalks, marls, marly chalks, chalky marls and calcarenites	Pakhna	Middle Miocene	NEOGENE	+2	0.75
3	Mm	Graywacke, marls, sandstones, siltstones, basal conglomerate	Kythrea	Middle Miocene	NEOGENE	+1.5	0.5
4	K ₃ -Ou	Chalks, marls, marly chalks, chalky marls with cherts in places as bands or nodules	Lefkara	Oligocene Eocene Palaeogene	PALAEOGENE	+1	0.5
5	Ku Tm-Km	Mammonia Complex	Agia Varvara Agios Photios Group Dhiazizos Group	Upper (Maastrichtian) Middle	CRETACEOUS TRIASSIC	-1	0
6	Jl-Kl	Recrystallised massive or medium to thick bedded limestones	Hilarion		JURASSIC	-1	1
7	Ku UPL LPL BG	Olivine, pillow lavas with occasional sheet flows, dykes and sills altered to zeolite facies	Upper Pillow Lavas Lower Pillow Lavas (Volcanic Sequence)	Upper (Campanian)	CRETACEOUS	-1	1
8	Db	Diabase dykes up to 3m wide, aphyric and clinopyroxene and plagioclase-phyric altered to greenschist facies	Sheeted Dykes (Diabase) (Intrusive Sequence)	Upper (Campanian)	CRETACEOUS	-1	1
9	y σ4 σ3 σ2 σ1 σ	Isotropic, urallite, and olivine gabbros, websterites, wehrlites, dunites, tectonized harzburgites, etc.	Gabbro Pyroxenite Wehrlite Dunite Harzburgite Serpentine (Mantke Sequence)	Upper (Campanian)	CRETACEOUS	-1	1

Table A-3. Magnitude and epicentral location of earthquakes in Cyprus (Solomis, 2002)

Earthquake No.	Date Time	φ°N	λ°E	Magnitude M _s	No. of readings
1*	09/10/96 13:10:52	34.41	32.12	5.74	1
2	13/01/97 10:19:26	34.27	32.37	5.25	3
3	25/05/99 17:15:29	34.49	32.30	4.69	4
4*	11/08/99 04:27:35	34.75	33.03	5.6	8
5	12/08/99 03:48:21	34.79	33	4.13	3
6	13/08/99 15:31:40	34.81	32.98	4.55	4
7	17/08/99 15:06:20	34.79	33.02	4.41	1
8	23/08/99 15:02:23	34.78	33.01	3.99	1
9	26/08/99 01:48:50	34.83	32.99	4.27	1
10	23/04/00 04:56:39	34.67	33.29	3.99	1
11	16/12/00 14:27:20	34.27	33.32	4.27	5
12	01/09/01 19:22:46	34.87	33.75	4.13	1
13	10/11/01 02:23:57	34.94	32.51	4.20	2
14	25/04/02 22:34:52	35.16	32.72	3.99	1
15	20/06/02 02:55:48	34.75	33.16	4.06	2

*. Data used for damage assessment

Table A-4. Strong-motion data and surface geology at the recording stations (Solomis, 2002)

Earthquake No.	Record Code	M_s	Intensity MMI	Distance R (km)	Depth (Km)	PGA (cm/sec ²)	Soil parameter (S)
1	YER	5.74	6	95	25	43	0.75
2	LMS	5.25	5	76	20	26	0
2	PSR	5.25	4.5	53	20	19	0.5
2	ARM	5.25	4.5	74	20	16	1
3	LMS	4.69	5	71	30	25	0
3	EVR	4.69	4	55	30	15	0.75
3	LWP	4.69	5	71	30	34	0.5
3	VAS	4.69	2	71	30	4	0
5	LMS	4.13	3.5	8	8	9	0
5	LMS	4.13	5	8	8	24	0
5	LWP	4.13	6	8	8	49	0.5
4	LMS	4.97	7	6	12	119	0
4	LWP	4.97	7	4	12	164	0.5
4	YER	4.97	7	5	12	135	0.75
4	LMS	4.13	6	10	8	39	0
6	LMS	4.27	2.5	14	5	6	0
4	LMS	3.99	4.5	10	5	16	0
6	LMS	4.06	3.5	17	3	10	0
6	LMS	4.13	3.5	16	5	9	0
6	LMS	3.99	3.5	8	20	10	0
4	LMS	4.06	4.5	22	5	15	0
4	LMS	4.55	5	13	5	25	0
4	YER	4.55	5	13	5	25	0.75
7	LMS	4.41	5.5	15	5	30	0
8	LMS	3.99	3	9	1	7	0
9	LMS	4.27	3	17	5	8	0
10	KAL	3.99	4	15	20	21	0.5
11	LMS	4.27	2.5	55	30	6	0
11	LWP	4.27	2	56	30	6	0.5
11	KOU	4.27	2	63	30	6	0.75
11	YER	4.27	3	56	30	9	0.75
11	LPS	4.27	2	52	30	5	0.5
12	KOU	4.13	2	77	40	5	0.75
13	KPF	4.20	2.5	22	10	6	0
13	PAF	4.20	2.5	28	10	5	0
14	KOU	3.99	2	51	35	4	0.75
15	LMS	4.06	5	14	8	25	0
15	LHL	4.06	5	14	8	26	0.5

Table A-5. Representative sample of damage data

Municipality	Building Type	No. of floors	Total building Area (m ²)	Damage (repair in CY£)	Construction Date	Vulnerability (repair/m ²)
Town centre	RC	2	120	£750.00	1997	6.25
*	RC	2	140	£1,035.00	1985	7.39
*	RC	1	240	£800.00	1974	3.33
*	RC	2	140	£310.00	1983	2.21
*	RC	1	120	£185.00	1985	1.54
*	RC	2	150	£1,500.00	1996	10.00
*	RC	1	200	£690.00	1993	3.45
*	RC	2	130	£920.00	1989	7.08
*	RC	1	160	£510.00	1993	3.19
*	RC	1	140	£355.00	1995	2.54
*	RC	1	140	£210.00	1992	1.50
*	RC	2	380	£555.00	1995	1.46
*	RC	1	130	£505.00	1957	3.88
*	RC	1	180	£845.00	1990	4.69
*	RC	1	140	£440.00	1990	3.14
*	RC	1	95	£640.00	1988	6.74
*	RC	2	120	£950.00	1993	7.92
*	RC	2	120	£950.00	1997	7.92

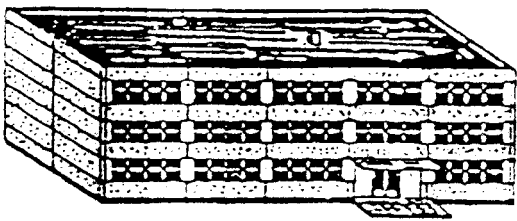
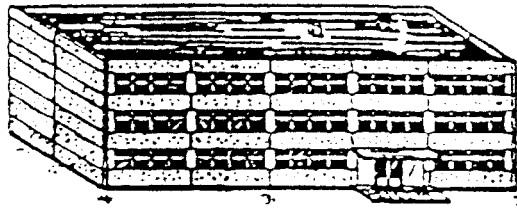
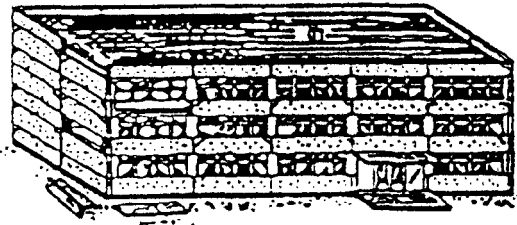


	<p>Grade 1: Negligible to slight damage (no structural damage, slight non-structural damage) Fine cracks in plaster over frame members or in walls at the base. Fine cracks in partitions and infills.</p>
	<p>Grade 2: Moderate damage (slight structural damage, moderate non-structural damage) Cracks in columns and beams of frames and in structural walls. Cracks in partition and infill walls; fall of brittle cladding and plaster. Falling mortar from the joints of wall panels.</p>
	<p>Grade 3: Substantial to heavy damage (moderate structural damage, heavy non-structural damage) Cracks in columns and beam column joints of frames at the base and at joints of coupled walls. Spalling of concrete cover, buckling of reinforced rods. Large cracks in partition and infill walls, failure of individual infill panels.</p>
	<p>Grade 4: Very heavy damage (heavy structural damage, very heavy non-structural damage) Large cracks in structural elements with compression failure of concrete and fracture of rebars; bond failure of beam reinforced bars; tilting of columns. Collapse of a few columns or of a single upper floor.</p>
	<p>Grade 5: Destruction (very heavy structural damage) Collapse of ground floor or parts (e. g. wings) of buildings.</p>

Figure A-1. Damage Grade classification scheme for RC buildings (EMS-1998)

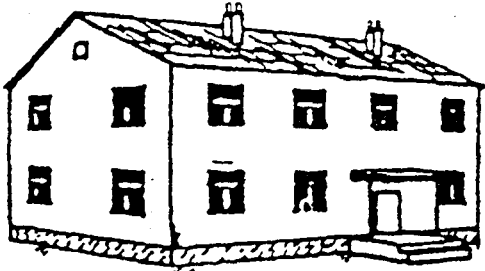
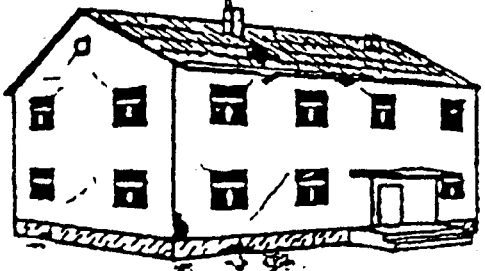
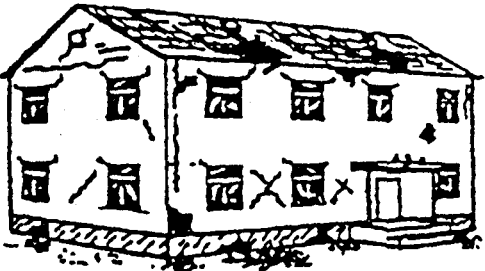


	<p>Grade 1: Negligible to slight damage (no structural damage, slight non-structural damage) Hair-line cracks in very few walls. Fall of small pieces of plaster only. Fall of loose stones from upper parts of buildings in very few cases.</p>
	<p>Grade 2: Moderate damage (slight structural damage, moderate non-structural damage) Cracks in many walls. Fall of fairly large pieces of plaster. Partial collapse of chimneys.</p>
	<p>Grade 3: Substantial to heavy damage (moderate structural damage, heavy non-structural damage) Large and extensive cracks in most walls. Roof tiles detach. Chimneys fracture at the roof line: failure of individual non-struc- tural elements (partitions, gable walls).</p>
	<p>Grade 4: Very heavy damage (heavy structural damage, very heavy non-structural damage) Serious failure of walls: partial structural failure of roofs and floors.</p>
	<p>Grade 5: Destruction (very heavy structural damage) Total or near total collapse.</p>

Figure A-2. Damage Grade classification scheme for Masonry buildings (EMS-1998)

Appendix B

SIMULATION VALUES FOR PROBABILISTIC VUNERABILITY CURVES

Table B-1. Simulation values for key parameters (Pre-seismic buildings)

fc (Mpa)	fy (Mpa)	s	l f(d)
24.4	465	275	21
31.3	429	198	26
26.3	426	286	22
27.3	446	243	23
22.3	368	255	19
35.9	377	240	29
25.6	411	233	22
29.8	483	295	25
33.2	353	282	27
19.6	393	309	17
32.4	421	217	27
38.6	460	237	31
37.3	389	266	31
40.3	435	212	33
21.5	405	273	19
29.3	424	227	24
24.0	454	270	20
43.1	402	254	35
18.2	386	251	16
49.2	418	263	39
15.3	415	224	14
34.5	440	260	28
35.6	399	196	29
28.8	409	248	24
31.2	445	232	26

Table B-2 Simulation values for key parameters (Basic seismic buildings)

fc (Mpa)	fy (Mpa)	s	l f(d)
30.1	575	205	36
36.1	540	128	31
31.8	537	216	31
32.6	556	173	33
28.2	477	185	23
40.1	487	170	25
31.1	521	163	29
34.9	592	225	38
37.8	462	212	21
25.9	503	239	27
37.1	531	147	30
42.5	570	167	35
41.4	500	196	26
44.0	545	142	32
27.6	515	203	28
34.4	535	157	31
29.7	565	200	34
46.4	512	184	28
24.7	496	181	26
51.8	529	193	30
22.1	526	154	30
38.9	550	190	33
39.9	510	126	28
33.9	520	178	29
36.0	556	162	33

Table B-3. Simulation values for key parameters (Modern seismic buildings)

fc (Mpa)	fy (Mpa)	s	l / f(d)
50.1	573	118	47
34.7	482	108	43
52.2	561	59	48
43.6	554	93	46
46.0	547	90	42
43.0	597	144	46
41.7	564	66	41
54.0	588	80	51
51.3	593	112	44
56.8	539	97	47
38.4	585	100	43
42.5	603	72	50
48.1	610	103	46
37.4	544	54	44
49.7	568	164	45
40.5	535	133	42
49.0	522	107	49
45.7	559	140	43
45.1	530	78	45
47.7	553	85	45
39.8	583	89	47
47.1	573	129	41
34.1	661	117	40
44.7	626	125	44
41.5	580	47	49

Appendix C

CROSS-SECTIONAL DETAILS OF SIMULATED FRAMES

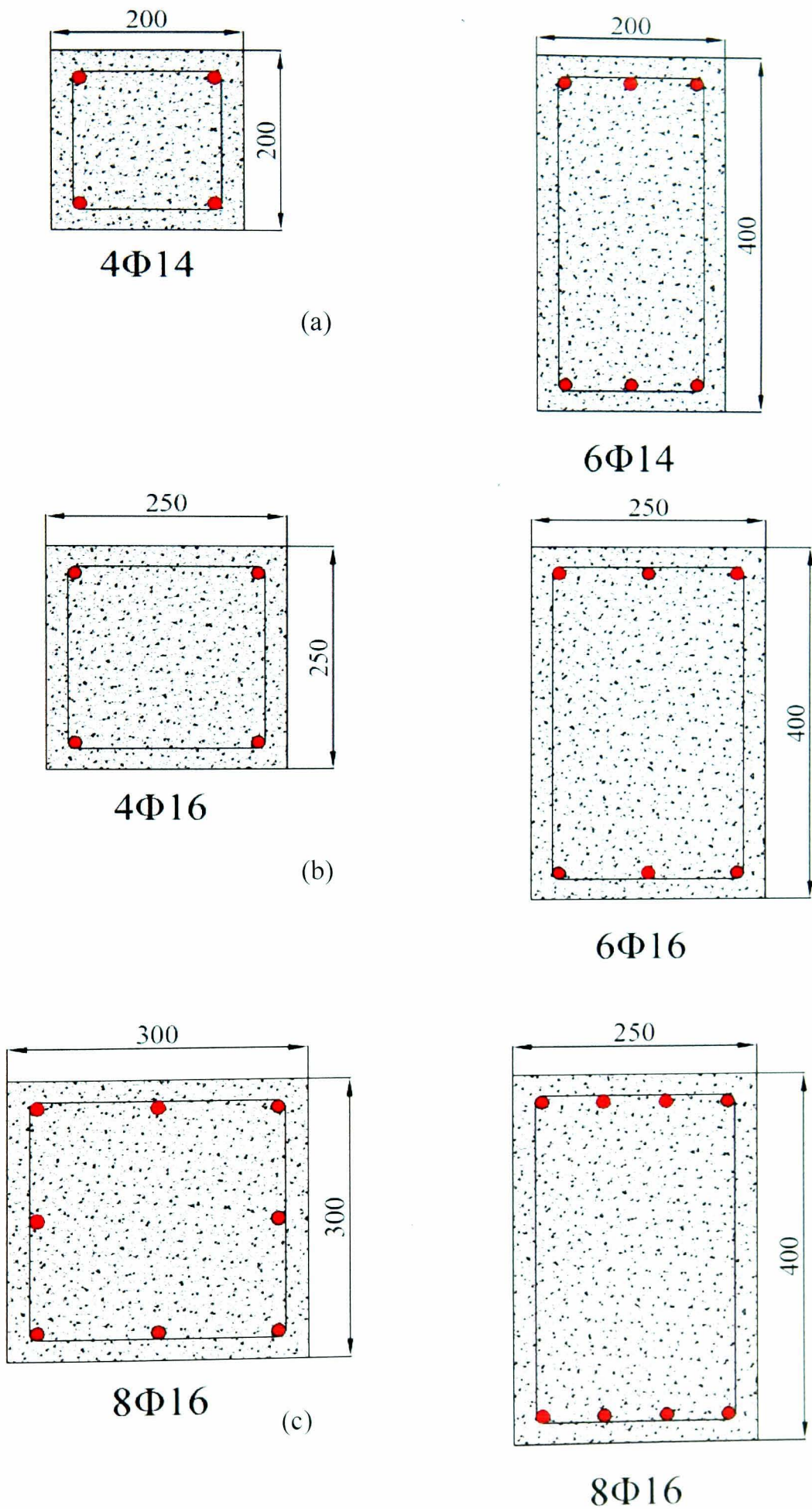


Figure C-1. Cross-sectional design detail of LR frames for (a) Pre., (b) Basic and (c) Modern seismic design (columns on the left hand side).

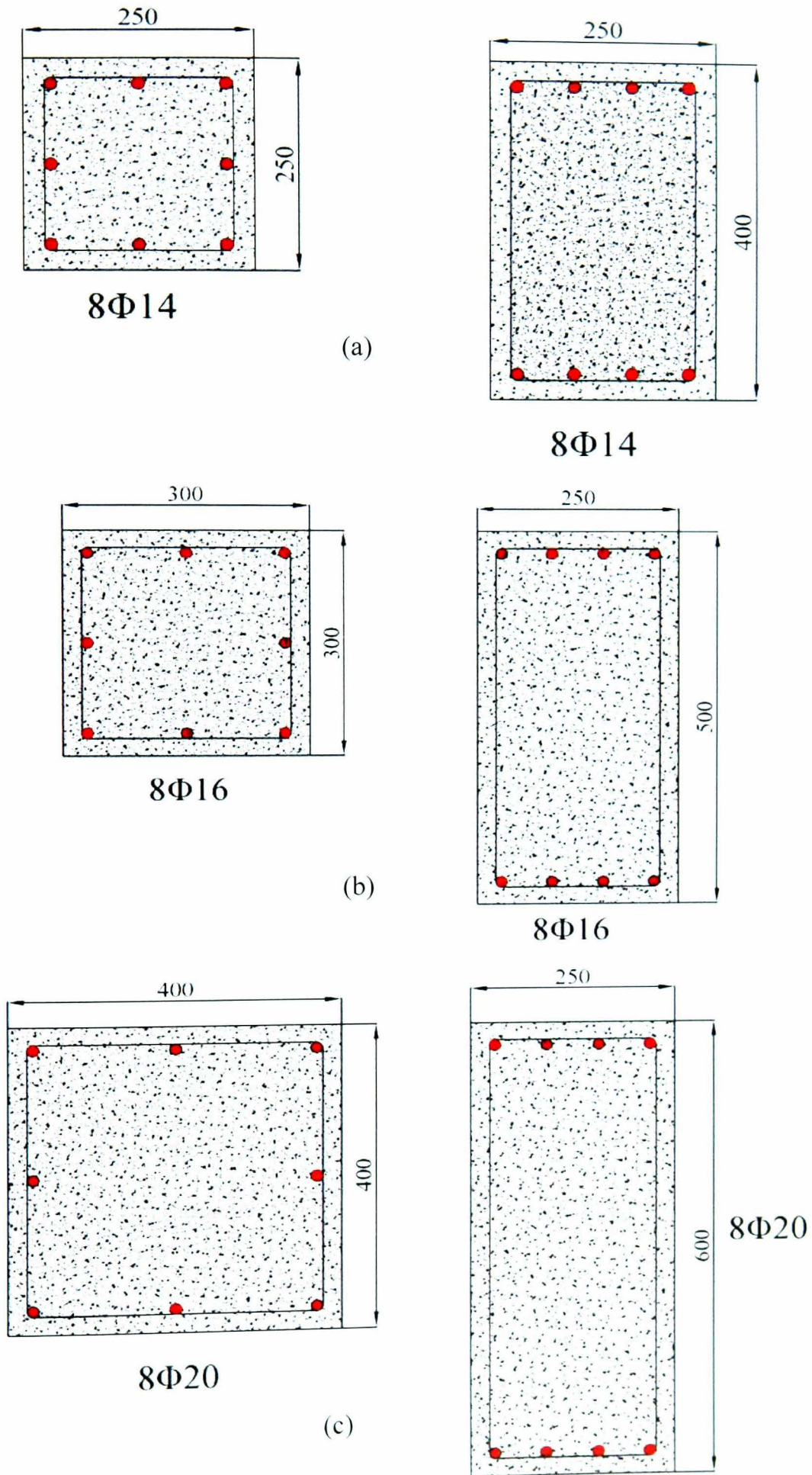


Figure C-2. Cross-sectional detail of MR frames for (a) Pre, (b) Basic and (c) Modern seismic design (columns on the left hand side).